UNIVERSITY OF SOUTHAMPTON

FACULTY OF NATURAL AND ENVIRONMENTAL SCIENCES

Chemistry

Volume 1 of 1

Application of Chromatography and Mass Spectrometry to the Analysis of Gasoline

by

Edward Michael John Wilmot

Thesis for the degree of Doctor of Philosophy

December 2017

UNIVERSITY OF SOUTHAMPTON

<u>ABSTRACT</u>

FACULTY OF NATURAL AND ENVIRONMENTAL SCIENCES

<u>Chemistry</u>

Thesis for the degree of Doctor of Philosophy

APPLICATION OF CHROMATOGRAPHY AND MASS SPECTROMETRY TO THE ANALYSIS OF GASOLINE

Edward Michael John Wilmot

The introduction of increasing stringent emission legislation placed on vehicle manufactures has resulted in the development of more efficient gasoline engines, namely, the development of gasoline direct injection (GDI) engines. GDI provides increased efficiency when compared to previous fuel injection systems. Although, GDI injectors are susceptible to injector nozzle deposits due to the elevated pressures and temperatures experienced within the combustion chamber. The presence of deposits within the injector nozzle impact the spray pattern produced and the flow of gasoline, reducing the efficiency of GDI. It is postulated that the formation of deposits is linked to gasoline composition, thus it is essential to comprehensively understand the chemical make-up of gasoline. Mass spectrometry and chromatography are extremely versatile tools to investigate gasoline composition, providing selectivity and detailed structural information for the compounds present.

EI GC-MS is the industry standard technique for gasoline analysis. It affords high chromatographic resolution and detailed structural information from energetic fragmentation for the hydrocarbon base fuel and volatile additives in gasoline. Although it is limited to thermally stable and low molecular weight compounds. Gasoline samples can often appear near identical, with just varying concentrations of the compounds present.

The use of atmospheric pressure ionisation mass spectrometry (API-MS) (*i.e.* electrospray ionisation, atmospheric pressure photo-ionisation and atmospheric pressure chemical ionisation) has permitted the detection of thermally labile and high molecular weight compounds within the gasoline matrix, while providing selectivity for the polar fraction of the gasoline, eliminating the hydrocarbon matrix. Differences between gasoline samples, which appeared identical by GC-MS are readily apparent, further selectivity was achieved by using ionisation additives.

Due to gasoline's increase solubility in supercritical CO_2 when compared to the mobile phases of liquid chromatography, ultra-high pressure supercritical fluid chromatography (UHPSFC) was used to separate components of the gasoline samples prior to ionisation to reduce the effect of ion suppression.

Two derivatised polyisobutylene detergent additives and one derivatised polypropylene glycol fluidiser additive. The additives were identified in finished gasoline samples at typically doping concentrations, without the use of pure standards for each polymeric additive. The gasoline samples required little sample preparation (*i.e.* a 5 % gasoline in methanol, and the addition of an ionisation additive).

Optical microscopy was used to identify performance reducing deposits within GDI injectors from test engines in an attempt to correlate the presence of deposits with compounds within the gasoline matrix.

SpectralWorks AnalyzerPro[TM] was used to provide a gauge on the similarity of the GC-MS data of ten gasoline samples, which look near identical when interpreting manually. One gasoline was identified as being very different compared to the other nine gasoline samples. This gasoline is thought to be a fuel designed to produce deposits within a test engine, and is described by a reference fuel patent (US 8764854 B).

UHPSFC coupled to API-MS was used to investigate the presence deposit precursors, named by the patent, within the gasoline samples (diolefins and peroxides).

Table of Contents

List of Tables

List of Figures

x

DECLARATION OF AUTHORSHIP

I, **Edward Michael John Wilmot** declare that this thesis and the work presented in it are my own and has been generated by me as the result of my own original research.

APPLICATION OF CHROMATOGRAPHY AND MASS SPECTROMETRY TO THE ANALYSIS OF GASOLINE

I confirm that:

1. This work was done wholly or mainly while in candidature for a research degree at this University;

2. Where any part of this thesis has previously been submitted for a degree or any other qualification at this University or any other institution, this has been clearly stated;

3. Where I have consulted the published work of others, this is always clearly attributed;

4. Where I have quoted from the work of others, the source is always given. With the exception of such quotations, this thesis is entirely my own work;

5. I have acknowledged all main sources of help;

6. Where the thesis is based on work done by myself jointly with others, I have made clear exactly what was done by others and what I have contributed myself;

7. None of this work has been published before submission

Signed: ....

Date:..

Acknowledgements

Firstly, I would like to express my sincere gratitude to my supervisor Prof. John Langley for his continuous support throughout my time at the University of Southampton. I could not have wished for a better advisor and mentor, his patience, motivation, and immense knowledge has helped me develop into a scientist.

I would also like to thank Julie Herniman for her advice and technical assistance in the lab.

I am extremely grateful to Innospec Ltd. and the EPSRC for providing me with the opportunity to undertake this project. In particular, I would like to thank Dr Jim Barker and Jacqueline Reid for their guidance throughout.

I would like to thank the members of the Langley group, past and present, for making the office an enjoyable place to work. You have all been fantastic friends.

I appreciate Andreas' and Dimitris' arduous attempt at teaching me Greek and introducing me to σουβλάκι to which I am now addicted. I would like to thank our excellent social secretary, Dovile, for the continuous supply of Jägerbombs and high quality banter. And a special thanks to Maria, for our and in-depth ion trap and fragmentation conversations. I would also like to thank Placido for his uplifting attitude. And a thank you to Steph and Ana. I feel very lucky to have met you all.

I would like to give a special thanks to Andy, from meeting you at Merton Road you have been a loyal and dependable friend. Be it barbecuing in January, humiliating me on the go-kart track or consistently losing the pub quiz, you have made my time in Southampton thoroughly enjoyable.

Thank you to my fiancée, Charlene, for her continuous love and support.

I would like to thank my Mum and Dad for their unending encouragement and financial assistance for as long as I can remember. I would also like to thank them for introducing me to the structure of the atom at 9 years old.

A special thank you to Glyn Wellington, my A level chemistry teacher for inspiring me to pursue chemistry at University, had it not been for him, I would not be a chemist today.

I would also like to take this opportunity to thank Percy, for taking my mind off work and helping me through the rough terrain of a PhD.

Definitions and Abbreviations

AC   Alternating Current

APCI   Atmospheric Pressure Chemical Ionisation

API   Atmospheric Pressure Ionisation

APPI   Atmospheric Pressure Photo-ionisation

BPICC   Base Peak Ion Current Chromatogram

BSFC   Brake-Specific Fuel Consumption

CCD   Combustion Chamber Deposits

CI   Chemical Ionisation

CID   Collision Induced Dissociation

CIDI   Compression Ignition Direct Injection

CRM   Charge Residue Model

DC   Direct Current

DCA   Deposit Control Additive

DCM   Dichloromethane

DI   Direct Injection

DISI   Direct Injection Spark Ignition

ECU   Electronic Control Unit

EI   Electron Ionisation

EPA   Environmental Protection Agency

ESI   Electrospray Ionisation

FID   Flame Ionisation Detector

FT-ICR   Fourier Transform Ion Cyclotron Resonance

GC   Gas Chromatography

GDI   Gasoline Direct Injection

HETP   Height Equivalent Theoretical Plate

HPLC   High Pressure Liquid Chromatography

HSS   High Strength Silica

I.D.   Internal Diameter

IEM   Ion Evaporation Model

isCID   In-Source Collision Induced Dissociation

IVD   Intake Valve Deposit

LC   Liquid Chromatography

m/z Mass to Charge Ratio

MS   Mass Spectrometry

MS/MS   Tandem Mass Spectrometry

MTBE   methyl tert-butyl ether

NHTSA   National Highway Traffic Safety Administration

NIST   National Institute of Standards and Technology

PAH   Polyaromatic Hydrocarbon

PEG   Polyethylene Glycol

PFI   Port Fuelled Injection

PIB   Polyisobutylene

PIBA   Polyisobutylene Amine

PPG   Polypropylene Glycol

QIT   Quadrupole Ion Trap

QqQ   Triple Quadrupole

RF   Radio Frequency

RICC	Reconstructed Ion Current Chromatogram
SFC	Supercritical Fluid Chromatography
SI	Spark Ignition
SIM	Selective Ion Monitoring
SORI	Sustained Off-Resonance Irradiation
SQD	Single Quadrupole Detector
SRM	Selective Reaction Monitoring
T90	Temperature where 90% of Fuel is Vaporised
TBI	Throttle Body Injection
TD	Thermal Desorption
TD	Time Domain
TEL	tetra-ethyl Lead
TICC	Total Ion Current Chromatogram
TR	Retention Time
UHPLC	Ultra-High Pressure Liquid Chromatography
UHPSFC	Ultra-High Pressure Supercritical Fluid Chromatography

Chapter 1:   Introduction

The introduction of increasingly stringent regulations placed on manufacturers in Europe and the USA to lower the emissions of carbon dioxide (CO_2) from motor vehicles has increased the demand for a more efficient engine design. In 2009 the EC regulation No. 443/2009 entered into force, with the aim of reducing CO_2 emissions of new cars to 130 g/km by 2015 and a further decrease to 95 g/km by 2020. In 2012 the Environmental Protection Agency (EPA) and the Department of Transportation's National Highway Traffic Safety Administration (NHTSA) set similar targets in the USA (EPA 2025) with the aim of reducing CO_2 emissions from passenger cars and light duty trucks to a final standard of 163 g/mile by 2025.

To fulfil the new standards, gasoline composition and spark ignition (SI) engine design must evolve. The two have an interdependent relationship, with changes in gasoline composition influencing SI engine design and *vice versa*. Examples include the introduction of hardened exhaust valve seats to SI cylinder heads in response to the removal of the anti-knock additive, *tetra*-ethyl lead from gasoline[1, 2] which protected the valves from damage. Conversely, the chemistry of deposit control additives has evolved with a developments in fuel injection technology[3], *i.e.* from carburettors to port fuelled injection (PFI).

It is vital for both automotive manufacturers and the petrochemical industry to understand the detailed composition of gasoline blends (*i.e.* fuel additive packages and potential deposit precursors), in addition to the bulk properties. Mass spectrometry and chromatography are extremely powerful tools for the detailed characterisation of gasoline blends.

The majority of gasoline analysis methods utilise gas chromatography - mass spectrometry (GC-MS), which is suitable for hydrocarbon analysis, but limited by the volatility and thermally labile nature of the various analytes. This allows for characterisation of the hydrocarbon base fuel, although chromatograms can be complex and appear similar between different gasoline samples.

Determination of subtle differences between gasoline samples is essential, particularly for the investigation of deposit precursors and fuel additives.

The application of atmospheric pressure ionisation mass spectrometry (API-MS) (*i.e.* electrospray ionisation, atmospheric pressure photo-ionisation and atmospheric pressure chemical ionisation) to gasoline analysis provides access to the higher molecular weight compounds while reducing the complexity of the sample. Essentially removing the non-polar components of the base fuel and highlighting the fuel additives and polar compounds possibly related to injector deposit formation. The selectivity of the different API techniques allows for the identification of subtle

differences between gasoline compositions, which may appear near identical by conventional methods.

1.1 Spark ignition engine

1.1.1 Four-stroke engine

The vast majority of motor vehicles around the world utilise a four-stroke internal combustion engine, also known as the Otto engine afters its German inventor Nikolaus August Otto. These engines contain a reciprocating piston within a cylinder, two classes of valves (intake and exhaust), a spark plug in the case of spark ignition (SI) engines and a fuel injection system, to introduce the fuel into the combustion chamber.

Fuel injection methods have advanced significantly from carburation, through port fuelled injection (PFI) to state of the art direct injection (DI) since the first iteration of the gasoline engine (*vide infra*). Although, the basic principle of the operation of the reciprocating piston and valves within a 4-stroke gasoline engine has not changed.

For carburation and PFI engines, fuel is mixed with air prior to entering the cylinder, the air-fuel mixture is then drawn into the cylinder on the intake stroke, when the piston moves from the top to the bottom of its travel with the opening of the intake valve. As the piston moves back up the cylinder, the compression stroke, the intake valve closes and the piston compresses the air-fuel mixture between the piston top and the cylinder head (the factor by which the intake charge is compressed is known as the compression ratio). In a SI engine, a spark produced from the sparkplug ignites the air-fuel mixture and a flame passes smoothly across the combustion chamber. The burning of the fuel increases the gas temperature, raising the pressure, driving the piston down, the expansion/power stroke, generating power to propel the vehicle, *via* rotation of the crankshaft. When the piston reaches the bottom of its travel, the exhaust valve opens, and as the piston returns towards the top, *via* momentum and power from the other cylinders, the exhaust gases are pushed out into the exhaust manifold, this is the exhaust stroke[4]. The series of 4 strokes is common for all fuel injection types, although within a direct injection engine, the fuel is injected directly into the cylinder rather than through the intake valve, which only allows the passage of air.

1.1.2 Two-stroke engine

Both the intake and exhaust stroke can be thought of as the air exchange part of the Otto cycle, and if this part could be condensed into a much smaller part of the cycle, then the expansion

stoke would represent a larger portion of the entire cycle, maximising power output from the engine.

This is the objective of the two-stroke engine, both the intake of the air/fuel mixture and removal of exhaust gases occur at the same point during the cycle, thus reducing the number of strokes required. This has many advantages, including reduced weight, increased power and decreased manufacturing costs when compared to a comparable 4-stroke engine.

Although due to the introduction of the fuel/air mixture and release of exhaust gases at the same moment in time, it is possible for the incoming mixture to continue out the exhaust without combusting, reducing efficiency and increasing emissions of the engine.

Unlike the 4-stroke engine, the 2-stroke engine requires the lubricating oil to be mixed with the fuel mixture as the crankcase is part of the induction tract, unlike the sealed crankcase of the 4-stroke[5]. The introduction of oil to the fuel system, results in further increases of emissions and could lead to spark plug fouling.

These factors have made the use of 2-stroke engines within automotive applications virtually obsolete since about 1970[6].

1.1.3   Fuel injection

A mixture of air and vaporised gasoline is required in a ratio in the range of about 7:1 to 20:1[6] within the region of the spark plug for combustion to occur. From the first iteration of the gasoline engine various approaches have been applied to meter the correct air/fuel ratio to the combustion chamber, three of which will be briefly described.

1.1.3.1   Carburettors

The first form of fuel injection incorporated into the gasoline engine was the carburettor. Fuel is pumped from the fuel tank of the vehicle to a reservoir on the carburettor known as the float chamber (Figure 1). A float within this chamber controls the entry of fuel, maintaining a constant head of gasoline within the carburettor.
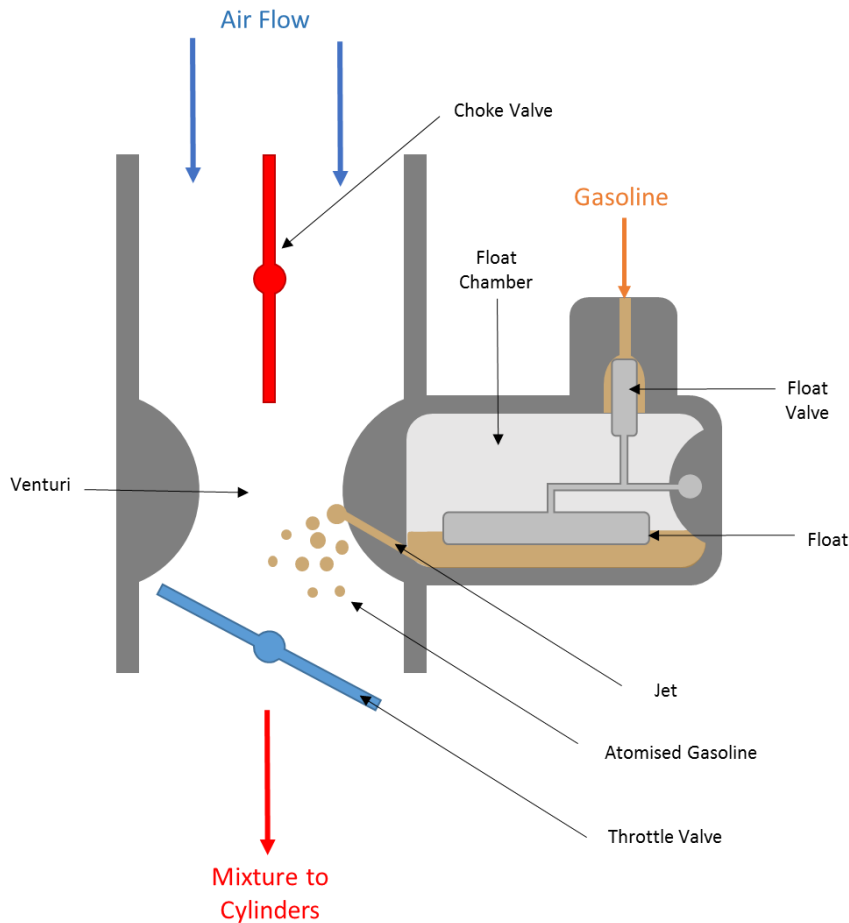
Figure 1 – Schematic of the carburettor

The carburettor is situated on the intake manifold, before the cylinders. The motion of the pistons in the cylinders draws air through the intake valve, which in turn draws air though the intake manifold and the carburettor. As air is drawn though the carburettor, the air experiences the Venturi effect[7] as the throat of the carburettor narrows, this increases the velocity of the air and thus decreases the pressure within this area. This partial vacuum draws fuel from the float chamber *via* the fuel jets situated within the throat of the carburettor, atomising the fuel and mixing it with the passing air.

Thus the amount of fuel introduced to the engine is proportional to the amount of air passing through the carburettor. To control the amount of air passing through the throat, a throttle valve is introduced, blocking the majority of the air and therefore fuel allowing the engine to idle. To increase the revolutions of the engine, the throttle valve can be opened, progressively allowing more air and fuel into the engine.

Differing driving conditions may require different air to fuel ratios, *i.e.* for a cruising vehicle, a leaner fuel to air mixture would be more appropriate to decrease fuel consumption, whereas a richer mixture would provide more power although at the cost of increase fuel consumption. The

air fuel mixture is adjusted manually by changing the aperture of the fuel jets, to increase or decrease the amount of fuel introduced for a given volume of air. The jets are typically set for the range of driving conditions to be experienced. Although, upon start up, the mixture is required to be very rich, this is achieved with the use of a choke, similar to the throttle valve, the choke blocks the passage of the majority of the air, enriching the mixture.

The carburettor is cheap to manufacture, lightweight and simple within its design, although suffers from a number of issues.

A typical, four-cylinder vehicle would have a single carburettor located on the intake manifold, distributing the air/fuel mixture to the four cylinders from a single point. This usually resulted in an uneven amount of air/fuel mixture reaching each combustion chambers, preventing each cylinder from running a peak performance, decreasing the efficiency of the engine. Traditionally this issue was overcome with the introduction of further carburettors designated to a lower number of cylinders, although imprecise air fuel metering was still an issue.

Carburettors are also susceptible to icing due to the evaporative cooling brought about by the vaporisation of the gasoline. Formation of ice restricts the air or mixture flow through the carburettor, resulting in incorrect metering and poor drivability. Carb icing can be controlled with anti-icing additives.

In addition, carburettors could not be adjusted while a vehicle is in motion to the differing driving conditions, to provide power when needed without the cost to efficiency.

The use of carburettors in automotive applications began to be phased out with the introduction of throttle body injection (TBI) and port fuelled injection (PFI) in the mid-1980s. Although, carburettors are still used to date, typically on light petrol powered machinery. This is due to their cheap cost and their lightweight nature, as they do not require expensive and heavy high pressure fuel injection pumps and injectors.

1.1.3.2 Throttle body injection (TBI)

Throttle body injection was first introduced to negate the issues experienced with carburettors. Essentially, a single high pressure injector replaced the carburettors Venturi and fuel jets, this improve power output. Although, many of the same issues experienced with the carburettor were still experienced, such as poor cylinder to cylinder performance, due to the single injector feeding all cylinders. Similarly to increasing the number of carburettors, the use of multiple throttle body injectors could also be used to increase performance. This use of multipoint injection (MPI) led to the introduction of port fuelled injection (PFI).

1.1.3.3   Port fuelled injection (PFI)

PFI engines consist of multiple high pressure injectors, typically one injector per cylinder. The injectors are located within the intake port for each cylinder. The spray produced by the injector is directed onto the inner wall of the inlet duct and the back of the valve tulip (Figure 2), forming a puddle where fuel air mixing occurs by fuel evaporation, with the scope of producing a homogeneous mixture (uniform fuel-air ratio). Upon opening of the intake valve, the mixture is drawn into the cylinder for combustion. By measuring the volume of air passing through the throttle body at various throttle apertures, the volume of fuel to be injected can be calculated by the engine control unit (ECU) to provide the correct air/fuel ratio.
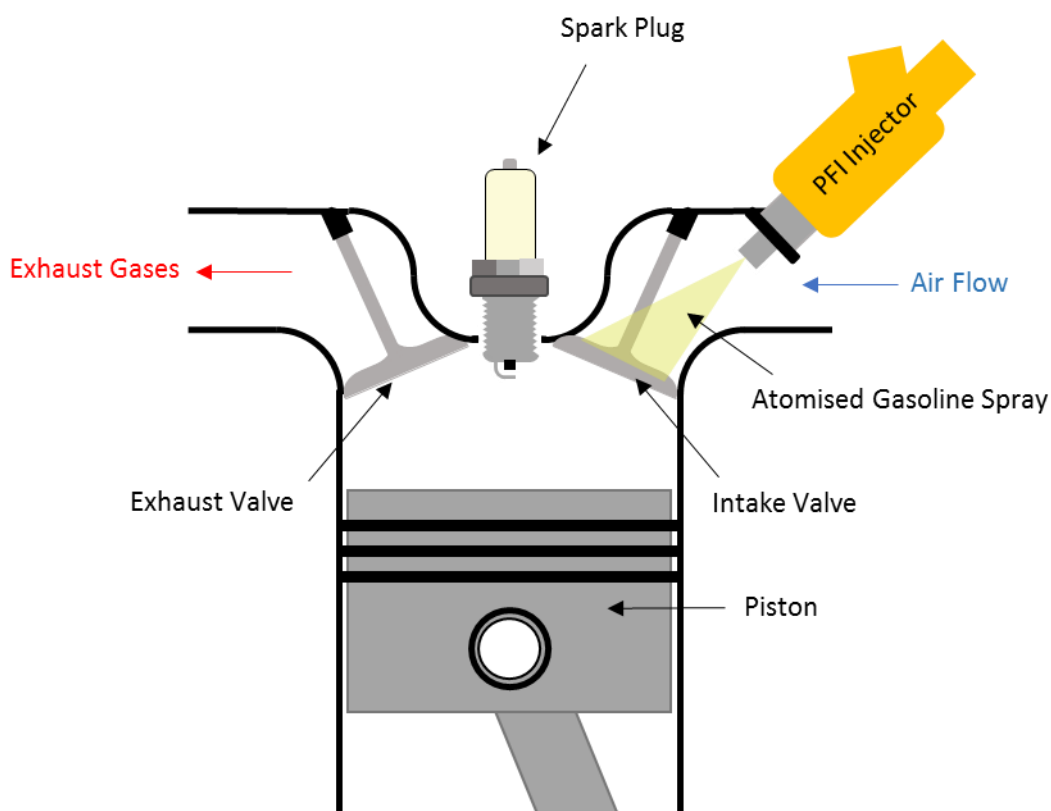
Figure 2 – Schematic of PFI system for a single cylinder

Two types of injectors exist, mechanical and electronic, with electronic being the most commonly used today.

Mechanical injectors consist of a spring, which when overcome by fuel pressure, will open the injector, releasing and atomising the fuel. These injectors produce a continuous spray while the engine is on.

Electronic injectors have a solenoid valve, which opens the injector prior to the opening of the intake valve, and shuts the injector off once the desired amount of fuel has been injected. As the intake stroke occurs once in every four strokes, the ECU controlling the injectors must know the position of the piston within the cycle, this is typically achieved with a crank shaft sensor.

PFI provided a means of meeting the demands of increase power output, lower fuel consumption, higher torque at lower engine speed, reducing emissions and improved drivability and performance[6].

Although, even if the engine is fully warmed up it is unlikely that the period between the point of injection and the opening of the intake valve is sufficient to achieved adequate mixing to produce a homogenous mixture. When the engine is cold, the temperatures are not sufficient for complete evaporation, droplets of liquid fuel are introduced into the cylinder, and residual fuel remains in the intake duct. The amount of fuel introduced into the cylinder is not the same as the amount of fuel injected by the injector and a delay in fuel delivery occurs. Consequences of this include: imprecise fuel metering; incomplete combustion and deposit formation due to inlet valve wetting. Cold cranking of the engine is a critical condition where low temperature and low turbulence limit fuel evaporation; it may be necessary to inject 4-5 times the stoichiometric amount of fuel at this time, causing increased unburnt hydrocarbon and carbon monoxide emissions[8], this problem was particularly prevalent with mechanical injectors due their continuous spray.

1.1.3.4 Direct injection (DI)

Port fuel injection (PFI) is currently the most common form of fuel injection in SI engines. The brake-specific fuel consumption (BSFC) of PFI engines is surpassed by compression ignition direct injection (CIDI) engines, diesel engines, mainly due to the significantly larger compression ratio. Although, diesel engines tend to be loud, suffer from a limited speed range, and increased particulate emissions. Attempts to produce an internal combustion engine with the BSFC of a diesel engine and the power output of a PFI engine have resulted in the design of the gasoline direct injection (GDI) engine, also known as direct injection spark ignition (DISI)[8].

The GDI engine satisfies emission regulations without compromising engine performance, thus leading to the rapid growth in vehicles featuring GDI engines. The market for GDI engines is projected to be the fastest growing market segment over the next 10 years[9].

The major difference between PFI and GDI, is the mixture preparation strategies, GDI is a form of fuel injection whereby fuel is injected directly into the combustion chamber and the air enters separately *via* the intake valve. This eliminates inlet valve wetting and decreases fuel transport time significantly. Thus, the actual amount of fuel entering each cylinder on given cycle can be

more accurately controlled. The higher fuel pressure utilised by GDI systems significantly increases atomisation and vaporisation of fuel entering the cylinder[8].
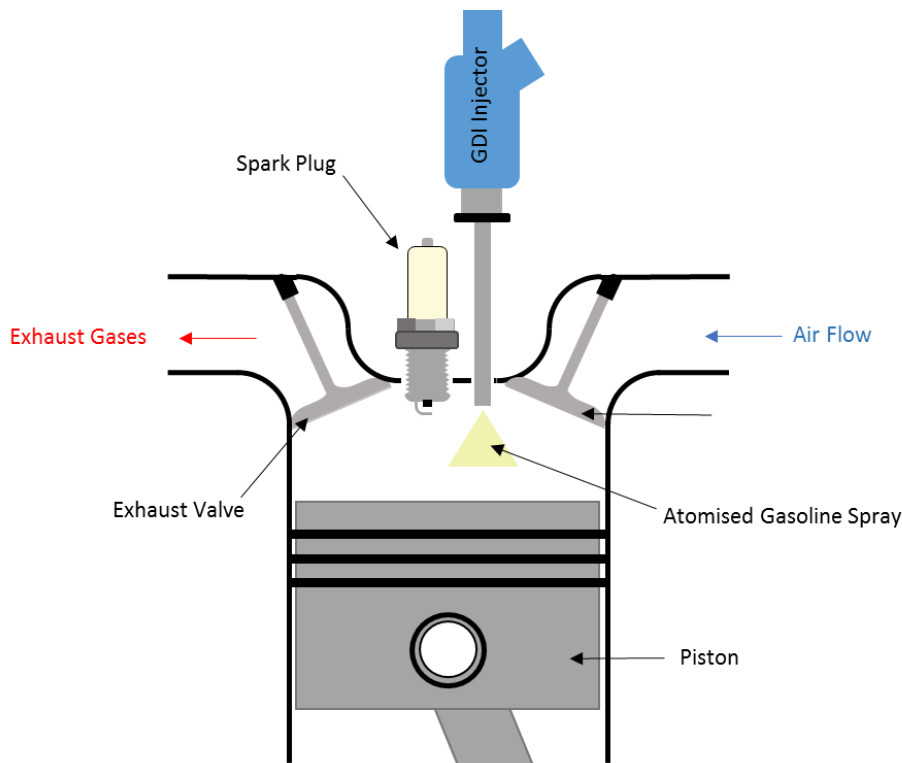
Figure 3 – Schematic of GDI system for an individual cylinder

Depending upon the working condition, air/fuel mixture in a GDI engine can have a homogenous charge or stratified charge. Homogenous charge is a uniform air to fuel ratio within the combustion chamber, as in PFI. In a stratified charge, there are space gradients in the air to fuel ratio across the combustion chamber, richer near the spark plug and getting progressively leaner with distance from the spark plug. Homogenous charge can be achieved with early injection, actuated at the beginning of the air induction phase, allowing adequate time for evaporation and mixing to produce the uniform distribution. Generally, such a condition is promoted at high load operation. To obtain a stratified charge, fuel must be injected shortly before the time of ignition (during the upward stroke of the piston), hence the need for direct injection[10]. Stratified fuel charge combustion allows for load control without throttling, improved fuel efficiency and decreased hydrocarbon emissions. The GDI engine offers a leaner combustion, less cylinder to cylinder variation in air-fuel ratios and lower operating BSFC values.

The main problem associated with GDI engines is injector fouling. As the injector tip is within the combustion chamber, it is subject to high temperatures and pressures, and an increase deposition within the injector nozzle has been observed when compared to PFI, which can impact on the fuel

flow rate and spray pattern. In turn the formed deposits can increase the hydrocarbon emissions (twice that of PFI engines)[10], limiting the performance and BSFC of the GDI system. It is therefore important to understand the composition of injector deposits and the mechanism of their formation.

1.2 Gasoline & gasoline additives

1.2.1 Gasoline production

More than 95% of the world's transportation fuels come from fossil fuels. Gasoline is primarily derived from crude oil that is an extremely complex mixture of hydrocarbons, derived from organic matter deposited with sediment millions of years ago. Oil deposits exist in many locations around the world, with different organic precursors, and having experienced a different temperature and pressure history. Due to these variations, the physical properties and chemical composition of crude oil varies greatly with location[4], making it difficult to determine the exact composition, although the various hydrocarbons can be divided into classes such as paraffins, olefins and aromatics.

After the recovery of crude oil, it is converted into useful products within a refinery. The first step involves removing impurities, *i.e.* water, suspended solids and inorganic salts, which have the potential to damage the equipment within the refinery. The step is usually referred to as 'desalting'.

The second step involves the separation of compounds based of their volatility, this is undertaken by distillation, *i.e.* separation of the hydrocarbons into fractions based on their boiling point. The lightest fraction typically consists of dissolved gases with a carbon number range of C_2-C_4. Gasoline typically contains hydrocarbons with carbon number of C_4 to C_{12} with an average carbon number of $C_{6.8}$, while diesel covers the range of C_{10}-C_{28}. Crude oil has a molecular weight distribution skewed toward heavier products, with the greater demand for lower weight products, cracking of larger molecules to smaller ones is required. This is achieved through catalytic cracking, hydrocracking and thermal cracking, thus allowing each barrel of oil in the US to be converted into gasoline (45%) and diesel (21%)[4].

Alcohols and ethers may also be blended into gasoline when demand requires, although issues can arise when oxygenate gasoline is used within vehicles designed for conventional gasoline. The increased oxygen content can affect the air/fuel ratio entering the cylinders or have adverse effects on the materials forming the fuel system.

1.2.2 Gasoline additives

Additive packages, containing a range of compounds are added to the base gasoline to provide the desired properties of the gasoline.

In general there are three applications for additives within gasoline: Additives to improve gasoline stability, additives to protect the engine and additives than influence the combustion of gasoline.

Types of additives include, octane boosters, corrosion inhibiters, detergents, friction modifiers, metal deactivators and oxygenated compounds. Dyes may also be added to fuels for identification purposes.

1.2.2.1 Additives influencing combustion

1.2.2.1.1 Octane boosters

Abnormal combustion, commonly known as engine knock, is an undesirable effect, whereby a fraction of the unburnt fuel mixture detonates before it can be consumed by the flame produced by the spark plug.

On the compression stroke of the piston, the fuel and air mixture is compressed before it is ignited by a spark. Detonation is caused by a fuels' intolerance to this compression. An octane rating is a standard rating given to fuels to describe their tolerance to knock.

The octane scale was developed with the use of two reference compounds n-heptane, which has a high tendency to knock and iso-octane, which has a high knock resistance. These two compounds were given arbitrary values of 0 and 100 respectively. A gasoline's tendency to knock can be compared against the tendency to knock of a blend of these two compounds. The volume percentage of iso-octane to n-heptane which results in the same tendency to knock as the gasoline sample in a test engine under test conditions can be used to calculate an octane rating[11, 12]. It is possible to have octane ratings of over 100 if a gasoline's resistance to knock is greater than that of pure iso-octane.

The higher the octane rating, the higher compression the fuel can experience without pre-detonation, this is particularly important with performance engines with high compression ratios.

The use of gasoline with low octane ratings will result in abnormal combustion, which in turn will result in a decrease in performance and in extreme cases, damage to the engine.

Suppression of knock with low octane fuels can be achieved with the addition of octane boosters to the gasoline to increase the octane number which in turn increases engine compression,

performance. These octane boosting compounds increases the activation energy of the fuel (the amount of energy require to initiate combustion), thus it is less likely these fuels will detonate prematurely at any given compression.

In 1921 *tetra*-ethyl lead (TEL) (Figure 4) was tested for its anti-knock properties for the first time in gasoline, and leaded gasoline became commercially available in 1923.
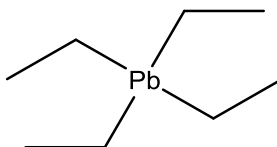
Figure 4 – Structure of *tetra*-ethyl lead (TEL)

The mechanism behind its anti-knock performances, involves its decomposition to lead oxide particles in the unburnt gasoline prior to arrival at the flame. These particles scavenged radicals formed from low temperature oxidation reactions of the fuel, thereby inhibiting pre-flame chain branching that leads to auto ignition[4]. Coupled with its octane boosting capabilities, TEL also protected against micro welds forming between the exhaust valves and their seats. As TEL is combusted, the lead oxide covers the valve seat and valve, cushioning the impact of the closing valve and prevents the formation of micro-welds. The opening of these micro welded valves would result in in valve seat recession, allowing gases to escape, reducing compression and therefore decreasing the engine performance.

The phase out of TEL in petrol began in the 1970s, because of cumulative neurotoxicity concerns and the fouling of catalytic converters, the latter being mandatory on cars from 1975 in the US. The decrease in leaded petrol was aided by the introduction of other octane boosters such as methyl *tert*-butyl ether (MTBE), which also acted as oxygenate, reducing carbon monoxide (CO) and soot emissions. Vehicle manufactures began producing cylinder heads with hardened valve seats to combat valve seat recession with the absence of lead.
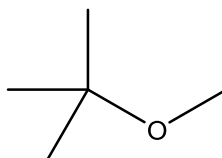
Figure 5 – Structure of methyl *tert*-butyl ether

The use of MTBE has declined in the United States due to environmental concerns. The high solubility of MTBE allows it to spread through soil and ground water more easily than other gasoline components, *e.g.* leaking from petrol stations or underground storage tanks. As part of the energy policy act of 2005 in the United States, MTBE was replaced by ethanol in gasoline.

Ethanol is a high octane fuel produced from biomass, and to a lesser extent from petroleum. It has been added to gasoline since the 1970s as an alternative to TEL[13]. More recently ethanol has been used in combination with gasoline within the fuel mixture to decrease greenhouse gas emissions. All studies have indicated that the production of ethanol is much less petroleum intensive than the production of gasoline, *i.e.* the energy require to obtain and refine crude oil to gasoline, is much greater than the energy required for the extraction of ethanol for a given volume. Although the use of ethanol produces similar greenhouse gas emissions to that of gasoline[14]. From 2007 to 2008, the percentage of ethanol blended with gasoline globally increased from 3.8% to 5.5%[13]. It has been predicted by 2022 that ethanol will have displaced 20% of the gasoline used in the USA[15].

1.2.2.2 Additives for engine protection

1.2.2.2.1 Deposit control additives (DCAs)

Deposit control additives are added to gasoline to prevent formation and remove deposits in the engine fuel system, cylinder and valve regions. These deposits are formed from combustion and can reduce fuel and air flow throughout the engine, decreasing performance and increasing emissions.

DCAs typically consist of a molecule with a polar group at one end and a long non-polar group at the other end. The polar groups are attracted to surfaces within the fuel system forming a thin film, the non-polar groups are soluble within the fuel, preventing the adhesion of deposit precursors onto the surface of fuel system components. It is also possible for DCAs to form thin layers around particulate matter within the fuel, forming a micelle, effectively solubilising any particulate matter into the fuel, carrying it to the combustion chamber for combustion.

DCAs were first introduced in gasoline in 1954, as a result of carburettor gumming which caused symptoms such as rough idling which would require the constant manual adjustment of the idle mixture, and eventually the disassembly of the carburettor for cleaning[16]. These early DCAs consisted of low-molecular weight surfactants, used at low concentrations, treat rates were typically between 20 to 100 ppm. They were effective at preventing deposits on the throttle bodies, although not effective in other parts of the intake system[3].

Surfactant additives are normally multi-functional, additives primary designed for deposit control may also have other benefits such as anti-icing or anticorrosion effectiveness[6].

Due to the increasing complex design of engine intake systems, these additives were no longer sufficient to control engine deposits. In 1968, a new class of additive was introduced, detergent

dispersants. These additives consisted of polyisobutylene succinimides (Figure 7), utilised in concentrations 3 to five times higher than the previous. They produced good results of preventing intake valve, and intake manifold deposits, although performed poorly at reducing carburettor and injector deposits. The performance of these additives was sometimes increased with the use of a petroleum fluidiser[3]. Fluidisers are thermally stable structures (*e.g.* poly-ethers and poly-glycols (Figure 6)), which form thin films on the internal engine surfaces preventing partially combusted particles from adhering to the hot metal surfaces. The build-up of high viscosity deposits can prevent valves from closing upon start up. The use of fluidisers prevent the formation of these deposits[17].

Where X = H, CH$_3$
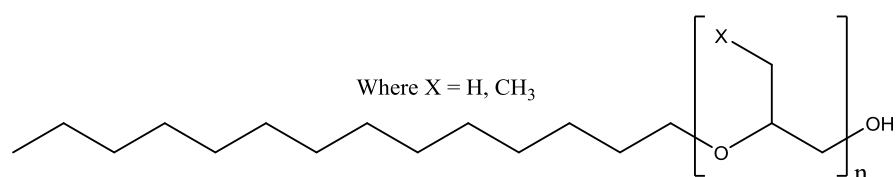
Figure 6 – Structure of alkyl polyalkylene glycol ether fluidiser

With the introduction of fuel injection, even small deposits within an injector nozzle could have large effects on vehicle drivability. The use of DCAs designed for deposit prevention within carburettors were no longer sufficient to control the different type deposits formed at higher temperatures within the injectors.

In the 1970s and 1980s DCAs were further improved with the introduction of an additive based on polybutene amine chemistry (Figure 7), these proved successful at reducing deposits throughout the intake system and fuel injectors. Although, with the phase out of TEL in gasoline and the use of this additive in unleaded petrol, an increase in combustion chamber deposits (CCD) was observed[18]. In response to this, the next generation of additive was developed for used with unleaded gasoline, based on polyether amine chemistry. The use of these yielded similar results to that of polybutene amine in leaded fuel, although the effect on CCD decrease, but still remained.

PIB-Mannich   PIB-amine   PIB-succinimide
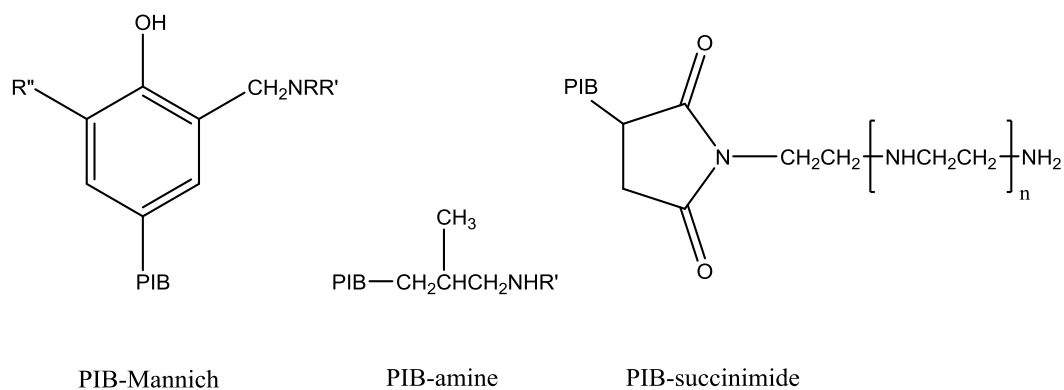
Figure 7 – Structure of PIB-Mannich, PIB-amine and PIB-succinimide

With growing environmental concerns for air quality, in 1995, the U.S. the Environment Protection Agency clean air act required that all gasoline sold in the country must contain deposit control additives.

In direct injection, the injector is now located within in the cylinder and subject to severe operation conditions. DCAs must be able to maintain clear injector nozzles, or the performance gain of direct injection will be neutralised. PFI DCAs have been tested for effectiveness within the direct injection system, with poly-isobutylene amine (PIBA) demonstrating that it could keep injectors clean, although could not remove deposits already present at the treat rate used[10]. PIBA was also demonstrated to work better than any polyether amine. Mannich DCAs were also shown to perform better than both polyether amine or polyisobutylene amine[19].

DCAs are critical for maintaining effective operation of the injectors. Due to the harsh environment in which the injector is operating, the decreasing size of injector nozzles and the derogatory impact of deposits of injector spray patterns, direct injection engines will require a new type of additive chemistry, in a similar manner to the move from carburettor to PFI engines.

1.2.2.2.2 Corrosion inhibiters

When water in the fuel system makes contact with metal surfaces, corrosion can occur. In modern fuel systems, fuel pumps and injectors use precise metering to deliver optimal engine performance, corrosion can affect these components resulting in imprecise metering. Rust particles produced by corrosion can also block fuel filters and pipes. It is therefore essential to protect against corrosion using corrosion inhibitors.

Typically, corrosion inhibitors have a structure consisting of a polar head group, which attaches to metal surfaces within the fuel system forming a protective film over the metal surfaces. The molecule also contains a non-polar hydrocarbon tail, providing solubility within the fuel matrix, ensuring delivery of the corrosion inhibitor to the vulnerable surfaces throughout the fuel system. Treat rates are typically around 5 mg/kg Typical examples of corrosion inhibitors include carboxylic acids (Figure 8), esters and amine salts[20].
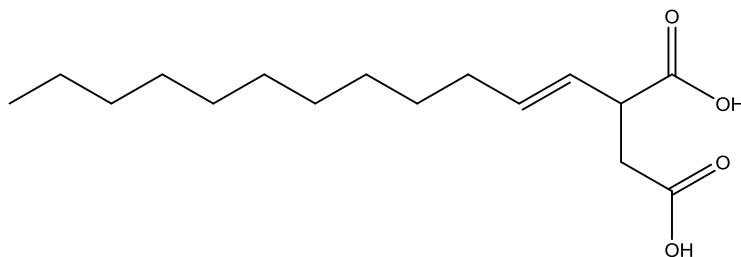
Figure 8 – Example of corrosion inhibitor (dodecenyl succinic acid)

1.2.2.3   Additives to improve oxidative stability

1.2.2.3.1   Antioxidants

Unstable olefins within the gasoline produce free radicals which combine with oxygen to produce further free radicals, *via* auto-oxidation reactions. This process will continue forming gums *via* polymerisation reactions, these gums are responsible for fouling of injectors, filters and fuel lines (*vide infra*).

Antioxidants disrupt the polymerisation process by acting as radical traps, preventing large molecular weight gums from being formed. Typical antioxidants include sterically hindered phenols (typically 5 to 100 mg/kg) and aromatic diamines (5 to 20 ppm). Aminophenols are also used, although their solubility in water can cause them to be lost in water at the bottom of storage tanks.

1.2.2.3.2   Metal deactivators

Metals, such as copper, within gasoline can catalyse oxidation reactions within the fuel. Metals in gasoline can originate from the crude oil or be dissolved into the gasoline v*ia* acidic compounds.

Metal deactivators are added to the gasoline at a treat rate of around 10 ppm. They act as chelating agents, forming complexes with the metals present in the fuel. A common metal deactivator is n,n'-disalicylene-1,2-propanediamine (Figure 9)[21].
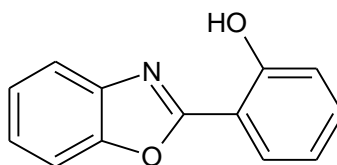
Figure 9 – Structure of metal deactivator n,n'-disalicylene-1,2-propanediamine

1.3   Gasoline engine deposits

The burning of commercial gasoline within the internal combustion engine results in the deposit of carbon on the interior parts, both from the incomplete combustion of fossil fuels and the thermal cracking of lubrication oil contaminants within the combustion chamber. During thermal stressing, the hydrocarbon composition of gasoline changes. Fuel related deposits can be created through two distinct free radical pathways: low temperature auto-oxidation and high temperature pyrolysis. Autoxidation reaction occur during fuel storage and exposure to high temperature in fuel lines, resulting in a series of liquid oxidation reactions of alkyl radicals generating oxidised products, which are believed to be responsible for solid deposit formation[22].

At elevated temperatures (>350°C), carbonaceous deposits form *via* two different roots: Decomposition of hydrocarbons to elemental carbon and hydrogen, or the polymerisation/condensation of hydrocarbons to form larger polycyclic aromatic hydrocarbons (PAHs) which can then nucleate to produce carbonaceous solids. The metal substrate of the injector surface can provide a site for catalysis[22].

Fuel stability play a large role within deposit formation. The oxidation of the olefin content of the gasoline is thought to be the main contributor towards fuel instability, particularly conjugated di-olefins[23], with patents for deposit forming fuels specifically mentioning the presence of these compounds[24]. Antioxidant additives are designed to prevent oxidation of compounds during fuel storage, but are ineffective at preventing oxidation during the injection event, where pre-flame oxidation reaction occur, possibly causing compounds to polymerise to form gums within the injectors.

Hallett[25] conducted a study investigating the effect of octane number of the gasoline and the amount of deposition on the surface of a metal alloy. It was found that the greater the octane number the lower the deposition.

In a conventional PFI system, the deposits can be classified as intake vale deposits (IVD), occurring on the tulip of the intake valve. And combustion chamber deposits (CCD), occurring on the cylinder head of the cylinder and the crown of the piston. The deposits in these areas are attributed to components within the gasoline and lesser extent the lubricating oil, especially in modern cars which burn less lubricating oil, although, deposits are frequently found to contain small quantities of Ca, Zn, and Mg deriving from lubricant additives. Concentrations of these elements is usually a few times higher in deposits formed on the piston crown, suggesting oil plays a greater role in the formation of piston deposits in the area of the engine head[18].

Combustion chamber deposits (CCD) forming on both the piston crowns and cylinder head can adversely affect the engines operation. Deposit accumulation can lead to abnormal forms of combustion, for example, resulting from deposit heat storage and thermal insulation effects leading to auto ignition knock[26].

According to Mayers *et al.,* the most critical components of fuel with regard to surface deposition are those with the greatest boiling points[27]. Therefore, with consideration to the major components of gasoline, aromatic hydrocarbons are the most prone to deposition, olefins significantly less and paraffins are the least prone[18]. Carlisle *et al.*[28] conducted a study on the effect of fuel composition on a GDI, and also concluded that the aromatic hydrocarbon content has a significant effect of deposition.

It has been reported that intake valve deposits (IVD) can be treated and controlled through the use of additives, although simultaneously increasing CCD[18]. It has also been reported, that the use of additives can actually increase the amount of CCD observed than when compared to base fuel. This is possibly due to the higher boiling point components of the additives compared to that of base fuel[29].

In PFI systems, injector deposits are formed during the "hot soak" period after the engine has been turned off. Residual fuel in the injector nozzle is subject to elevated temperatures for a prolonged time, this heat degrades the gasoline into a hard varnish, initiating deposit formation. This effect is amplified when the vehicle is used for numerous short trips.

In general, GDI engines produce greater level of deposits when compared to PFI engines, namely fuel injector deposits. This is likely to be a result of the severe operating conditions a GDI injector faces when compared to a PFI. Located within the cylinder, not only are the temperatures and pressures higher, but the injector is the subject of direct exposure to flame front and combustion gases. As the injector body is located within the engine block, rather than in the manifold as with PFI, the body of the injector is subjected to increased heat soak temperatures[6].

The stratified charge cycle of a GDI engine produces a greater level of injector fouling than the stoichiometric cycle[18], this is possibly due to the favourable deposit conditions produced by the leaner mixture, lower gas and surface temperatures.

It has been reported that GDI engines produce over twice the amount of IVD deposits compared to PFI lean cycle conditions on base fuel and about equal on rich cycle[30]. Although, in GDI engines, fuel does not come directly in contact with the tulip of the intake vale, as fuel is injected directly into the combustion chamber. Lubricating oil can be a significant factor for IVD, as oil has direct pathways to the valve tulip *via* the valve stems. Intake valve deposits due to the combustion of fuel must be considered to act only in a secondary fashion. Although at the same time, no fuel is washing over the valve, as in PFI, so detergents do not come into contact with the valve tulip explaining the increase in IVD seen in GDI engines[18].

The effect of GDI design with relation to injector deposits has been investigated, two forms of GDI design have been adopted "spray guided" and "wall air-guided" combustion systems[3]. The feature of the spray guided system, is that the injector is placed centrally in the top of the cylinder in close proximity to the spark plug. This type of system is more susceptible to injector coking, due to its proximity to the combustion event and a greater amount of fuel remains on the injector time. The wall air guided system is less susceptible to coking, as the injector is mounted at an angle causing the spray to deflect of the top of the piston, the combustion event is at a greater distance from

the tip of the injector, decreasing the temperature at that point and a greater movement of air around the tip reduces residual fuel[3, 8].

The design of modern fuel injectors incorporates the use of several smaller holes, to increase atomisation and enhance spray patterns. These smaller holes increasing susceptible to fouling (Figure 10).The effect of these deposits on the injector manifest in two ways, a decrease in the spray quality delivered by an alteration in the spray skew, angle and symmetry. A reduction of fuel flow through the injector, thus less fuel injected on each injection. In the case of GDI, the temperature and pressure experience at the tip can result in the polymerisation of components within the gasoline leading to a waxy residue within the passage. For most GDI injectors, early deposits do not result in significant flow reduction, although substantial changes in the spray pattern can result[8].
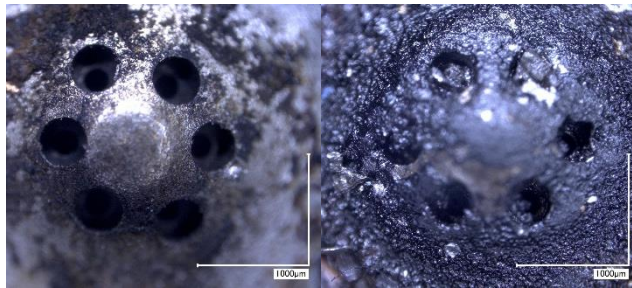
Figure 10 – Comparison of clean injector *vs* heavily deposited injector

Kinoshita *et al.*[31] conducted a study where the injector deposit formation mechanism was investigated. The study focused on two aspects of deposition: the soot formed on the nozzle and needle; fuel polymerisation by thermal decomposition to form gum type deposits within the injector. The internal injector deposits were found to occur where fuel resides after the end of each injection. Both the nozzle temperature and fuel distillation characteristics were found to dominate the deposit build up; when the nozzle temperature exceeded the T90 (the distillation temperature where 90% of the fuel is vaporised), the flow rate of fuel is significantly decreased. A mechanism is offered by Kinoshita *et al.*[31] to explain this result. When the nozzle is subject to elevated temperatures, thermal decomposition of the fuel can occur, where the deposit precursors are formed. When the nozzle temperature is below that of the T90 (Figure 11b), most of the fuel will remain as a liquid, continued presence of liquid fuel ensures that the deposit precursors are washed away during the next injection event. When the nozzle temperature exceeds that of the T90 (Figure 11c), the majority of the fuel will vaporize. As a consequence the deposit precursors are distributed on the nozzle surface.
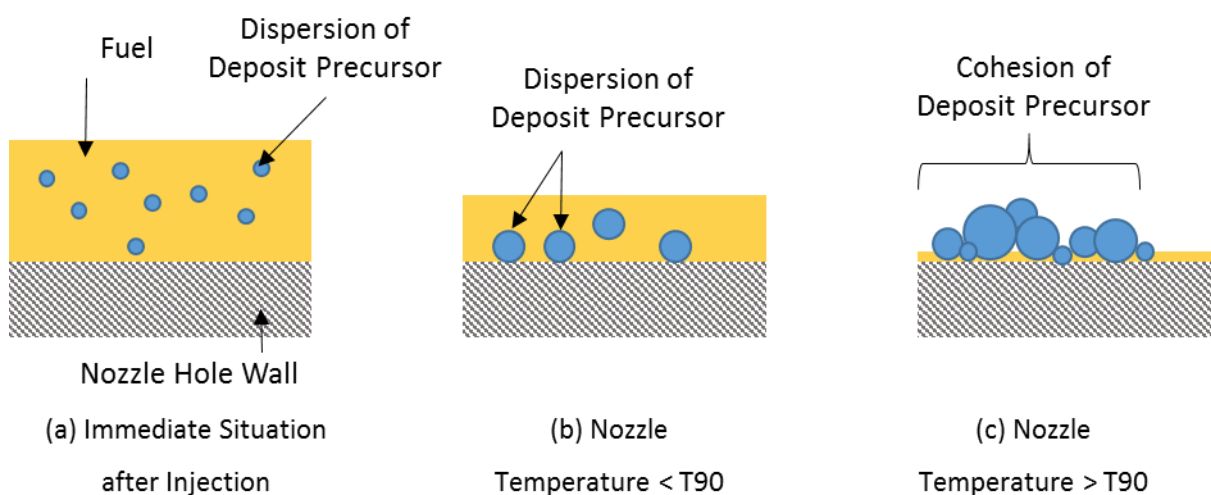
Figure 11 - Kinoshita *et al.* deposit formation model for injector nozzle[31]

However, Arters and Macduff[32] found that fuels with a higher T90 correlated with increased injector deposits, suggesting that fuels with a higher volatility would lead to decreased injector deposits. This was also observed by Sandquist *et al.*[10], they also found that injector fouling was the main cause of hydrocarbon emissions.

It has also observed that deposition occurs early, and decreases in rate with the accumulation of deposits, suggest the injector surface plays a critical role in deposit formation. Indeed, it has been seen that coated surfaces were found to delay the onset of deposition, but once a deposit layer had formed the coated and uncoated surface displayed very little difference in carbon deposition[8].

Dearn *et al.*[33] conducted a study to characterise the deposits of a GDI injector. The physical and chemical properties of the internal surfaces of mechanically cracked injector were analysed. It was concluded that the deposits in different locations consisted of different amounts of typical fuel and lubrication elements, although the dominating elements within the injector were found to be C, S, Ca and O. The percentage of carbon within the deposits increases, while the percentages of sulphur and calcium decrease with proximity to the combustion chamber. The surrounding environment at different locations within the injector have a significant effect of the chemical composition of the deposits.

1.4   This study

This study will focus on the application of chromatography and mass spectrometry (with a focus on atmospheric pressure ionisation techniques) to qualitatively asses the composition of fuel

samples. This includes the development of methods and strategies for the detection and identification of compounds within the complex gasoline matrix, *i.e.* polymeric additives.

An investigation into how the composition of gasoline samples influence the severity of DI injector fouling will also be conducted.

Initially, a range of gasoline samples have been provided, some of which display injector deposits under test conditions. The use of the following instrumentation will be employed to identify differences between deposit forming and non-deposit forming fuels, in an effort to identify deposit precursors within the fuel matrix.

Chapter 2:   Instrumentation

2.1   Chromatography

Chromatography is the term for techniques involving the separation of mixtures[34]. The initial mixture is carried by a mobile phase through an immobile stationary phase. Components within the mixture will experience different affinities to the mobile and stationary phases due to their structures and chemistries. Compounds that are soluble in the mobile phase, will have a high mobility through, and adversely, compounds that are have large interactions with the stationary phase will have a low mobility.

As a result of these mobilities, compounds will begin to separate from each other as they travel over the stationary phase. Following the separation the individual components within the mixture can be detected.

2.1.1   Chromatographic resolution

Chromatographic resolution is the measurement of how well two eluted peaks can be separated. Chromatographic resolution is affected by three parameters; selectivity, efficiency and retention which can be amalgamated into Equation 1[35].

Equation 1: $$R_S = \frac{\sqrt{N}}{4} \times \left(\frac{\alpha-1}{\alpha}\right) \times \frac{k}{k+1}$$

Where N is the number of theoretical plates (the hypothetical distance in which the analyte establishes and equilibrium between the mobile and stationary phase), α is the selectivity factor and k is the retention factor.

2.1.1.1   Retention factor

Retention time (T_R) of a compound in a chromatographic separation is the time taken from injection to the peak maximum to be eluted from the column. The retention factor is equal to the ratio of the retention time of an analyte on the column to the retention time of a non-retained compound. Thus the non-retained compound has no interaction with the stationary phase, and the time from the injection to the elution of the non-retained compound is the "dead time". The retention factor is given by Equation 2.

Equation 2: $$k = \frac{(t_R-t_0)}{t_0}$$

Where t_0 is the retention time of the non-retained compound. This is effectively a measure of the time a molecule spends in the stationary phase, when compared to the mobile phase. The ratio is also independent of mobile phase flow rate and the physical dimensions of the column.

Adjusting the retention factor can be achieved by altering both the solvent and solvent ratio within the mobile phase.

2.1.1.2   Selectivity factor

The selectivity factor is a measure of chromatographic system to separate "chemically" between two different sample components. It is measured *via* the ratio of two different components retention factors, and is given by Equation 3.

Equation 3: $$\alpha = \frac{k_2}{k_1}$$

Where k_1 and k_2 are the retention factors for peaks 1 and 2 respectively. As selectivity depends on the chemical nature of the analytes of interest, altering the mobile and stationary phases will affect the selectivity factor.

2.1.1.3   Chromatographic efficiency

Efficiency of a chromatographic peak is a measure of how the band of analyte disperses as it travels through the column. Ideally the analyte band should spread out as little as possible during the separation, excessive spreading will result in a loss of resolution.

The efficiency of a column may be expressed by the number of theoretical plates on the column (N), the term was derived from a comparison with a fractional distillation column. Each plate is the hypothetical distance for an analyte to reach one equilibrium between the mobile and stationary phase within the column. Therefore, a higher number of theoretical plates will result in a higher number of equilibriums, increasing the quality of the separation. The number of theoretical plates within a chromatographic column can be calculated using Equation 4.

Equation 4: $$N = 16 \left(\frac{t_R}{w_b} \right)^2 = 5.54 \left(\frac{t_R}{w_h} \right)^2$$

Where w_b is peak width at the base and w_h is peak width at half height.

In order for columns of different lengths to be compared, efficiency can be expressed as the height equivalent to a theoretical plate (HETP). This can be calculated using Equation 5, where L is the length of the chromatographic column.

Equation 5: $$HETP = \left(\frac{L}{N} \right)$$

2.1.1.3.1 Van Deemter equation – packed columns

The physical parameters effecting band broadening in a packed column are described the Van Deemter equation[36] (Equation 6), the equation relates HETP with the linear velocity of the mobile phase flowing through the column.

Equation 6:
$$HETP = A + \frac{B}{u} + Cu$$

Where the A term, relates to the Eddy diffusion, the B term relates to longitudinal diffusion, the C term relates to the resistance to mass transfer and u is the linear velocity of the mobile phase flowing through the column. The various terms can be plotted on a graph to obtain optimal efficiency (Figure 12). The optimum efficiency is identified at linear velocity corresponding to the shortest HETP.
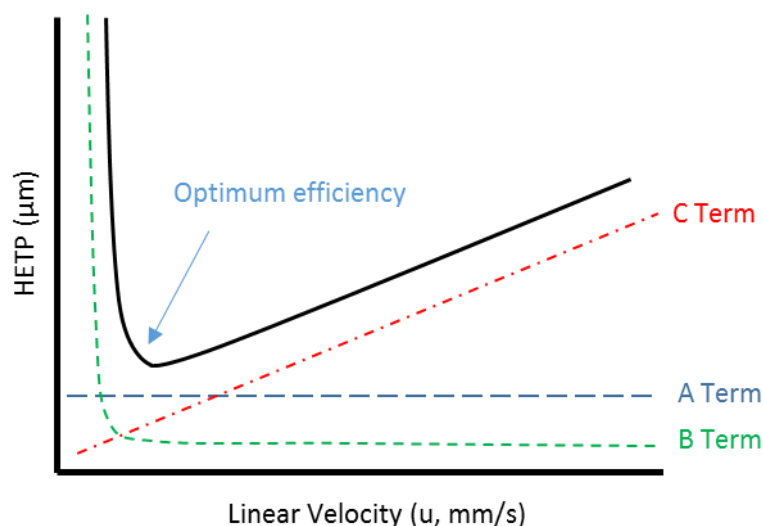
Figure 12 – Plot of the three parameters that comprise the van Deemter equation for efficiency

The three physical parameters, Eddy diffusion, longitudinal diffusion and resistance to mass transfer are described in more detail.

2.1.1.3.1.1 Eddy diffusion

Eddy diffusion is a description on the random path analyte molecules can take around the stationary phase particles within a packed chromatographic column. Large variations in time taken for analyte molecules to transverse the column will result in increased band broadening.
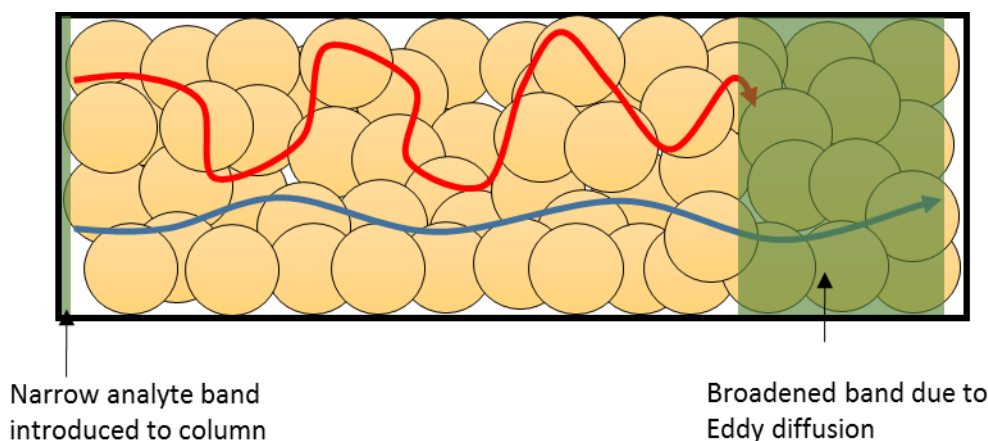
Figure 13 – Representation of Eddy diffusion within a packed chromatographic column

If the most extreme case is considered (Figure 13), both analyte molecules are introduced to the column at the same point in time, therefore the initial band of analyte is narrow. The analyte molecule represented by the blue line (Figure 13), moves through the column quickly, taking the shortest path available. Conversely, at the same time, the analyte molecule represented by the red line (Figure 13), takes a longer path, due to the nature of the stationary phase present. Upon reaching the end of the column, both molecules have transverse the column within different times, broadening the band.

Eddy diffusion can be minimised with the use of more uniformly packed and smaller stationary phase particle sizes. A small size distribution of the packing material is also desirable. All of these factors tend to standardise the length of the various paths within the column experienced by an analyte molecules.

2.1.1.3.1.2   Longitudinal diffusion

The molecules of any analyte within a fluid will diffuse in all directions with time due to the concentration gradient present at the outer edges of the band. Within a chromatographic column, the greatest scope for diffusion is along the axis of the column, due to the tubular nature, hence the name longitudinal diffusion. As an analyte band travels along the column, the band will broaden due to this diffusion. From the van Deemter plot (Figure 12), it can be seen that the effect on HETP is particular prevalent at low linear velocities. The use of tubing and unions with large internal volumes will maximise longitudinal diffusion, and hence increase band broadening.

2.1.1.3.1.3   Resistance to mass transfer

A packed column contains porous beads of packing material coated in stationary phase. The porous nature increases the surface area present for interaction with analytes within the mobile

phase. Although, to access the stationary phases within the pores, the analytes molecules must defuse through the stagnant mobile phase which occupies the voids within the porous beads.
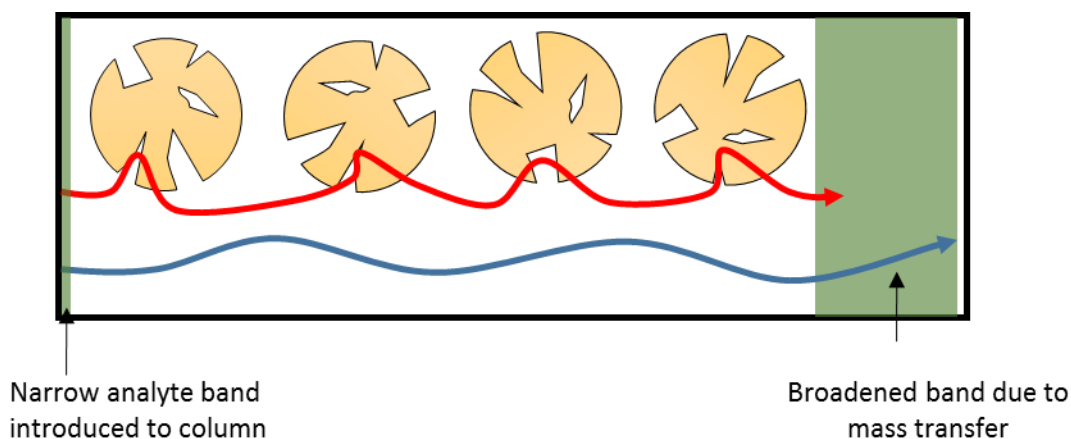
Figure 14 - Representation of resistance to mass transfer within a packed chromatographic column

Again, if the most extreme case is considered, a simplified column is presented (Figure 14). The blue path corresponds to an analyte molecule, traveling through the column, little interaction with the stationary phase of the column. The red path corresponds to an analyte molecule which diffuses into all the pores within the beads upon its route through the column, the rate of diffusion and the increased distance into the pore will increase the time taken for the analyte molecule to travel the length of the column. Thus, the difference in time results in band broadening.

From the van Deemter plot (Figure 12), it can be seen, the effect of mass transfer increases with increasing flow rates. Smaller particles size will decrease the effects of mass transfer as the pores will be shallower, reducing the time taken for an analytes molecule to enter and leave the pore.

2.1.1.3.2   Golay equation – capillary columns

Similarly to the Van Deemter equation for packed columns, the Golay equation[37] (Equation 7) describes band boarding in a capillary column. As there is no packing material within a capillary column, there is no eddy diffusion term (A term) in the Golay equation (Equation 7), although contains two terms for mass transfer C_M and C_S (mass transfer into the mobile phase and stationary phase respectively).

Equation 7:
$$HETP = \frac{B}{u} + (C_S + C_M)u$$

As described for the Van Deemter equation, the C term describes the rate at which an analyte molecule can diffuse between the mobile phase and stationary phase. Fast transition into the

stationary phase (C_S) results in reduced band broadening, this is typically achieved with a thin stationary phase film thickness, reducing the distance that analyte molecules have to travel.

Band broadening from diffusion of the analyte molecules into the mobile phase (C_M) occurs due to non-turbulent flow of an analyte band within a column. As a band moves down a column, the analyte molecules in the centre of the column will travel faster when compared to analyte molecules near the wall of the column. This effect can be reduced by minimising the internal diameter of the column, thus reducing the distance for mass transfer to occur.

The various terms can be plotted on a graph to obtain optimal efficiency (Figure 15). The optimum efficiency is identified at linear velocity corresponding to the shortest HETP.
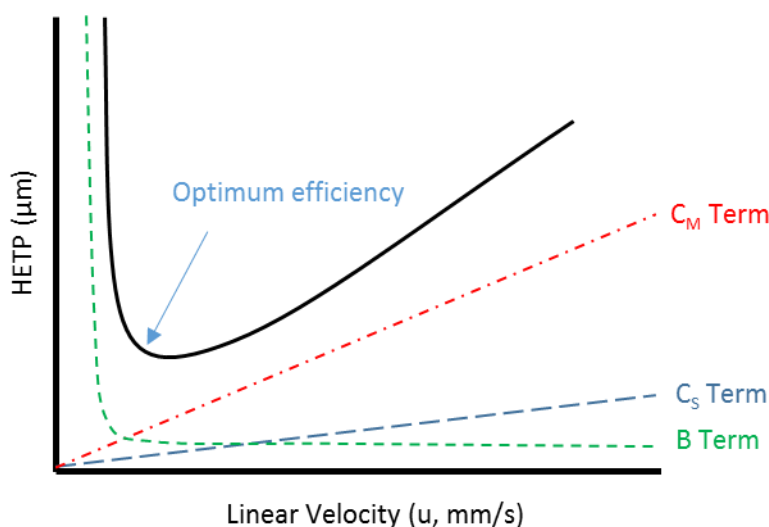
Figure 15 - Plot of the three parameters that comprise the Golay equation for capillary columns for efficiency

2.1.2   Gas chromatography (GC)

A gas chromatograph (Figure 16) consists of a column located within an oven. The oven allows for control of the temperature of the column, typically between 40 and 350 °C. Gas chromatography utilises an inert gas as the mobile phase, typically nitrogen, helium or hydrogen. Typically a heated injection port is used to introduce the sample, and a heated interface is utilised post-column to transfer the eluent to a suitable detector.
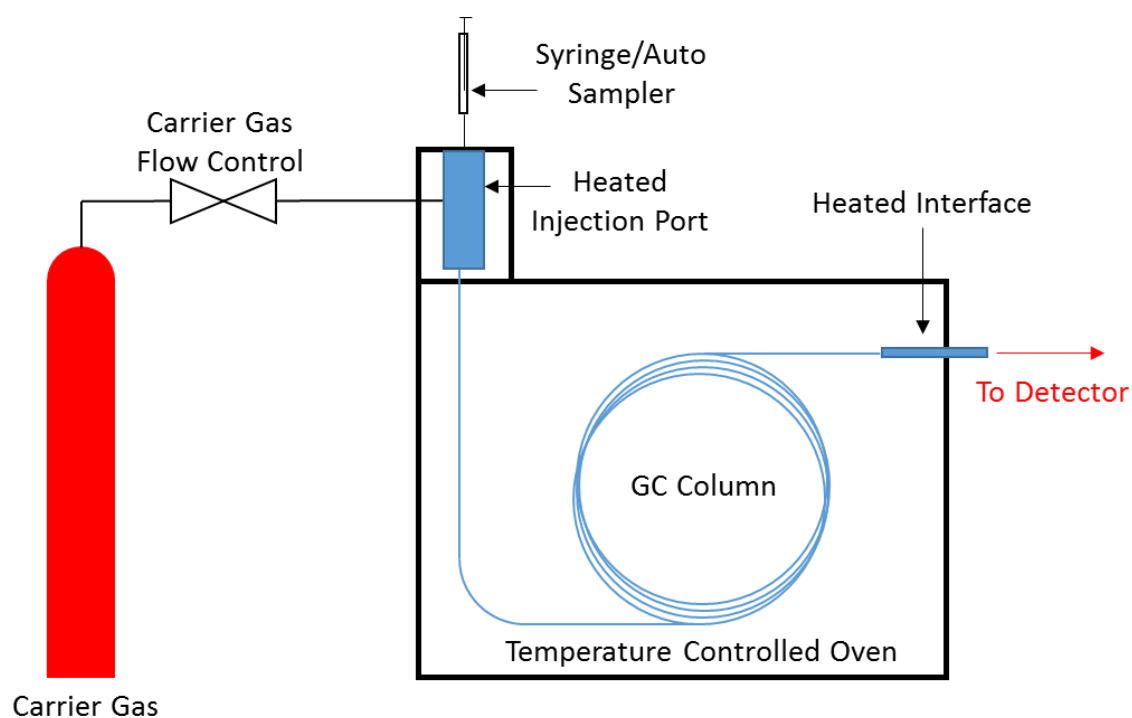
Figure 16 – Schematic of a gas chromatograph

There are two general types of column available to GC, packed columns and capillary columns. Packed columns consist of a finely divided, inert solid support structure, coated with the liquid stationary phase. These columns, are typically between 1.5 – 10 m in length, with an internal diameter of 2 – 4 mm.

Capillary columns[38], are open bore, with and internal diameter typically between 0.1 – 0.5 mm. The ridged base of the column is constructed from fused silica, the inside surface is coated with a thin film of stationary phase (0.25 – 0.50 µm thick). The outside of the fused silica is covered with a polyimide coating which strengthen the fused silica and protects the column from the elevated temperatures experienced within the GC oven. Capillary columns can be longer (60+ m) than packed columns due to their open tubular nature resulting in the lower backpressures. Thus capillary columns have an increased efficiency when compared to packed columns. The absence of particles within a capillary column, also negates the effect band broadening from Eddy diffusion experienced by packed columns.

Capillary wall coated open tubular columns are more commonly used in GC analysis when compared to packed columns, due to their increase efficiency.

A known volume of liquid sample is injected into the heated injection port, where it is vaporised and carried onto the column by the carrier gas, where the sample condenses, providing the temperature of the column is lower than that of the samples boiling point. As the temperature of the oven increases, low temperature boiling point compounds vaporise and travel down the

column, impeded by adsorption to the stationary phase. The characteristics of the compound and stationary phase define the amount interaction between the two. Compounds with a low affinity to the stationary phase travel through the column quicker, and compounds with a high affinity to the stationary phase travel slower. As the oven temperature increases further, higher boiling point compounds begin to vaporise and travel down the column. GC separates mixtures on their boiling points and interactions (*i.e.* dispersive, dipole and hydrogen bonding interactions) with the stationary phase.

Typically, there are two types of stationary phase, polar and non-polar. Separation of polar compounds can be achieved on a polar column, *i.e.* a polyethylene glycol (PEG) (Figure 17), *via* intermolecular interactions between the analyte of interest and the stationary phase.
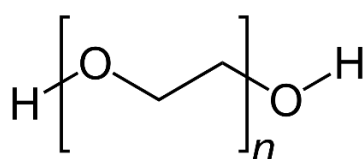
Figure 17 – Structure of PEG stationary phase

Whereas, non-polar compounds can be typically separated on the non-polar diphenyl dimethyl polysiloxane stationary phase (Figure 18), separated *via* the boiling points of the various analytes.
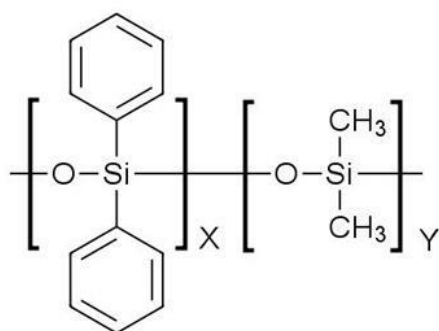
Figure 18 – Structure of diphenyl dimethyl polysiloxane stationary phase

The diphenyl unit is interactive with molecules in the mobile phase, the relative number of diphenyl units to methyl units in the stationary phase effects the retention of compounds. Where X is 5% and Y is 95% as in an RTX-5 column, compounds experience little interaction with the stationary phase, and are mainly separated based on their boiling points, these are commonly known as boiling point columns. Where X is increased to 50%, interactions of compounds with the stationary phase plays an important role in separation.

GC is limited to compounds that are volatile or semi-volatile otherwise they will not enter a gaseous phase, remaining in the injection port. Compounds must also be thermally stable, or they

will degrade upon heating. The decreased volatility of higher molecular weight molecules limits the maximum molecular weight of compounds.

Gas chromatography can be interfaced with many different detections methods, most commonly, flame ionisation detectors or mass spectrometry.

Flame ionisation detectors (FID) are used extensively in the GC analysis of fossil fuels due to their high sensitivity and good reliability. The FID response is proportional to the amount of oxidisable material being ionised in the flame, and does not vary significantly with the chemistry of the compound *i.e.* aromatic and aliphatic compounds of the same carbon number give a similar response. The FID detector is considered a universal detector for oxidisable carbon compounds and provides a fingerprint for the petroleum samples containing the major chemical components, although detailed structural information cannot be obtained from a single analysis. The comparison of retention times to standard compounds is required to identify individual components within a mixture.

Gas chromatography can be coupled to mass spectrometry (GC-MS)[39]. Electron ionisation and chemical ionisation are the most commonly used ionization techniques when coupling a mass spectrometer to a GC. GC-MS equipped with an electron ionisation provides invaluable structural information from the extensive fragmentation achieved each component eluting the GC column. Chemical ionisation can also be interfaced, typically producing protonated and adducted molecules with minimal fragmentation. Low fragmentation permits the calculation of the molecular weight of the detected compounds. GC-MS is an extremely valuable tool in mixture analysis.

Gas chromatography (GC) is widely used in the analysis of petroleum products. GC is applicable to low-molecular weight, volatile and thermally stable hydrocarbons, *i.e.* the base fuel.

GC-MS is frequently used for the analysis of gasoline, to detect adulterants to gasoline and the presence of additives, such as MTBE, with little to no sample preparation[40][41][42].

Dearn *et al.*[33] outlined the used of thermal desorption GC-MS (TD-GCMS) method for analysing injector deposits. Test mixtures of different high boiling point compounds were analysed, to investigate whether these compounds could be successfully desorbed, captured and analysed by GC-MS. The resulting spectra showed that all mixtures were successfully analysed with good detection limits and very little cross contamination.

When using gas chromatography, compounds of a similar boing point can co-elute from the column, making identification of each component difficult[43]. Phillips and Beens[44] reported the use

of two-dimensional gas chromatography (GC x GC) to increase the separation. This method of analysis employs the use of two columns with different separation mechanisms, the columns are connected orthogonally. The sample is injected into the first column where the primary separation occurs, the sample is collected in a modulator, and is then transferred into the second column where secondary separation occurs. The two dimensional chromatogram has a greater peak capacity that than of one dimensional, so is much more accommodating to complex mixtures. Frysinger and Gaines[43] reported, while GC x GC provides significant separation and grouping of petroleum components, the absolute identification of individual peaks, is time consuming and near impossible if standards do not exist. With the addition of a mass spectrometer in the third dimension (GC x GC-MS) the ability to identify minor components within petroleum products is significantly increased[44].

2.1.3   High pressure liquid chromatography (HPLC)

HPLC involves forcing a liquid mobile phase through a column packed with stationary phase at high pressure, a schematic of a HPLC system is present (Figure 19).
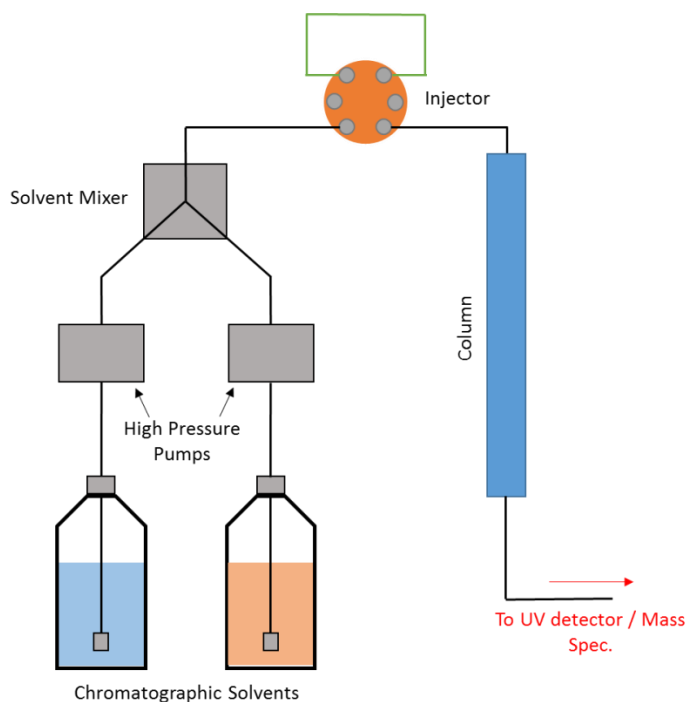
Figure 19 – Schematic of HPLC system

The mobile phase is generally a mixture of solvents, (*e.g.* water/methanol), the solvent composition alters the polarity of mobile phase and plays a major role in the separation process. Separation by HPLC is generally achieved through adjusting the ratio of solvents in the mobile phase over the course of a chromatograph run, giving the mobile phase different characteristics at different points.

The column is packed with silica beads, to which stationary phases may be chemically bonded (

Figure 20).

Silica Surface to which stationary phases may be bonded
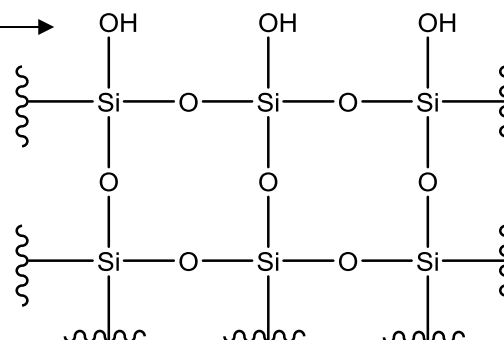
Figure 20 – Structure of silica support material within a chromatographic column

Depending on the relative polarity of the mobile and stationary phases, there are two different variants of HPLC, normal phase and reversed phase.

2.1.3.1   Normal phase liquid chromatography

Normal phase HPLC[45], involves the use of a non-polar solvent such as hexane and a relatively more polar stationary phase. Typical stationary phases include bare silica and bonded stationary phases, *e.g.* amino and cyano (Figure 21).
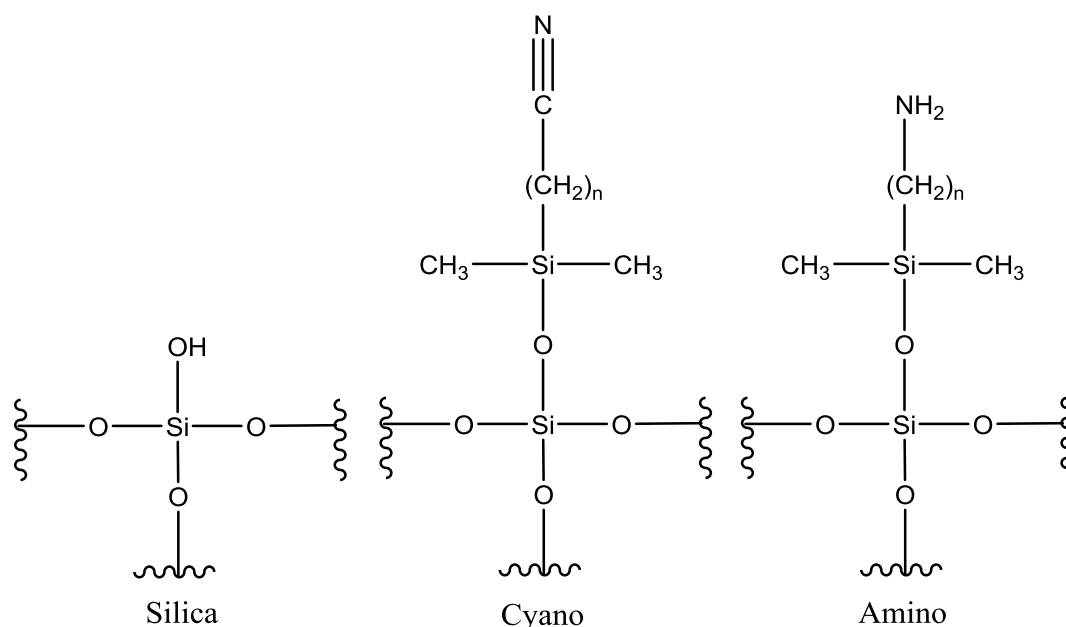
Figure 21 – Structures of three normal phase stationary phases

Retention in normal phase chromatography is achieved *via* polar adsorption of solvent or analyte molecules to the stationary phase. Solvent molecules are adsorbed to the stationary phase, and if an analyte contains a sufficiently polar functional group, it is possible for the analyte molecule to displace the solvent molecule and gain retention. The analyte molecule will then be displaced from the stationary phase *via* mass action (an effect whereby a more concentrated species may displace a less concentrated species), causing it to elute from the column. In normal phase chromatography, polar analytes within the mixture remain on the column longer, thus have an increased retention time when compared to non-polar components.

Hydrocarbon determination for petroleum mixtures is usually undertaken using normal phase HPLC, this is due to the good solubility of the gasoline components within the saturated hydrocarbon solvents normally used.

2.1.3.2   Reversed phase liquid chromatography

Reversed phase chromatography utilises a relatively polar solvent when compared to the stationary phase. The bare silica stationary phase is modified to become non-polar by adding long hydrocarbon chains to the surface of the silica support material *e.g.* C18 and C8 (Figure 22).
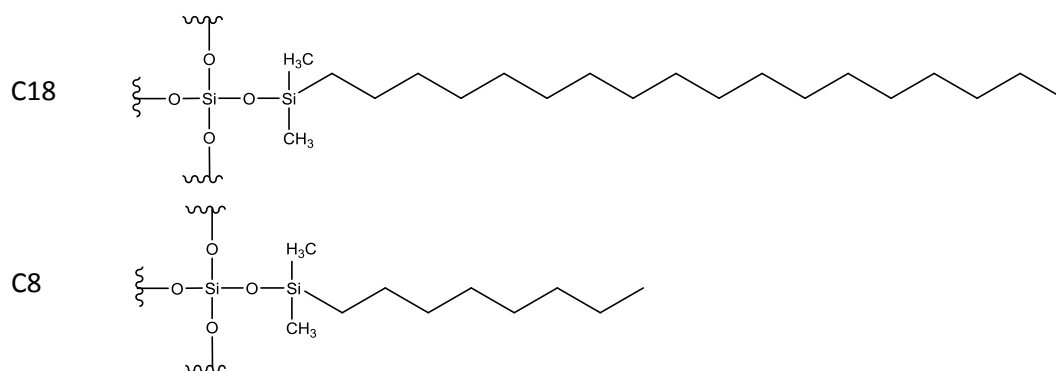
Figure 22 – C18 and C8 column used in reversed phase chromatography

The mobile phase typically consists of water and an organic modifier (*i.e.* methanol), this organic modifier lowers the polarity of the mobile phase, altering the retention time of analytes.

Retention in reversed phase chromatography is governed by the degree an analyte is partitioned into the stationary phase. The water content of the mobile phase forces non-polar analytes out of the mobile phase onto the non-polar stationary phase, as the presence of non-polar analytes interferes with the hydrogen bonding between the water molecules. The analytes molecules will reside in the stationary phase until they partition back into the mobile phase and then elute from the column. Thus non-polar components within the mixture have an increase retention time when compared to the polar constituent.

2.1.3.3   Ultra-high pressure liquid chromatography (UHPLC)

Efforts to increase the efficiency (and hence a reduction of analysis time) of HPLC separation has led to the development of ultra-high pressure liquid chromatography (UHPLC). UHPLC utilises smaller stationary phase particle sizes (sub 2 μm) and a narrower size distribution. The increase in surface area achieved with the use of smaller particles increases the efficiency of the separation. Although, higher pressures are required to force the mobile phase through the stationary phase due to increased density of the packed bed when using the smaller particle sizes.

2.1.3.4   Liquid chromatography and gasoline

In general liquid chromatography has a much lower resolving power than that of GC in the separation of complex hydrocarbon mixtures, therefore, it is employed to separate mixtures on compound class or type, rather than individual isomers[46]. HPLC is useful for higher boiling point and thermally labile compounds that cannot be analysed by GC. Interfacing with an ESI-MS ionisation source allows soft ionisation and detection of polar components with gasoline, previously unattainable by GC, although the aqueous nature of reversed phase is incompatible with the organic nature of gasoline.

2.1.4   Ultra-high pressure supercritical fluid chromatography (UHPSFC)

UHPSFC can be considered as a form of normal phase chromatography, which is used for the analysis of low to moderate molecular weight compounds. The principle of operation is similar to that of HPLC, although UHPSFC utilises supercritical CO_2 or a similar supercritical fluid as the mobile phase.

A supercritical fluid is a substance above its critical temperature and critical pressure, this is known as the critical point. Above this point distinct liquid and gas phases do not exist, this is illustrated in the phase diagram for CO_2 (Figure 23).
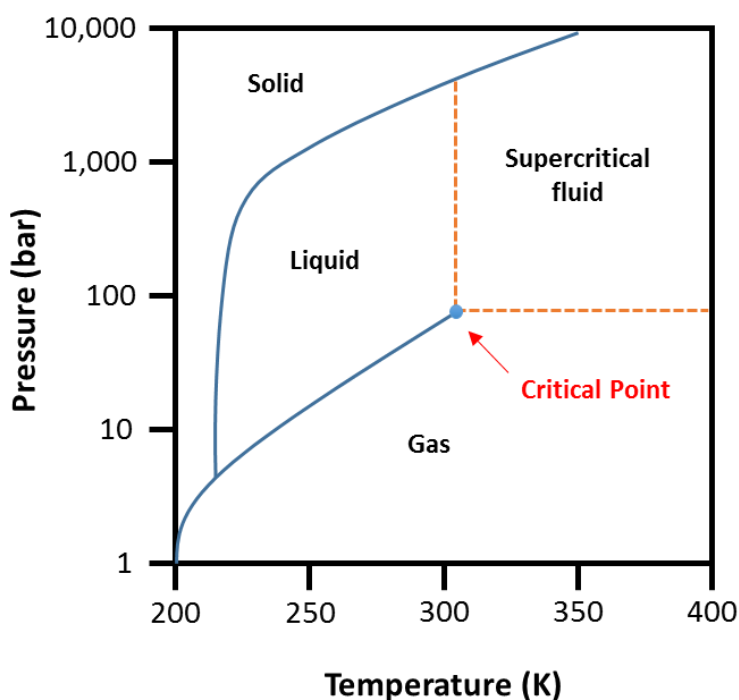
Figure 23 - Phase diagram for CO_2

The properties of a supercritical fluid are between that of a liquid and a gas, providing the dissolving power of liquids, but the diffusivities of gases, placing UHPSFC as a technique between HPLC and GC. Although the separating power of GC is superior to that of SFC, the resolution achievable by SFC is comparable to UHPLC[47].

CO_2 is a good choice as the mobile phase in the analysis of thermally labile compounds due to its low critical conditions (31.3°C and 72.8 atm.). Although due to the low polarity of CO_2 it is unable to elute polar compounds, modifiers (co-solvents) can be used to increase the polarity of the mobile phase, methanol is the most commonly used[48].

The use of SFC for the analysis of gasoline is particularly useful as it is compatible with electrospray ionisation mass spectrometry, allowing the detection of polar compounds within the gasoline matrix, previously unseen by gas chromatographic methods. This method is advantageous to that of UHPLC due to gasoline's increased solubility in supercritical CO_2 compared to the mobile phases of UHPLC.

2.2   Mass spectrometry

Mass spectrometry (MS) is one of the most widely used analytical techniques. It allows the identification of compounds by measuring the mass to charge ratio and the abundance of gas phase ions.
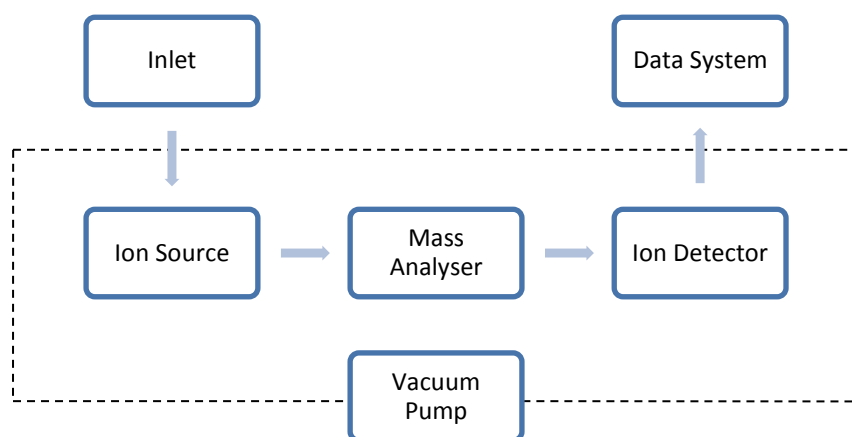
Figure 24 – Schematic of mass spectrometer

Mass spectrometers can be divided into three main fundamental parts, the ion source, the mass analyser and the detector (Figure 24). Samples are introduced to the mass spectrometer *via* the inlet into the ionisation source of the instrument. Here the sample molecules are ionised into positive or negative gas phase ions, these ions are then extracted into the mass analyser, where they are separated by their mass to charge ratios (*m/z*), provided they are present in a gaseous form, and carry a net charge. Once separated the ions are then detected, and a signal is sent to a data system where the *m/z* and relative abundance for each ion are collated and presented in the form of a mass spectrum.

2.2.1   Ionisation

Mass spectrometers use magnetic and electrical fields to direct and detect charged particles within a vacuum. Therefore, for a sample to be analysed it must carry a charge, *i.e.* it must be an ion. Ionisation is the process that yields an ion from an atom or molecule. Additionally, these ions must be introduced to the mass spectrometers vacuum in the gas phase, this can be achieved by heating the sample (*i.e.* electron ionisation, chemical ionisation and atmospheric pressure ionisation), although many analytes can decompose on heating. Or by desolvation of ions within a liquid (i.e. electrospray ionisation).

A variety of ionisation techniques are used in mass spectrometry. The selection of ionisation technique is dictated by the physicochemical parameters of the analyte of interest, the type of information required from the analysis and, to a degree, the interfacing with the any chromatography or sample introduction method.

Ionisation methods can be very energetic, inducing extensive fragmentation, other techniques are softer, and typically produce very few fragment ions, with only the ions of the molecular species.

2.2.1.1   Electron ionisation (EI)

Electron ionisation is a highly energetic form of ionisation, producing extensive fragmentation of the ions produced, with the absence of the molecular ion being commonplace. EI is only suitable for gas phase molecules, thus its use is limited to those compounds that are volatile and thermally stable.
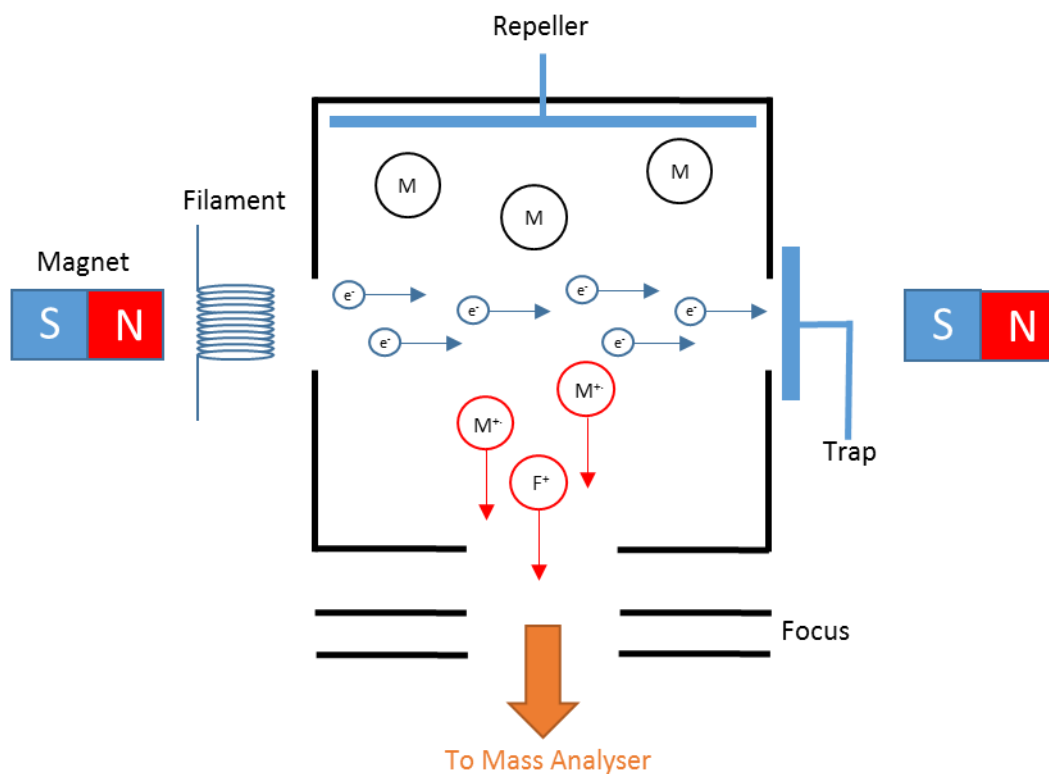
Figure 25 – Electron ionisation source

The process of electron ionisation involves the interaction of the gaseous sample with an electron beam. A tungsten or rhenium wire filament is heated to a temperature where it produces free electrons, these electrons are accelerated towards the anode (trap) to an energy of 70 eV. A magnetic field is used to keep the electron beam focussed across the ion source and onto the electron trap (Figure 25). The sample is introduced perpendicular to the beam of electrons, this allows the close passage of the highly energetic electrons with the neutral sample molecules, causes large fluctuations in the electric field of the sample molecules and induces ionisation (by expulsion of an electron) and fragmentation. The resulting radical cations are directed towards the mass analysers by a repeller electrode.
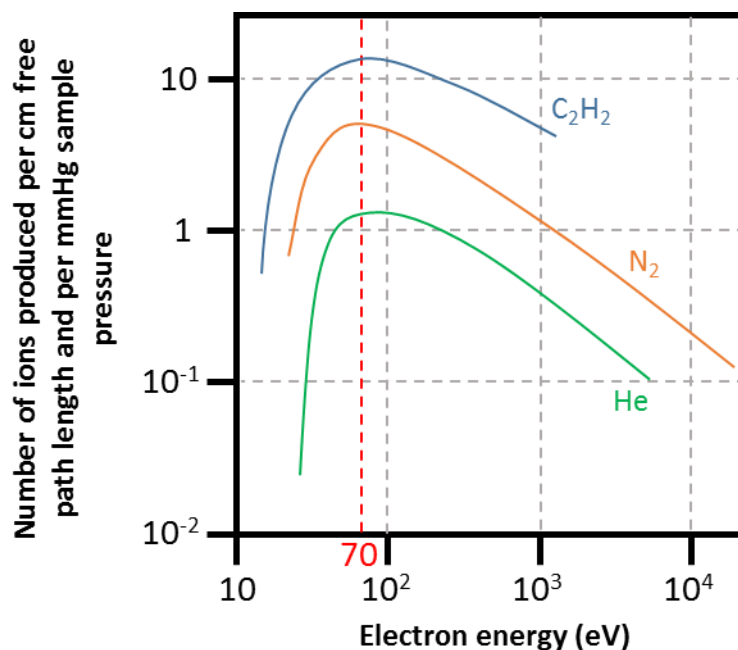
Figure 26 – Ion yield as a function of electron energy[49]

Figure 26 displays the typical curve observed of the ion yield obtained when acceleration potential of the electrons is varied, a maximum appears around 70 eV[50]. Hoffman and Stroobant[49] provide an explanation this phenomenon, with the use of the de Broglie wavelength equation (Equation 8).

Equation 8

$$\lambda = \frac{h}{mv}$$

Where λ is the de Broglie wavelength (in m), h is Planck's constant, m is the mass of the electron (in kg) and v is the velocity of the electron (in ms^{-1}).

This wavelength is 2.7 Å for a kinetic energy of 20 eV and 1.4 Å for a kinetic energy of 70 eV. When this wavelength is close that of the bond lengths in a molecule, the bond becomes complex. If one of the frequencies has an energy corresponding to a transition in the molecule, an energy transfer can occur, allowing the molecule to enter various excited states. When there is enough energy, an electron can be expelled, ionising the molecule.

At lower potentials the energy is lower that the molecules ionisation energy, and at higher potentials the wavelength becomes too small, and molecules become transparent to the electrons.

The primary reason for using an electron energy of 70 eV, is that the greatest ion yield is achieved. Typically ~10 eV is enough to ionise most organic molecules, the remaining energy induces

37

fragmentation within the molecules, providing invaluable structural information about the molecule, although a molecular ion may not be seen. If a reduction in fragmentation is required, the electron energy can be reduced, although this will also reduce the ion yield (Figure 26). Another advantage of using a standard of 70 eV allows reproducible mass spectra for comparison and library matching.

The ionisation of the sample molecule to a radical cation is given by Equation 9, the ionisation process provides excess energy above that required to ionise the molecule. The remaining energy can break bonds within the molecule resulting in fragmentation. The radical cations can fragment in two ways, by elimination of a neutral radical Equation 10 or by elimination of an even electron molecule Equation 11.

Equation 9: $$M + e^- \rightarrow M^{+\cdot} + 2e^-$$

Equation 10: $$M^{+\cdot} \rightarrow A^+ + B^\cdot$$

Equation 11: $$M^{+\cdot} \rightarrow C^{+\cdot} + D$$

2.2.1.2   Chemical ionisation (CI)

Chemical ionisation uses a similar source to that of electron ionisation. Analyte ions are produced by colliding the analyte molecule with ions of a reagent gas. A 'softer', less energetic form of ionisation is achieved, resulting in reduced fragmentation of the analyte and a spectrum in which the molecular species can be easily recognised, thus is complementary to electron ionisation.

A reagent gas is pumped into the ionisation source to maintain a pressure of approximately 0.60 mbar[49]. The reagent gas is first ionised by electron ionisation, to yield reagent gas ions (Equation 12).These initial ions further undergo reactions with the neutral reagent gas molecules, producing the ionisation plasma (Equation 13).

Equation 12: $$NH_3 + e^- \rightarrow NH_3^{+\cdot} + 2e^-$$

Equation 13: $$NH_3^{+\cdot} + NH_3 \rightarrow NH_4^+ + NH_2^{\cdot}$$

When the sample is introduced, the reagent gas ions collide with the sample, to produce protonated molecules (Equation 14) and adduct ions (Equation 15).

Equation 14: $$NH_4^+ + M \rightarrow NH_3 + [M + H]^+$$

Equation 15: $$NH_4^+ + M \rightarrow [M + NH_4]^+$$

The partial pressure of the sample gas is small compared to that of the reagent gas (10^3-10^4 fold excess reagent gas), this effectively shields the sample and prevents the ionisation of the sample by electron ionisation[51]. Other reagent gases include methane and isobutane.

An analyte must be volatile and thermally stable to ionise by CI. The analytes must also have a greater proton affinity than the reagent gas ions for proton transfer to take place.

2.2.1.3   Electrospray ionisation (ESI)

ESI is an ionisation process that involves the conversion of condensed-phase species into gas phase ions[52][53]. There are three major steps in this process: (a) production of charged droplets in the ESI capillary tip; (b) the shrinkage of the charged droplets due to solvent evaporation and repeated charge induced droplet disintegrations leading ultimately to highly charged droplets capable of producing gas phase ions; (c) the actual mechanism by which gas phase ions are produced from these droplets[54]. All three of these stages occur under atmospheric pressure, and therefore ESI is a form of atmospheric pressure ionisation.
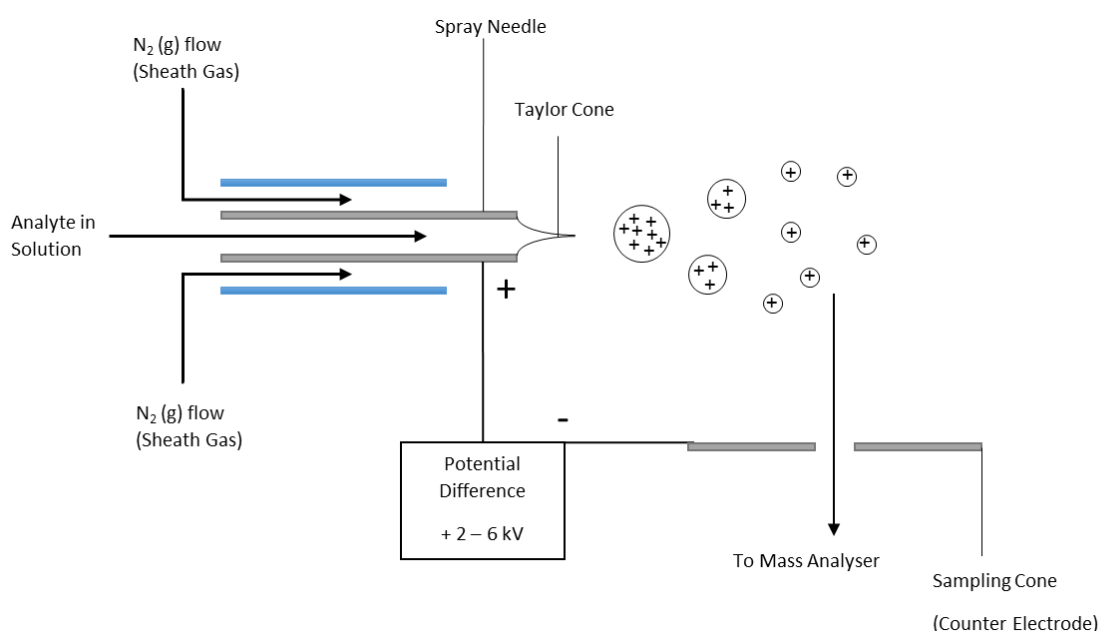
Figure 27 – Schematic of electrospray source

ESI is produced by applying a strong electric field, to a liquid flowing through a capillary under atmospheric pressure. A potential difference of + 2 – 6 kV is applied between the capillary and a counter electrode (Figure 27), located 1 – 3 cm from the capillary, achieving a field strength of approximately 10^6 V m^{-1} [54].

This strong electric field causes positive ions within the solution to congregate at the liquid surface of the solvent, located at the end of the capillary, and the negative ions to move away from the meniscus. The meniscus will then begin to distort, due to the polarisation, into a cone pointing towards the anode. This cone is known as the Taylor cone (Figure 27)[54][55]. If the applied

electric field is great enough, the tip of the cone becomes unstable and can breaks causing the dispersion of the sample solution into an aerosol of highly charged electrospray droplets.

The use of nitrogen as a sheath gas, injected coaxially to the capillary, results in better nebulisation and aids in directing the spray towards the mass spectrometer. This is pneumatically-assisted electrospray ionisation, most often referred to as electrospray ionisation.

The initial droplets expelled from the Taylor cone have a radii in the micro-meter range, each droplets is positively charge due to the abundance of excess positive ions. Protons are often the net contributor to the droplet charge, partly because many analyte solutions are acidic, but mainly from the generation of protons at the metal/solution interface inside the metal capillary (Equation 16)[52, 56].

Equation 16: $$2 H_2O \rightarrow 4 H^+ + 4 e^- + O_2$$

The droplets undergo rapid solvent evaporation (aided by heating), the charge density on the shrinking droplets increases until the surface tension is balanced by Columbic repulsion, this point is known as the Rayleigh limit. Droplets at the Rayleigh limit produce even smaller droplets by fission and solvent evaporation, with a radii of a few nanometres. From these droplets gas phase ions are produced for detection[52].

The process by which gas phase ions are created is still in debate and remains an active area of research[57], and two models have been proposed, the ion evaporation model (IEM)[58] and the charge residue model (CRM)[59].

The ion evaporation model was initially proposed by Iribarne and Thompson[58], to explain the production of atomic ions from charged droplets in a spray atomiser. In this model the droplets shrink by evaporation until the field strength at the droplet surface is sufficiently large, that the solvated ions can be ejected from the droplet. The energy gain in the strong electric field, compensates for the required energy to enlarge the droplet when the ion is expelled[60] (Figure 28).
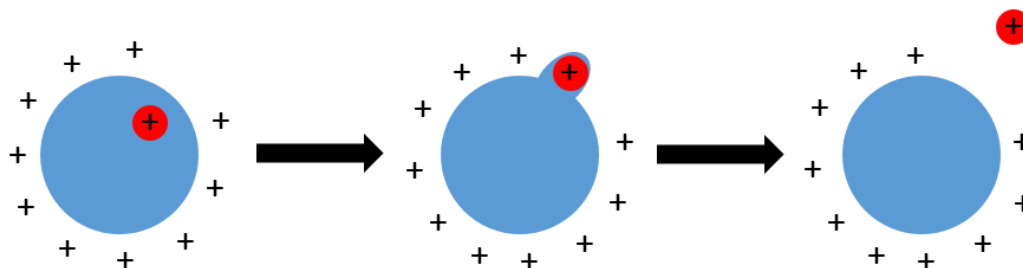
Figure 28 – Summary of the ion evaporation model, achieving gas phase ions from an ESI droplet

The charge residue model was initially proposed by Dole *et al.*[59], it proposes that the electrospray droplets undergo evaporation and disintegration, leading to many smaller droplets. The final droplets will contain no more than one analyte molecule, the remaining solvent evaporates leaving the analyte molecule with the charges it carried (Figure 29).
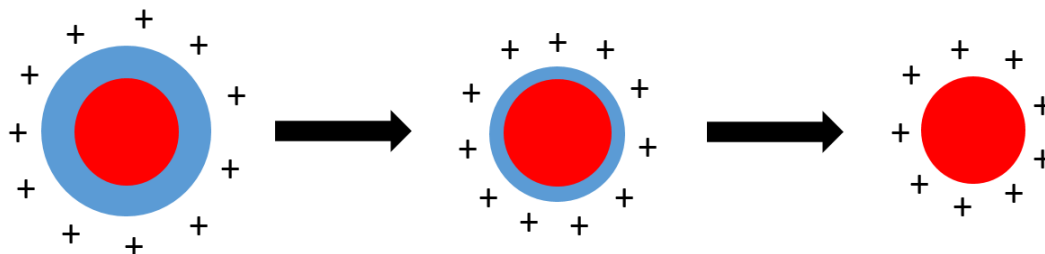
Figure 29 – Summary of charge residue model, achieving gas phase ions from an ESI droplet

ESI is another example of a 'soft' ionisation technique with little fragmentation, typically producing a protonated molecule represented by $[M + zH]^{z+}$ where *z* is the number of protons. Both singly charge and multiply charge ions are commonplace[52].

Adduct ions can also be formed: cationised molecules, such as $[M + Na]^{+}$ $[M + NH_4]^{+}$; and anionised molecules such as $[M + Cl]^{-}$.

ESI is typically suited to molecules with medium to strong polarity, but fails to give good ionisation yields for analytes of low polarity[61]. Petroleum contains both non-polar compounds and polar compounds, typically 90% and 10% respectively[62], Electrospray ionisation has been demonstrated to successfully ionise the polar hydrocarbons in gasoline (approximately 10%), but for the remaining non-polar fraction is undetected, and therefore invisible in the mass spectrum.

Although, this is a small fraction of the components that make up the mixture, they are typically additives or active compounds containing nitrogen, oxygen and sulfur which can be problematic with respect to fouling and deposition[18], thus are of great interest.

A major benefit of ESI as an ionisation method, is the ability to interface with chromatography, for online separation of complex mixtures prior to MS, specifically HPLC and SFC.

Zhan and Fenn[63] reported the successful use of ESI-MS on gasoline samples, allowing identification of the polar compounds within the mixture. Rostad[64] described the process of screening gasoline samples for polar compounds using an electrospray ionisation source in negative ion mode, interfaced to HPLC. Negative ion ESI was shown to produce simple spectra, allowing the identification of a range of alkylated phenols within the gasoline. Haddad *et al.*[65]

observed a series of alkyl pyridines within gasoline using positive ion ESI. Carraze *et al.* described the detection of some polymeric fuel additives by positive ion ESI[66].

2.2.1.4   Atmospheric pressure chemical ionisation (APCI)

Atmospheric pressure chemical ionisation (APCI) is similar to that of chemical ionisation previously described, but occurs under atmospheric pressure. In APCI, primary ions are produced by corona discharges on a solvent spray.

The analyte is present within the capillary as a solution (Figure 30). As the solution emerges from the capillary, it is surrounded by a flow of nitrogen gas. Both the eluent and nitrogen gas is heated, causing the eluent to rapidly evaporate producing a fine aerosol. A corona electrode is placed within the region of the aerosol, the discharge of the high potential applied to the electrode (2 – 4 kV) produces electrons, which in turn ionise the gas phase molecules within the aerosol.
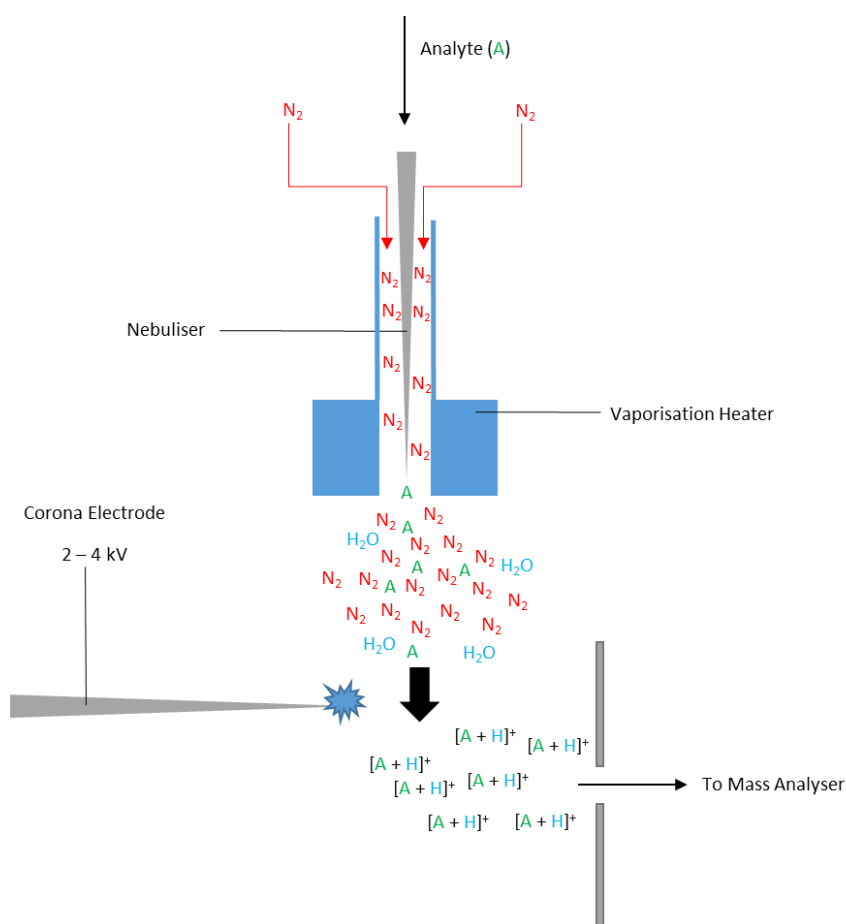
Figure 30 – Schematic of APCI source

In a nitrogen atmosphere, the electrons emitted from the discharge, ionise the N_2 molecules within the source by electron ionisation to produce primary ions of $N_2^{+\cdot}$ and $N_4^{+\cdot}$. These primary ions then collide with vaporised solvent molecules producing a cascade of secondary ions,

resulting in cluster ions. The following equations display the production of these cluster ions, assuming nitrogen is used as the nebuliser gas and water vapour is present within the source.

Equation 17 $\qquad N_2 + e^- \rightarrow N_2^{+\cdot} + 2e^-$

Equation 18 $\qquad N_2^{+\cdot} + 2N_2 \rightarrow N_4^{+\cdot} + N_2$

Equation 19 $\qquad N_4^{+\cdot} + H_2O \rightarrow H_2O^{+\cdot} + 2N_2$

Equation 20 $\qquad H_2O^{+\cdot} + H_2O \rightarrow H_3O^+ + OH^\cdot$

Equation 21 $\qquad H_3O^+ + H_2O + N_2 \rightarrow H^+(H_2O)_2 + N_2$

Equation 22 $\qquad H^+(H_2O)_{n-1} + H_2O + N_2 \rightarrow H^+(H_2O)_n + N_2$
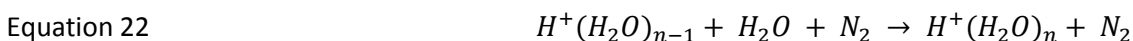
The protonated analyte molecules are formed by gas-phase reactions between the cluster ions and the analyte molecules. As the source is at atmospheric pressure, there is a high frequency of collisions, resulting in a high ionisation efficiency.

It is important to prevent solvent cluster ions from entering the mass analyser as this will increase the noise within the mass spectrum. This can be achieved with a counter-flow of nitrogen gas, a heated capillary or in source collision induced dissociation (CID) of the clusters prior to mass analysis.

APCI is typically suited to compounds below a molecular weight of 1000 gmol^{-1}, which are of medium to low polarity. Analytes should also display some degree of volatility and should be thermally stable, as heating is required for nebulisation.

2.2.1.5 Atmospheric pressure photo-ionisation (APPI)

Initially developed by Robb *et al.*[67] Atmospheric pressure photoionisation (APPI) is a form of atmospheric ionisation whereby ions are formed by the detachment of electrons induced by photons emitted from a lamp within the source.
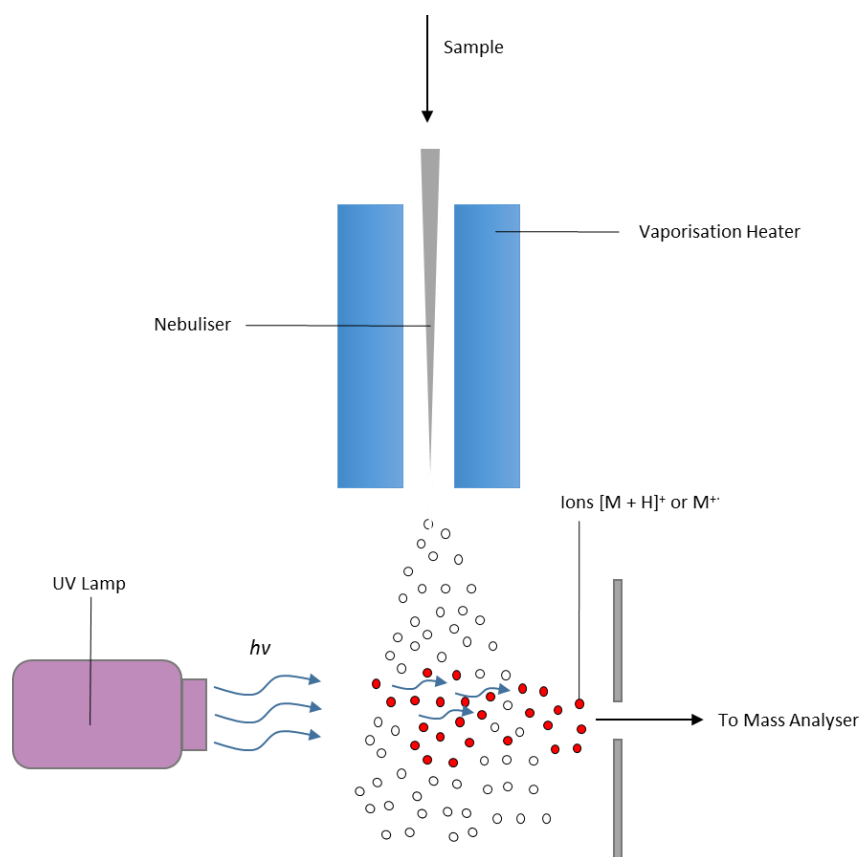
Figure 31 – Schematic of APPI source

The sample is introduced to the APPI source (Figure 31) through the nebuliser, which atomises the sample into a fine mist, the desolvation and atomisation of the sample is aided by the vaporisation heater. The sample is sprayed across the source towards the mass analyser entrance.

UV radiation with energy *hv,* produced from a krypton lamp (10.6 eV), passes through the atomised sample, these energetic photos interact with the analyte molecules producing photoions which are then transferred to the mass analyser.

As in ESI, two ionisation possibility are available, APPI: positive and negative. Typically in positive ion APPI, the predominate ion of $[M + H]^+$ is observed, although in some instances, which seem to correlate with molecules of low proton affinity, the $M^{+\cdot}$ ion is observed[68], this is explained v*ia* the two distinct ionisation pathways, direct analyte photoionisation, and dopant-assisted ionisation.

2.2.1.5.1   Direct photoionisation

Direct photoionisation produces molecular radical ions, this is achieved with the direct absorption of a photon by the analyte molecule, followed by the ejection of an electron from the molecule. This is possible if the irradiating photon energy (*hv*) exceeds that of the ionisation potential of the molecule[68]. This is displayed in Equation 23.

Equation 23 – Direct photoionisation of analyte molecule

$$M + hv \rightarrow M^* \rightarrow M^{+\cdot} + e^-$$
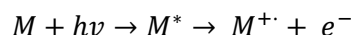
The statistical likelihood of direct ionisation of the analyte molecules is very low, in part because of competing reactions between the photons and the solvent, *e.g.* photoexcitation, photo dissociation and radiative decay of the excited state[69]. If the ionisation potential (IP) of the analyte is greater that than of the emitted photo energy, direct ionisation will not take place. Although most organic molecules have an ionisation potential in the range of $7 - 10$ eV[67], within the range of a krypton lamp.

2.2.1.5.2 Dopant-assisted photoionisation

If the IP of an analyte is greater than the energy of the photon, dopant assisted ionisation is utilised. This involves the addition of an excess of dopant molecules that are ionised by the photons (Equation 24). If the dopant is selected such that its photo-ions (an ion produced through photoionisation) have a relatively high recombination energy, or a low proton affinity, then the dopant photo-ions may react by charge exchange (Equation 25) or proton transfer (Equation 26) with the species present in the ionisation region. Because the ionisation region is at atmospheric pressure, the high collision rate will ensure that the charge on the photo-ions is effectively transferred to the analyte[67].

Equation 24 – Direct photoionisation of dopant molecule

$$D + hv \rightarrow D^{+\cdot} + e^-$$
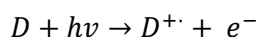
Equation 25 – Charge transfer from dopant ion to analyte molecule

$$D^{+\cdot} + M \rightarrow D + M^{+\cdot}$$
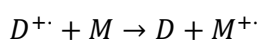
Equation 26 – Proton transfer from dopant ion to analyte molecule

$$D^{+\cdot} + M \rightarrow [M + H]^+ + [D - H]^{\cdot}$$
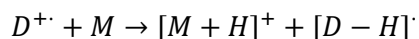
APPI is typically suited to compounds of low to no polarity, which do not ionise by electrospray, providing complementary data to ESI analysis for complex mixture containing compounds of different structure and polarity.

2.2.2   Mass analysers

The purpose of a mass analyser is to separate ions based on their mass to charge ratio (*m/z*) and output them to a detector. Several different mass analysers have been developed, all separating ions on their *m/z*, using static or dynamic electric or magnetic fields, most of the differences between these mass analysers is how these fields are applied to achieve the desired separation. Each analyser has its own characteristics, benefits and limitations[49].

2.2.2.1   Quadrupole mass analyser

The quadrupole mass analyser consists of four parallel hyperbolic shaped rods (although cylindrical rods are typically used as they are cheaper to manufacture), made of metal or ceramic coated in metal. The filtering aspect of the quadrupole is achieved by placing a constant voltage (*U*) and an oscillating voltage (*V*) on the rods, where ω is the angular frequency (in radians per second = 2 π*v* where *v* is the frequency of an RF field) (Figure 32*)*.
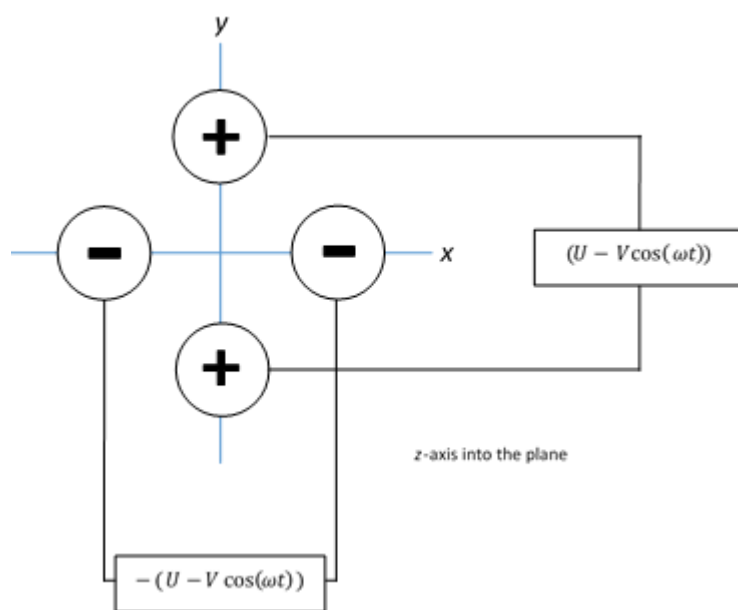
Figure 32 – Schematic of quadrupole, viewed down z-axis.

If considered qualitatively, each pair of rods can be considered a separate mass filter, the rods with the constant positive voltage permitting heavier ions to have a stable trajectory through the quadrupole and the negative rods permitting the lighter ions to have a stable trajectory.

If only rods on the *y*-axis are considered. The oscillating potential (*V*) applied to the rods spends half of the cycle at a positive potential and the other half at a negative potential. When the potential is positive, the positive ions are focused on the centre line of the quadrupole. When the potential is negative, the positive ions are accelerated towards the rods, if the ions make contact with the rods they become neutralised and removed from the analyser *via* the vacuum pump. The

acceleration and trajectory of the ion is governed by multiple physical factors including the frequency of the oscillations, the position of the ion within the quadrupole and the *m/z* of the ion.

As a positive ion travels down the *z*-axis the positive constant potential (*U*) repels the positive ion, effectively holding it on a stable trajectory through the quadrupole. If the ion is heavy and the frequency of the oscillating potential is rapid, the heavy ion tends to only respond to the average potential applied, which is the constant potential (*U*) as the average of *V* is 0. Therefore the periods when the oscillating potential is negative will have little effect on the trajectory of heavy ions, keeping them on the centre line. In contrast, light ions may be affected greatly by the oscillating potential, light ions experience a larger acceleration when compared to heavy ions and during the negative potential oscillation, they may experience a large enough acceleration to collide with the rods, neutralising them. Therefore, below a lower limit of *m/z*, ions will be filtered out, with ions above this limiting continuing unimpeded, this is the role of the *y*-axis rods in this case (Figure 32).

The *x*-axis rods (Figure 32) in this case have a constant negative potential. Once again the heavy ions tend to respond to the average potential, and therefore in this case, they accelerate towards the rods, causing them to collide and neutralise. The lighter ions are also attracted to the rods, although they experience a greater effect of the oscillating potential, when the potential is positive it causes the ions to be repelled back to the centre of the quadrupole, giving them a stable trajectory. These rods act as a filter, filtering out the high masses[70].

It is only possible for an ion to travel though the quadrupole mass analyser if the ion has a mass in the mass region where both mass filters will permit a stable trajectory. This provides a small window of which ions of a certain mass may pass and be detected. This mass window can be moved by altering the voltages applied to the rods, allowing a scanning function of the quadrupole.

From the equations of movement, the characteristic parameters for an ion in an electric field are given by a and q, resulting in Equation 27 and Equation 28[49].

Equation 27:

$$a_u = \frac{8zeU}{m\omega^2 r_0^2}$$

Equation 28:

$$q_u = \frac{4zeV}{m\omega^2 r_0^2}$$

Where r_0 is the distance from the *z-axis* and *u* represents the *x* or *y* transverse displacement, *e* is the charge on an electron and *m* is mass of an ion.

For a given quadrupole, r_0 and ω are maintained constant, therefore *a* and *q* are proportional to *U/m* and *V/m* respectively.

Stability of ion trajectories in a quadrupole electric field can be represented in an a_u and q_u diagrams.
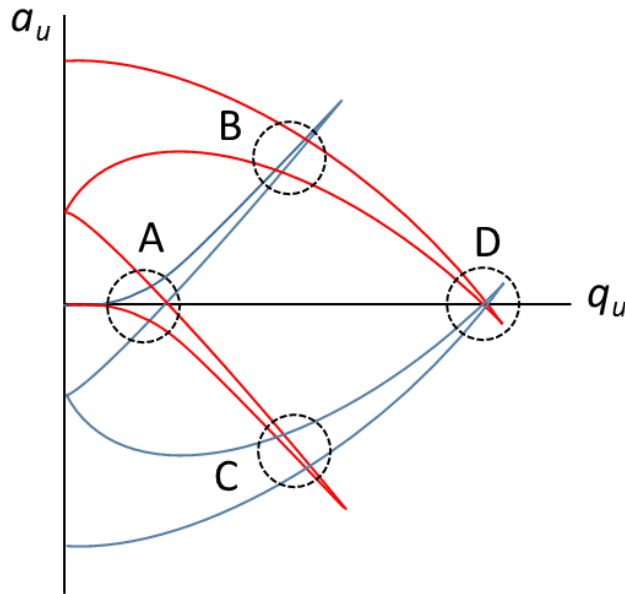
Figure 33 – Stability diagram for an ion along x and y, with the four stability areas labelled A to D[49].

The diagram (Figure 33) is a combination of the stability areas in a_u - q_u space for the individual *x*-axis and *y*-axis. The regions where each plot intersects (A to D) represent areas where an ion of a certain mass will have a stable trajectory in both the *x* and *y axis*.

Typically, quadrupoles are operated in positive area region A (Figure 33), other regions would require very high DC and AC voltages.
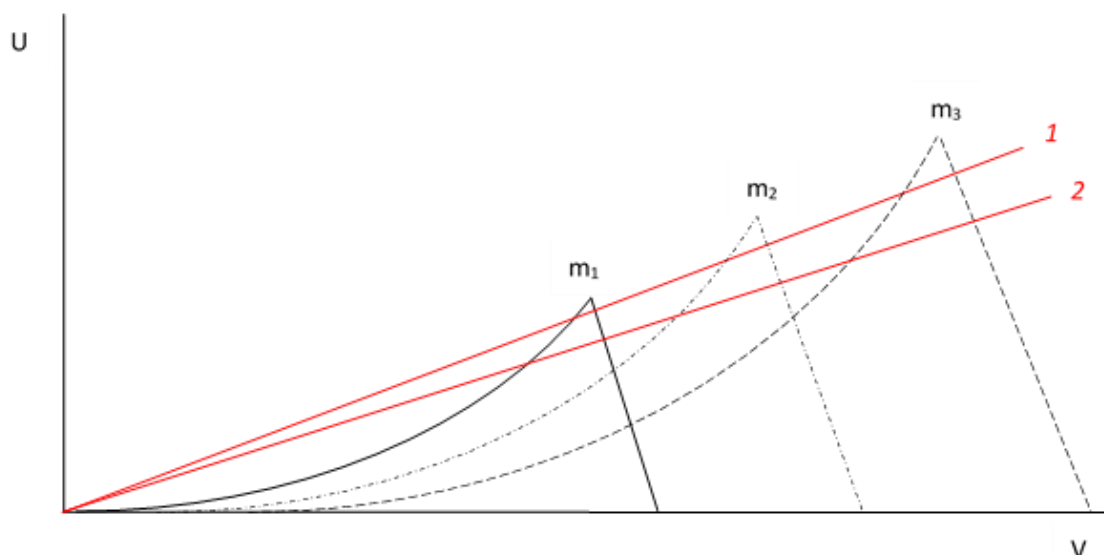
Figure 34 – Stability areas of an ion within a quadrupole as a function of U and V for three ions of different masses ($m_1 < m_2 < m_3$). Two scan lines with a constant U/V ratio (lines 1 and 2) display the effect of increased sensitivity on resolution

Figure 34 displays the stability of ion trajectory in the working region of a typical mass spectrometer (Figure 33, Region A). For each different mass there is a combination of U and V values allowing a stable trajectory of that mass. Areas under the 'triangles' are stable regions, outside the triangles the ion trajectories are unstable.

By scanning along a line, maintaining a constant U/V ratio (Figure 34, line 1) allows the successive detection of the different masses[49], displaying the areas above the line as a mass spectrum. If the gradient of the line is decreased (Figure 34, line 2), the sensitivity of the quadrupole increases, displayed as a greater area above the line, although, the resolution will decrease, displayed as increase in peak width.

Usually, quadrupoles are operated at unit mass resolution and are therefore low-resolution mass analysers.

Until now the quadrupole has been described operating in scan mode, whereby all *m/z* are scanned for between two designated *m/z* values. Quadrupoles can also be operated in selective ion monitoring (SIM) mode, where an increase in sensitivity between 10 and 100-fold can be obtained. The quadrupole is set to only allow ions with a selected *m/z* through, typically 2 to 3 ions. Therefore, the quadrupole spends a greater amount of time permitting a stable trajectory for each mass. This method is particularly useful when the analyte is of low concentration and a known mass.

Chapter 2

2.2.2.2   Fourier transform ion cyclotron resonance (FT-ICR)

An ion in a magnetic field experiences a force that is perpendicular to both the direction of its velocity and the magnetic field, this force is known as the Lorentz force. This causes an ion to travel in a circular orbit that is perpendicular the magnetic field[71]. If the velocity is low and the magnetic field is intense, the radius of the trajectory becomes small, thus an ion can become trapped on a circular trajectory in a magnetic field[49].

The forces acting upon an ion in a magnetic field on a circular trajectory are the centripetal force (Equation 29) and the centrifugal force (Equation 30), where force is F, magnetic field is B, velocity is v, the charge on the ion is q and the radius of the trajectory is r.

Equation 29 – Centripetal force

$$F = qvB$$

Equation 30 – Centrifugal force

$$F' = \frac{mv^2}{r}$$

An ion is on a stabilised trajectory when both the centrifugal and centripetal forces are balanced giving Equation 31.

Equation 31 – Balances centripetal and centrifugal force

$$qB = \frac{mv}{r}$$

The ion completes a circular trajectory of $2\pi r$ with a frequency (f) (Equation 32).

Equation 32 – Angular frequency

$$f = \frac{v}{2\pi r}$$

Angular velocity ω is related to angular frequency by Equation 33.

Equation 33 – Angular Velocity

$$\omega = 2\pi f$$

When f is substituted with Equation 32:

Equation 34

$$\omega = \frac{v}{r}$$

When *v/r* is substituted with Equation 31, angular velocity is only dependant on three physical parameters the strength of the magnetic field *B*, the mass of an ion *m* and the charge on an ion *q* (Equation 35) and are thus independent of the velocity. However the radius of the trajectory increases for a given ion, in proportion to the velocity[49].

Equation 35

$$\omega = \frac{qB}{m}$$

Thus the frequencies of an ion is related to the mass to charge when in a constant magnetic field.

In practice, the circular trajectory of ions is achieved in an open ended cylindrical cell (Figure 35), where the magnetic field (produced by a superconducting magnet) aligns with the principle axis of the cylinder.
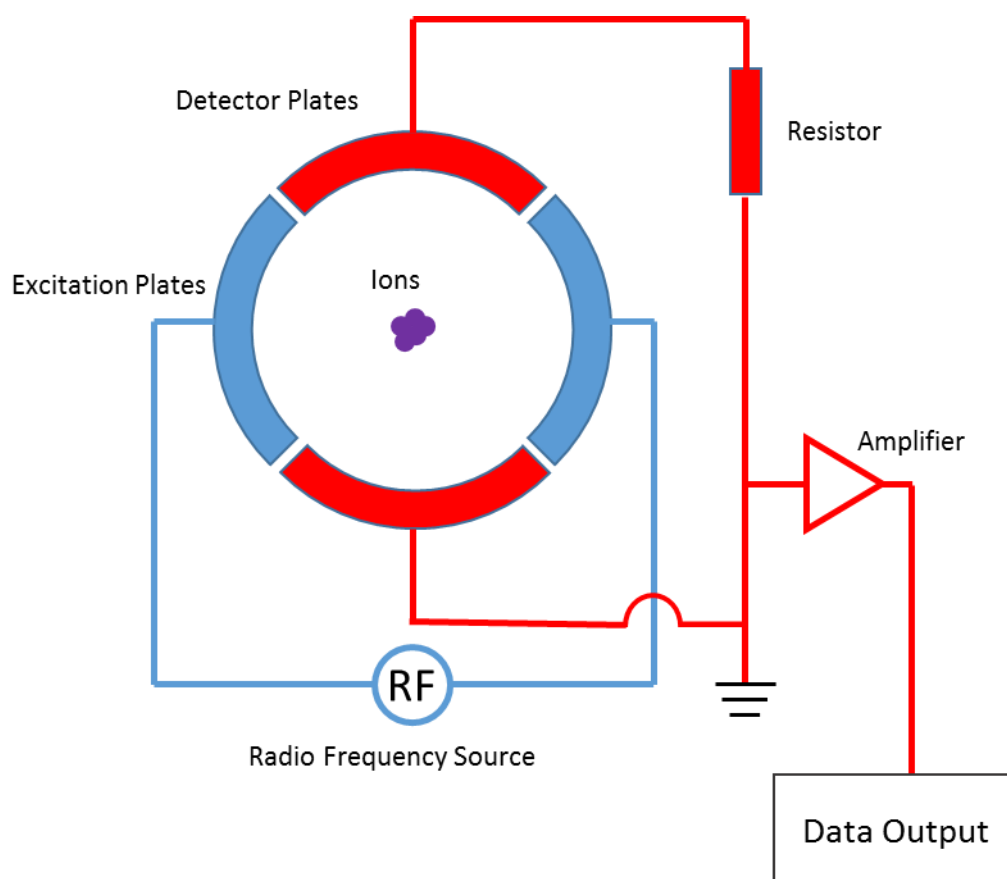
Figure 35 – FT-ICR MS analyser cell schematic, viewed down the principle axis of the cylinder

A trapping electrode exists at each end of the cylinder, maintaining the ions within the cell. The cylinder is divided into four paired electrodes, the excitation electrodes and the detector electrodes.

Ions of a specific *m/z* in an ion-cyclotron orbit does not itself produce an electric current for two reasons:

(a) An ion may start its cyclotron motion at any point around the circumference of its orbit. Thus for an group of ions, any charge induced on one detector plate will be balanced by an equal charge induced on the other detector plate (*i.e.* by an ion with opposite phase), so that the net different in charge between two plates is zero[72].

(b) Generally the radius of the orbits are too small to be detected even when all ions are in phase[72].

Therefore the ions must be excited. This is achieved by creating an oscillating radio frequency electric field v*ia* the excitation plates, with a frequency in resonance with that of ions of a specific *m/z.* This causes the oscillating ions to spiral outwards towards the walls of the chamber, this spiralling effect causes the ions to group up, eliminating the cancelling out effect, inducing an alternating current when passing the detector plates, this is known as the imaging current. The image current is proportional to that of the number of orbiting grouped ions.

The cyclotron motion of the ions is circular, although due to the three dimensional field formed from the magnetic field and electric potential, a further motion is experienced by the ions. This motion is known as magnetron motion, and is independent of cyclotron motion, the mass of the ion and its charge, but rather the geometry of the ICR cell. The radius of magnetron motion is usually much smaller than that of the cyclotron motion. The combination of cyclotron and magnetron motions results in a spiral type orbit (Figure 36)[71].
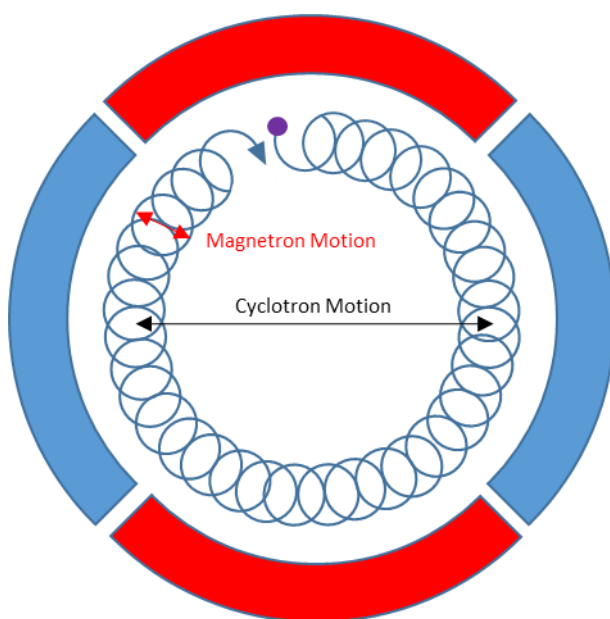
Figure 36 – Ion motion within FT-ICR cell

In the 1950s the principle of ion cyclotron resonance was first incorporated into a mass spectrometer called the "Omegatron", by Sommer *et al.*[73]. This involved irradiating with an electromagnetic wave that had the same frequency as an ion in the cyclotron, transferring energy to the ion, increasing its kinetic energy, which causes and increase in the radius of the trajectory.

The passage of these ions circulating within the cell past the detector plates, induces the image current. In this case only ions of a single mass can only be targeted due to the unique frequency of excitation.

Fourier transform mass spectrometry (FTMS), first described by Comisarow and Marshall in 1974[74], allows the detection of ions of many masses in one scan. The technique involves excitation of all ions present in the cyclotron by rapidly scanning a large frequency range within a times span of about 1 μs[49]. This will cause all the ions with cyclotron frequencies in this frequency range to be excited into large cyclotron orbits of the same radius.

The passage of these packets of ions near the detector plates induces an image current for all of the ions present creating a complex wave, in units of current per time, this is typically known as the time domain. To obtain the *m/z* data, the time domain signal must be converted to a frequency domain v*ia* Fourier transform. This effectively degrades the time domain, into each of its frequency components, which are characteristic of the ions of each *m/z*.

The frequency plot can be mass corrected to obtain the mass spectrum for ions present.

2.2.2.2.1   FT-ICR MS resolution

FT-ICR MS offers ultrahigh mass resolving power (m/Δm$_{50\%}$ > 300,000 at 9.4T in which m is ion mass and Δm$_{50\%}$ is the mass spectral peak full width at half-maximum peak height for ions of 200 < *m/z* < 1000) and mass resolution (m$_2$ – m$_1$ .0.003 Da) for complex mixtures of up to several thousand different elemental compositions[72].

Resolving power in FT-ICR MS can be thought of the number of cyclotron orbits an ion makes during the data acquisition period[75]. The amplitude of the transient signal decays with time as collision between ions and neutrals within the analyser cell destroy the coherence of the ion packet. Thus ultrahigh vacuum is required for FT-ICR MS, typically $10^{-8} - 10^{-10}$ mbar[71].

2.2.2.3   Quadrupole ion trap (QIT)

The principle of a QIT is similar to that of the quadrupole. Although unlike the quadrupole, where ions of a specific *m/z* are permitted a stable trajectory at any one time, within the QIT, ions of many *m/z* values are present together, and are expelled according to *m/z* to form a spectrum. It is

also possible to undertake MS^n experiments within a QIT due to its ability to trap ions within an area of space.

A QIT is formed from three electrodes, a hyperbolic ring electron and two end cap electrodes (Figure 37) producing a three dimensional electrical field, when a RF voltage is applied to the ring electrode and the end cap electrodes are held at ground. One end cap electrode has a single aperture in the centre of the electron, through which ions from the ion source can be gated. The other end cap electrode has several small apertures, through which the ions can be expelled to a detector post storage.
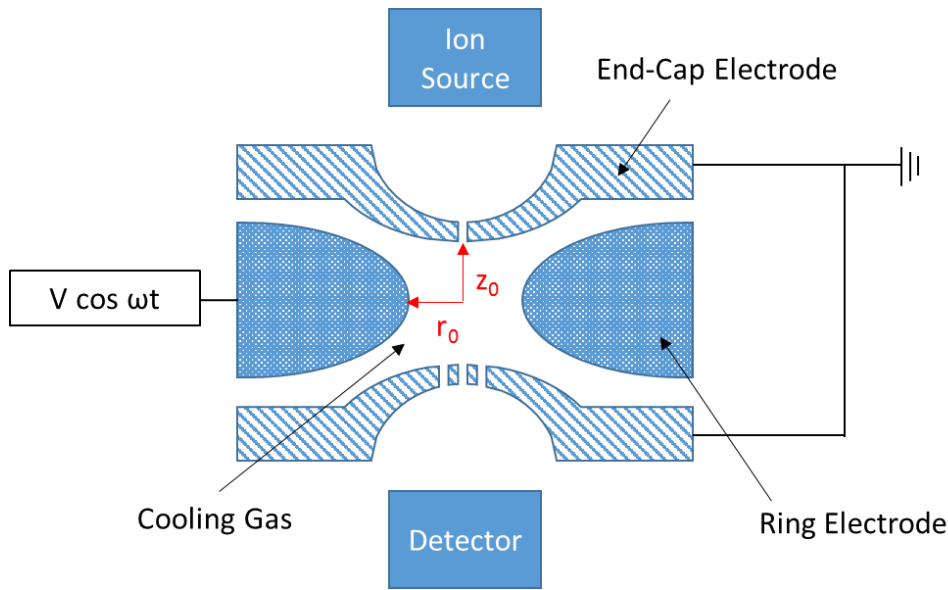
Figure 37 – Cross section schematic of quadrupole ion trap

As with the quadrupole, Mathieu equations can be utilised to identify parameters whereby an ion has a stable trajectory within the trap, *i.e.* not exceeding the trap dimensions (z_0 and r_0 (Figure 37)). Within a quadrupole the trajectory is manipulated in two dimensions, and movement in the z-axis is a result from the momentum of the ion entering the quadrupole. Within an ion trap, stable trajectory must be achieved in three dimensional space. The Mathieu equations for a quadrupole ion trap are presented (Equation 36 and Equation 37).

Equation 36:

$$a_u = a_z = -2a_r = \frac{-16zeU}{m(r_0^2 + 2z_0^2)\omega^2}$$

Equation 37:

$$q_u = q_z = -2q_r = \frac{8zeV}{m(r_0^2 + 2z_0^2)\omega^2}$$

Where r_0 is the radius of the ring electrode, z is the distance from the centre of the trap to the end cap electrode (thus $2z_0$ is the distance between the two end cap electrodes) and u represents either r or z. Where e is the charge on an electron, z is the number of charges on an ion and m is mass of an ion. U is the DC voltage applied and V is the AC voltage, alternating with a radio frequency with an angular frequency of ω.

Solutions to the Mathieu equations will result in either stable or unstable trajectory for an ion. An ion with a stable trajectory will be stored within the trap. Ions with an unstable trajectory will be ejected from the trap, either lost or detected externally. Solutions for a and q in the z and r plane from the Mathieu equations can be plotted, on a Mathieu stability diagram, (Figure 38).
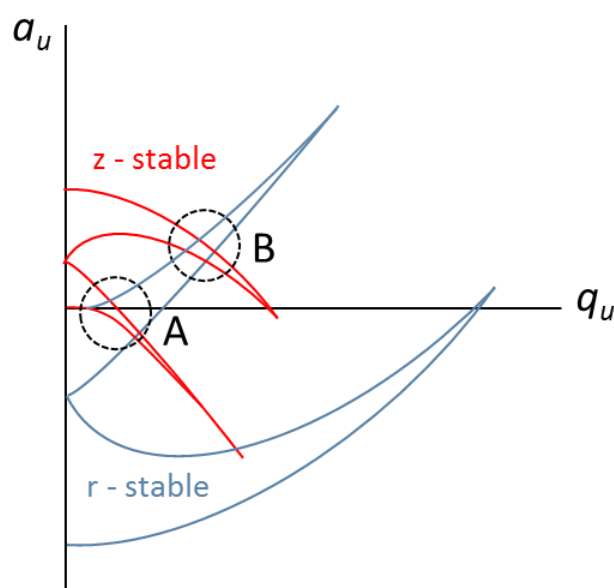
Figure 38 – Mathieu stability diagram for quadrupole ion trap

The boundaries of the diagram represents when an ions trajectory is no longer stable within the confines of the trap. Ions will remain within the trap provided they have a stable trajectory within r and z simultaneously, this is displayed on the diagram (Figure 38) where the r-stable and z-stable areas intersect. In practice region A is used within commercial ion trap mass spectrometers.

Another important parameter is β_u which is closely related to the amplitude and frequency of the oscillations performed by the ions within the ions trap. A value of β_u between that of 0 and 1 is required for an ion to have a stable trajectory. In order for an exact value of β_u to be calculated a continued fraction in terms of a_u and q_u must be used. Although a simpler expression for β_u can be achieved through the Dehmelt approximation[76] (Equation 38).

Equation 38
$$\beta_u = [a_u + (q_u^2/2)]^{1/2}$$

Although this approximation only holds true for $q_r < 0.2$ and $q_u < 0.4$.

Area A from the stability diagram (Figure 38) is enlarged and presented, iso-β are have also been superimposed (Figure 39).
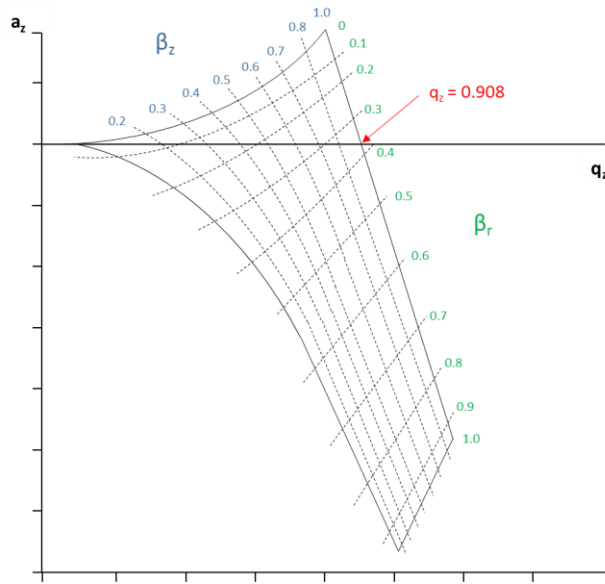
Figure 39 – Enlarged area A of Mathieu stability diagram for quadrupole ion trap with superimposed iso-β lines

As a_u and q_u are proportional to U and V respectively a plot of voltages and stability could also be produced.

2.2.2.3.1   Mass analysis in the quadrupole ion trap

2.2.2.3.1.1   Stability limit ejection

As ions of different m/z values are stored in the ion trap together, they must be scanned out according to their mass for detection. As described previously ion traps operate with a RF voltage to the ring electrode, the frequency of which is constant although the amplitude can be varied. The end cap electrodes are held at ground, although additional RF voltages may be applied at various frequencies and amplitudes.

As no DC voltage is applied (a_u = 0), so only q_u is to be considered (Equation 37). For mono-charged ions with a trap of fixed dimensions and a fixed RF frequency, q_u will increase with increasing V and decreasing m, *i.e.* for a given V, a larger ion will have a smaller q_u value to that of a smaller ion.

By increasing V the q_u for an ion of a given mass will increase. As a_u = 0, once a q_u value of 0.908 of an ion is achieved, β will be equal to 1, and thus the ion will be on its stability limit (Figure 39). Further increases in V will result in an unstable trajectory for an ion, resulting in an ejection of the

ion from the trap. Further increases in V, will result in the sequential ejection of ions of increasing mass.

2.2.2.3.1.2   Resonant excitation

Ions of different masses within the trap subjected to an RF voltage with angular velocity $\omega = 2\pi v$, (where v is the frequency), will not all oscillate at the same frequency due to their inertia. Rather, at a secular frequency f, lower than v and decreasing with increasing masses, this relationship between the RF frequency applied and the secular frequency on an ion is presented in Equation 39.

Equation 39 $$f_{\zeta} = \beta_{\zeta}\, v\, /\, 2$$

As β_{ζ} increases if q_{ζ} increases it is possible to calculate a value of V to be applied for ions of a given mass to oscillate at their secular frequency f [49].

If small supplementary RF voltage at frequency f is applied to the end caps of the trap, *i.e.* along the ζ-axis of the trap, ions with the corresponding mass will resonate and oscillate. This applications of an ion trap can be used in two ways.

i) If the amplitude of the RF voltage frequency is sufficient, the oscillations of the ions will be so large, they will be ejected from the ion trap. Single ions or groups of ions can be removed from the trap, possibly to leave a single ion trapped; this is particularly useful in MS/MS experiments which is discussed in detail later.

ii) Excitation of the ions will increase their kinetic energy; collisions of these energetic ions with the helium cooling gas present within the trap will result in CID fragmentation, also important in MS/MS experiments. As the secular frequency is unique to a specific mass, fragments can only originate from the excited ion, as fragments ions will not oscillated on the precursor ions secular frequency.

It is also important to balance kinetic energy uptake so that ion internal energy may be accumulated incrementally and rapidly so that ejection of both the isolated ion and fragments is prevented [76].

2.2.2.3.2   Space charge effects

An ion trap can only contain a limited amount of ions before the repulsive forces between the ions begin to influence each other. The ion located around the outside of the trap will act as a shield, modifying the effect of the field for the ions within the centre. This can lead to a loss of resolution and shift in mass calibration. Thus it is essential that number of ions within the trap is

considered. Regulation of ions within the trap can be achieved by automatic gain control (AGC). AGC accomplishes this by monitoring of the ion production from the ion source with the use of pre-scans. Thus the number of ions entering the trap can be adjusted during operation by altering the ion accumulation time.

2.2.3 Tandem mass spectrometry (MS/MS)

MS/MS is the acquisition and study of the spectra of the product ions and precursor ions of a selected m/z. In tandem MS, ions are formed in the ion source and separated by m/z within the mass analyser, ions of a chosen m/z can then be isolated, under-go fragmentation and then can be detected, thus providing valuable structural information. This is particularly useful for mixtures of compounds, whereby an individual compound can be isolated and fragmented.

For the MS/MS of the polymeric additives two different forms of tandem MS have been employed, MS/MS in time and MS/MS in space, this was achieved with the use of an 3-D ion trap and quadrupole Fourier transform ion cyclotron resonance mass spectrometer (Q-FT-ICR MS) respectively, each form of instrument has benefits and drawbacks, although are complementary when used in combination.

2.2.3.1 MS/MS in space

In MS/MS in space the different processes are physically separated and distinct, an example of this would be the triple quadrupole mass spectrometer, a simplified schematic of a triple quadrupole mass spectrometer operating in product scan mode is presented (Figure 40).
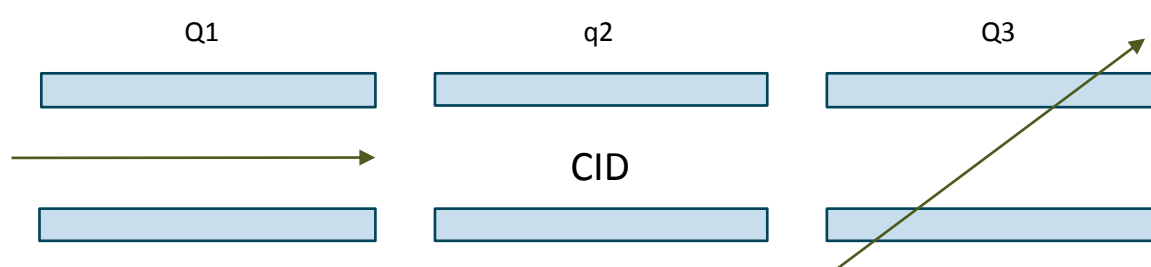
Figure 40 – Schematic of triple quadrupole mass spectrometer

Ions from the ion source are directed ion to quadrupole 1, which only allows the stable trajectory of one or more selected m/z values. The selected ions then enter quadrupole 2, which acts as a collision cell, to fragment the ions by collision induced dissociation (CID). The quadrupole operates in RF mode only permitting the stable trajectory of all ions. The cell is filled with an inert gas, *e.g.* argon, as the ions pass through this quadrupole, they collide with the inert gas molecules causing the ions to fragment, these fragment ions can also undergo further collisions to produce

fragments of fragments. The voltage applied to the collision cell affects the kinetic energy of the ions, increasing the energy increases fragmentation, so the degree of fragmentation can be controlled. The fragments ions produced will then enter quadrupole 3, which will sequentially allow the stable trajectories of different *m/z* values in a scanning function, which will permit the passage of ions to the detector. This mode of operation for a triple quadrupole mass spectrometer is called a product ion scan, as the product ions of a selected precursor are investigated.

There are three other main modes in which a triple quadrupole can be operated:

Firstly, precursor ion scan, whereby Q1 is set to scan, and selected *m/z* values are permitted in Q3. This allows for the precursor origin of a specific product ion to be identified.

Secondly, selective reaction monitoring (SRM), whereby, selected *m/z* values are permitted in both Q1 and Q3, thus the precursor and product *m/z* will be known. As the quadrupole spends its entire time permitting the stable trajectory of one ion, rather than scanning, lower detection limits can be obtained by SRM.

Finally, neutral loss scan, whereby both quadrupoles are set to scan, although an offset between the scans is applied. This offset will be set to correspond to a neutral loss that is commonly observed with the class of compound of interest.

These scan types are specific to tandem MS in space, it is not possible to operate all of these modes in tandem MS in time.

For some of the following product ion scan experiments, the FT-ICR MS has been utilised for tandem MS in space. The initial quadrupole isolates the precursor ion, the ions undergo CID in the collision cell and finally the ions are detected simultaneously within the ICR cell. Due to principle of utilising cyclotron frequencies to detect ions within the ICR cell, accurate mass data can be acquired for the product ions, allowing elemental formulae to be deduced. Although, utilising this form of CID, fragments of fragment ions can be obtained, *i.e.* the product ions observed in the product ion mass spectrum, may not have originated directly from the selected precursor ion, and rather be the result of multiple stages of fragmentation/rearrangements. The ICR cell operated with no quadrupole fragmentation can perform MS/MS in time, v*ia* sustained off-resonance irradiation (SORI) CID although this has not been utilised for these experiments.

2.2.3.2   MS/MS in time

MS/MS in time is accomplished by trapping the ions in the same physical place with multiple processes, *i.e.* isolation, fragmentation and detection, occurring at different points in time. There are two main advantages of this process:

All the product ions detected have originated from the selected precursor ion *i.e.* there are no fragments of fragments, this is due to the way ions are isolated and fragmented. This allows for fragmentation pathways to be constructed, aiding structural elucidation.

Secondly, MS^n (where n is the number of sequential fragmentation experiments) experiments can be performed, this is due to the ions being trapped and the processes occurring in time. To preform multiple stages of MS using a tandem MS in space instrument, an extra collision cell and quadrupole would be required for each sequential fragmentation, increasing the size of the instrument.

Tandem mass spectrometry in an ion trap occurs in time, and occurs v*ia* the following process: An ion of a specific *m/z* is selected and all of the other ions are then expelled from the trap. This ion is then fragmented, by collisions with helium gas. This fragmentation can be improved by providing energy to the ions by exciting them at their secular frequency[49]. The product ions can then either be scanned out of the trap for detection, or another ion can be selected for further fragmentation by ejecting all of the other ions and repeating the process to provide MS^n spectra. The excitation of an ion by irradiation at its secular frequency means only this ion is excited and therefore fragments. Products of this ion are not excited by this frequency therefore do not undergo further fragmentation, unlike the multiple collisions that ions undergo in the quadrupole.

2.2.4   The vacuum system

The analyser, detector and usually the ionisation source (unless atmospheric pressure ionisation) are held under high vacuum, this is necessary to allow the ions to travel through the mass spectrometer without colliding with air molecules.

At low vacuum (> 10^{-3} mbar), collisions occur between the analyte ions and the background gaseous molecules, these collisions can alter the trajectory of the ion, causing neutralised on the internal surfaces of the mass spectrometer, losing its charge, resulting in a loss of sensitivity. Alternatively, ions and gaseous molecules can undergo undesirable reactions, including charge neutralisation or formation of a new species, resulting in a loss of sensitivity and an increased complexity to the mass spectrum[49].

The distance the ions travel within the mass spectrometer, between the ionisation source and the detector dictates the mean free path required for the instrument, and therefore the pressure required to achieve an unimpeded path for the ions.

The relationship between pressure, P (in Pa) and mean free path, L (in m) is given by

Equation 40.

Equation 40:

$$L = \frac{kT}{\sqrt{2p\sigma}}$$

Where k is the Boltzmann constant, T is the temperature (in K) and σ is the collision cross sectional area (in m^2); $\sigma = \pi d^2$ where d is the sum of the radii of the stationary molecule and the colliding ion (in m). Under normal conditions the equation can be simplified to give an approximation of the mean free path of an ion in a mass spectrometer using Equation 41, where L is in centimetres and pressure p is in pascals.[49]

Equation 41:

$$L = \frac{0.66}{p}$$

Mean free paths and the pressures required for a variety of mass analysers are displayed in

Table 1.

Table 1 – Mean free paths and pressures required for a variety of mass analysers [77]

Analyser	Pressure (mbar)	Mean Free Path
FT-ICR MS	$< 10^{-10}$	500 km
Magnetic Sector	$< 10^{-6}$	50 m
TOF	$< 10^{-6}$	50 m
Quadrupole	$< 10^{-4}$	50 cm
Ion Trap	$< 10^{-4}$	50 cm

Typically, vacuums are maintained *via* rotary vacuum pumps and turbo-molecular pumps. These pumps work in conjunction with each other, the rotary pumps typically reduce the vacuum to approximately 10^{-2} mbar, prior to the high vacuum turbo-molecular pump establishing the required analysis vacuum (as high as 10^{-10} mbar).

The pumping capacity of rotary pumps is limited to 10^{-3} mbar due to the vapour pressure of the oil used, there is potential risk of the sealing oil tracking back into the mass spectrometer in the case of a sudden loss of vacuum. These issues are not experienced with turbo-molecular pumps.

Chapter 3:   Experimental

10 gasoline samples were provided by Innospec Ltd (Ellesmere Port, UK), numbered 155, 156, 158, 159, 160, 161, 162, 164, 166 and 167.

Indene, isoprene, dicyclopentadiene, anthracene, di-*tert*-butyl peroxide, dicumyl peroxide and 1,1-di(t-butylperoxy)-3,3,5-trimethylcyclohexane were purchased from Acros Organics (Geel, Belgium).

Methanol (LC-MS grade), ethanol (LC-MS grade), acetonitrile (LC-MS grade), toluene (HPLC grade) and dichloromethane (HPLC grade) were purchased from Fisher Scientific (Loughborough, UK). Formic acid, ammonium acetate, sodium formate and lithium acetate were purchased from Fisher Scientific (Loughborough, UK).

Liquefied CO_2 was of food grade and purchased from BOC Special Gases (Manchester, UK).

3.1   Gas chromatography-mass spectrometry (GC-MS)

70 eV electron ionisation mass spectra were recorded using a ThermoQuest Trace™ GC 2000 gas chromatograph coupled to a Thermo Finnigan trace MS quadrupole mass spectrometer (Thermo Finnigan, Manchester, UK).

Xcalibur v1.1 was used for control of the GC–MS and data acquisition. Individual mass spectra were compared against the National Institute of Standards and Technology (NIST) EI mass spectral Library (NIST05) and NIST mass spectral search program (version 2.0d).

3.1.1   GC-MS of gasoline

1.0 μL of gasoline was injected into a Grob split/splitless injector (240 °C), a split ratio of 50 with helium carrier gas at a constant flow rate of 1 mL/min.

The GC-MS was initially equipped with an RTX-5 fused silica capillary column (Thames Restek, High Wycombe, UK), (30 m × 0.25 mm i.d., 0.25 μm film thickness). The oven temperature programme for the RTX-5 column was initially 40 °C for 5 minutes, ramped at a rate of 20 °C/minute to 320 °C and held for 7 minutes.

Subsequently, the GC-MS was equipped with a HP-INNOwax column (Santa Clara, CA, USA) (60 m 0.25 mm i.d., 0.50 μm film thickness). The oven temperature programme for the HP-INNOwax

column was 40 °C for 5 minutes, ramped at a rate of 20 °C/minute to 240 °C and held for 8 minutes.

Electron ionisation (EI) mass spectra were acquired between m/z 40 – 500 at a scan rate 2 scans/second. No solvent delay was used.

3.1.2   GC-MS of peroxides and diolefins

1.0 µL of peroxide and diolefin samples in DCM were initially injected into a Grob split/splitless injector (240 °C), as a splitless injection. Helium was used as carrier gas at a constant flow rate of 1 mL/min.

The GC-MS was equipped with an RTX-5 fused silica capillary column (Thames Restek, High Wycombe, UK), (30 m × 0.25 mm i.d., 0.25 µm film thickness). The oven temperature programme for the RTX-5 column was initially 40 °C for 4.5 minutes, ramped at a rate of 20 °C/minute to 320 °C and held for 7 minutes.

Subsequent experiments utilised lower temperatures due to the decomposition of dicumyl peroxide. Injector temperatures of 100 °C and 60 °C were investigated. A transfer interface between the gas chromatograph and the mass spectrometer was held at a temperature of 120 °C. The oven temperature programme was changed to 90 °C for 4.5 minutes, ramped at a rate of 30 °C/minute to 120 °C, held for 25 minutes and then ramped at 30 °C/minute to 320 °C.

Electron ionisation (EI) mass spectra were acquired between m/z 40 – 500 at a scan rate 2 scans/second. No solvent delay was used.

3.2   Fourier transform ion cyclotron resonance mass spectrometry (FT-ICR MS)

The high resolution mass spectrometry measurements were undertaken using a Bruker Daltonics (Billerica, MA, USA) 4.7 Tesla Fourier transform ion cyclotron resonance mass spectrometer. The spectra were averaged over various numbers of scans depending on sensitivity (ranging from 32 to 256 per analysis), in the range of m/z 54 – 1500 with a TD of 1M, although the m/z range was subsequently increased to m/z 200 – 2000.

Data acquisition and processing was performed using Solarixcontrol v1.5.0.

3.2.1   ESI+ FT-ICR MS

50 μL of gasoline was diluted in methanol to a total volume of 1 mL, subsequently ionisation additives were introduced depending on the analyte of interest (*i.e.* 25 mM formic acid, 25 mM ammonium acetate & 25 mM lithium acetate). The resulting solutions were directly infused into an electrospray source using a 100 μL Hamilton syringe at a flow rate of 2 μL/min. A capillary voltage of -4 kV, drying temperature of 180 °C, drying gas flow rate of 4.0 L/min and nebuliser pressure of 1.2 bar was used. Calibration was preformed using 10 mM sodium formate in methanol.

3.2.1.1   ESI+ FT-ICR MS/MS

MS/MS experiments were undertaken by isolating the desired precursor ion in the quadrupole of the instrument and inducing fragmentation by collision induced dissociation (CID) with argon gas. The selection of the precursor ion *m/z* and CID voltages were dependant on the analyte of interest and are described in the results and discussion section.

3.2.2   ESI- FT-ICR MS

50 μL of gasoline was diluted methanol and 25 mM ammonium hydroxide to a total volume of 1 mL. The resulting solutions were directly infused into an electrospray source using a 100 μL Hamilton syringe at a flow rate of 2 μL/min. A capillary voltage of +4 kV, drying temperature 180 °C, drying gas flow rate of 4.0 L/min and nebuliser pressure of 1.2 bar was used. Calibration was preformed using 10 mM sodium formate in methanol.

3.2.3   APPI+ FT-ICR MS

50 μL of gasoline was diluted in toluene to a total volume of 1 mL. The solutions were directly infused into a APPI II (Bruker) source using a 100 μL Hamilton syringe at a flow rate of 5 μL/min. The source was equipped with a krypton lamp (10.2 eV). A capillary voltage of 3 kV, drying temperature of 200 °C and a drying gas flow rate of 3.0 L/min was used. A vaporisation temperature of 300 °C was utilised. Calibration was preformed using a mixture of purine, hexamethoxyphosphazene, (2, 2-difluoroethoxy) phosphazene, 1H, 1H, 3H-tetrafluoropropoxy) phosphazene, (1H, 1H, 5H-octafluoropentoxy) phosphazene and (1H, 1H, 7H-dodecafluoroheptoxy) phosphazene.

3.3   ESI+ quadrupole ion trap (QIT)

The analyses were undertaken Thermo Finnigan LCQ ion trap (Thermo Finnigan, Manchester, UK).

Initially 400 µL of gasoline was diluted in methanol to a total volume of 1 mL. Further samples were diluted in the presence of an ionisation additive. 400 µL of gasoline was diluted in methanol + 25 mM formic acid to a total volume of 1 mL. 50 µL of gasoline was diluted in methanol + 25 mM lithium acetate to a total volume of 1 mL.

The resulting solutions were directly infused using a 100 µL Hamilton syringe at a flow rate of 5 µL/min into an electrospray source. A spray voltage of 3.5 kV, capillary temperature of 200 °C, sheath gas flow rate of 30 arb. units and an auxiliary gas low rate of 10 arb. units. Automatic gain control was enabled, with a maximum injection time of 50.00 ms and 3 microscans and data acquired between a m/z range of 150 – 2000. Data were acquired using Xcalibur v1.1.

3.3.1   ESI+ QIT tandem MS

MS^n experiments were undertaken by isolating the desired precursor ions with an isolation window of 5 m/z units. Fragmentation of these ions was achieved by collisions with a helium buffer gas. The precursor ion m/z values, collision voltages and m/z ranges selected are described in the results and discussion section.

3.4   Ultra-high pressure super critical fluid chromatography-mass spectrometry single quadrupole detector (UHPSFC-MS SQD)

3.4.1   UHPSFC-ESI+ SQD MS of gasoline

The analyses were undertaken using a Waters Acquity UPC^2 (UltraPerformance Convergence Chromatography) (Waters Corp., Milford, MA, USA).

2 µL of gasoline was injected onto a High-Strength Silica (HSS) C18 Column (1.8 µm x 3.0 mm x 100 mm) maintained at 40 °C. A mixture of supercritical CO_2 and methanol + 25 mM NH_4OAc was used as the mobile phase at a flow rate of 1.50 mL/min, quantities of which were varied over the 3 minute analysis time, as outlined in Table 2.

Table 2 – Solvent gradient for gasoline UPC^2 method

Time / min.	CO_2 / %	MeOH + 25 mM NH_4OAc / %
0.00	90	10
2.50	60	40
3.00	60	40

Ionisation additives were introduced prior to the ionisation source, methanol + 25 µM ammonium acetate and methanol + 1 % formic acid were used at a flow rate of 0.45 mL/min.

Detection was achieved with a Waters SQ Detector 2 single quadrupole mass spectrometer with ESCi multi-mode ionisation source operated in ESI+, with the following parameters:

A capillary voltage of 3.2 kV, source temperature of 150 °C and a desolvation temperature of 200 °C was used. Nitrogen was used as the desolvation gas at a flow of 550 L/h. Data were acquired between m/z 400 – 1500. Various cone voltages were investigated, and selection was dependant on the analyte of interest. Data were recorded using MassLynx v4.1.

3.4.2   UHPSFC-ESI+ SQD MS of peroxides

The analysis was undertaken using a Waters Acquity UPC^2.

The peroxide samples were prepared at various concentrations in methanol, 2 µL of which was injected onto a High-Strength Silica (HSS) C18 Column (1.8 µm x 3.0 mm x 100 mm) maintained at 40 °C. A mixture of supercritrical CO_2 and methanol + 25 mM NH_4OAc was used as the mobile phase at a flow rate of 1.50 mL/min, quantities of which were varied over the 5 minute analysis time, as outlined in Table 3.

Table 3 - Solvent gradient for peroxides in gasoline UPC^2 method

Time / min.	CO_2 / %	MeOH + 25 mM NH_4OAc / %
0.00	100	0
1.50	100	0
2.30	60	40
5.00	60	40

Methanol + 25 µM ammonium acetate was added as an ionisation additive prior to the ionisation source at a flow rate of 0.45 mL/min.

Detection was achieved with a Waters SQ Detector 2 single quadrupole mass spectrometer with ESCi multi-mode ionisation source operated in ESI+, with the following parameters:

A capillary voltage of 3.2 kV, source temperature of 150 °C and a desolvation temperature of 200 °C was used. Nitrogen was used as the desolvation gas at a flow of 550 L/h. Data were acquired between m/z 400 – 1500. Various cone voltages were investigated, and selection was dependant on the analyte of interest. Data were recorded using MassLynx v4.1.

3.4.3   UHPSFC-APPI+ SQD MS of diolefin samples

The analysis was undertaken using a Waters Acquity UPC^2.

2 µL of a 100 ppm per component toluene solution of anthracene, indene and dicyclopentadiene was injected onto a High-Strength Silica (HSS) C18 Column (1.8 µm x 3.0 mm x 100 mm) maintained at 40 °C. A mixture of supercritical CO_2 and methanol + 25 mM NH_4OAc was used as the mobile phase at a flow rate of 1.50 mL/min, quantities of which were varied over the 3 minute analysis time, as outlined in

Table 4 - Solvent gradient for diolefins UPC^2 method

Time / min.	CO_2 / %	MeOH + 25 mM NH_4OAc / %
0.00	90	10
2.50	60	40
3.00	60	40

Toluene was added as an ionisation additive prior to the ionisation source at a flow rate of 0.45 mL/min.

Detection was achieved with a Waters SQ Detector 2 single quadrupole mass spectrometer with APPI source operated in APPI+, with the following parameters:

A vaporisation temperature of 600 °C and a cone voltage of 30 V. The quadrupole was set to scan between m/z 50 – 1000. Data were recorded using MassLynx v4.1.

3.5   Triple quadrupole mass spectrometer

3.5.1   MS/MS of polyisobutylene in gasoline

50 % gasoline in methanol + 1 % formic acid was driectly infused into Waters TQ Detector 2 tandem quadrupole mass spectrometer with ESCi multi-mode ionisation source positive ion ESI data were acquired using the following parameters:

A capillary voltage of 3.2 kV, source temperature of 150 °C, desolvation temperature of 200 °C and a cone voltage 60 V was used. Nitrogen was used as the desolvation gas at a flow of 550 L/h.

For each MS/MS experiment a protonated PIB m/z was selected and isolated within the first quadrupole. Fragmentation of the PIB would occur in the collision cell by CID with argon gas. A

CID voltage of 30 V was used. The third quadrupole was set to scan between *m/z* 40 - 1000. Data were recorded using MassLynx v4.1.

Chapter 4: Application of gas chromatography mass spectrometry to gasoline analysis

4.1 GC-MS of gasoline

GC-MS analysis is applicable to low-molecular weight, volatile and thermally stable compounds. Thus, for gasoline analysis GC-MS is suitable for the majority of the base fuel which consist of hydrocarbons with a carbon number of C_4 to C_{12}. GC-MS is frequently used for the analysis of gasoline, with little to no sample preparation, for adulterants and the presence of some volatile additives[40-42]

EI is an energetic form of ionisation, after the initial ionisation of the molecule, the remaining energy induces fragmentation producing an abundance of fragment ions. These fragment ions provide valuable structural information, the use of a standard 70 eV electron energy allows for reproducible mass spectra, which in turn allows for rapid matching of mass spectra to library mass spectra as the ions fragment in a characteristic and consistent manner.

Ten gasoline samples that have been used to power DISI test engines, some of which have displayed injector deposit issues, have been analysed by GC-MS. The resulting GC-MS TICCs have then been compared by computational methods to identify the similarities between samples which the aim of identifying a correlation between compound composition and deposit formation.

4.1.1 Screening of DISI gasoline samples by GC-MS

The analyses was undertaken using a ThermoQuest Trace™ GC 2000 gas chromatograph coupled to a Thermo Finnigan trace MS quadrupole mass spectrometer. 1.0 µL of gasoline was injected into a Grob split/splitless injector (240 °C) with a split ratio of 50. Samples were transfer to a RTX-5 fused silica capillary column (30 m x 0.25 mm i.d., 0.25 µm film thickness) by a 1.0 mL/min helium carrier gas. Initially the column oven was held a 40 °C for 5 min. then ramped to 320 °C at 20 °C/min. and held for 7 min. The quadrupole was set to scan between *m/z* 40 and 500 . The solvent delay was set to 0 min. to record the most volatile compounds in the gasoline matrix.

The resulting GC-MS TICC for gasoline 159 is displayed (Figure 41).
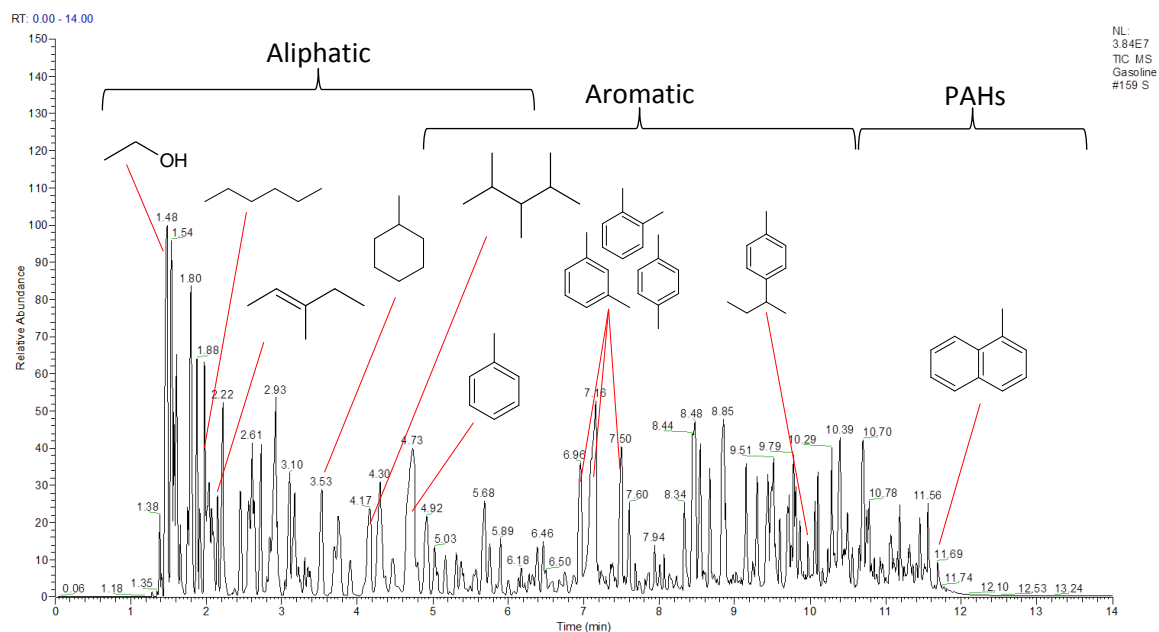
Figure 41 – GC-MS (EI) TICC of gasoline 159 with a split ratio of 50 (RTX-5 column)

Library matching of the individual mass spectra for the chromatographic peaks allows for rapid identification of the components within the gasoline matrix. The TICC (Figure 41) displays a range of hydrocarbons originating from the base fuel and blending components such as ethanol and toluene.

Aliphatic, aromatic and polyaromatic hydrocarbons can be identified within distinct regions of the TICC (Figure 41). The most volatile aliphatic compounds eluting first, followed by the aromatics, and finally the higher boiling point polyaromatic hydrocarbons. This behaviour is consistent with the use of the RTX-5 column (containing 5 % diphenyl siloxane), compounds experience little interaction with the stationary phase, and are mainly separated based on their boiling points. Increased retention of the more polar components of the gasoline sample can be achieved by using PEG based stationary phase.
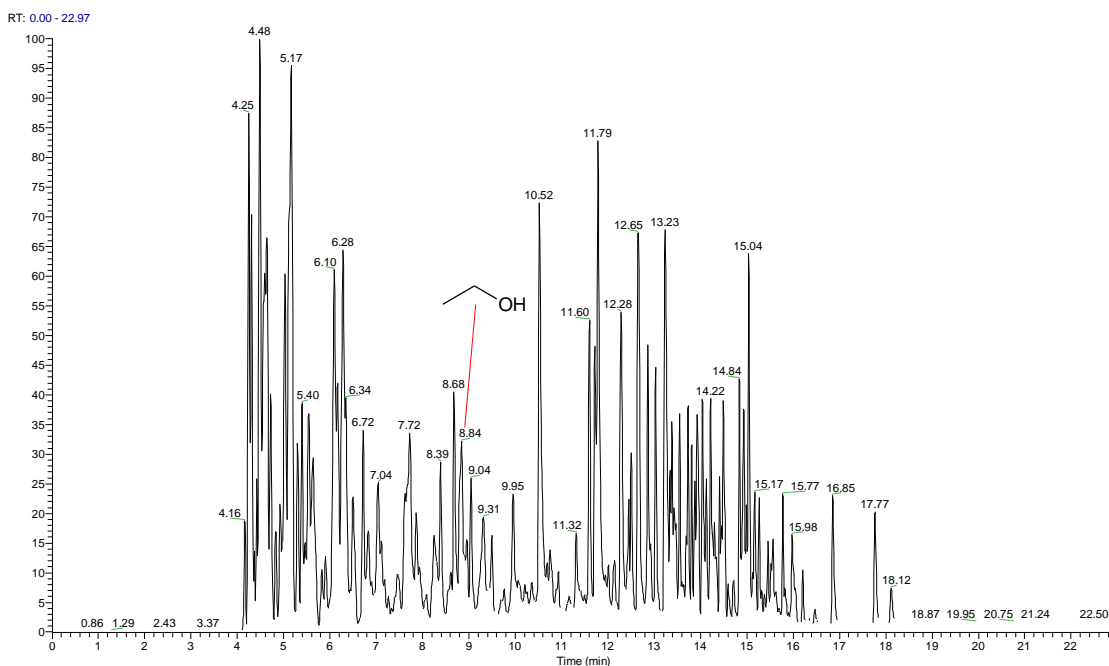
Figure 42 - GC-MS (EI) TICC of gasoline 159 with a split ratio of 50 (HP-INNOwax column)

The increased retention of the more polar compounds prevents coelution with the non-polar hydrocarbons with similar volatility. Ethanol, added to gasoline as a blending component, is an example of this, although volatile and eluting early (T_R: 1.48 min.) on the RTX-5 column (Figure 41), a retention time of 8.84 min. is observed when using the HP-innowax column (Figure 42). Non-polar compounds are retained less on the column innowax column when compared to polar compounds, although increased retention times can be seen across the range when compared to RTX-5 column, this is due to the HP-innowax increased column length of 60 m compared to 30 m of the RTX-5 column.

The 10 gasoline samples were screened using the RTX-5 column and a split ratio of 50, and the TICCs were compared.
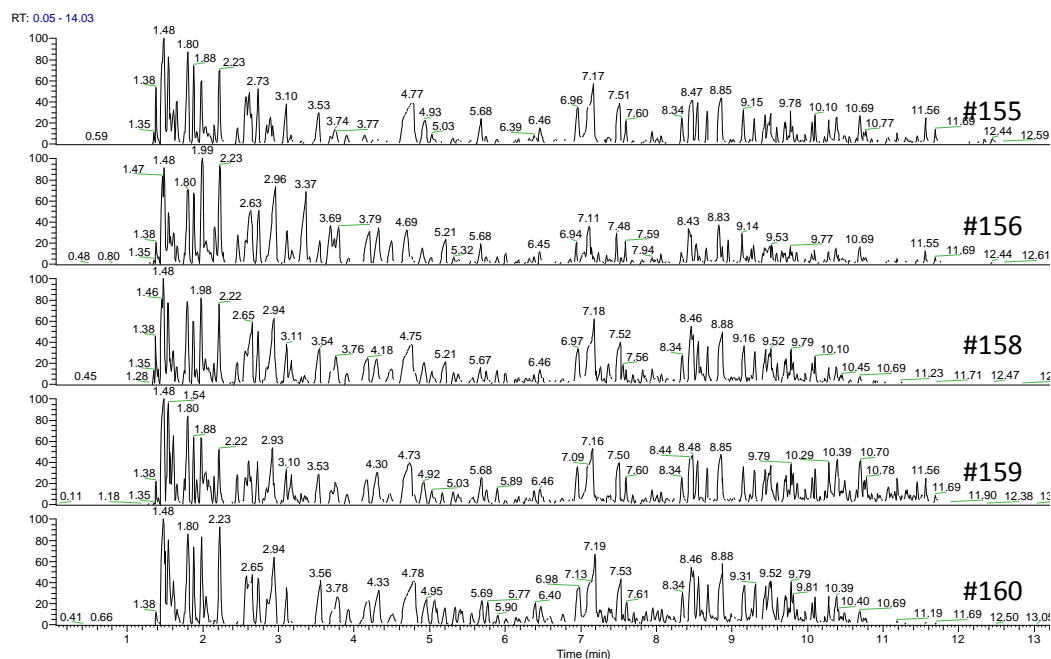
Figure 43 – GC-MS TICC for gasolines 155, 156, 158, 159 and 160
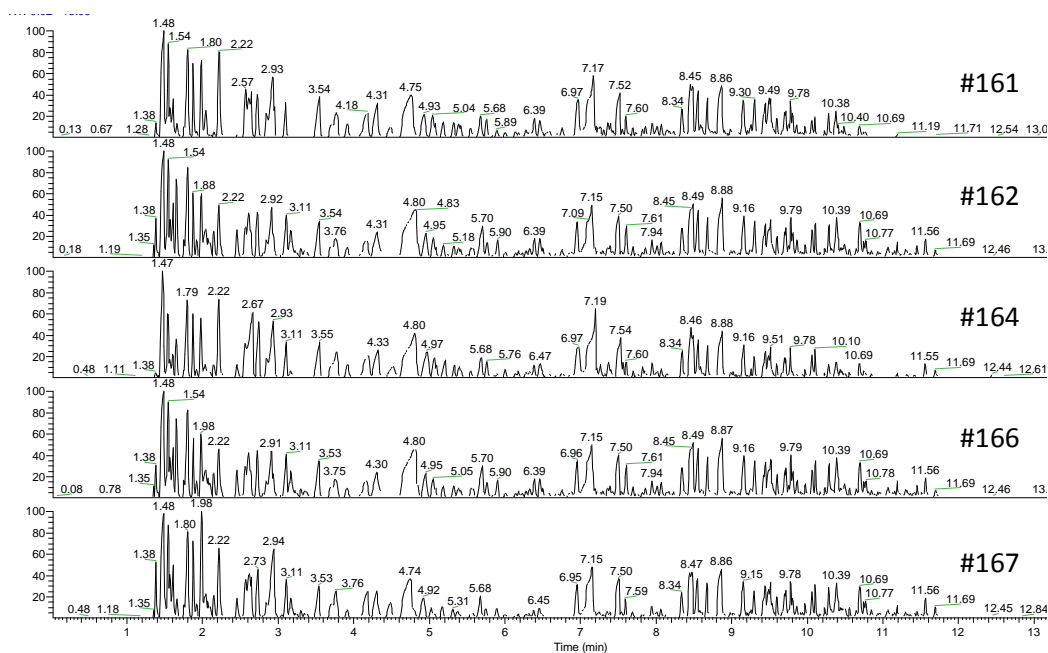
Figure 44 – GC-MS TICC for gasolines 161, 162, 164, 166 and 167

Differences within the composition of the gasoline samples are not readily apparent by comparison of the TICCs (Figure 43 & Figure 44). Approximately 300 compounds are detected and identified, the majority of which are present in all of the gasoline samples, although in varying concentrations. Very few unique compounds, identified by library matching, are detected. These compounds are usually isomers or closely related hydrocarbons with differing chain lengths to the compounds already detected. The gasoline samples appear near identical when analysed by GC-MS; the additive packages are not observed.

4.1.2   Automated comparison of GC-MS data for gasoline samples

If there is a correlation between hydrocarbons in the base fuel and whether deposits are formed within DISI injectors, the identification of subtle differences within the GC-MS TICCs is essential. Manual comparison of the GC-MS TICCs display few differences between samples.

Automated processing of the GC-MS TICCs allows for rapid identification of peaks within a gasoline sample. The peaks detected can be compared to the peaks present in other gasoline samples, and the similarity of the gasolines can be compared. Subtle differences between the EI ionisable portion of the gasoline samples can be highlighted.

SpectralWorks AnalyzerPro^{TM} software was utilised for to identify subtle differences between the gasoline samples. AnalyzerPro^{TM} identifies components in the GC-MS TICCs by comparing the peak shape of RICCs for *m/z* values at each retention time, an identical peak shape in the RICCs for two or more ions identify these ions are from the same compound. These identified ions are used to produce a mass spectrum for the detected component, *i.e.* the resulting mass spectra only contains ions originating from a sinlge component, free from ions originating from coeluting chromatographic peaks and background ions. An example is shown for three components within a gasoline sample (Figure 45).

Figure 45 – (Left): GC-MS TICC with the RICC for each *m/z* overlaid (Right): Three identified components

Table 5 – NIST library matches for identified components within AnalyzerPro[TM] (Figure 45)
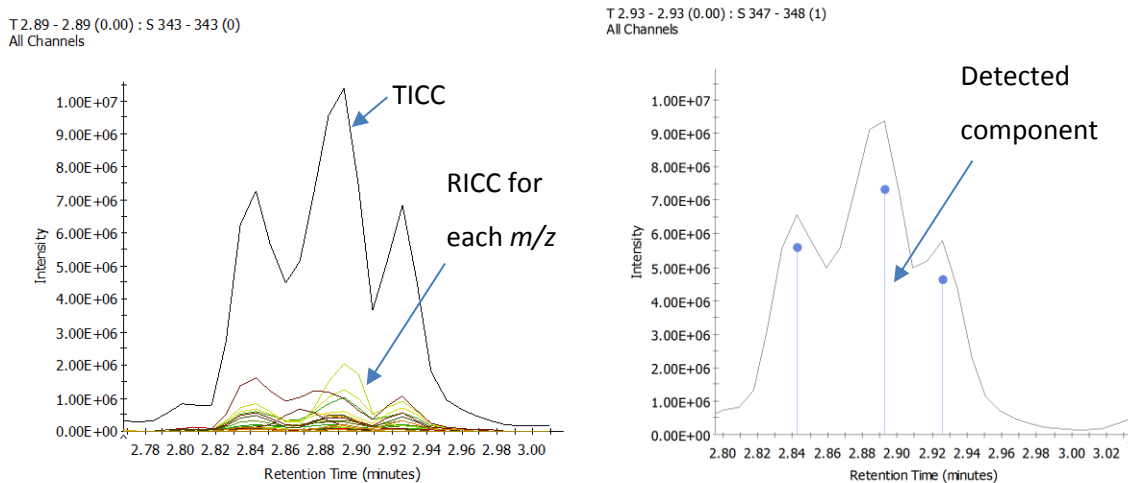
RT (min)	Scan	Start RT (min)	End RT (min)	Area	Confidence %	Forward	Reverse	CAS #	Name
2.7926	331	2.7683	2.8128	189963					
2.8426	337	2.8111	2.8549	7061873	88.55	881	896	2453-00-1	Cyclopentane, 1,3-dimethyl-
2.8926	343	2.8535	2.9328	10488324	83.65	832	847	926-82-9	Heptane, 3,5-dimethyl-
2.9259	347	2.9094	2.9981	4084190	82.30	820	830	1192-18-3	Cyclopentane, 1,2-dimethyl-, cis-
3.0426	361	3.0068	3.0568	216958	91.80	918	918	4914-89-0	3-Hexene, 3-methyl-, (Z)-
3.1093	369	3.0292	3.1438	31857540	90.09	897	910	142-82-5	Heptane
3.1426	373	3.0769	3.1427	654238	85.88	857	863	15232-95-8	Cyclohexene,3-(2-propenyl)-

The resulting mass spectra for each peak can be searched against the NIST mass spectral library to identify the component (Table 5). Although, the identification of a compound is not necessary to determine the presence of said compound in different gasoline samples. The presence of a peak with an identical mass spectrum at an identical retention time within two samples would infer the compound is present within both samples, providing the same GC-MS method is used.

Each gasoline can be characterised by the mixture of components identified. This component fingerprint can be compared to the fingerprint of other gasoline samples and the similarity of the samples can be assessed. The presence and absence of compounds within difference gasolines can be highlighted, thus identifying subtle differences, which in turn may correlate to the presence of injector deposits.

The GC-MS TICCs for the 10 gasolines acquired with a split ratio of 50 (section 4.1.1) were compared using AnalyzerPro[TM]. For a component to be identified, a minimum peak area of 500 arb. units, a minimum retention time width of 0.01 min. and a minimum peak height of 0.1 % were used as the peak detection threshold values.

For a mass spectral match of a component to an entry in the NIST mass spectral database a minimum forward and backward similarity index of 650 arb. units and an overall match confidence of 80 % was used.

The component fingerprint of each gasoline was produced and saved in a library as searchable entities. Each gasoline sample component fingerprint was searched against this library producing a percentage similarity of the searched gasoline to each library entry. Strictly, this percentage value is the confidence that the searched gasoline component fingerprint is identical to that of the library entry, thus, more similar gasolines result in higher percentage similarities. When searching a drift window of T_R: 0.2 mins was used to account for slight differences in retention time.

As an example, the GC-MS TICCs for gasolines 155 and 159 with the component markers overlaid are displayed (Figure 46). A percentage similarity of 89.92 % was determined when searching gasoline 155 against gasoline 159.
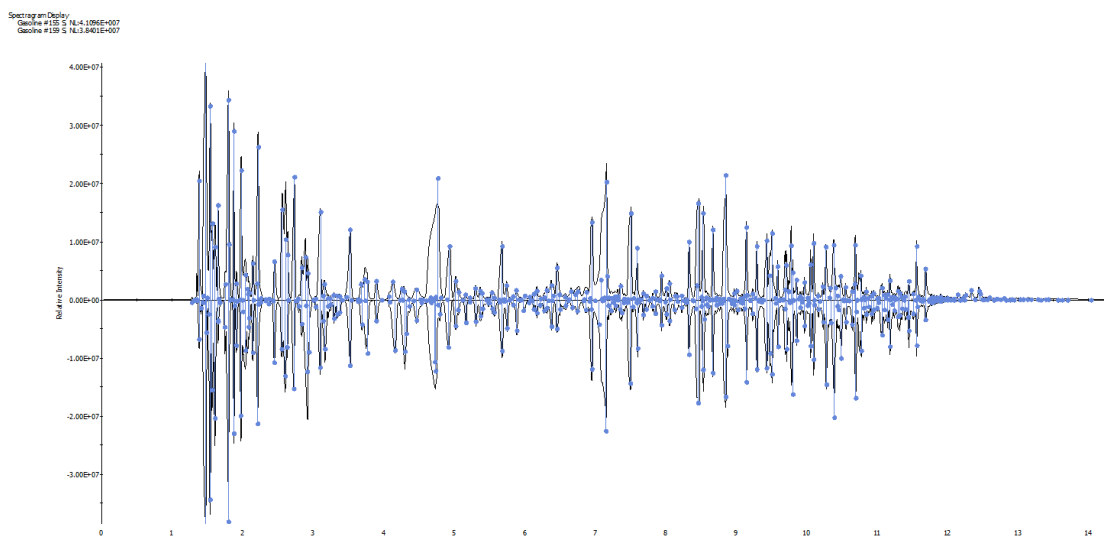

Figure 46 – GC-MS TICCs with overlaid component markers for (top): gasoline 155 (bottom): gasoline 159

The percentage matches are displayed in Table 6, matches of 100% are observed as each gasoline is matching with its own library entry.

Table 6 – Percentage similarity of the GC-MS TICCs of gasolines

	155	156	158	159	160	161	162	164	166	167
155	100.00	< 50	70.45	92.85	78.91	79.45	83.32	80.66	74.47	83.00
156	< 50	100.00	54.96	< 50	< 50	52.36	< 50	56.58	50.96	63.83
158	74.44	60.23	100.00	71.91	87.15	80.31	70.07	82.16	75.25	84.86
159	89.92	< 50	70.24	100.00	74.47	83.96	72.55	82.50	69.51	83.04
160	79.24	< 50	85.66	75.40	100.00	83.99	69.37	83.17	77.22	78.88
161	85.30	52.56	81.63	88.13	87.80	100.00	65.13	87.56	80.24	88.58
162	82.08	< 50	68.99	80.19	70.41	66.18	100.00	73.68	76.03	71.79
164	83.45	58.05	83.87	87.82	89.25	89.70	73.89	100.00	78.40	85.79
166	80.10	51.27	75.70	74.33	79.65	80.23	77.75	80.17	100.00	73.52
167	86.95	61.69	86.24	88.43	80.09	87.52	69.68	85.43	69.62	100.00

The heat mapped table (Table 6) where red is the most similar and green is the most dissimilar, displays high percentage similarities for the majority of gasolines with each other. Although, gasoline 156 has a maximum percentage similarity of 63.83 % with that of gasoline 167, and for the majority of other gasoline samples a match of less than 50 %. This would suggest that gasoline 156 is radically different in base fuel composition (readily detectable by GC-MS) to that of the other 9 gasoline samples.

4.1.3   GC-MS of gasoline conclusions

EI GC-MS affords high chromatographic resolution and detailed structural information from energetic fragmentation for the hydrocarbon base fuel and volatile additives in gasoline. Although it is limited to thermally stable and low molecular weight compounds. Gasoline samples can often appear near identical, with just varying concentrations of the compounds present. Subtle differences between the samples are difficult to identify manually. Automated processing of gasoline TICCs allows for rapid and comprehensive identification of compounds, and comparison between different samples. The use of SpectralWorks AnalyzerPro^{TM} provides a gauge on the similarity of gasoline samples, by comparing the component fingerprint of a gasoline to another. Gasoline 156 has been identified as being very dissimilar to the other 9 gasolines.

To further understand the differences between the samples, the presence and absence of compounds in each sample could be highlighted. The presence of each compound in each sample could be correlated to the presence of injector deposits within a DISI injector.

Chapter 5:   Polymeric additive determination

Deposit control additives (DCAs) are added to gasoline to prevent and remove deposits forming in the engine fuel system, cylinder and valve regions. These deposits are formed from combustion and can reduce fuel and air flow throughout the engine, decreasing performance and increasing emissions.

As discussed previously, the chemistry of the deposit control additives has changed with the evolution of fuel injection methods. DCAs can become ineffective at preventing deposits within new engine technology. This is particularly prevalent with the move from PFI to GDI, with many PFI additives become ineffective at protecting GDI injectors. This, coupled with the increased likelihood of deposits within GDI injectors, due to the severe operating conditions now experienced and the greater effect of deposition on smaller injector holes, it is important to understand the DCA packages added to fuels when considering direct injection deposits. Although, the composition of the various deposit control additive packages added to fuels are not readily available.

This chapter focuses on the detection and structural identification of the polymeric detergent additives present within the gasoline samples acquired, namely polyisobutylene (PIB) and polyethylene glycol (PPG) chemistry.

5.1   FT-ICR MS

Gas chromatography mass spectrometry (GC-MS) is typically used to assess fuel quality and profile the hydrocarbon content of gasoline[40, 42]. Many American standard test methods (ASTM) rely on GC-MS to report on fuel quality[78, 79]. Due to the nature of gas chromatography, only compounds which are volatile and stable upon heating are suitable for analysis by this technique, thus preventing detection of a variety of compounds within the gasoline mixture, *e.g.* thermally unstable polymeric detergent additive packages.

In contrast to GC-MS the nature of electrospray ionisation (ESI), in this case positive ion electrospray ionisation (ESI+), allows for the ionisation and detection of the higher molecular weight *i.e.* polymeric additives, and thermal labile compounds, which may play a role in deposit formation[80].

Petroleum contains both non-polar compounds and polar compounds, typically 90 % and 10 % respectively. The polar fraction of the fuel consists of additive packages introduced to the refined fuel, and polar compounds present in the base fuel. These polar compounds are likely to be active

in deposition mechanisms and other fuel related issues. Both classes of compounds are of great interest in gasoline analysis. Positive ion ESI will only ionise the polar fraction of the fuel, (*e.g.* molecules with a site for protonation *i.e.* amines) ~ 10 %, whilst rendering the remaining 90 % of the fuel invisible to analysis by this technique[81].

Atmospheric pressure ionisation techniques have been widely applied to the analysis of crude oil in the field of petroleomic mass spectrometry[82]. The application to the analysis of refined products is less documented, although previous work has focused on the adulteration and fingerprinting of gasoline samples[63-66].

The use of Fourier transform ion cyclotron resonance mass spectrometry (FT-ICR MS) has various advantages over that of quadrupole mass spectrometry, namely high mass accuracy and high resolving power.

FT-ICR MS involves the measurement of an ions cyclotron frequency, each frequency specific to a particular *m/z*, therefore a mass spectrum to be obtained. As the frequency can be measured with great accuracy, errors in the measured mass of an ion can be narrowed down to less than 1 millidalton (mDa)[83], allowing the molecular formula to be derived from the comparison of the accurate mass measured with the exact mass of various element compositions. Nominally isobaric compounds, with different chemical formulae, observed by low resolution mass spectrometry can also be resolved.

5.1.1   ESI+ FT-ICR MS

5.1.1.1   Initial sample preparation

The presence and concentration of polymeric fuel additives was initially unknown for the ten gasoline samples.

Therefore experiments were conducted to optimise the concentration of gasoline in methanol, prior to ESI+ FT-ICR MS analysis. Solutions of gasoline 164 were made in methanol to 1 ppm, 10 ppm, 100 ppm and 5% (50,000 ppm)(*v/v*), which were compared against a methanol blank.
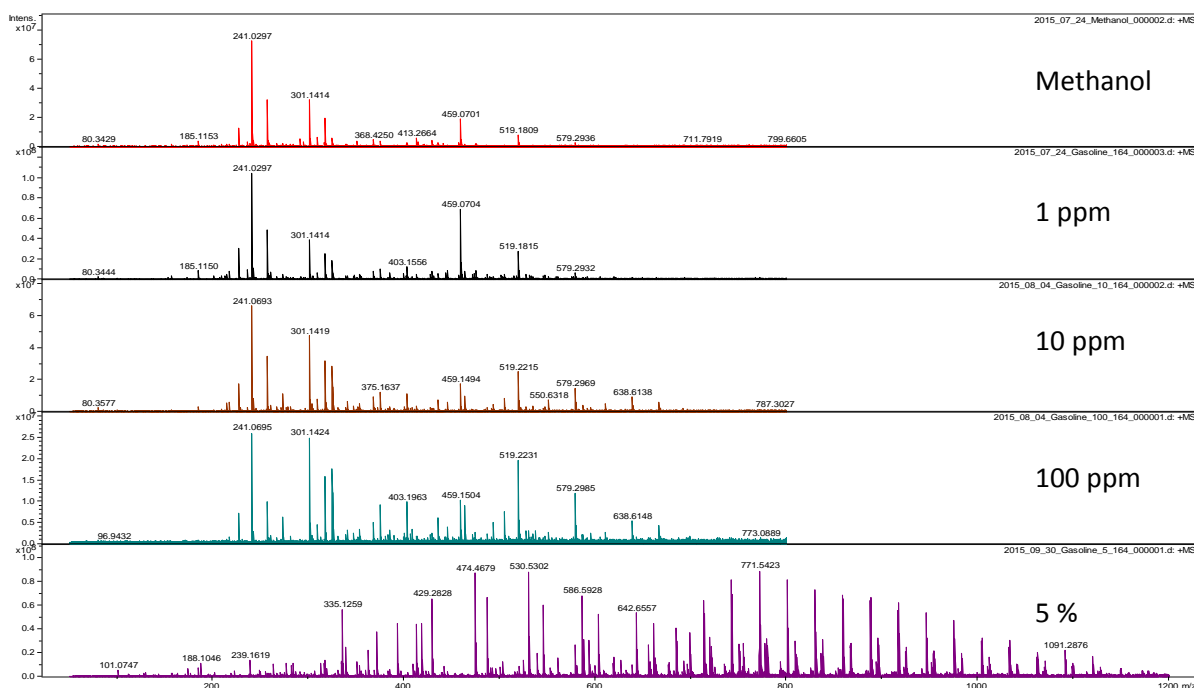
Figure 47 – ESI+ FT-ICR MS mass spectra for methanol and gasoline 164 at dilutions of 1 ppm, 10 ppm, 100 ppm and 5% in methanol.

The infusion positive ion ESI mass spectra (*Figure 47*) for concentrations of 1 ppm, 10 ppm and 100 ppm display identical peaks to that of the methanol blank, with no unique ions observable from the gasoline. Whereas the dilution of 5 % displayed a range of ions, evidently originating from the gasoline, rather than impurities in the methanol or artefacts within the mass spectrometer. This concentration is within the same range as other FT-ICR studies involving gasoline[65]. This concentration was used for all further samples.

Figure 48 – ESI+ FT-ICR mass spectra for gasoline samples

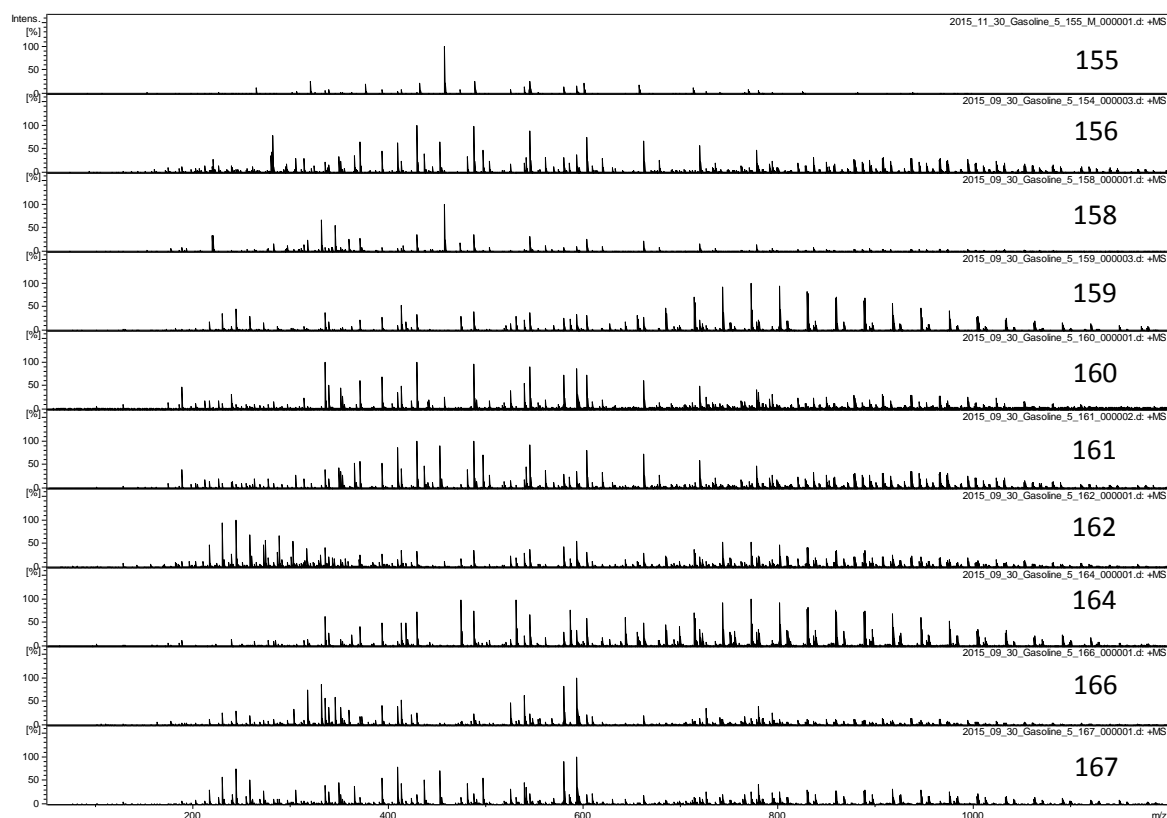The remaining nine gasoline samples were analysed by infusion ESI+ FT-ICR MS, at a concentration of 5% gasoline in methanol. The ESI+ FT-ICR mass spectra (*Figure 48*) display different profiles for each gasoline, each containing polymers and other series of compounds, which are discussed in more detail, in section 5.1.1.2.

Electrospray ionisation is evidently a powerful ionisation technique for identifying differences in the gasoline samples. ESI+ allows for the identification of non-volatile, higher molecular weight compounds, which was an issue experienced with the electron ionisation GC-MS data of the last chapter. A simplification of the mass spectra is also observed, only the polar component of the gasoline (ionisable by ESI+) is observable, thus highlighting additives and deposit precursors, while effectively rendering the base hydrocarbon fuel invisible.

5.1.1.2   Polymer type identification

Polymeric series are evident within the majority of the gasoline samples screened by ESI+ FT-ICR MS, although this could also be achieved with low resolution instrumentation. Various polymers types can be identified by the characteristic *m/z* spacing between the sequential ions within each polymeric series. Each successive ion within the series represents an increase in polymer chain length by one monomer unit, thus the difference in *m/z* between consecutive ions within a series

corresponds to the monomer mass for the given polymer. The ESI+ FT-ICR MS of gasoline 159 is used as an example (*Figure 49*).
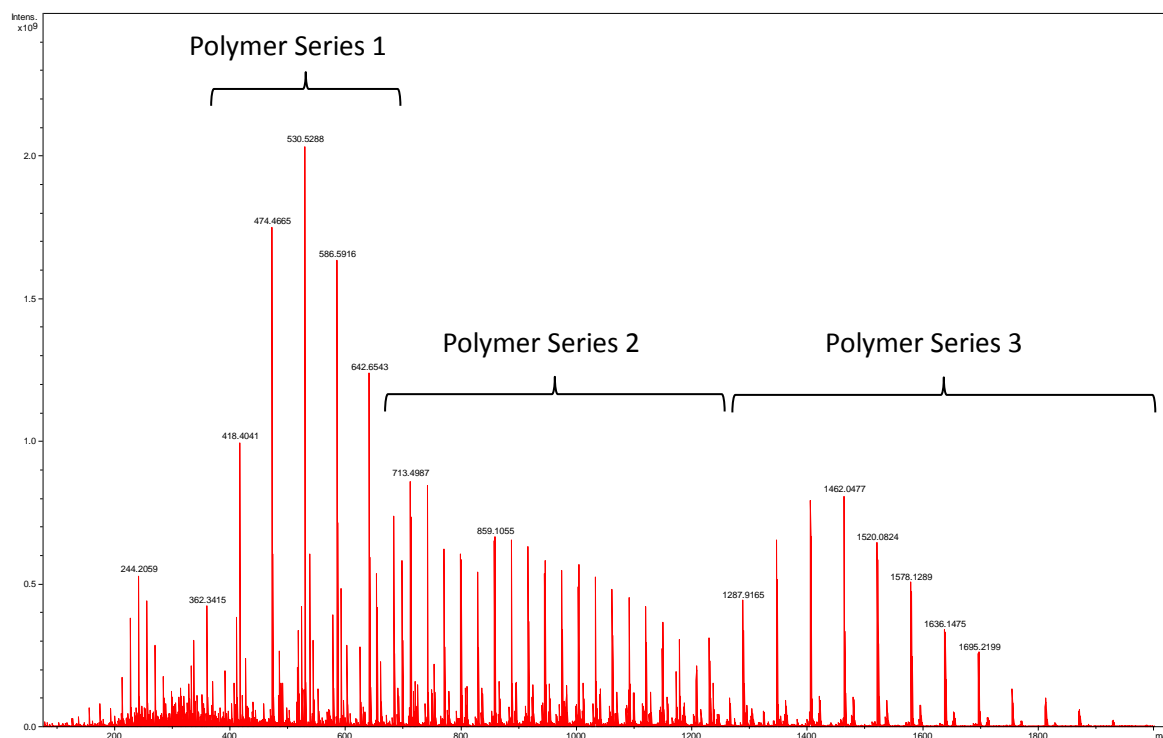

Figure 49 – ESI+ FT-ICR mass spectrum of 5 % gasoline 159 in methanol

Three distinct polymeric series can be identified from the mass spectrum (*Figure 49*). The most intense polymeric series of ions is observed between *m/z* 418 – 642 (polymer series 1), and can be characterised from the peak spacing between the sequential ions within the series of 56.062 *m/z* units corresponding to an elemental formula of C_4H_8 – an isobutylene monomer. From this mass spectrum (*Figure 49*), it is not possible to derive the exact structure of the polymer, although the peak spacing calculated from the accurate mass measure is sufficient to identify polymer series 1 as polyisobutylene. As discussed previously, PIB is typically added to gasoline blends as part of a detergent control package, to remove and prevent the formation of deposits within the fuel system and combustion chamber.

The series of ions between *m/z* 597 – 1265, (polymer series 2) can be characterised by a peak spacing of 29.0207 *m/z* units and a 0.5 *m/z* unit spacing between ^{12}C and ^{13}C peaks, indicative of a doubly charged species.

Upon calculation, a monomer mass of 58.0414 *m/z* units for a singly charged species can be determined, which is in good agreement with the exact mass of a propylene glycol monomer of 58.0419 *m/z* units (C_3H_6O).
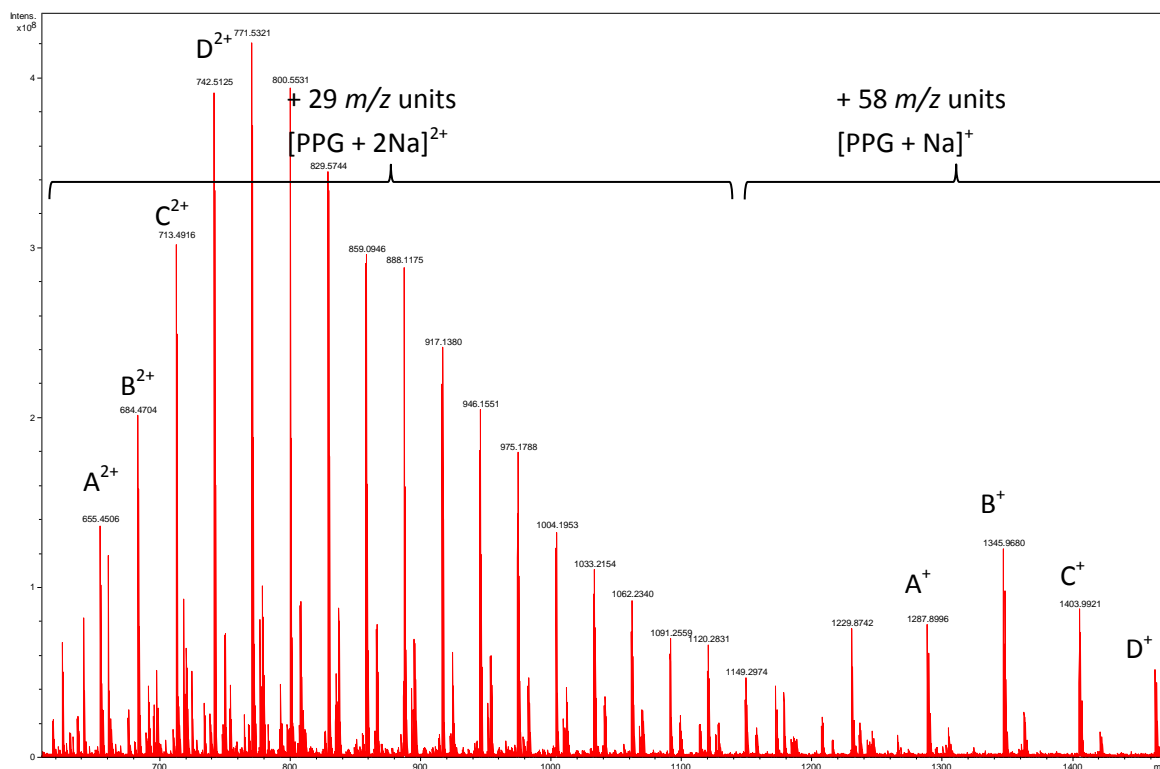
Figure 50 - ESI+ FT-ICR mass spectrum of 5 % gasoline 159 in methanol, *m/z* 600 – 1500

Polymer series 3, between *m/z* 1113 – 1984, is also identified as the same polypropylene glycol (PPG) as previously described, although present as the singly charged species, confirmed by deconvolution of the doubly charged species. This is represented in Figure 50.

The doubly charged PPG is present as the $[M + 2Na]^{2+}$ species, which can be calculated from the mass of the associated single charged ion, which is present as the $[M + Na]^{+}$ species (determined from the accurate mass measurement), these assignments are confirmed by the addition of ionisation additives to the solvent, which will be discussed later. Polypropylene glycols (PPG) are typically added to gasoline blends as a carrier oil in the deposit control packages.

The ESI+ FT-ICR mass spectra (Figure 50) for the gasoline sample displays the doubly charged PPG, it is suggested that the PPG is present as the sodiated molecule ($[PPG + 2Na]^{2+}$), calculated from the accurate mass measurement. Further evidence for the sodiated state is present in the form of the series of ions at + 8 *m/z* units with respect to the $[PPG + 2Na]^{2+}$ series, this corresponds to a series of $[PPG + Na + K]^{2+}$ ions.

The ESI+ FT-ICR mass spectrum (Figure 51) for gasoline 155 displays the presence of a different PIB series (characterised by the accurate mass measurement of the ion *m/z* spacing of the series) to that of the PIB identified within gasoline 159.

Henceforth, the PIB series identified in gasoline 159 will be referred to as PIB A and the PIB series identified in gasoline 155 will be referred to as PIB B.
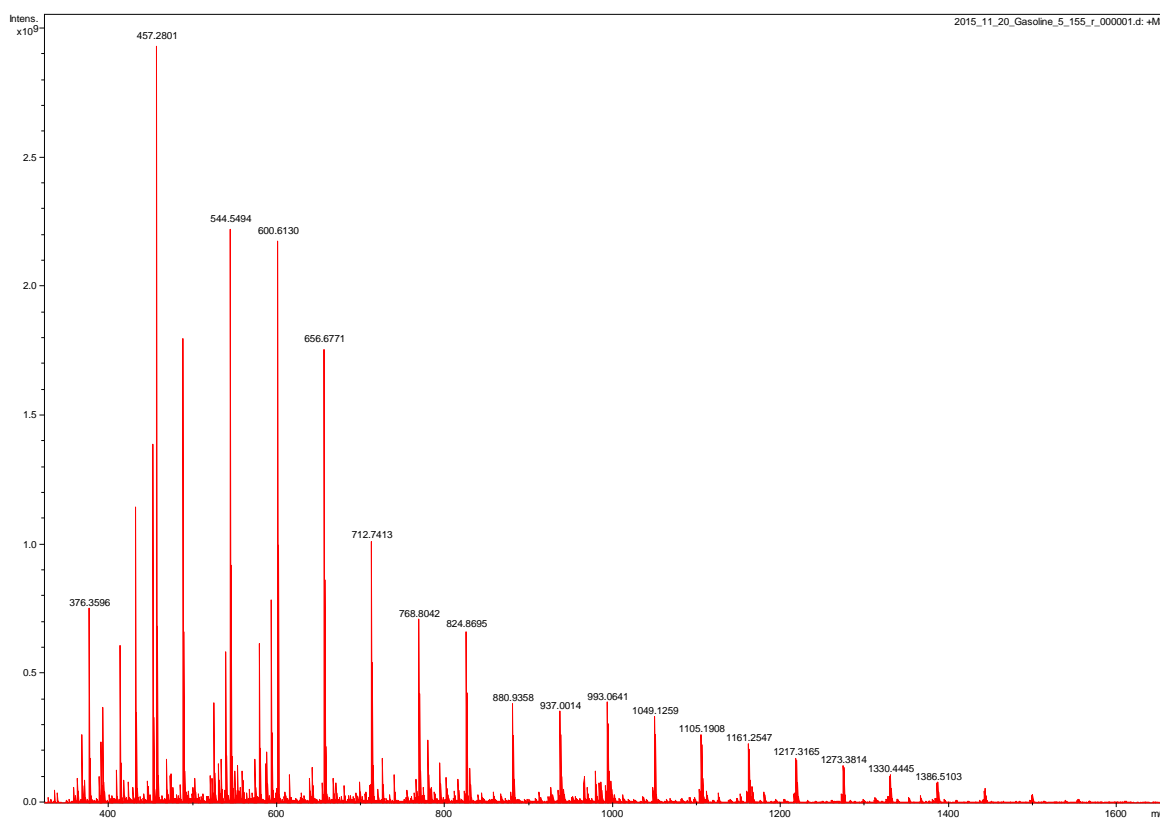
Figure 51 - ESI+ FT-ICR MS mass spectrum of 5 % gasoline 155 in methanol, *m/z* 350 -1600

The difference in *m/z* values between constituents of the PIB B series (Figure 52, bottom) when compared to the PIB A series (Figure 52, top) is + 14.0158 *m/z* units, this corresponds to an elemental formula of CH_2, this increase in *m/z* is likely the result of an increased chain length within the PIB B when compared to PIB A. Although for detailed structural information MS/MS experiments were undertaken (see sections 5.3.1.2, 5.3.2.2 & 5.3.3.1).

Figure 52 – ESI+ FT-ICR mass spectra of (Top): gasoline 159 (Bottom): gasoline 155

The gasoline samples were screened for the presence of polymeric additives, the presence of PIB A, PIB B and PPG are highlighted in Table 9.
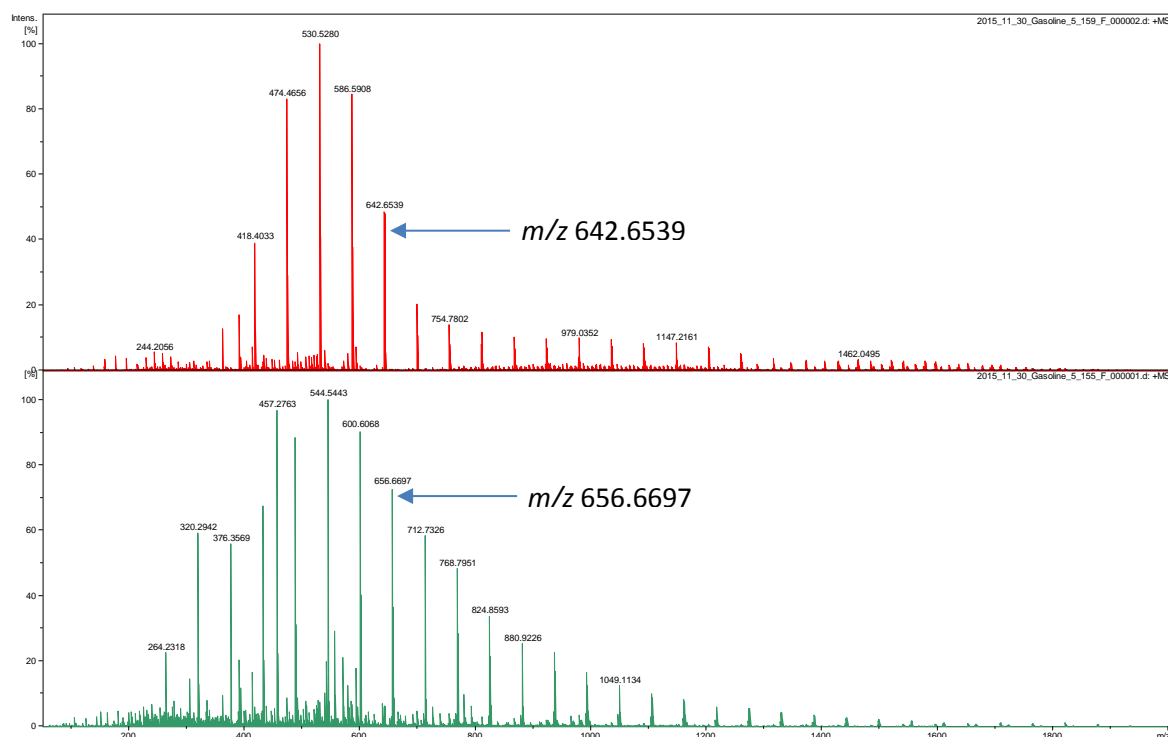
Table 7 – Presence of polymeric additives with gasoline samples

Series	Gasoline Sample #									
	155	156	158	160	162	167	159	161	164	166
PIB A	X	X	X	✓	✓	✓	✓	✓	✓	✓
PIB B	✓	X	X	X	X	X	X	X	X	X
PPG	X	X	X	✓	✓	✓	✓	X	✓	✓

5.1.1.3   ESI+ ionisation additives on polymer ionisation

The addition of an ionisation additive to the sample solvent, can promote the formation of a particular ionisation adduct. This can aid the structural elucidation, as well as provide a tool for selective ionisation of a particular compound within the complex gasoline matrix.

From the accurate mass measurement of the PIB and PPG molecules, it was determined that they are present as the protonated molecule and the sodiated molecule respectively. The addition of ionisation additives can influence the formation of an ion with the corresponding ionisation additive adduct, *i.e.* the addition of sodium formate, will promote the formation of a sodiated molecule. By producing the desired cationised molecule by ESI+, the molecular mass of the molecule responsible for to the detected ion can be calculated, aiding in identification.

Gasoline 159 was utilised to investigate the effect of ionisation additives on the ionisation of polymeric compounds as it contains both PIB (A) and PPG.

Upon the addition of ionisation additives, 25 mM formic acid or 25 mM ammonium acetate, to 5 % gasoline 159 in methanol, a similar profile of compounds is observed in the ESI+ FT-ICR mass spectrum when compared to the ESI+ FT-ICR mass spectrum for gasoline 159 in pure methanol (Figure 53). Although shifts in *m/z* and the suppression of the ionisation of particular compounds is observed, this is due to the preferential ionisation of particular compounds with a specific cation. This is influenced by the size and structure of the molecule, ionisation sites and steric effects.
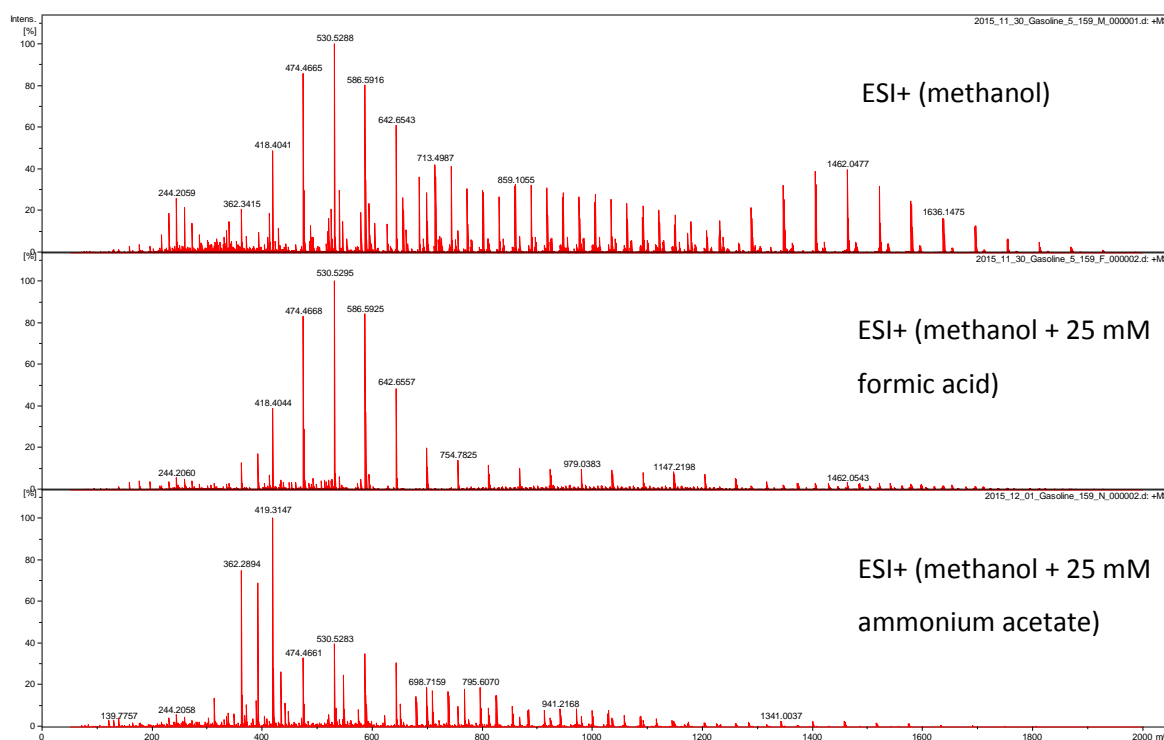
Figure 53 - ESI+ FT-ICR MS of 5 % gasoline 159 utilising various solvent compositions

5.1.1.3.1   Formic acid as an ionisation additive

With the addition of formic acid to the gasoline sample, the suppression of the ionisation of the PPG and the enhancement of the ionisation of the PIB is observed. An enlarged section of both methanol and methanol + 25 mM formic acid ESI+ FT-ICR mass spectra provides further detail (Figure 54).
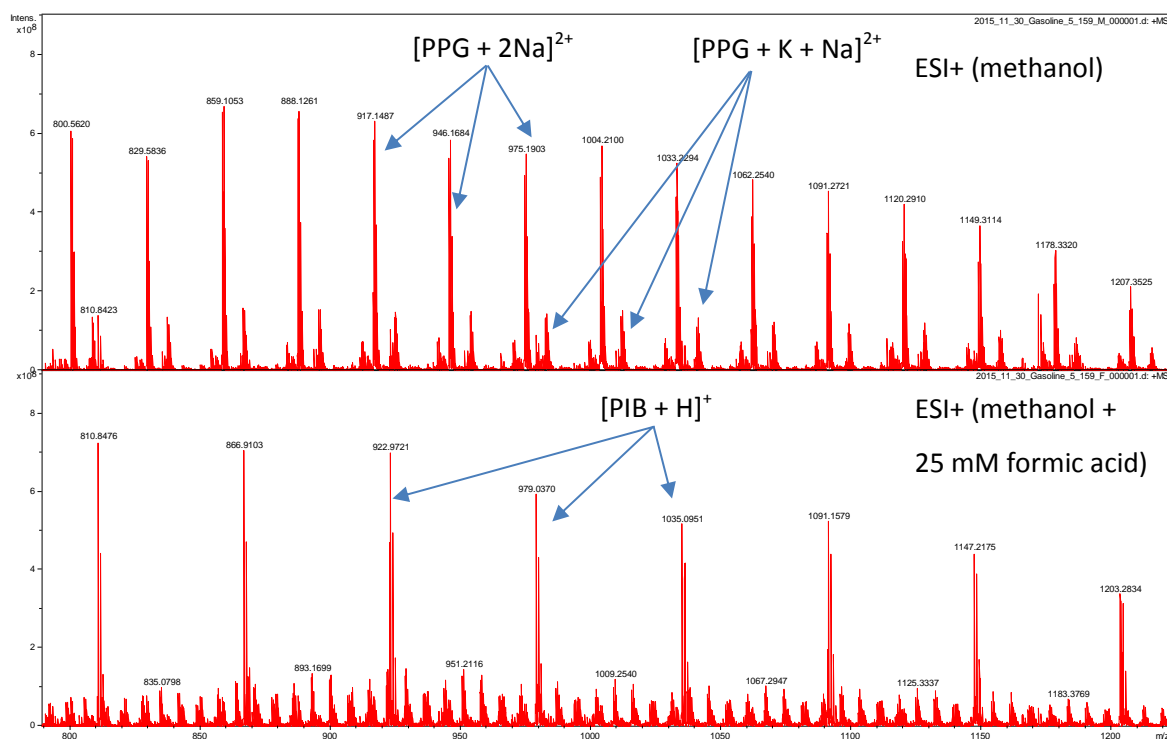
Figure 54 - ESI+ FT-ICR MS of 5 % gasoline 159 (*m/z* 700 – 1100) in methanol and formic acid additive to methanol

Upon the addition of formic acid, the *m/z* of PIB A remains unchanged when compared to the unadditised sample, this is coupled with a significate increase in intensity of the detected ion.

The observed increase in intensity of the PIB ions in the presence of protons provided by the formic acid would suggest that the molecule is protonated, as suggested by the elemental composition provided from the accurate mass measurement.

The identical *m/z* observed for the PIB in the methanol and when formic acid is introduced indicates that the PIB is protonated in both experiments.

The addition of formic acid to gasoline for ESI+ experiments selectively ionises the polyisobutylene within the gasoline sample, which could potentially be missed due to the low intensity and similar masses of the [PPG + Na + K]$^{2+}$ observed when no ionisation additive is used (Figure 54).

This is a powerful method for detecting the presence of derivatised polyisobutylene additives within gasoline samples with minimal sample preparation, as an example, gasoline 159 and 156 can be compared using this method (Figure 55).
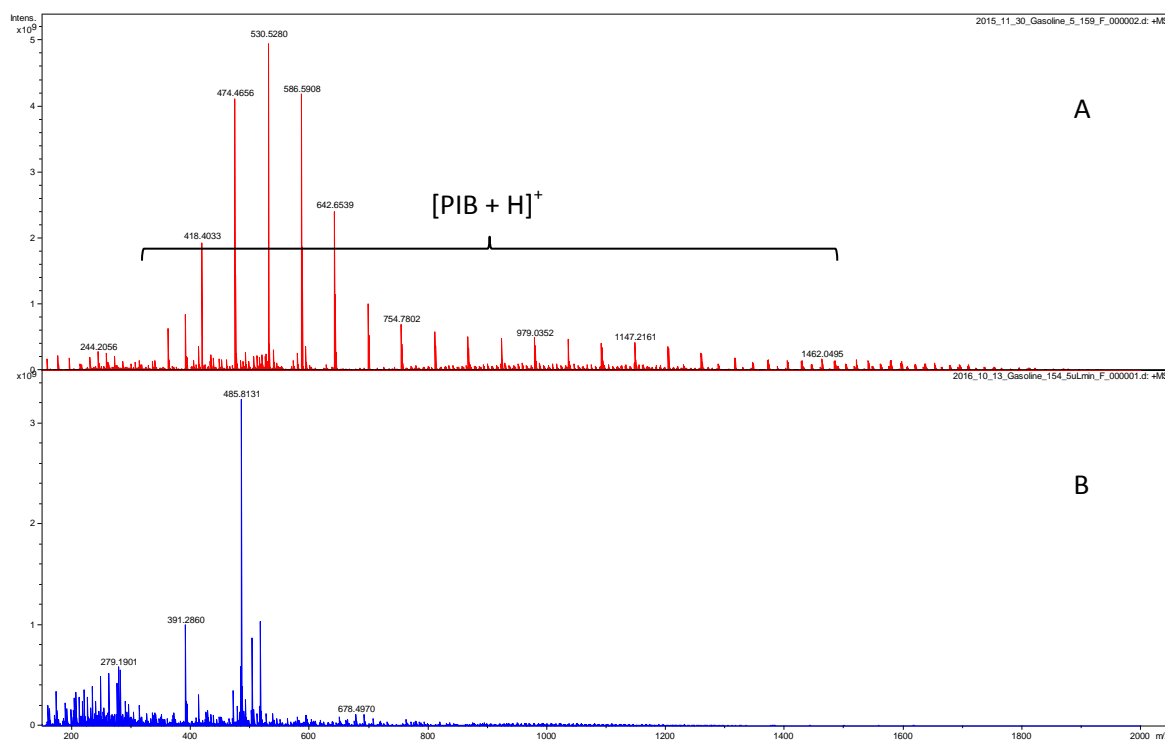
Figure 55 - ESI+ FT-ICR mass spectra comparison of 5 % gasoline samples in methanol + 25 mM formic acid (A): gasoline 159 (B): gasoline 156

It is evident from the ESI+ FT-ICR mass spectrum (Figure 55) that gasoline 156 polyisobutylene detergent compounds are absent, *i.e.* it is not additised with PIB.

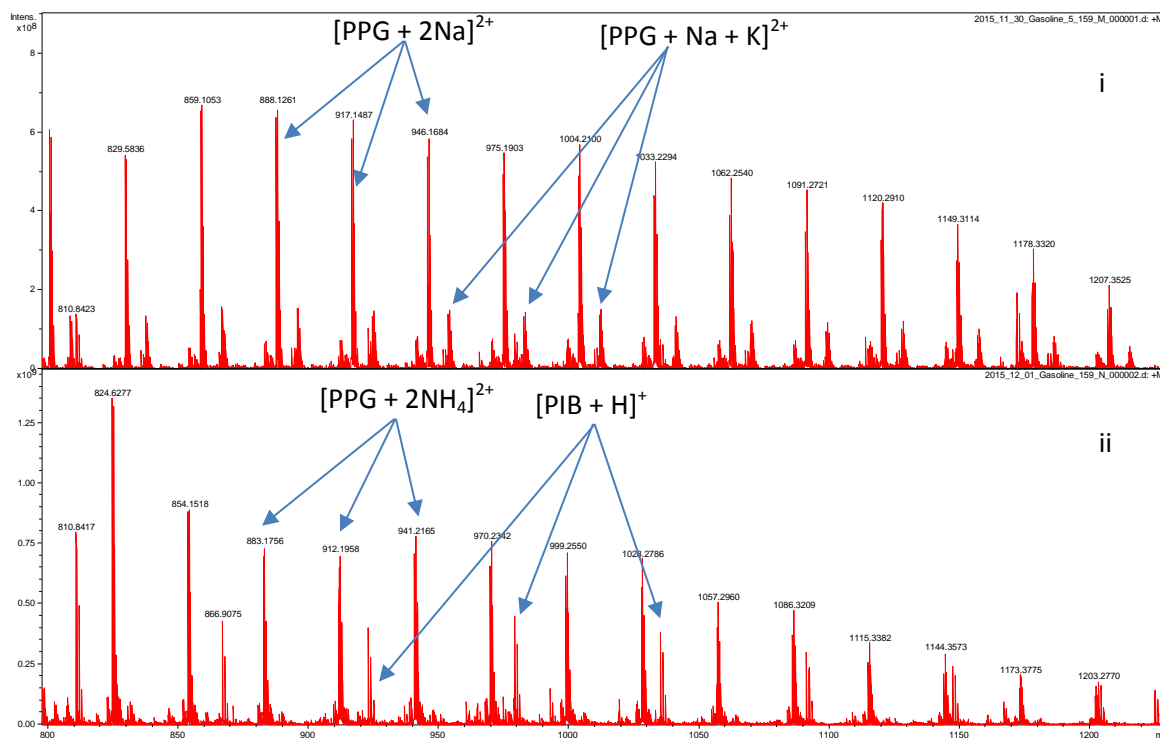### 5.1.1.3.2 Ammonium acetate as an ionisation additive

Figure 56 - ESI+ FT-ICR MS of 5 % gasoline 159 in (i): methanol and (ii): methanol + 25 mM ammonium acetate

The addition of ammonium acetate as an ionisation additive aids the formation of the ammoniated molecule during ionisation. Upon addition to gasoline 159 (Figure 56), the m/z of the double charged PPG oligomers previously described has reduced by 5 m/z units, this is characteristic of the difference between $[M + 2Na]^{2+}$ and $[M + 2NH_4]^{2+}$. It is therefore concluded, that upon the addition of ammonium acetate the PPG is present as the ammoniated molecule, and in the methanol sample, present as the sodiated molecule. This is in agreement with the element composition derived from the accurate mass measurement. The ammoniated molecule is of a similar intensity to that of the sodiated molecule within the methanol sample.

The PIB series within gasoline 159 is observable from ESI+ FT-ICR mass spectrum (Figure 56), without interference from the $[PPG + Na + K]^{2+}$ which is no longer present. The PIB ions remain in the protonated state, regardless of the addition of ammonium acetate.

The difference in ionisation behaviour between the PIB and PPG molecules results from the structure of each. The PIB chain is essentially a non-polar hydrocarbon with no basic sites for a cationisation event during ESI+, therefore it is concluded that the molecule must be protonated on a site located within the end group of the polymer. Conversely, the backbone of the PPG chain contains an oxygen atom for every monomer unit. Upon ionisation, it is possible for the PPG chain to surround the cation, allowing the oxygen atoms within the PPG molecules to form coordinate

bonds with the larger cations (sodium, ammonium and potassium). Due to the multiple oxygen atoms present in the PPG backbone it is possible for the larger PPGs to support addition cations and thus becoming multiply charged.

5.1.2   ESI- FT-ICR MS of polymeric additives

Gasoline 159 (containing PIB A and the PPG) and gasoline 155 (containing PIB B) were subject to ESI- FT-ICR MS experiments. For a molecule to ionise under negative ion electrospray ionisation conditions, the molecule must contain a site for deprotonation, the presence of deprotonated molecules within the mass spectrum provides further insight into the ion structure, *i.e.* the presence of a phenolic hydrogen.

For the ESI- experiments, the FT-ICR MS mass analyser parameters remained identical to that of the ESI+ experiments apart from the polarity of the electrospray source was switched to permit the desolvation of negative ions. Samples were made to 5 % gasoline in methanol, with 25 mM of NH$_4$OH to promote deprotonation. The resulting ESI- FT-ICR mass spectra for gasoline 155 and 159 is present (Figure 57).
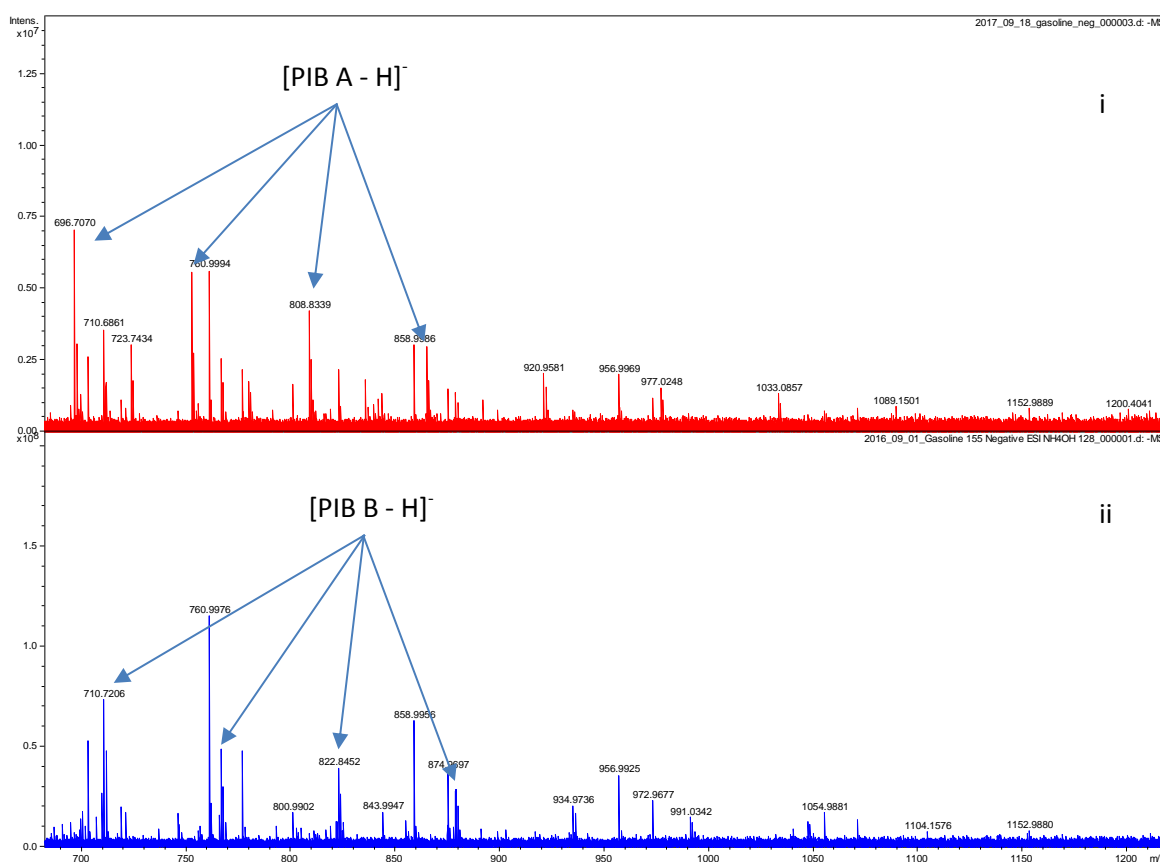

Figure 57 – ESI- FT-ICR mass spectra for 5 % gasoline in methanol + 25 mM NH$_4$OAc (i): gasoline 159 (ii): gasoline 155

From the mass spectra (Figure 57), PIB A can be observed within gasoline 159 in the deprotonated state, - 2 *m/z* units relative to that of the protonated molecules observed by ESI+. PIB B is also identified in the deprotonated state within gasoline 155. This ionisation event indicates the presence of a site for deprotonation within both PIB molecules, *i.e.* a phenolic PIB end group.

Ions corresponding to the PPG ion series are not identified within the ESI- FT-ICR mass spectra (Figure 57), suggesting the absence of a deprotonation site.

5.1.3   APPI+ FT-ICR MS of polymeric additives

For an analyte to be ionised by APPI, it must absorb a photons with a wavelength within the ultra-violet part of the electromagnetic spectrum, and have an ionisation potential lower than that of the energy of the photon. π-electron systems, *i.e.* aromatic, polyaromatic and conjugated dienes are suitable analytes for APPI.

APPI+ can be used to further probe the structure of the polymeric additives (PIB & PPG) within gasoline, if they ionise under APPI+ conditions the additives must contain a π-electron system. The ionisation of the analyte molecules can be achieved *via* two routes, direct ionisation and dopant assisted ionisation and both protonated molecules and molecular ions can be formed within the ion source. As the ionisation event takes place in the gas phase, it is not possible to form metal adduct ions, *e.g.* sodiated and ammoniated molecules as in ESI+.

Gasoline 159 was prepared at 5 % by volume in toluene (to act as an ionisation dopant). Utilising a vaporisation temperature of 350 °C, PIB A is identified within gasoline 159 *via* APPI+, thus the PIB molecules must contain a π-electron system.
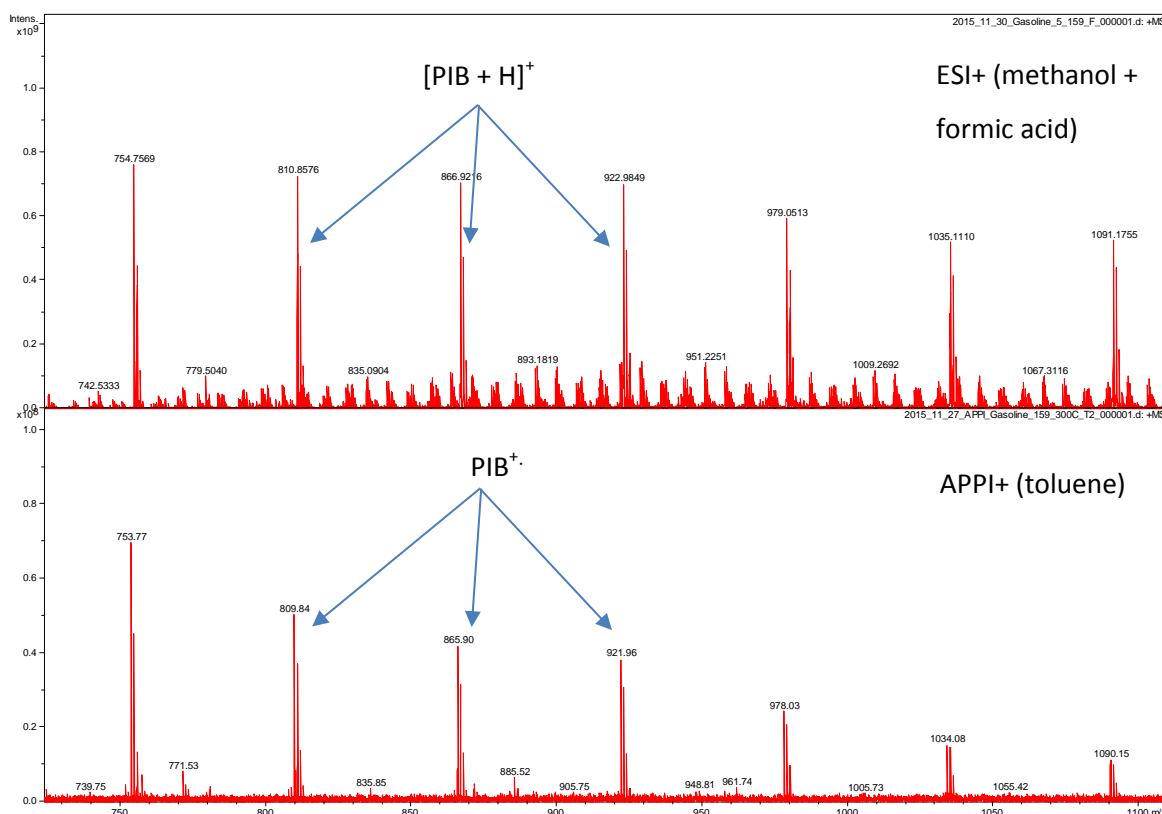
Figure 58 - ESI+ FT-ICR mass spectrum (*m/z* 700 – 1100) of 5 % gasoline 159 in methanol + 25 mM
formic acid (upper trace) compared to APPI+ FT-ICR mass spectrum (*m/z* 700 – 1100)
of 5 % gasoline 159 in toluene (lower trace)

When the *m/z* of the PIB A observed by ESI+ FT-ICR MS is compared to the *m/z* of the same PIB A
by APPI+ FT-ICR MS, a difference of − 1 *m/z* units is noted (Figure 58). This infers that under ESI+
conditions the PIB ion exists as the protonated molecule and under APPI+ conditions the
molecular ion is formed. This evidence confirms the protonated nature of the PIB within the
previous analysis.

PIB B is detected within gasoline 155 in a similar manner.

The PPG is undetected when APPI+ is applied to the gasoline sample, suggesting the absence of π-
electron system within the PPG molecule.

APPI is a selective ionisation technique for the analysis of these PIB additives and provides a
useful tool for the confirmation of the presence of π-bonding systems within molecules.

5.2   UHPSFC-SQD MS

FT-ICR MS experiments described thus far were direct infusion, whereby the sample is introduced
directly into the ion source, without prior chromatography. Therefore, constituents of the ion

population are susceptible to ion suppression effects, (*i.e.* as all analytes are present in the source at any one point, the presence of a particular compound may supress the ionisation of another compound present within the source). This can be negated with chromatography to some extent, as the analytes can be separated prior to ionisation.

The benefits of atmospheric pressure ionisation for the detection of polymeric additives within gasoline samples have been highlighted when compared to electron ionisation, as in gas chromatography mass spectrometry.

Interfacing API techniques to chromatography UHPSFC allows for the detection of high molecular weight, non-volatile compounds unobtainable by GC-MS, while negating ion suppression effects experienced by direct infusion FT-ICR MS. Although, the use of quadrupole mass analysers limits the mass resolution to 1 *m/z*, thus elemental composition cannot be obtained, as accurate mass measurement is not possible.

The non-polar, heptane like nature of the supercritical CO_2 mobile phase used in UHPSFC, has a good compatibility with the organic components of gasoline, when compared to the aqueous mobile phase of UHPLC.

5.2.1 PIB identification by UHPSFC-ESI+ SQD MS

Undiluted gasoline 159 was used to investigate the application of UHPSFC-ESI+ MS for polymeric gasoline additive detection. Initially, a HSS C18 column was used, with a 10-40 % gradient of methanol over 3 minutes. Formic acid in methanol was used to aid ionisation of the PIB.
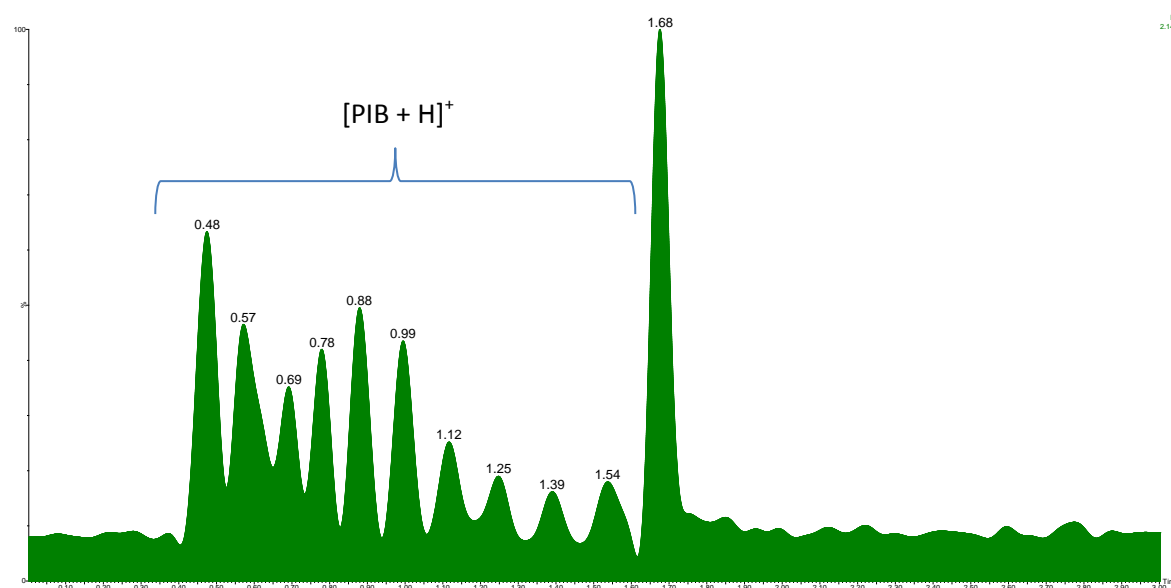

Figure 59 - UHPSFC-ESI+ SQD MS BPICC for gasoline 159

The series of peaks within the BIPCC (Figure 59) between T_R: 0.40 min. and 1.54 min. can immediately be identified as protonated PIB A from the *m/z* values in the mass spectra for this range of retention time (Figure 60). Each sequential peak corresponds to an increase in polymer chain length by one isobutylene unit (56 *m/z* units).
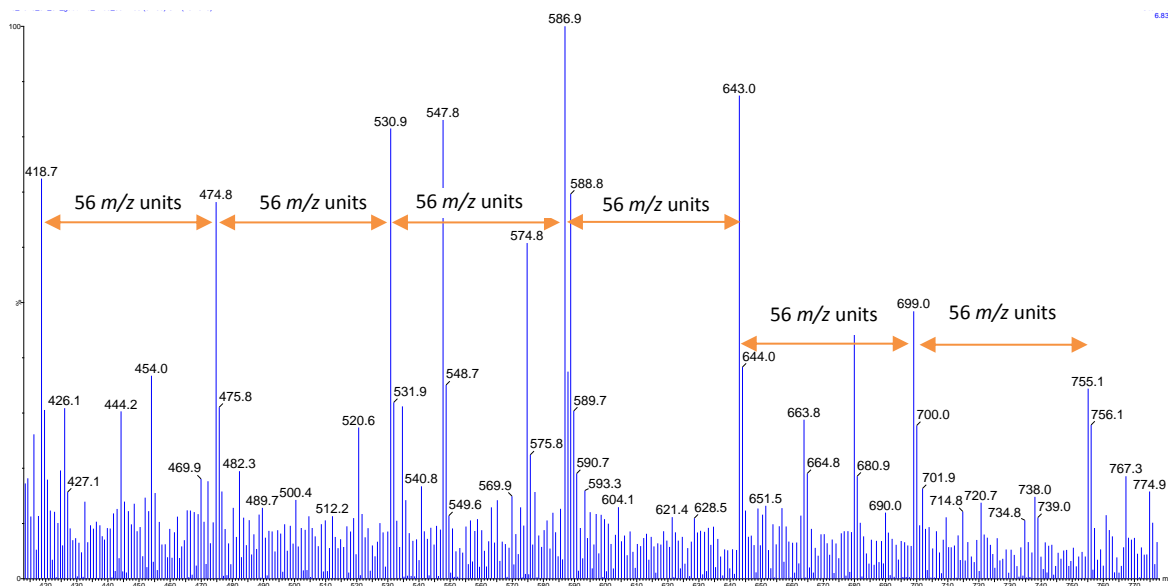

Figure 60 – UHPSFC-ESI+ SQD average mass spectrum between T_R: 0.40 min. and 1.53 min. (*Figure 59*)

The UHPSFC-ESI+ mass spectrum (Figure 60) is sufficient to identify the presence of PIB within a gasoline sample, from the characteristic 56 *m/z* unit peak spacing. Although the low resolution prevents any accurate mass measurement.

5.2.1.1   In-source collision induced dissociation (isCID) voltage on PIB intensity

The effect of in-source CID on the intensity of the polymer peaks was investigated (Figure 61), upon increasing the in-source CID voltage, the intensity of the polymer peaks increase, while the other peaks present in the spectrum decreased, due to the better transmission of the higher molecular weight polymers at higher cone voltages. Thus for the polymer detection and identification methods, a cone voltage of 60 V was selected. No fragmentation of the polymers was observed at any cone-voltage.
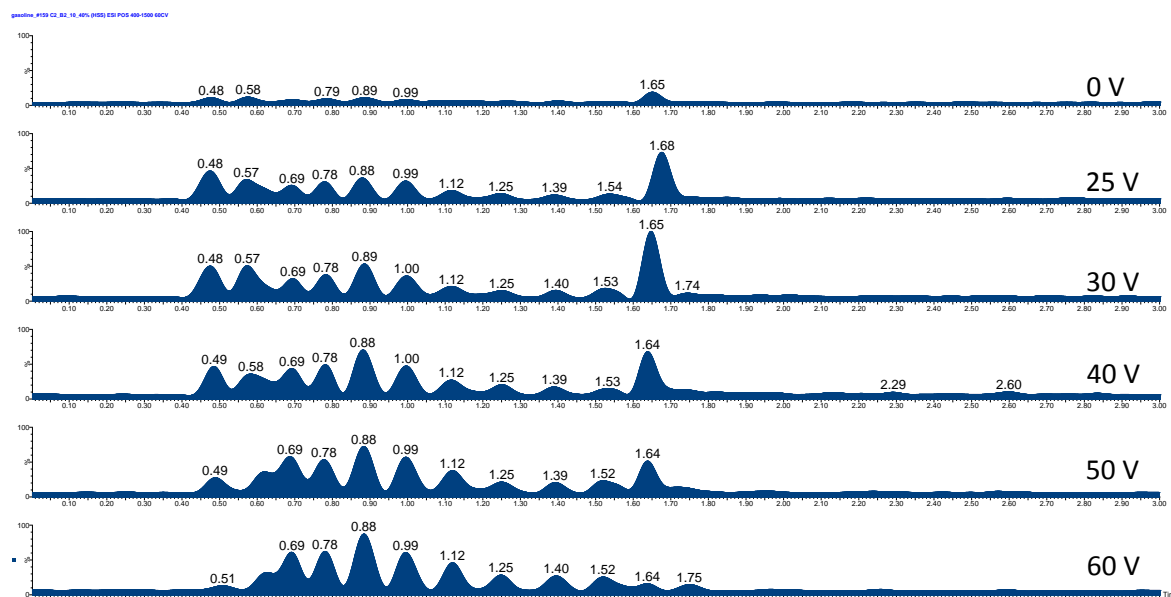
Figure 61 - UHPSFC-ESI+ MS BPICC for gasoline 159 at various cone voltages

The PIB peaks are identifiable within the untargeted BPICC. To reduce the interference from other compounds present in the gasoline and to highlight the presence of PIB, a targeted RICC can be created for the various [PIB A + H]$^+$ *m/z* values (Figure 62).
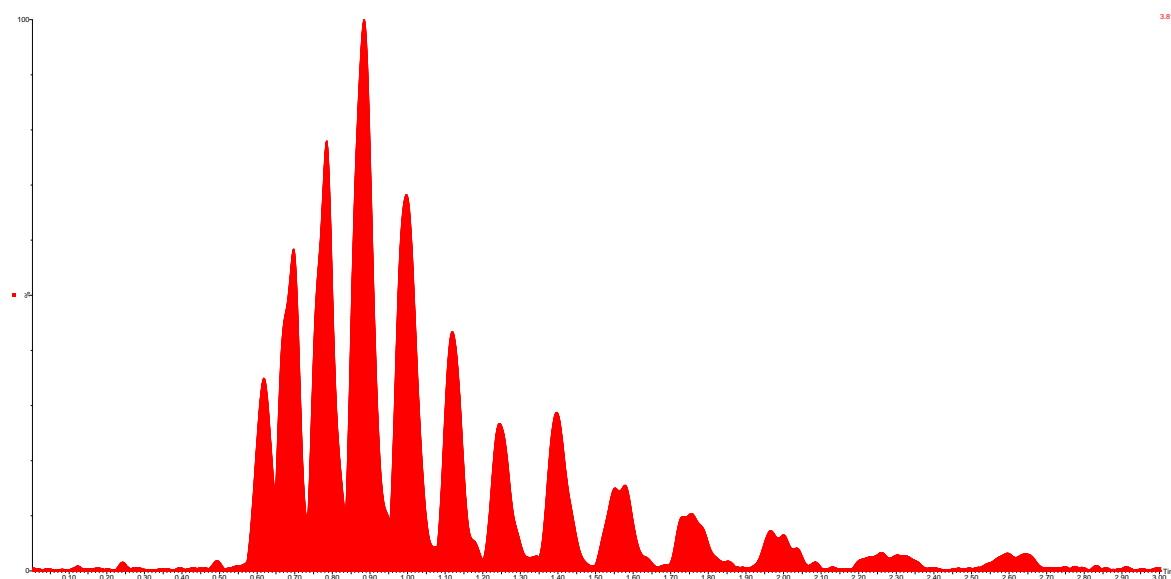

Figure 62 - UHPSFC-ESI+ MS RICC for PIB in gasoline 159 at various cone voltages

SIM methods could be adopted for the analysis of PIB to further increase the sensitivity, although this target approach may omit important information which can be seen within the untargeted TICC/BPICC.

5.2.1.2 Comparison of retention time for PIB A and B

PIB B, identified in gasoline 155 by ESI+ FT-ICR MS, differs from PIB A by a + 14 *m/z* unit difference, corresponding to a CH_2 unit, assigned by a comparison of accurate mass measurements. It was thought likely that this CH_2 group would be located within the end group of the molecule.

A difference of CH_2 in the end group of a polymer is unlikely to change the retention time of the molecule significantly, especially when taking into account, the lack of separation obtained, when increasing the polymer chain length by entire monomer units.

Gasoline 155 was analysed using the same method previously applied to gasoline 159, with an in-source CID voltage of 60 V for maximum sensitivity of the PIB compounds. A RICC was created (Figure 63) for the various *m/z* for PIB B identified within the BPICC.
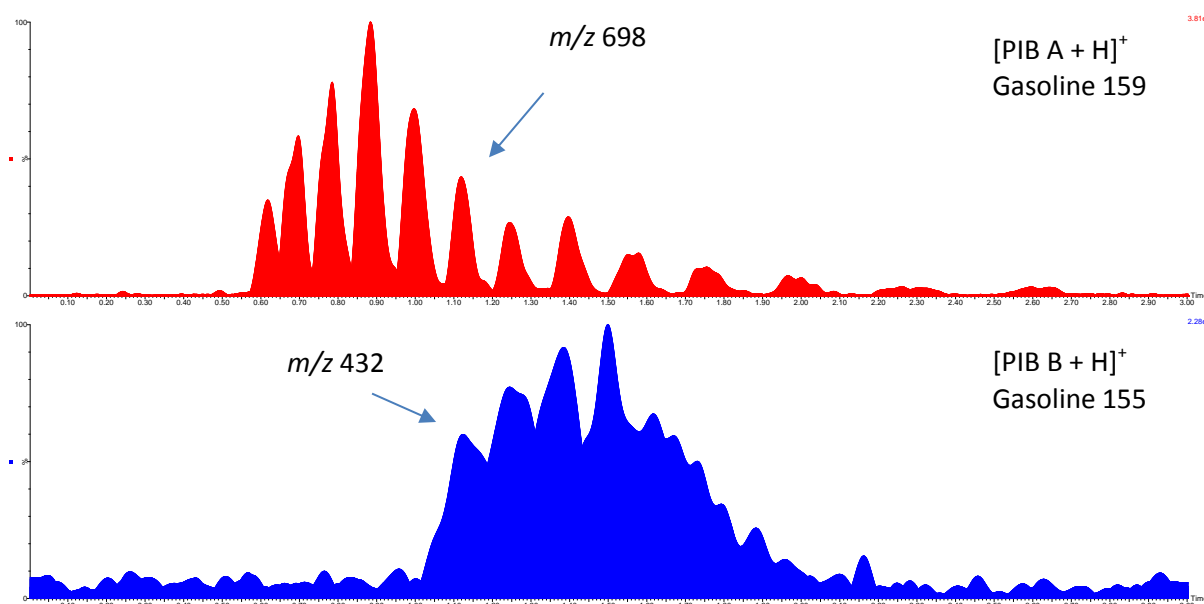

Figure 63 – UHPSFC-ESI+ SQD MS RICC for PIB A and PIB B

The RICC for PIB B within gasoline 155 (Figure 63) displays a complex, unresolved hump for all of the individual ions of the PIB B series. The chromatographic behaviour is different to that of PIB A, whereby chromatographic resolution was achieved for each individual PIB ions within the series.

A retention time overlap is observed between that of PIB A and B, although for a given retention time *e.g.* 1.12 min., the resulting masses are *m/z* 699 and *m/z* 433 for PIB A and B respectively. The data suggests that PIB B is more polar than PIB A, as the retention time is longer due to increased interaction with the stationary phase when compared to PIB A.

From the ESI+ FT-ICR MS data it was assumed they have similar structures differing by one CH_2 unit in the end group. Although, the presence of an additional CH_2 within a chain in the end group is not sufficient to warrant this difference in retention time.

The retention time for both PIB types suggests, that in fact the end groups of the polymers are different, although the total number of atoms they contain only differs by CH_2 (or 14 + n56, where n is a integer).

Thus the use of chromatography not only negates ion suppression effects but also highlights key differences in the chemistry of similar compounds, which are not immediately obvious from the mass spectrum alone, this is displayed in sections 5.3.1.2 & 5.3.2.2.

5.2.2   PPG identification by UHPSFC-ESI+ SQD MS

PIB A and B were readily identifiable from the BPICC of their respective gasolines, although the PPG ions identified by ESI+ FT-ICR MS are not observable within the chromatograms. This is likely due to the introduction of 1 % formic acid as an ionisation additive, it has been shown that PIB protonates regardless of the ionisation additive used, although with formic acid, the intensity of the ion peaks is enhanced. PPGs have been shown to sodiated and ammoniate rather than protonate. As with the ESI+ FT-ICR MS, the PPG ions are likely to be present, although their low intensity, due to the ionisation additive used, may prevent identification within the BPICC.

Gasoline 159 was analysed using the same method at previous, (1 % formic acid in methanol was used as an ionisation additive). An average mass spectra across the entire chromatographic range of gasoline 159 was constructed (T_R: 0.00 – 3.00 min.) (Figure 64).
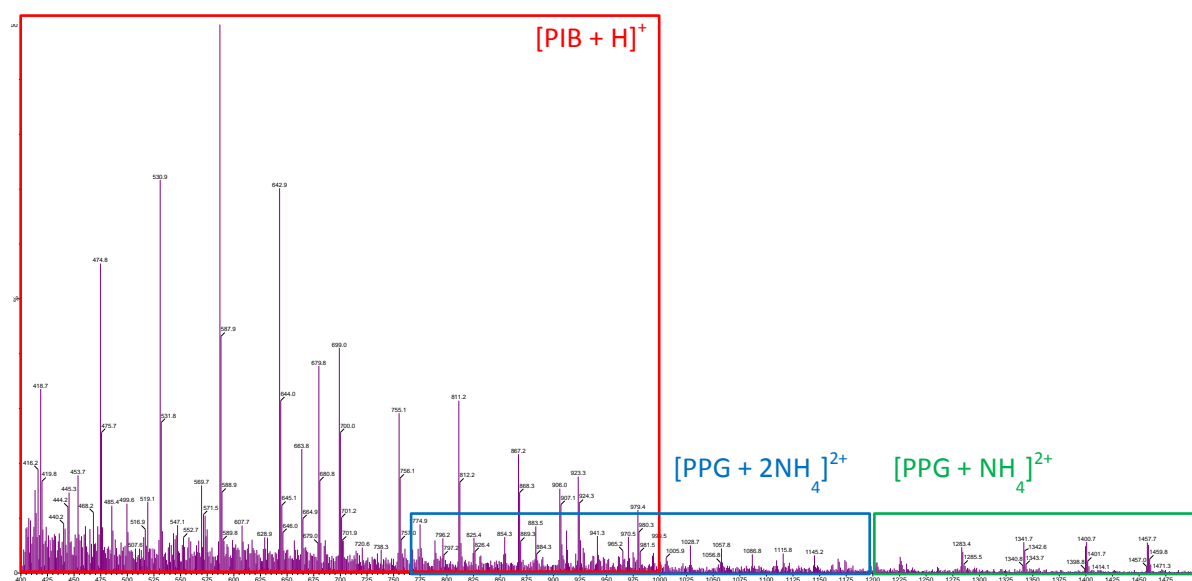

Figure 64 – UHPSFC-ESI+ SQD mass spectrum for T_R: 0.00 – 3.00 min. of gasoline 159

From the mass spectrum (Figure 64), the singly charged and doubly charged PPG are observable, as ammoniated molecules. The intensity of the ions is lower than that of the protonated PIB due to the addition of formic acid as an ionisation additive. The low intensity of the two PPG series is responsible for their absence from the TICC/BPICC.

The UHPSFC-ESI+ SQD average mass spectrum is comparable to that of the ESI+ FT-ICR mass spectrum, when ammonium acetate is used to aid ionisation (Figure 65).
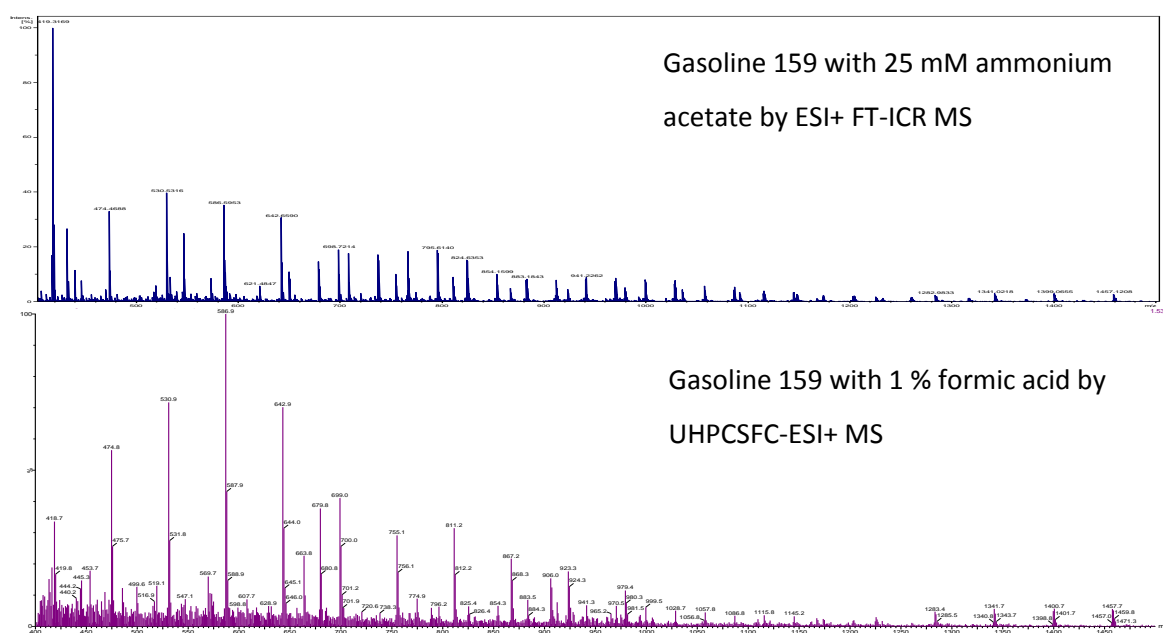

Figure 65 – Comparison of mass spectra. Top: Gasoline 159 with ammonium acetate by ESI+ FT-ICR MS. Bottom: Gasoline 159 by UHPSFC-ESI+ MS

The formation of the ammoniated molecule for both the singly charged and doubly charged PPG ions is likely the result of the relativity high concentration of ammonium acetate (25 mM) within the chromatographic modifier, supplying a source of ammonium ions.

The detection of ammoniated PPG molecules within gasoline samples by UHPSFC-ESI+ SQD is possible when formic acid is used as the ionisation additive, although the addition of sodium formate (5.2.2.1) was investigated as this was likely to increase the sensitivity, as observed in the ESI+ FT-ICR MS experiments.

5.2.2.1   Sodium formate as an ionisation additive

The make-up flow was changed from 1 % formic acid to 10 μM sodium formate, in an attempt to force the PPG to the sodiated form, which is readily observable by ESI+ FT-ICR MS.

On addition of the sodium formate, no sodium adducts were present in the mass spectra for the PPG (Figure 66). The PPG remained in the ammoniated form, this is possibly due to the relatively

high concentration (25 mM) of ammonium acetate in the chromatographic modifier flow, when compared the low concentration of sodium.
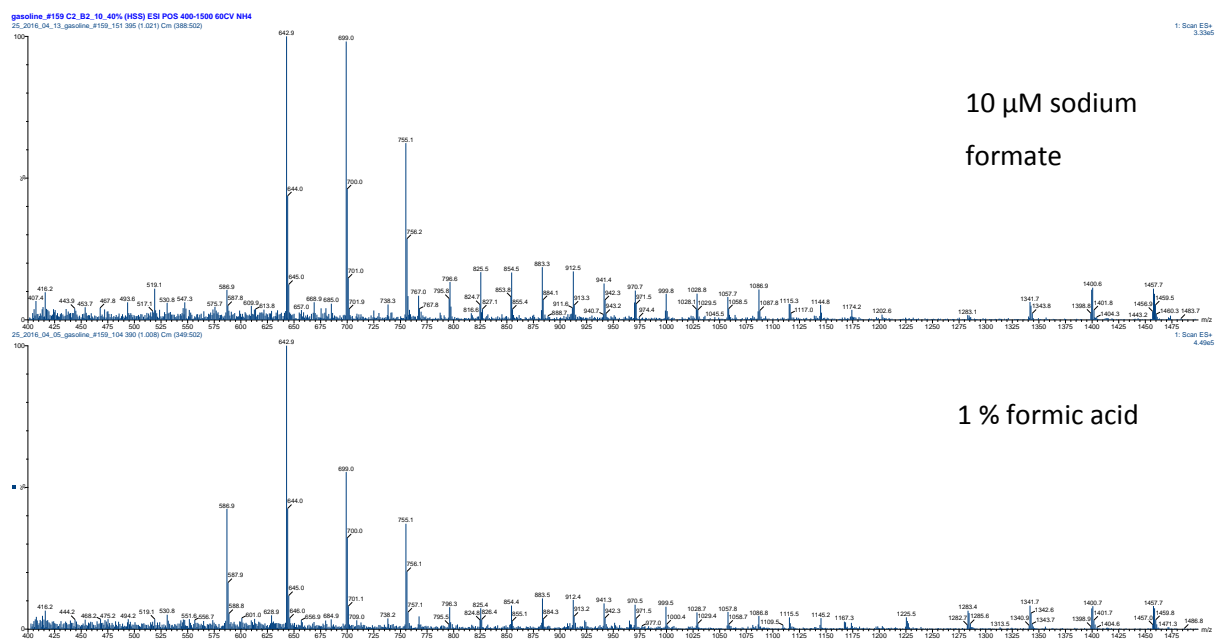
Figure 66 – UHPSFC-ESI+ SQD mass spectra comparison of 1 % formic acid and sodium formate as an ionisation additive

5.2.2.2   Chromatography of PPGs

The ammoniated PPG ions present in the UHPSFC-ESI+ SQD mass spectrum can be used to produce reconstructed ion chromatograms, to identify the retention times for each of the PPG molecules. The RICCs for the observable doubly and singly charged ions are presented (Figure 67 & Figure 68 respectively).

Figure 67 – UHPSFC-ESI+ MS RICC for doubly charged PPG
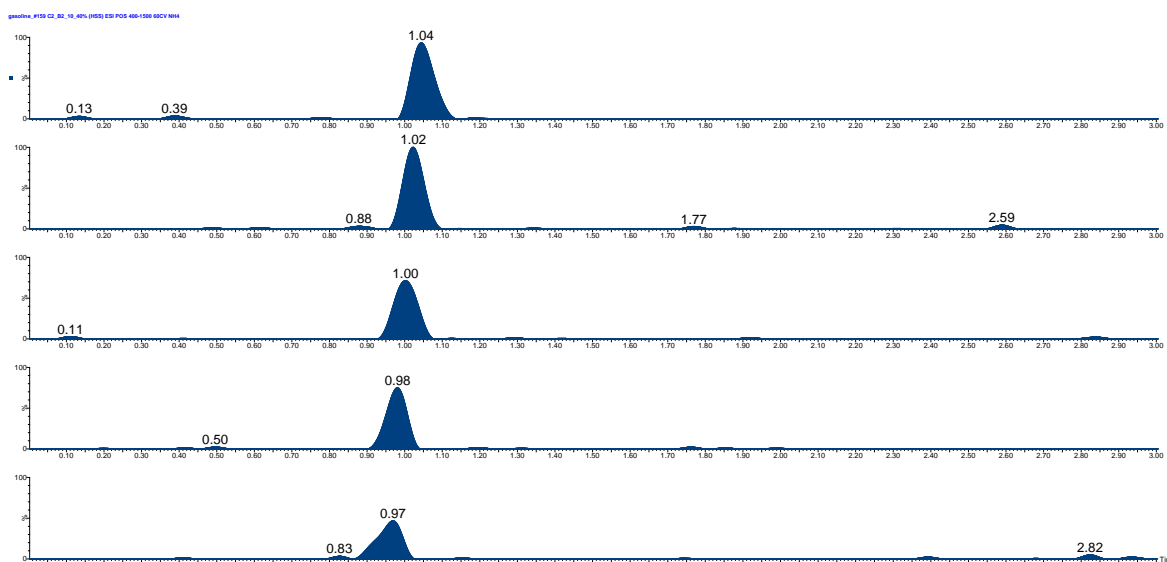
Figure 68 - UHPSFC-ESI+ MS RICC for singly charged PPG

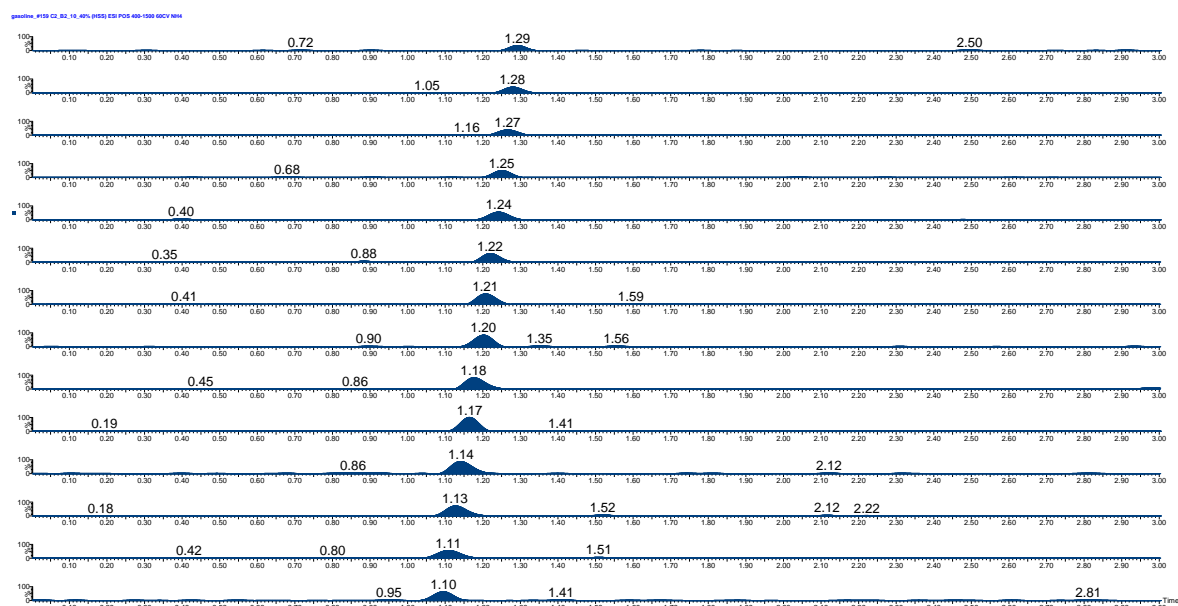Retention time increases with increasing chain length, although compounds increasing by one monomer units cannot be chromatographically resolved from the previous using this method. Further chromatographic separations were investigation using different stationary phases, mobile phase modifiers and changes in modifier gradient, although little effect on separation was observed.

This method is sufficient for detection of the polymers within a particular gasoline sample, by reconstructing ion current chromatograms for the specific ions of each polymer unit. A peak present at the correct retention time in these RICC indicates the presence of that specific oligomer. This screening method is presented for gasoline 159 (Figure 69).
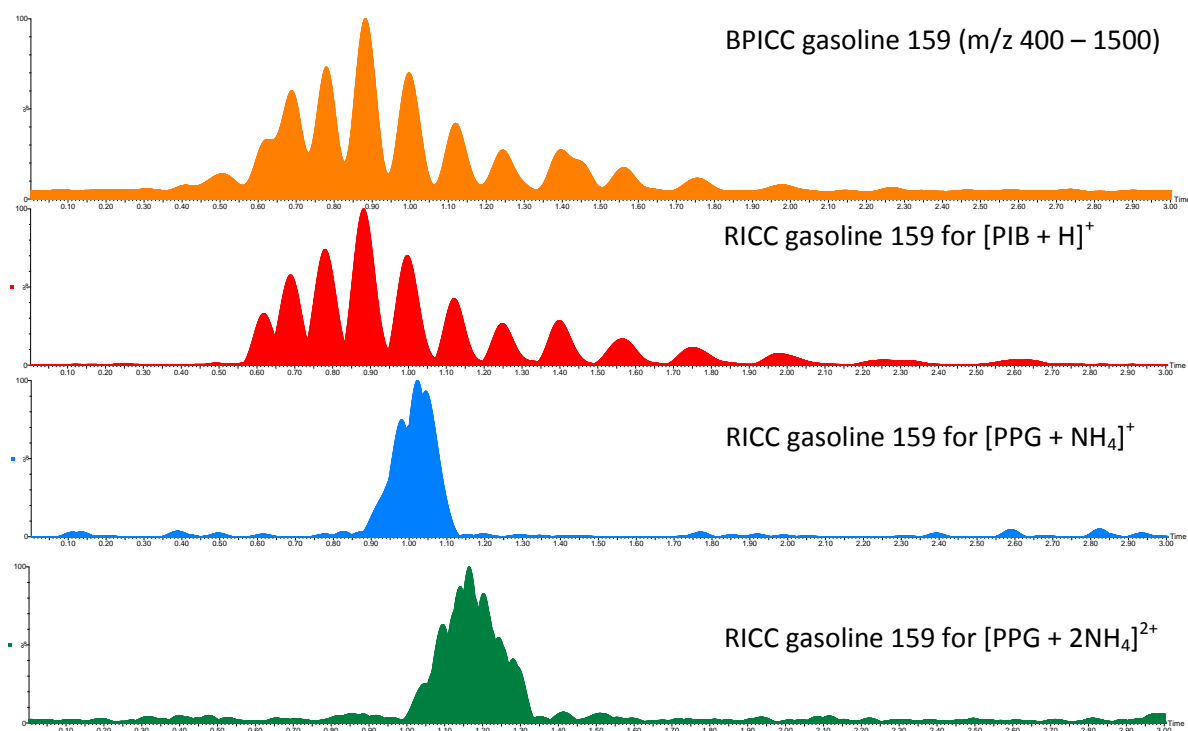
Figure 69 – UHPSFC-ESI+ MS RICCs for various polymers in gasoline 159

From the ESI+ FT-ICR MS data analysis (section 5.1.1.2) for the singly charged and doubly charged PPG ions within gasoline 159, it was calculated that the molecules were the same, although present in two different charge states. Although, if a [PPG + NH$_4$]$^+$ and a [PPG + 2NH$_4$]$^{2+}$ observed within the UPHPSFC-ESI+ mass spectrum can be attributed to a single molecule, the retention time by UHPSFC-ESI+ MS (Figure 69) of the singly charged PPG should be shared with that of the doubly charged PPG, which is not immediately evident within the UHPSFC chromatograms (Figure 69).

If the mass spectrum of gasoline 159 (Figure 70) is analysed, this phenomenon can be attributed to the constraints of the *m/z* range scanned, and the low ion intensity of the doubly charged species below *m/z* 738.

Figure 70 – UHPSFC-ESI+ SQD MS of gasoline 159

By calculation, the $[M + 2NH_4]^{2+}$ and $[M + NH_4]^+$ labelled in UHPSC-ESI+ mass spectrum (Figure 70) are ions of the same molecule in different charge states. This can be confirmed by a comparison of retention times between the singly charged and doubly charged ions.

It is observed from the RICCs (Figure 71) for both ions ($[M + NH_4]^+$ and $[M + 2NH_4]^{2+}$ (Figure 70)), that the retention time is identical, thus confirming a single PPG series is responsible for the two charge states observed. The RICC for the lower m/z members of the doubly charged series are limited by their low ion intensity, whereas the singly charged species is limited by the upper m/z range constraint.

Figure 71 – UHPSFC-ESI+ SQD MS RICC for ions A^+ and A^{++} (Figure 70)

5.3 Polymeric additive end-group determination

Polymeric gasoline additives can be identified as PIB or PPG from the ESI+ FT-ICR mass spectra and UHPSFC-ESI+ mass spectra, by the characteristic spacing between the peaks within the ion series, with *m/z* values differing by the mass of the monomer units. Ionisation additives can be used to manipulate the samples, enhancing ion intensity and simplifying the mass spectrum.

Different ionisation techniques provide further information on the ions structure. Ionisation by APPI+ indicates the presence of aromatic systems or conjugated double bonds within the molecule. Ionisation by ESI- indicates the presence of a site for deprotonation, *i.e.* a phenolic derivatised PIB, (e.g. a PIB Mannich).

Chromatography can be used to negate ion suppression issues, and also highlight differences between the chemistries of the additives *i.e.* PIB A and PIB B only differ by CH_2, although their chromatographic behaviour is different.

Identification and detection of the fuel additives thus far has been determined by the characteristic *m/z* spacing of the polymeric chain. The polymers contain an end group, which is responsible for the adhesion to metal surfaces and deposits within the engine, and thus, the effectiveness of the additives relies greatly on the structure of this end group.

A series of experiments has been developed to determine these end groups.

5.3.1 Polyisobutylene A end group determination

5.3.1.1 Linear regression of PIB A ion series from ESI+ FT-ICR mass spectrum

PIB A is present in gasoline 159, through previous experimentation it has been identified as singly charged and in the protonated form when analysed by ESI+. This was determined by comparison to the APPI+ spectrum for the sample fuel sample, a difference of − 1 *m/z* unit is observed between the positive ion APPI and ESI data, this is due to the formation of the molecular ion in the APPI+ ionisation event.

A series of possible end group masses can be calculated v*ia* linear regression[84].

If the mass of each polymer (measured mass · charge state) (y) is plotted against the number of monomer units (x) then the gradient of the line (m) is the monomer mass and the intercept (c) is the sum of the end group masses and cations. Although, the number of monomer units within the PIB chain for an ion of a specific *m/z* value is unknown. Thus, the number of monomer units is used as a place holder, as the final measured end group mass can be increased or decreased by

multiples of 56.0620 *m/z* units, to an upper limit equal to the mass of the ion with the lowest *m/z* observable within the PIB series, and a lower limit when $0 < m_e < 56$, (where m_e is the mass of the polymer end group). This results in a series of possible end group masses, corresponding to the various number of monomer units possible for each PIB ion.

Two possible end group masses for PIB A are calculated as an example v*ia* linear regression (where *m/z* 362.3393 corresponds to n = 4 (Figure 72) or n = 2 (Figure 74)), using the ESI+ FT-ICR MS of 5 % gasoline 159 in methanol with 25 mM formic acid, thus allowing calculation of the accurate mass of the end group.
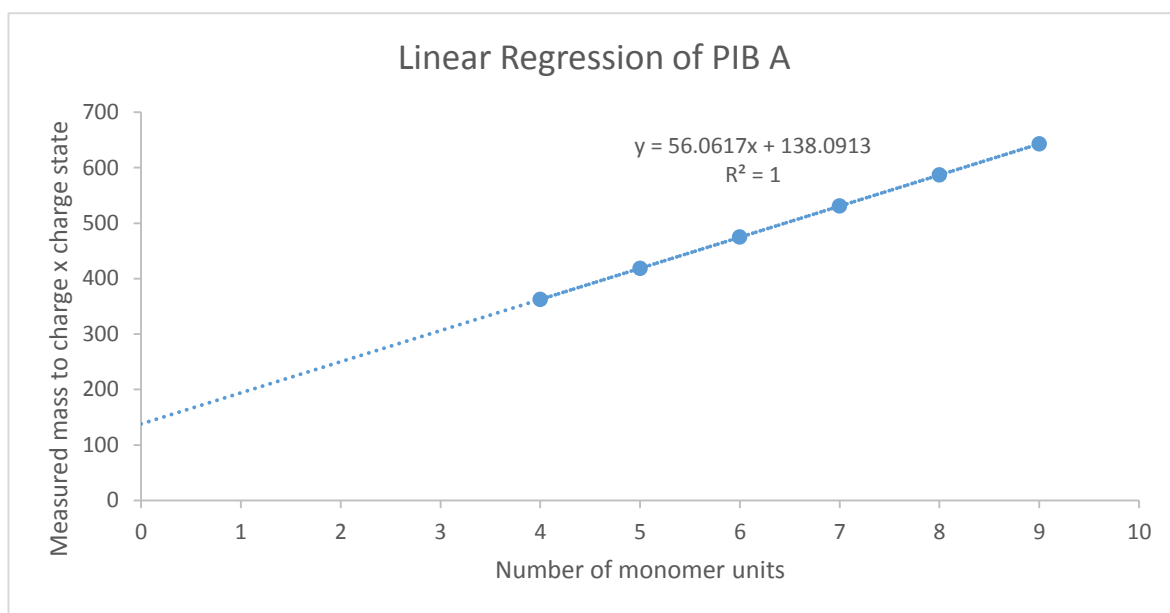

Figure 72 – Determination of PIB A end group mass by linear regression where *m/z* 362.3393 corresponds n = 4

When the gradient from the graph (Figure 72) (measured monomer mass) is 56.0617 *m/z* units which corresponds to an isobutylene monomer unit with an exact mass of 56.062 *m/z* units*.* The intercept was calculated at 138.0913 *m/z* units*,* this is the sum of the masses of the end groups plus the sum of the masses of any cations present on the molecules. This is a singly charged protonated molecule so, the cation mass is equal to 1.0078 gmol^{-1}. This can be subtracted to give the mass of the summed end groups as 137.0835 *m/z* units.

This corresponds to an elemental formula of $C_8H_{11}NO$ (4.1 ppm error, 0.6 mDa). The termination of the polymerisation of PIB results in one end group becoming a single hydrogen, so the other end group has an elemental formula of $C_8H_{10}NO$. This could correspond to a structure previously proposed for a PIB additive detected within gasoline[85] (Figure 73), the ions of which are isobaric to the PIB A ions observed in gasoline 159.
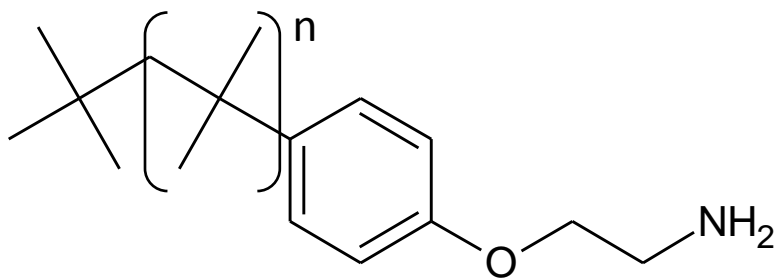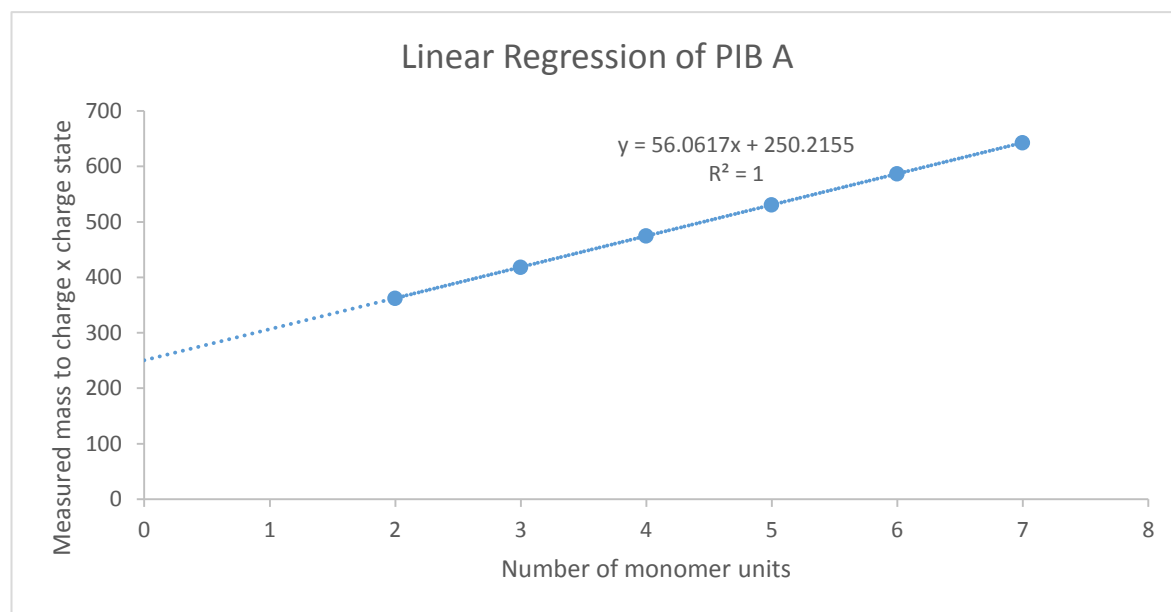
Figure 73 – Proposed PIB A Structure[85]

Figure 74 - Determination of PIB A end group mass by linear regression where m/z 362.3393 corresponds n = 2

When n = 2 (Figure 74) is assigned to m/z 362.3393, the line is translated horizontally, *i.e.* the gradient remains the same, but the intercept has increased, thus the end group mass has increased to m/z 250.2155. In the same manner as the previous, the mass of a hydrogen atom must be subtracted to calculate the mass of the end groups (protonated state), resulting in a calculated m/z of 249.2077. This corresponds to an elemental formula of $C_{16}H_{27}NO$ (6.0 ppm error, 1.5 mDa) for both end groups, one of which is a hydrogen atom, the other possible end group is $C_{16}H_{26}NO$.

Linear regression of the ion series observed in the ESI+ FT-ICR mass spectra can be used to obtain a series of accurate mass values for the end group of the molecule. The charge state and cation(s) must be known, which can be obtained from the m/z difference between the ^{12}C and ^{13}C ions and the use of ionisation additives respectively.

Although, from the use of linear regression in isolation, choosing the correct end group mass from the range and structural elucidation is not possible. Further experimentation is required, *i.e.* MS/MS.

5.3.1.2 Tandem MS (MS/MS) of PIB A

ESI+ FT-ICR MS/MS and ESI+ QIT MS/MS were utilised for the analysis of PIB A, providing accurate mass measurement and fragmentation information respectively.

Initially, 5 % gasoline 159 in methanol with 25 mM formic acid was analysed by ESI+ FT-ICR MS, the resulting mass spectrum is displayed (Figure 75).
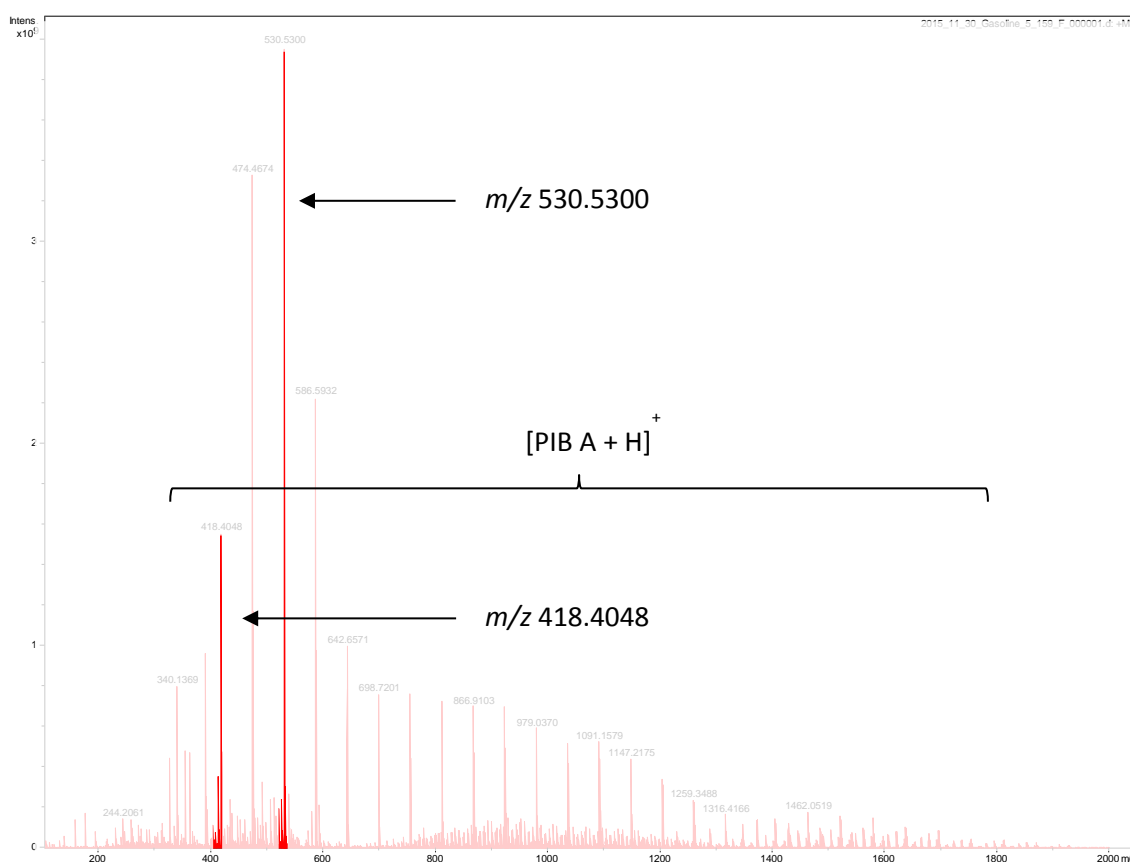

Figure 75 - ESI+ FT-ICR MS of 5 % gasoline 159 in methanol with 25 mM formic acid, isolated ions are highlighted

Ions of *m/z* 530.5300 and 418.4048 were selected for MS/MS experiments, and were isolated in the quadrupole, within separate experiments. The CID collision energy was varied to obtain optimal fragmentation (abundance of fragment ion peaks), 35 V for *m/z* 530 and 20 V for *m/z* 418. The resulting product ion mass spectra are displayed (Figure 76).
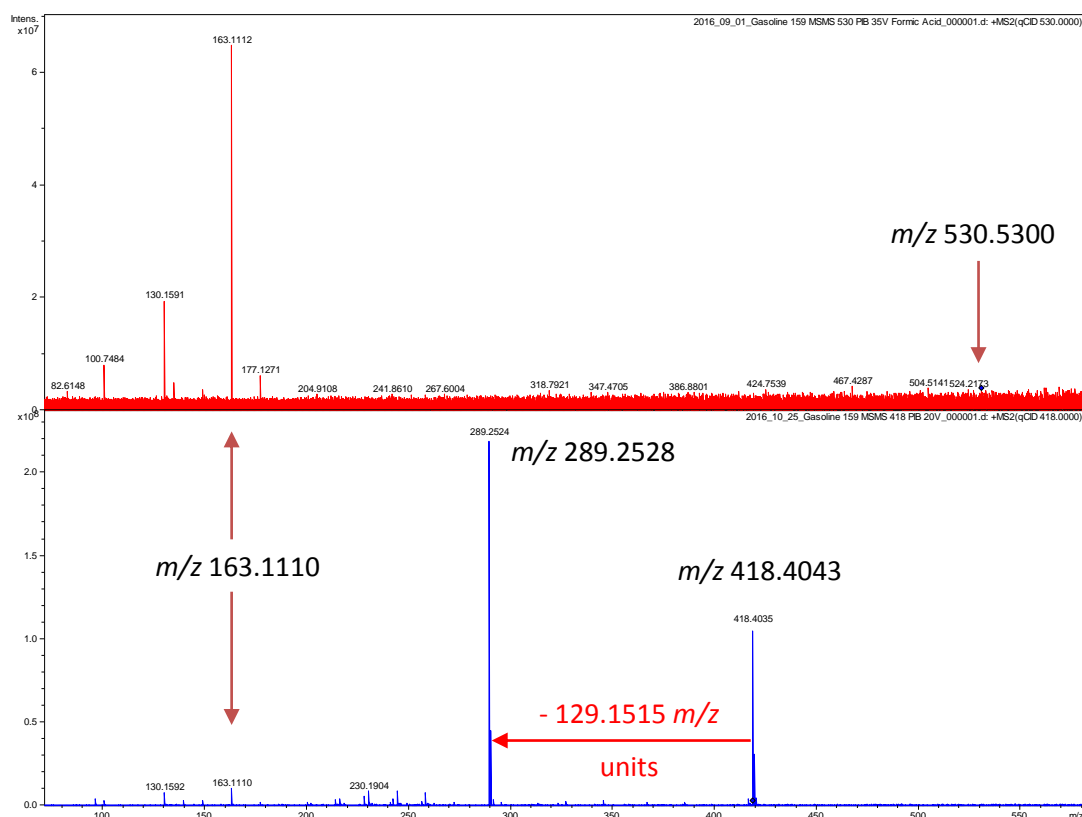
Figure 76 - Comparison of ESI+ FT-ICR product ion spectra for PIB A (Top): *m/z* 530 & (Bottom): *m/z* 418

The fragmentation of *m/z* 530 ([PIB A + H]$^+$) (Figure 76) results in a series of ions at nominal *m/z* 177, 163, 149, 135 and 130. The fragmentation of *m/z* 418 ([PIB A + H]$^+$) (Figure 76) results in the identical series of peaks when compared to the fragmentation pattern of *m/z* 530, although in addition to this an ion at *m/z* 289 is observed, which corresponds to a loss of 129 *m/z* units. The accurate mass for these ions is discussed in section 5.3.1.2. The rationale for these experiments was to compare the fragmentation of different PIB ions within the series, the identical *m/z* values of the some of the product ions would suggest they originate from the polymer end group.

Fragmentation of the [PIB A + H]$^+$ was also achieved by ion trap mass spectrometry, low *m/z* ions in the [PIB A + H]$^+$ series were isolated and fragmented. *m/z* 474, 418 and 362 were fragmented at collision energies of 30 %, these ions were chosen as they displayed the loss of 129 *m/z* units, whereas this loss is not readily observable within the product ion mass spectra for higher *m/z* ions. The resulting mass spectra are shown in Figure 77.
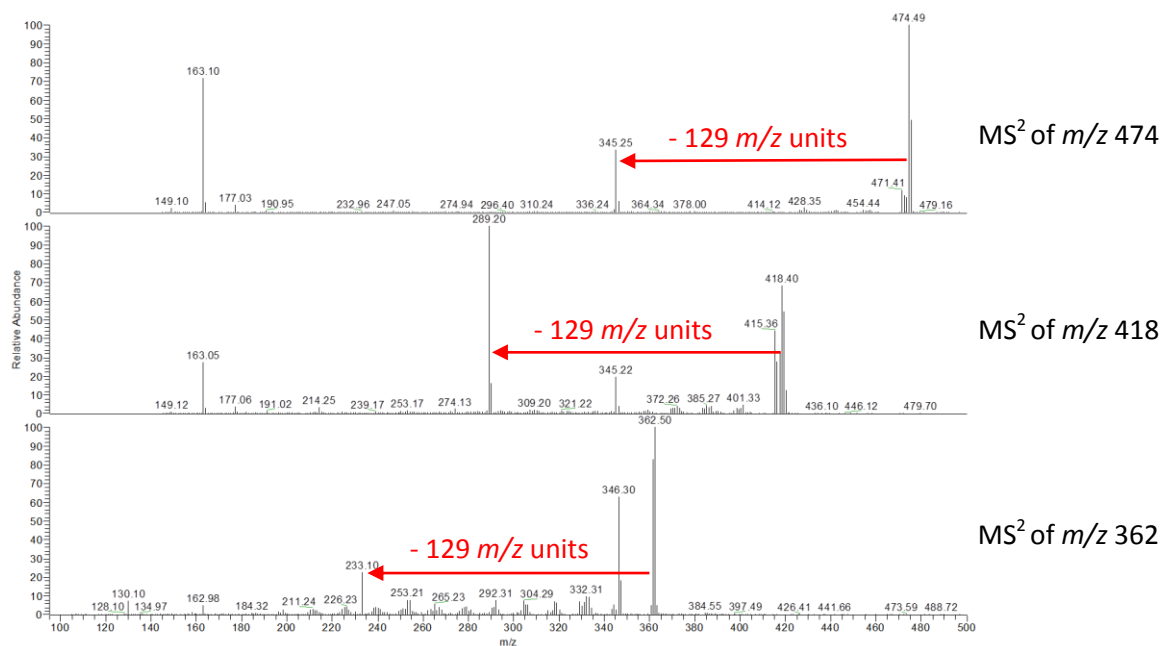
Figure 77 – Comparison of ESI+ QIT MS² product ion spectra of three PIB A ions

The MS² product ion mass spectra of PIB A (Figure 77) resembles that of the fragmentation observed in the FT-ICR MS/MS data (Figure 76), ions at m/z 177, 163, 149, 135 and 130 are observed. The protonated molecule is also observed to lose 129 m/z units in each case identical to the fragmentation of m/z 418 in the FT-ICR MS/MS experiments.

The accurate mass measurement of the loss of m/z 129 is identified as m/z 129.1515 which corresponds to an elemental formula of $C_8H_{19}N$ (1.5 ppm error, 0.2 mDa).

The accurate mass of the other ions common for all PIB molecules was investigated using m/z 530 as an example (Figure 78).
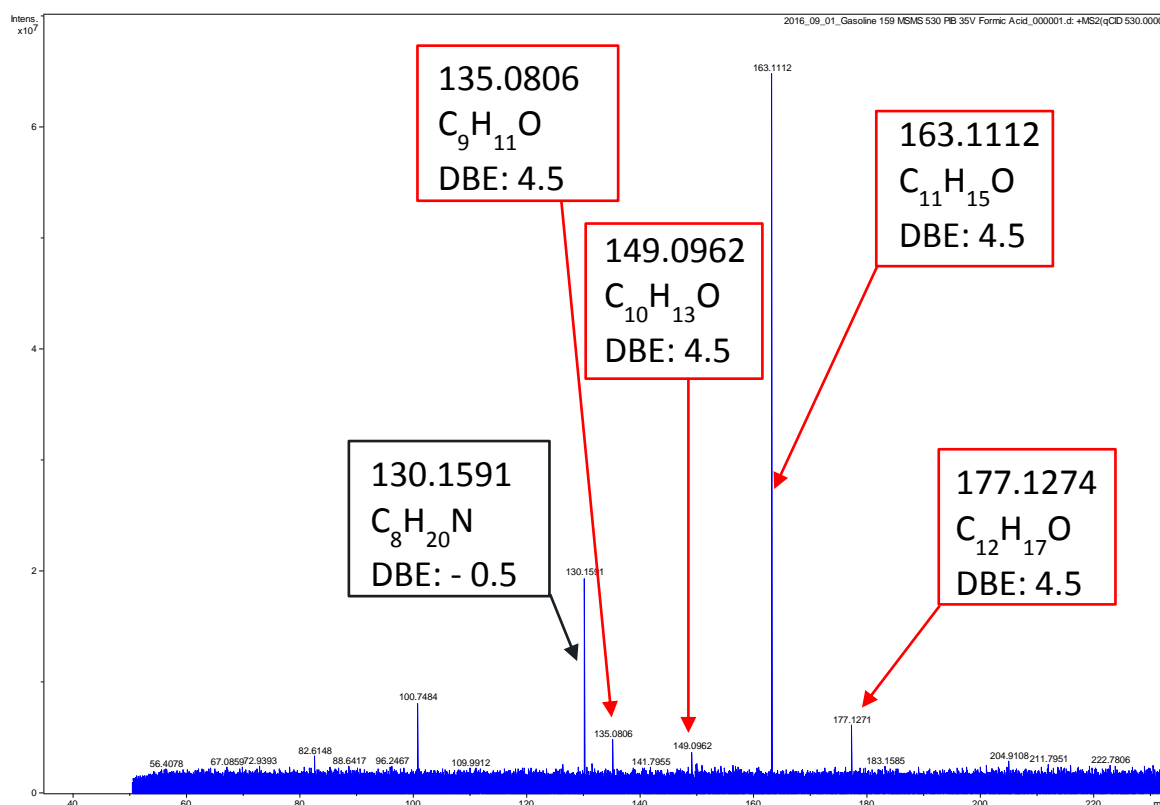
Figure 78 – ESI+ FT-ICR MS product ion spectrum of *m/z* 530.5300 (PIB A in methanol + 25 mM formic acid)

The ion at *m/z* 130.1591 (Figure 78) corresponds to an elemental formula of $C_8H_{20}N$ (3.0 ppm error, 0.4 mDa), this consistent with the protonated molecule of the corresponding neutral loss of *m/z* 129.1515 described previously. The remaining fragments within the ESI+ FT-ICR product ion mass spectrum (Figure 78) are observed when fragmenting both *m/z* 530 and *m/z* 418, therefore are likely to originate from the polymer end group. The accurate mass measurement suggests these fragments contain an oxygen atom. The oxygen containing fragment ions each differ by a CH_2 group, MS[3] of these ions identify that they are related, as *m/z* 135, 149 and 163 can be obtained from the fragmentation of *m/z* 177.

The ion at *m/z* 130.1591 was further investigated by MS[3] utilising the QIT, although at 1 *m/z* resolution *i.e. m/z* 130. *m/z* 418 was fragmented at 40 % collision energy, resulting in *m/z* 130, which was then isolated and fragmented at 25 % collision energy. The resulting product ion mass spectrum is presented, annotated with structural interpretations (Figure 79).
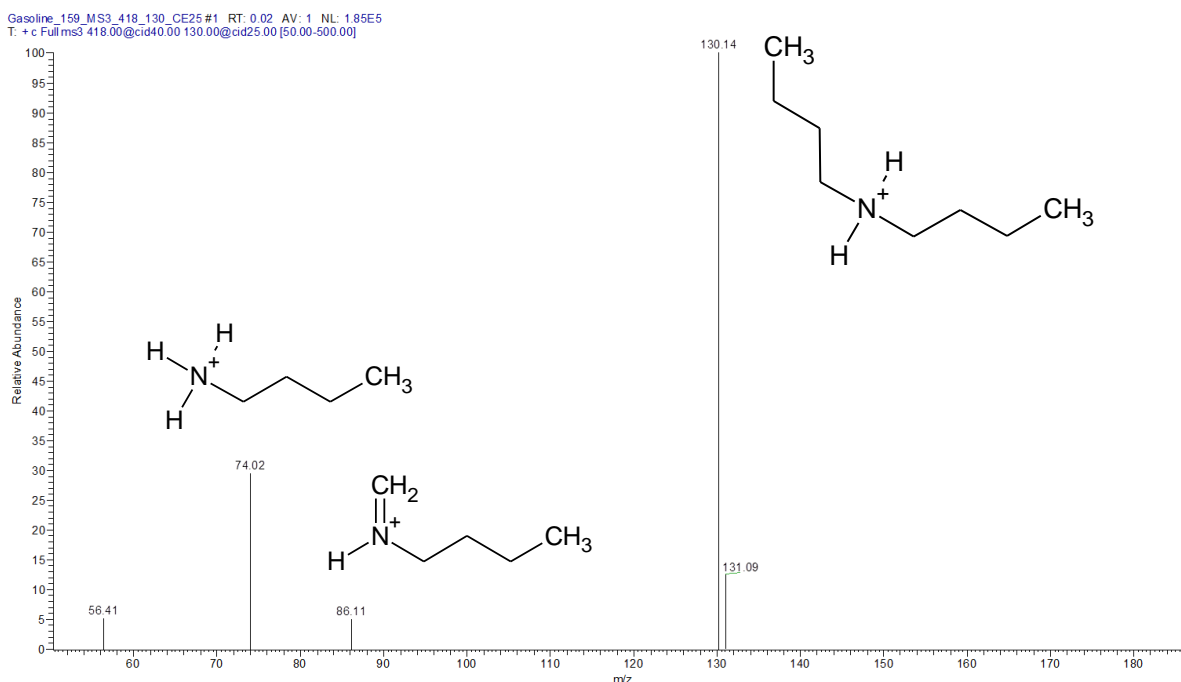
Figure 79 - ESI+ QIT, MS^2 product ion spectrum of *m/z* 418 at 40 % collision energy, and then MS^3 of *m/z* 130 at 25 % collision energy

The fragmentation of *m/z* 130 (Figure 79) is characteristic of protonated di-butyl amine, this is consistent with the accurate mass measurement for this ion. The neutral loss of 129 *m/z* units from the protonated PIB molecule, and the presence of the di-butyl amine at *m/z* 130 suggests that PIB A contains a di-butyl amine pendant arm (Figure 80), this is consistent with the structure of PIB Mannich deposit control additives (Figure 81).
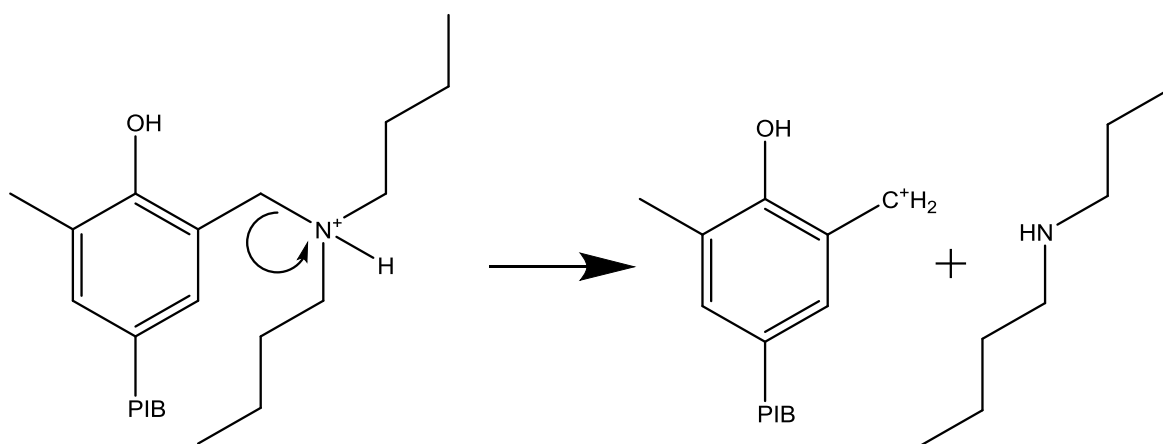

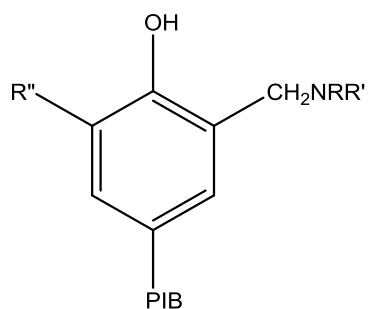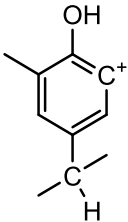Figure 80 - Suggested mechanism for the loss of di-butyl amine from PIB A
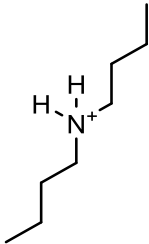
Figure 81 – Generic structure of PIB-Mannich DCA

Elemental formula have been assigned to the fragment ions produced during the FT-ICR MS/MS experiments *via* accurate mass measurement. MS^n experiments within the ion trap have allowed for the determination of the presence of a di-butyl amine pendant arm. Assignment of structures to the fragment ions observed are displayed in Table 8, the fragmentation of protonated PIB A with an *m/z* of 418 is used as an example.

Table 8 – Proposed structures of precursor ion and fragment ions for protonated PIB A (*m/z* 418)

Ion *m/z*	Proposed Structure
418	
289	
177	
163	

149	
130	

5.3.1.3   Deuteration of PIB A

Deuterium exchange experiments were undertaken to confirm the number of exchangeable hydrogen atoms within a molecule.

The ESI+ FT-ICR MS method described in section 5.1.1.3.1 for the detection of PIB was utilised, although, deuterated methanol replaced methanol in the sample preparation. Formic acid was also replaced with deuterated formic acid.
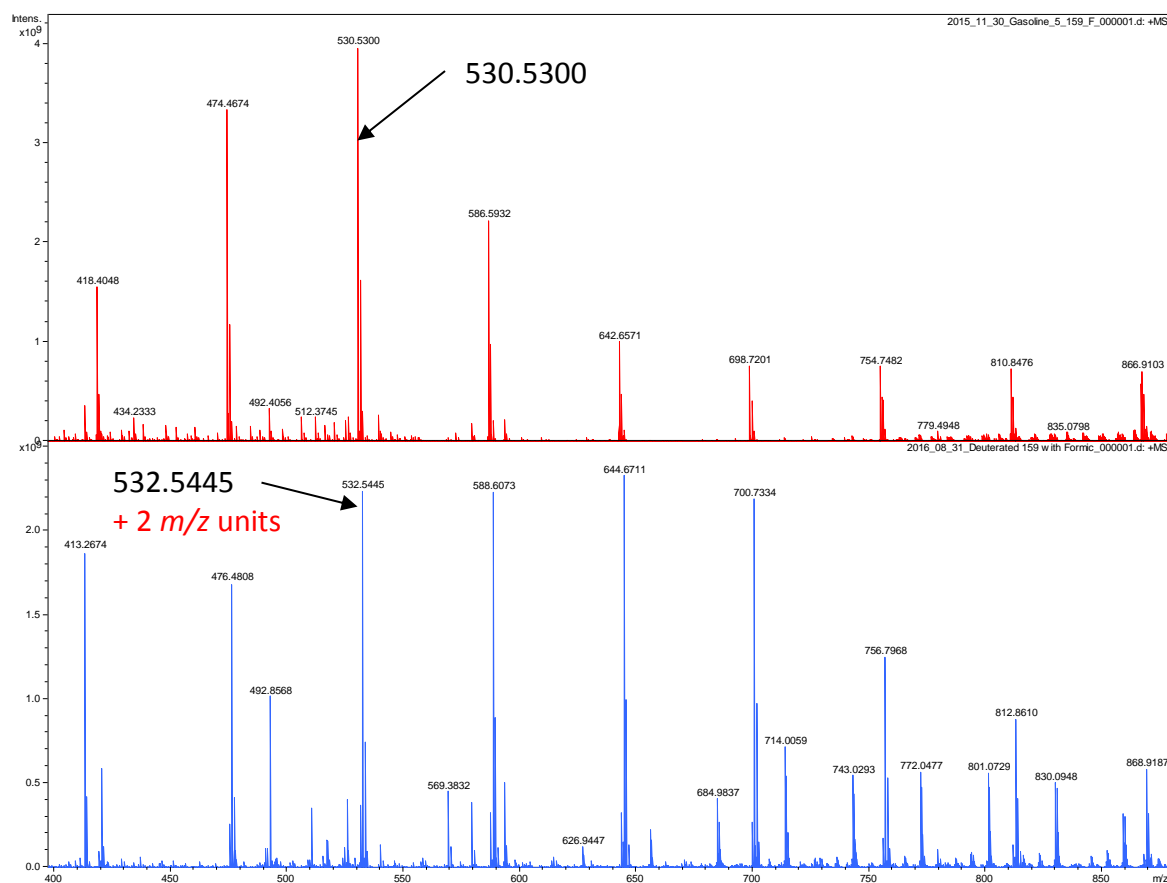
Figure 82 – ESI+ FT-ICR mass spectra of 5 % gasoline 159 (Top): in methanol + 25 mM formic acid
(Bottom): in deuterated methanol + 25 mM deuterated formic acid

A comparison between the ESI+ FT-ICR mass spectrum for un-deuterated and deuterated 5 % gasoline samples is displayed (Figure 82). Upon the addition of deuterated solvent, an increase in 2 m/z is observed for the PIB A series, suggesting the presence of two exchangeable hydrogen atoms. One of which will be the proton from the ionisation event, thus leaving one exchangeable hydrogen atom within the molecule.

The presence of an OH groups suggested by the negative ion experiments would be responsible for this exchangeable hydrogen atom. If this were to be the case, then the nitrogen present (determined from the accurate mass and nitrogen rule) would have to be either tertiary or quaternary, *i.e.* not bonded to any exchangeable hydrogen atoms. This is consistent with the proposed determination of the di-butyl amine pendant arm from the MS/MS data described in section 5.3.1.2.

MS/MS experiments can be undertaken for the deuterated molecule to further investigate the structure and the position of the exchangeable hydrogen atoms within the ion. m/z 532.5445 was isolated and fragmented at collision energy of 30 V within the FT-ICR MS, the resulting product ion mass spectrum is shown in Figure 83.
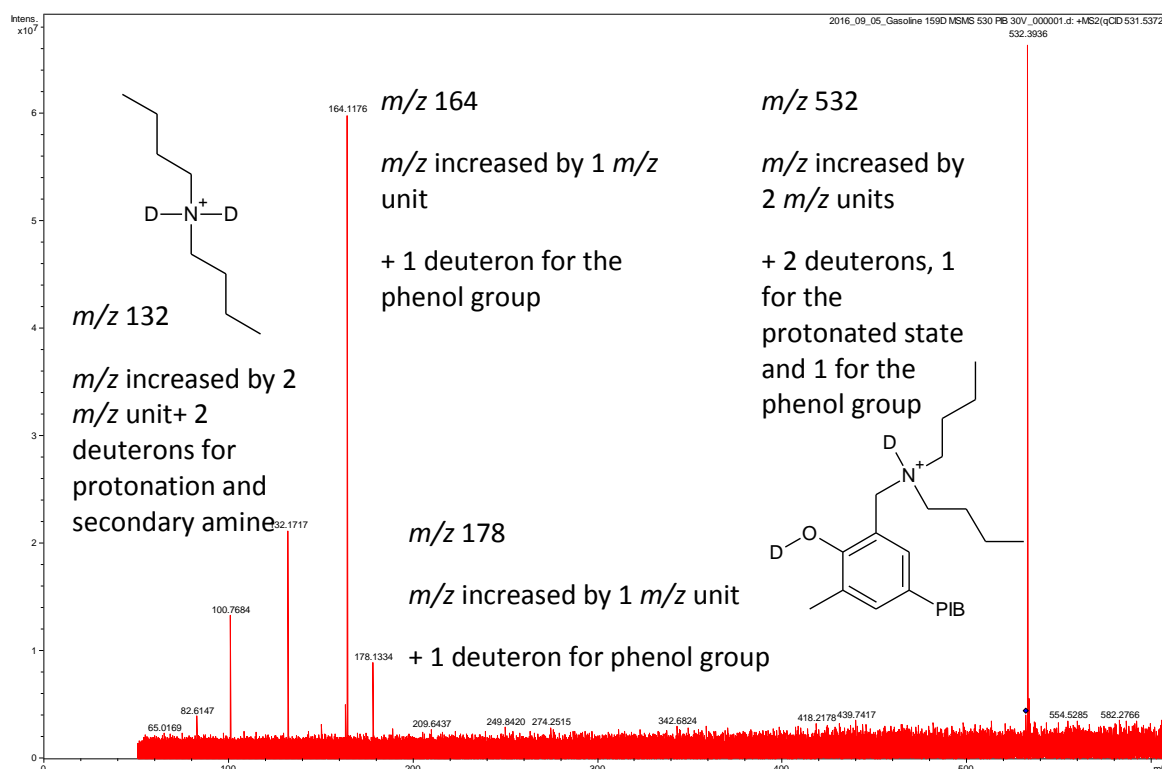
Figure 83 – ESI+ FT-ICR product ion spectrum for *m/z* 532 at a collision energy of 30 V (5 % gasoline 159 in deuterated methanol + 25 mM deuterated formic acid)

The product ion mass spectrum of *m/z* 532 can be compared against the product ion mass spectrum of the corresponding peak within the un-deuterated sample (*m/z* 530) (Figure 76 top). All of the oxygen containing peaks previously described (section 5.3.1.2, Figure 78) have increased by 1 *m/z* unit corresponding to the exchange of the phenol proton with a deuteron. The species previously observed in the non-deuterated sample at *m/z* 130, is now observed at *m/z* 132, corresponding to there being two exchangeable hydrogen atoms on the protonated di-butyl amine (proton for protonated state and a proton on the amine).

5.3.2   Polyisobutylene B end group determination

The determination of PIB B was achieved utilising the same methodology as for PIB A. PIB B displayed similar ionisation characteristics to PIB A, formation of a protonated molecule under positive ion ESI conditions, formation deprotonated molecule under negative ion ESI conditions and formation a molecular ion under positive ion APPI conditions. Although, the *m/z* of the PIB B series is + 14 *m/z* units when compared to the PIB A series, and displays different chromatographic behaviour when compared to the PIB A by UHPSFC.

The use of deuterated solvents and MS/MS techniques were utilised to further investigate the structure of PIB B and the differences to PIB A. Gasoline 155, which contains PIB B was used for all further PIB B experimentation.

5.3.2.1   Deuteration of PIB B

The protonated PIB B series displays an increase of 2 *m/z* units in the presence of a deuterated solvent, when compared to un-deuterated sample (section 5.1.1.2, Figure 51). Identical behaviour to that of PIB A.

5.3.2.2   Tandem MS of PIB B

5 % gasoline 155 in methanol + 25 mM formic acid was analysed by ESI+ FT-ICR MS, an ion of *m/z* 376 (PIB B) was isolated and fragmented by CID at a collision energy of 20 V, the resulting product ion mass spectrum is presented (Figure 84).
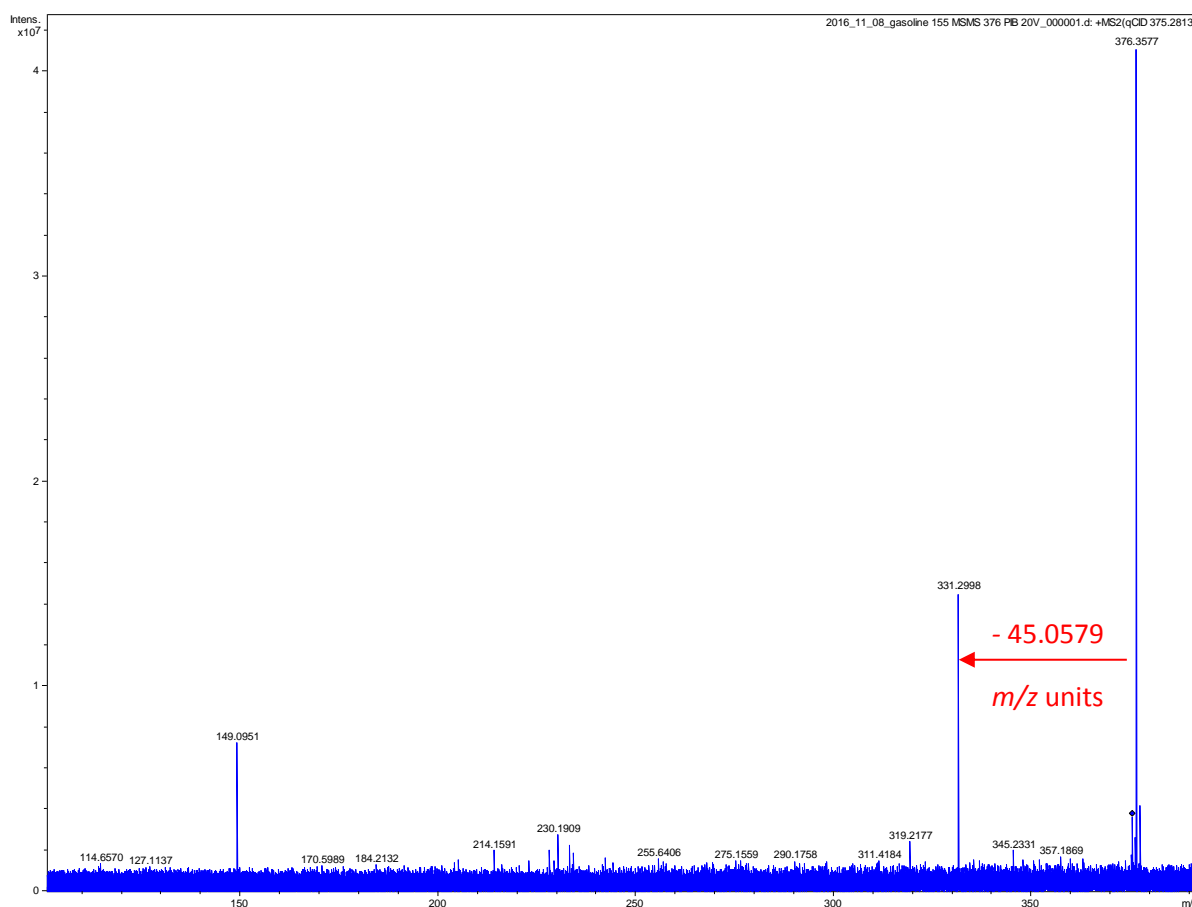
Figure 84 – ESI+ FT-ICR product ion spectrum for *m/z* 376 at collision energy of 20 V (PIB B in 5 % gasoline 155 in methanol + 25 mM formic acid)

A loss of 45.0579 *m/z* units is observed from the precursor ion upon CID (Figure 84) corresponding to an elemental formula of C_2H_7N. No ion is observed in the ESI+ FT-ICR product ion mass spectrum (Figure 84) for a loss of 129.1515 *m/z* units, previously observed for PIB A, accompanied with the absence of *m/z* 130.1591.

The loss of 45 *m/z* units can be attributed to the loss of di-methyl amine (Figure 85), in a similar manner to the loss of di-butyl amine from PIB A.

m/z 376.3577
$[C_{25}H_{45} NO + H]^{+}$

m/z 331.2998
$C_{23}H_{39}O^{+}$

Exact Mass:
45.0578 gmol^{-1}
C_2H_7N

Figure 85 – Suggested mechanism for the loss of di-methyl amine from PIB B

Similarly to PIB A, the corresponding protonated di-methyl amine would be expected within the ESI+ FT-ICR product ion mass spectrum (Figure 84) and *m/z* 46, although due to frequency constraints of the FT-ICR MS, it is not possible to obtain data for this low *m/z*. The presence of this low *m/z* fragment ion was confirmed by repeating the MS/MS experiment using triple quadrupole mass spectrometer .A product ion scan for *m/z* 376 at a CID voltage at 30 V resulted in the fragmentation of the protonated PIB B molecule (Figure 86), displaying a fragmentation pattern similar to that of the ESI+ FT-ICR MS/MS experiments (Figure 84), although now with 1 *m/z* unit resolution. The predicted ion at *m/z* 46 is present, corresponding to the protonated dimethylamine pendant arm, thus confirming the suggested structure.
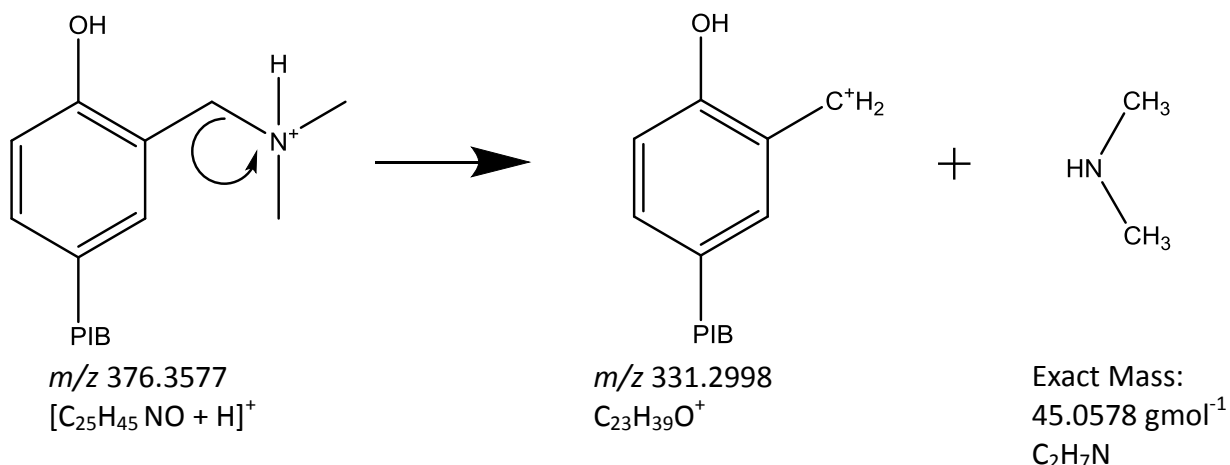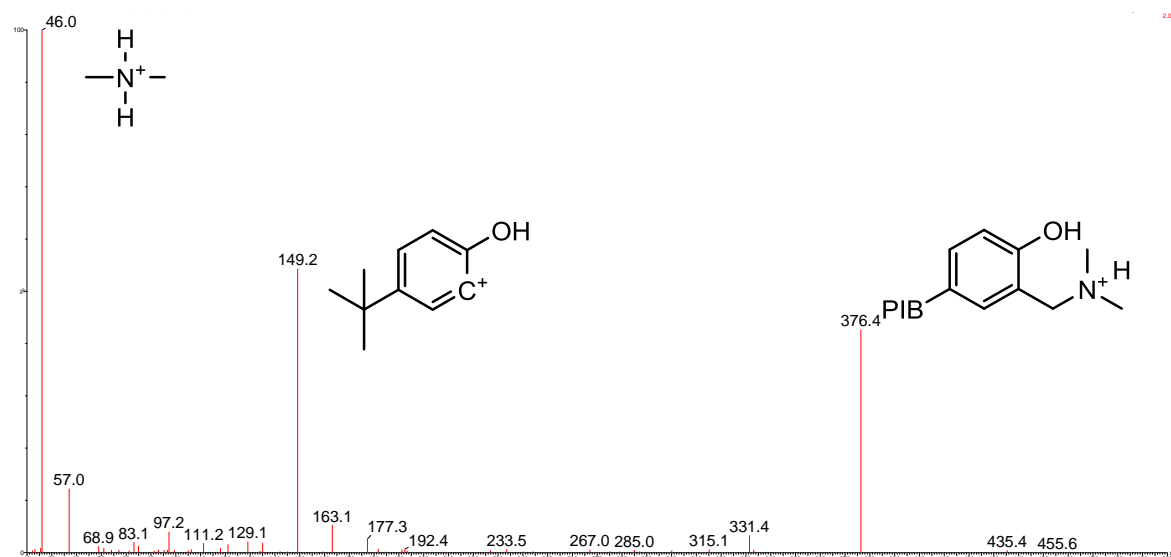
Figure 86 – UHPSFC-ESI+ product ion of *m/z* 376 at a collision energy of 30 V (PIB B in gasoline 155 in methanol + 25 mM formic acid)

The use of both the FT-ICR MS and triple quadrupole instruments are complimentary. The FT-ICR MS provides high resolution and high mass accuracy, although the lower *m/z* range is restricted by the frequency parameters. The triple quadrupole instrument allows for this low *m/z* range to be probed, at the cost of low resolution.

The suggested structures do not include the methyl group in the *ortho-* position as observed with PIB A, as this is not consistent with the measured *m/z* of the PIB B ions. The presence of the di-methyl amine pendant arm has been identified, thus either the methyl group on the aromatic ring is absence or the PIB chain is shorter by a CH_2 unit.

The di-methyl amine pendant arm of the PIB B is smaller than that of the di-butyl amine pendant arm of PIB A by - 84 *m/z* units. The absence of the *ortho-* methyl group in PIB B when compared to PIB A results in a further difference of -14 *m/z* units.

Thus PIB A will have an increased mass of 98 *m/z* units (84 + 14 *m/z* units) when compared to a PIB B with the same PIB chain length. The observation of the PIB B series as having an increased *m/z* of + 14 *m/z* units when compared to PIB A is due to an increased length of the PIB chain by 2 PIB monomer units (112 *m/z* units)

The differences between increased PIB chain length of PIB B and the increased end group mass of PIB A results in the apparent 14 *m/z* unit difference (112 – 98 = 14 *m/z* units). An example is displayed in Figure 87.

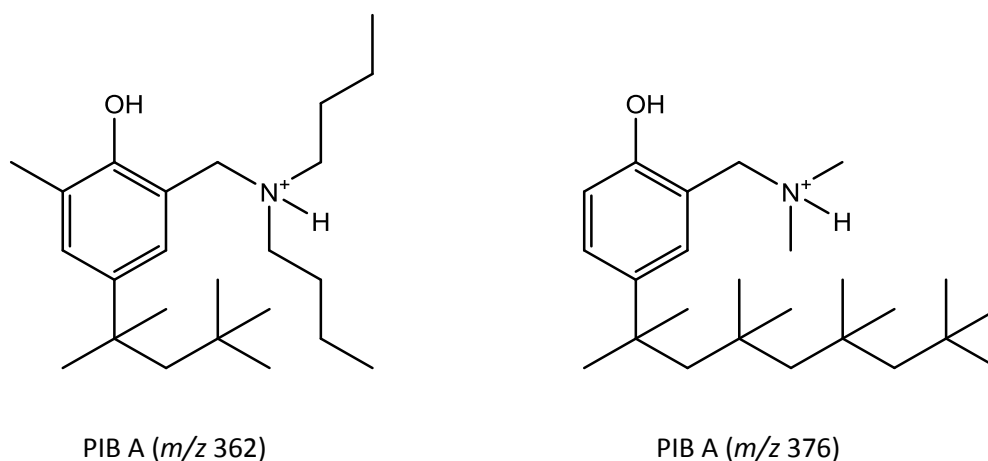PIB A (*m/z* 362)   PIB A (*m/z* 376)

Figure 87 – Structure of PIB A (left) and PIB B (right), 14 *m/z* unit difference

This is highlighted by comparison of the ESI+ FT-ICR product ion mass spectrum of the PIB A and B (Figure 88).
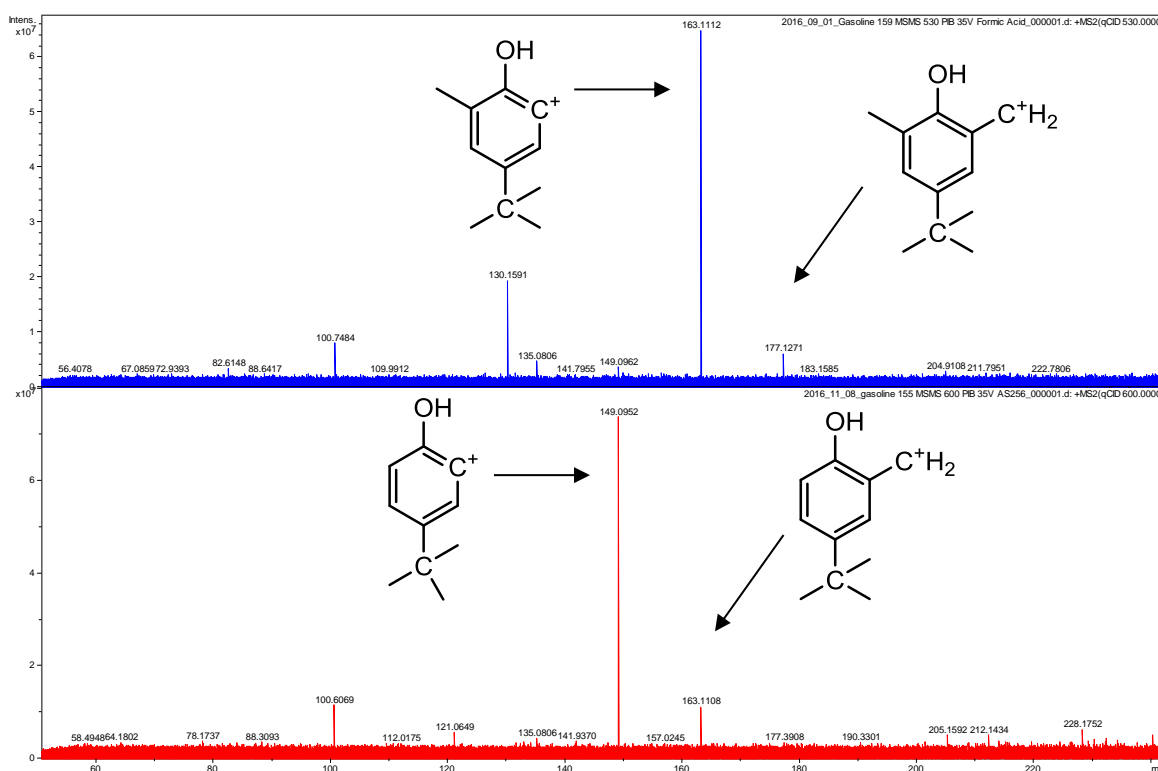
Figure 88 – ESI+ FT-ICR product ion spectrum of (Top): PIB A (*m/z* 530 at 35 V) (Bottom): PIB B (*m/z* 600 at 35 V)

Ions for *m/z* 163 and 149 are present in both MS/MS, although the intensities of the peaks is different. The base peak of ESI+ FT-ICR MS product ion mass spectrum for PIB A (Figure 88, top) is *m/z* 163 whereas for PIB B the base peak is *m/z* 149 (Figure 88, bottom). The base peak for each mass spectra is interpreted as a fragment ion with the charge located on the aromatic ring, due to

its increased stability. The difference of +14 *m/z* units between the base peak of PIB A and PIB B is indicative of an addition methyl group on the aromatic ring within the PIB A molecule.

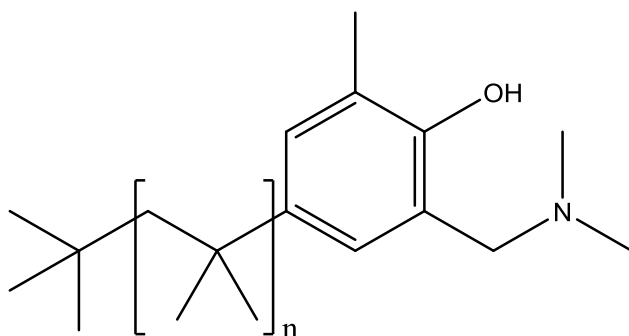Thus a proposed structure for PIB B is presented in Figure 89.

Figure 89 – Proposed structure of PIB B

The difference in chromatographic behaviour observed by UHPSFC could be explained by the difference in the amine group and the corresponding difference in PIB chain length for molecules of similar mass, due to the shorter amine side group.

5.3.3   Polypropylene glycol end group determination

The determination of PPG was achieved utilising the same methodology as for PIB molecules. The presence of PPG was identified within gasoline 159 by ESI+ FT-ICR MS and UHPSFC-ESI+ MS, thus gasoline 159 was utilised for structural determination.

In the absence of ionisation additives (5 % gasoline in methanol), the series of PPG ions were identified as sodiated molecules, the addition of ammonium acetate forced the ammoniated molecules and the addition of formic acid suppressed the ionisation of the PPG series to undetectable levels.

The PPG does not ionise by APPI+, suggesting the absence of an aromatic centre or conjugated double bonds within the molecule. The PPG does not ionise by negative ion ESI, suggesting the absence of a site for deprotonation.

The PPG ion series is present in the +2 and +1 charge state, determined by the 0.5 *m/z* unit spacing between the ^{12}C and ^{13}C ions within the series.

5.3.3.1   Tandem MS of polypropylene glycol

ESI+ FT-ICR MS/MS was utilised for the isolation and fragmentation of the doubly sodiated PPG molecule.

Ions of *m/z* 771 and 858 were selected for MS/MS experiments and for a comparison of fragmentation between two members of the series (Figure 90).
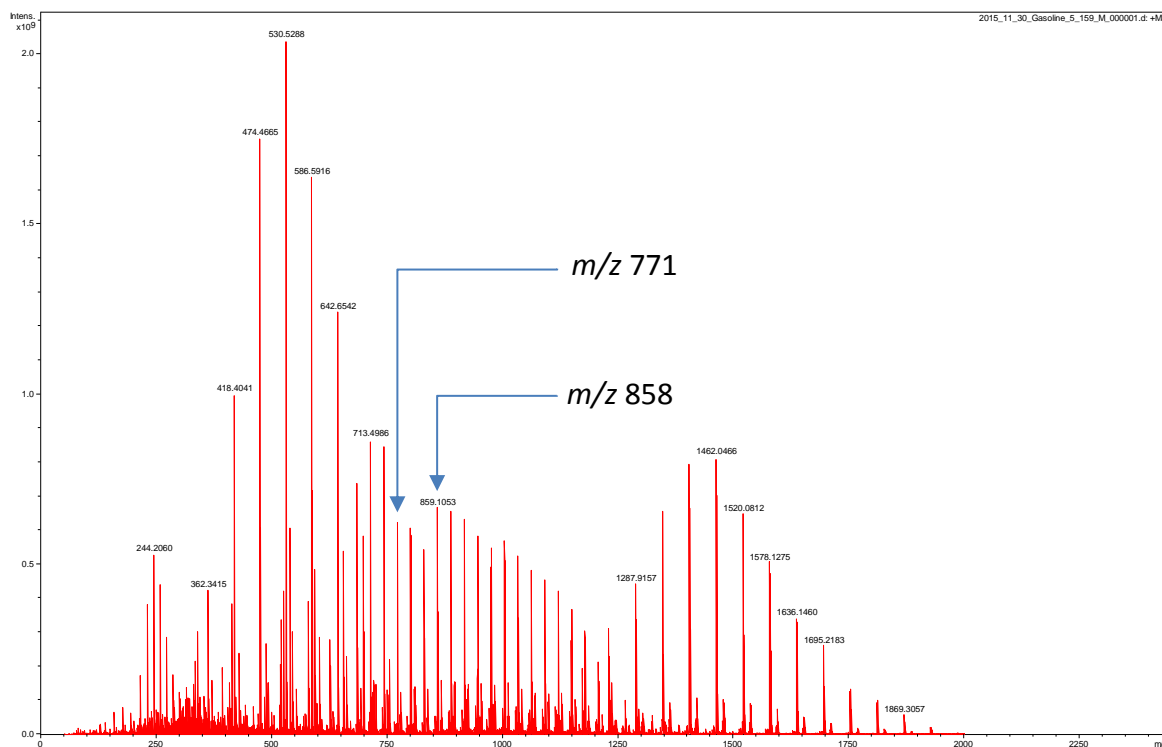

Figure 90 – ESI+ FT-ICR mass spectrum of 5 % gasoline 159 in methanol (nominal *m/z* for precursor ions for PPG MS/MS experiments are highlighted)

The resulting ESI+ FT-ICR product ion mass spectra at a collision energy of 50 V and 55 V for *m/z* 771 and *m/z* 858 respectively are presented (Figure 91).
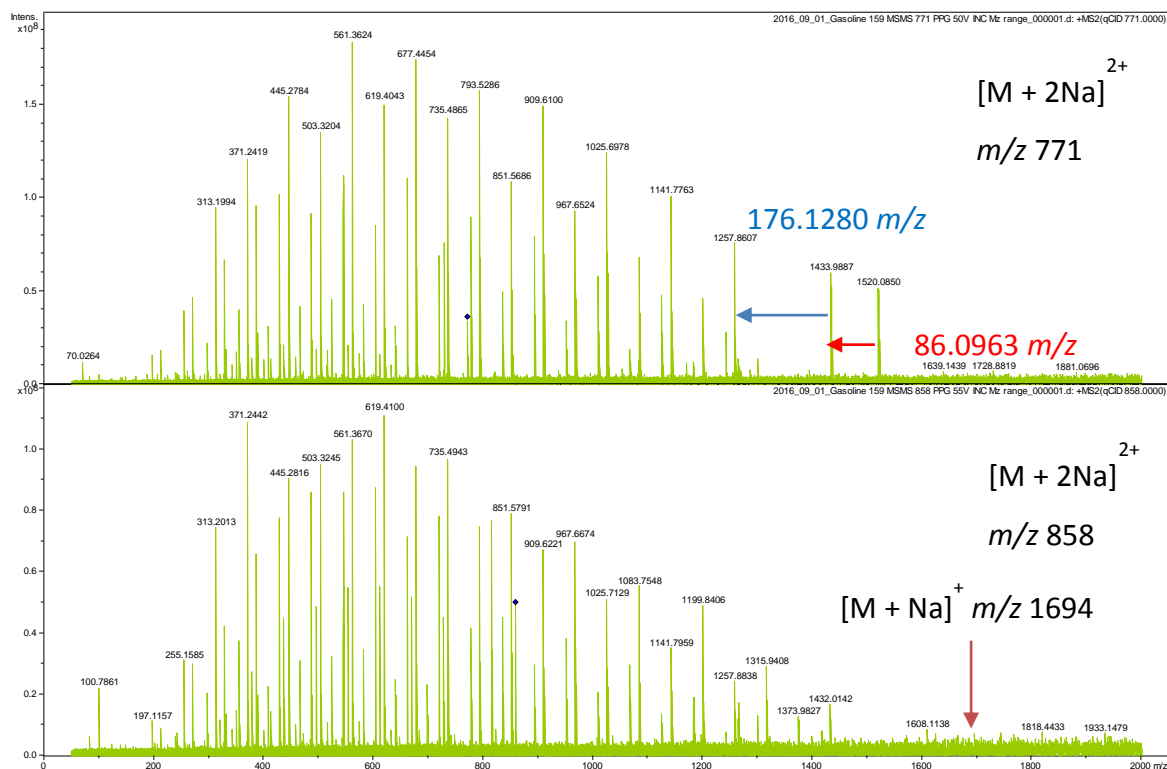
Figure 91 – ESI+ FT-ICR product ion spectra for 5 % gasoline 159 in methanol (Top): nominal *m/z* 771 at 50 V (Bottom): nominal *m/z* 858 at 55 V

Upon CID (Figure 91) both [PPG + 2Na]$^{2+}$ ions fragment in a similar manner. A series of ions separated by 29 *m/z* units is observed at a lower *m/z* to that of the precursor ion, this is attributed to the sequential loss of PPG units from the doubly charged precursor ion. The PPG is also observed in the singly charged state, at *m/z* 1520 (MS/MS of *m/z* 771) and *m/z* 1694 (MS/MS of *m/z* 858), these *m/z* correspond to the [M + Na]$^{+}$ ion for each PPG. A series of singly charged fragments are also observed.

The singly charged sodiated molecules display at loss of 86.0963 *m/z* units, followed by a loss of 176.1280 *m/z* units.

From the ion corresponding to a loss of 176.1280 *m/z* units, the fragmentation proceeds v*ia* four series. Each peak within each series is separated by 58 *m/z* units, the PG repeat unit. These series are further investigated v*ia* ion trap experiments (section 5.3.3.1.1.1).

5.3.3.1.1   Addition of lithium acetate to PPG

It has previously been indicated that more structural information was obtained by means of CID of polyethers when lithium ions are used to ionise the oligomeric series[86]. The effect of lithium ions as an ionisation additive for PPGs in gasoline was investigated.
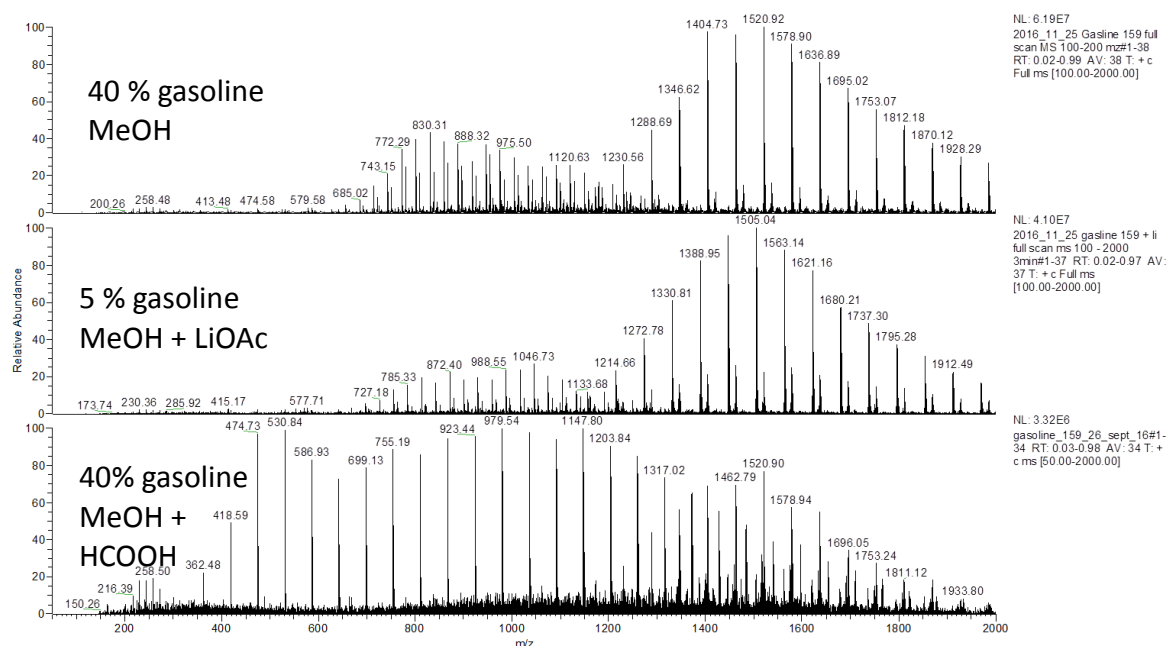
Figure 92 – ESI+ QIT mass spectra of gasoline (Top): 40 % gasoline in MeOH (Middle): 5 % gasoline in MeOH + LiOAc (Bottom): 40% gasoline in MeOH + HCOOH

The ESI+ QIT mass spectra obtained (Figure 92) highlights the application of different ionisation additives. With the absence of an ionisation additive and a 40 % concentration of gasoline, the singly and doubly charged PPG series are observed as the sodiated form. Upon the addition of lithium acetate, the same peak intensity of the lithiated molecule can be obtained with a concentration of 5 % gasoline when compared to the sodiated molecule at a gasoline concentration of 40 %. The lithium acetate also allows for the selective ionisation of the PPG molecules within the gasoline sample. A difference of 16 *m/z* units between the sodiated PPG series in the unadditised sample and the PPG series observed within the LiOAc sample, this is indicative of the difference between sodium and lithium ions.

The effect of the addition of lithium acetate to the gasoline samples is not only limited to increasing the intensity of the PPG ions, but increase in the number of fragment ions was observed when compared to the sodiated species upon MS/MS (Figure 93).
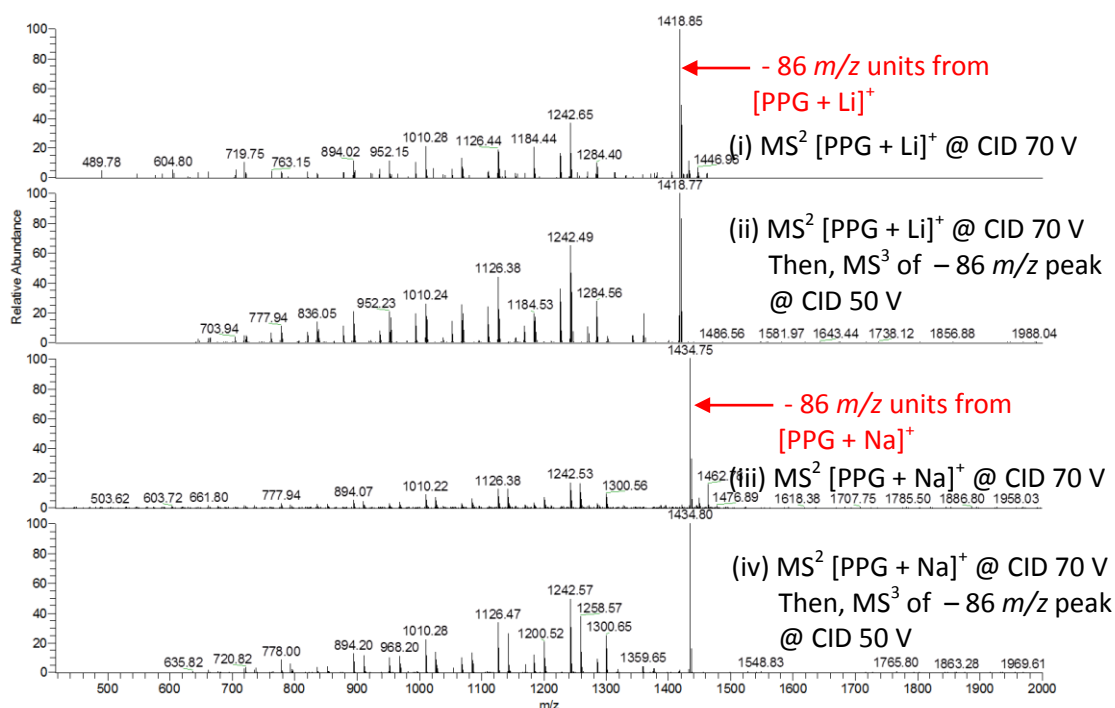
Figure 93 – ESI+ QIT product ion mass spectra comparison of lithiated and sodiated PPG molecules (i): MS^2 of *m/z* 1504 [PPG + Li]$^+$ at a CID of 70 V (ii): MS^3 of *m/z* 1504 [PPG + Li]$^+$ at a CID of 70 V, then 1418 at CID 50 V (iii): MS^2 of *m/z* 1520 [PPG + Na]$^+$ at a CID of 70 V (iv): MS^3 of *m/z* 1520 [PPG + Na]$^+$ at a CID of 70 V, then 1434 at CID 50 V

The effect of lithium and sodium cations on the fragmentation of the PPG cationised molecules was investigated. The fragmentation of lithiated and sodiated molecules corresponding to single PPG molecule was compared. The fragmentation was investigated utilising MS^n within the QIT, initially isolating and fragmenting each respective cationised molecule of the PPG, and then subsequently fragmenting the base peak ion of each product ion mass spectrum.

MS^2 of both the lithiated and sodiated molecule, *m/z* 1504 (Figure 93, first) and *m/z* 1521 (Figure 93, third) respectively, resulted in an intense ion corresponding to a loss of 86 *m/z* units, previously observed by ESI+ FT-ICR MS. This [M + (Li or Na) – 86]$^+$ ion was subsequently fragmented in MS^3 experiments, *m/z* 1418 for the lithiated species and *m/z* 1434 for the sodiated species.

Similarly to the ESI+ FT-ICR product ion mass spectra for the sodiated molecules (Figure 91), the fragmentation of the sodiated and lithiated PPG ions proceeds by four fragmentation series (ions within each series are separated by 58 *m/z* units) (section 5.3.3.1.1.1), within the QIT, although the fragmentation pattern for the lithiated PPG is – 16 *m/z* units relative to the sodiated PPG due to the difference in *m/z* of the lithium and sodium cation. This also demonstrates that the

fragment ions retain the cation upon fragmentation, which is plausible due to the oxygen containing backbone of the PPG molecule.

The fragmentation pattern of the lithiated molecule displays a more intense and intricate series of fragment ions, when compared to the sodiated species. Additional fragment ions are observed via the addition of lithium acetate, including a peak corresponding to the loss of 176 *m/z* units, previously observed by ESI+ FT-ICR MS.

Lithium was utilised as an ionisation additive for further PPG experiments, as the number and intensity of the lithiated fragment ions was greater than that observed from the fragmentation of the sodiated molecule.
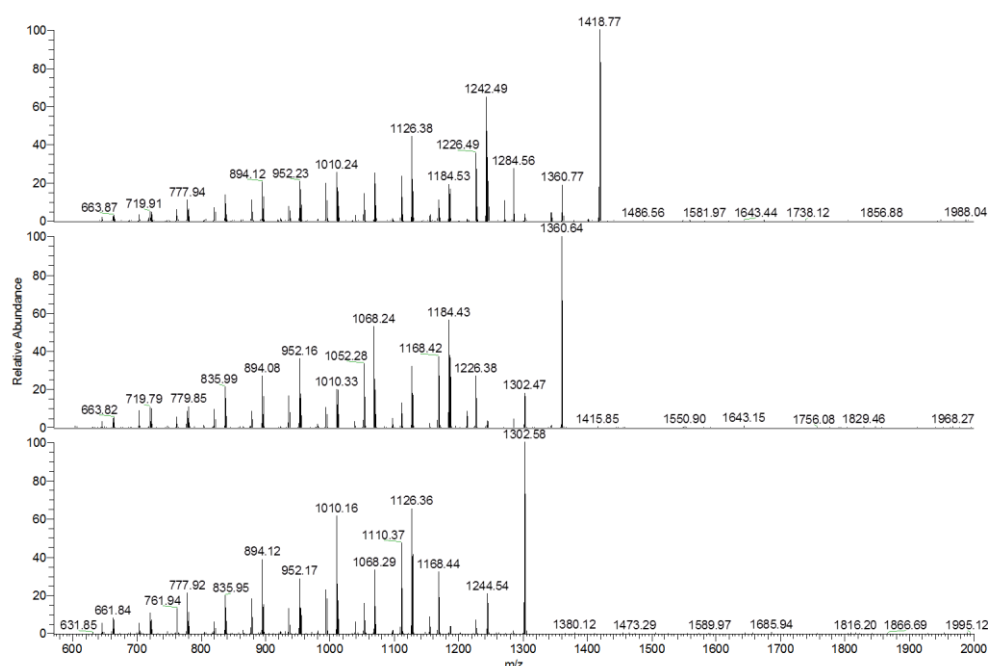

Figure 94 – ESI+ QIT MS³ product ion spectrum of three lithiated PPG ions (Top): *m/z* 1504
(Middle): *m/z* 1446 (Bottom): *m/z* 1388

Fragmentation of different PPG ions within the series results in a similar fragmentation pattern (an initial loss of 86 *m/z* units, followed by fragment ions originating from the fragmentation of the PPG backbone) (Figure 94).

5.3.3.1.1.1   PPG fragmentation series

The four fragmentation series observed within the FT-ICR ESI+ MS and the ESI+ QIT product ion mass spectra are to be investigated. The ESI+ QIT MS³ mass spectra for a precursor ion of *m/z* 1505 (lithiated PPG), and a second precursor ion of *m/z* 1418 (lithiated PPG – 86 *m/z* units), is presented (Figure 95).
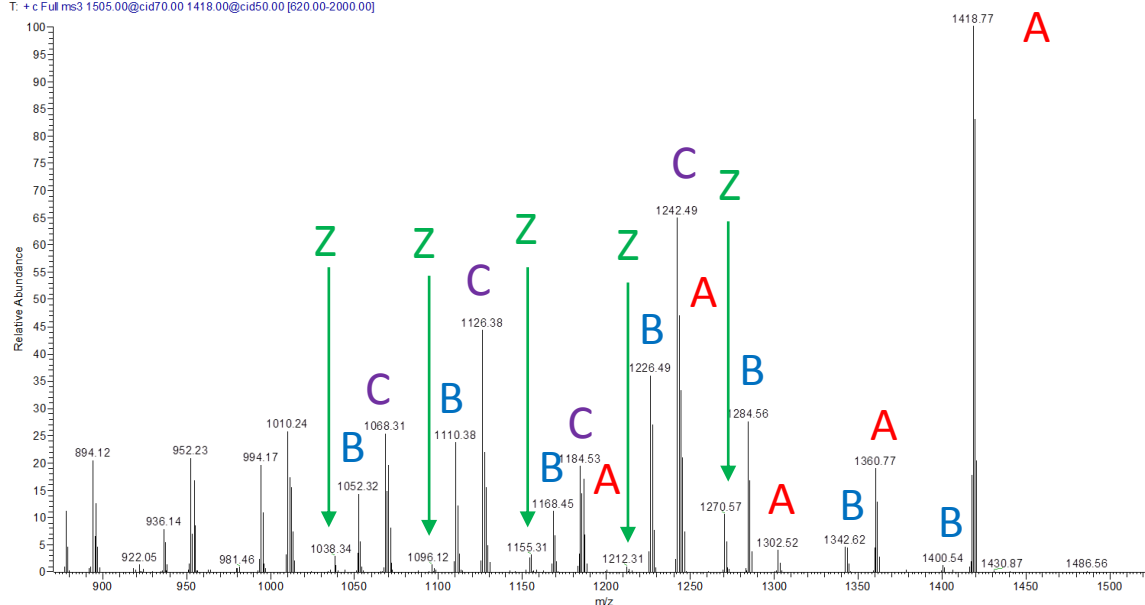
Figure 95 – ESI+ QIT MS³ product ion spectrum of *m/z* 1504 at CID of 70 V then *m/z* 1418 at 50 V displaying the four fragmentation series (A, B, C & Z)

The four series labelled A, B, C and Z in accordance with previous lithiated PPG fragmentation studies[86]. All the peaks in each series are separated by 58 *m/z* units. The different series can be attributed to different fragmentation along the PPG chain. Four different types of structures are suggested (Figure 96) for these fragment ions (6 PPG unit chain used as an example):

Figure 96 – Suggested structures for the A, B, C and Z series observed in the ESI+ QIT product ion
mass spectra of the PPG

As increased fragmentation of the PPG was observed when the lithiated molecule was
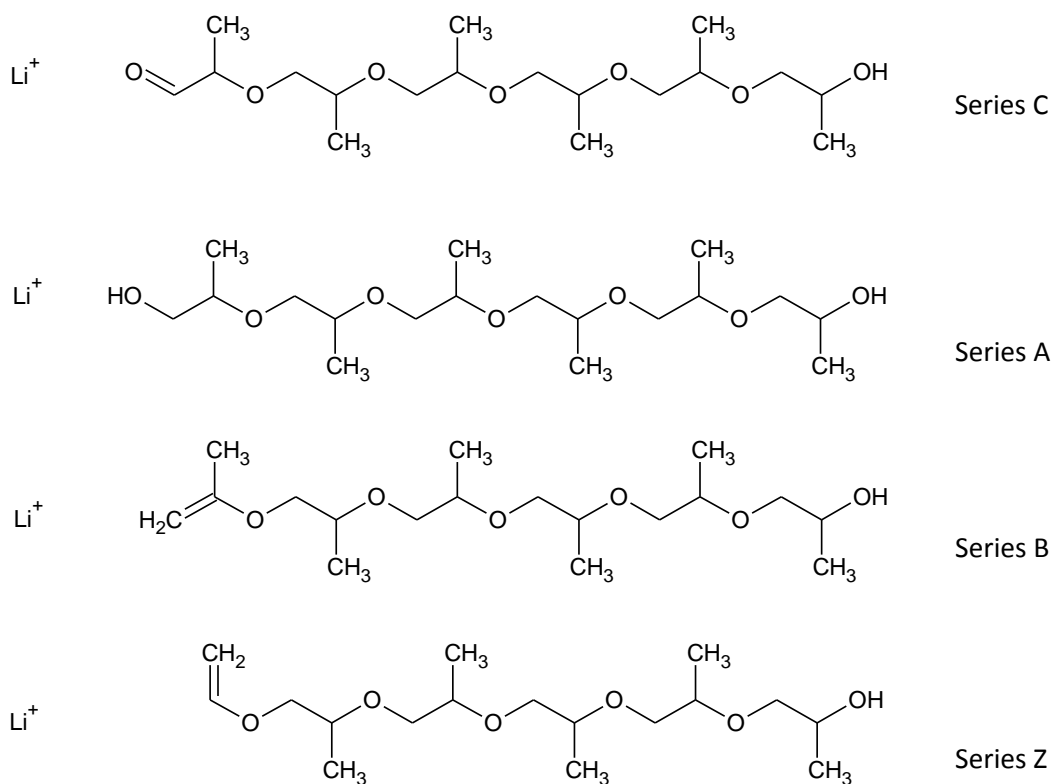fragmented when compared to the sodiated molecule within the QIT, the effect of lithium ions as
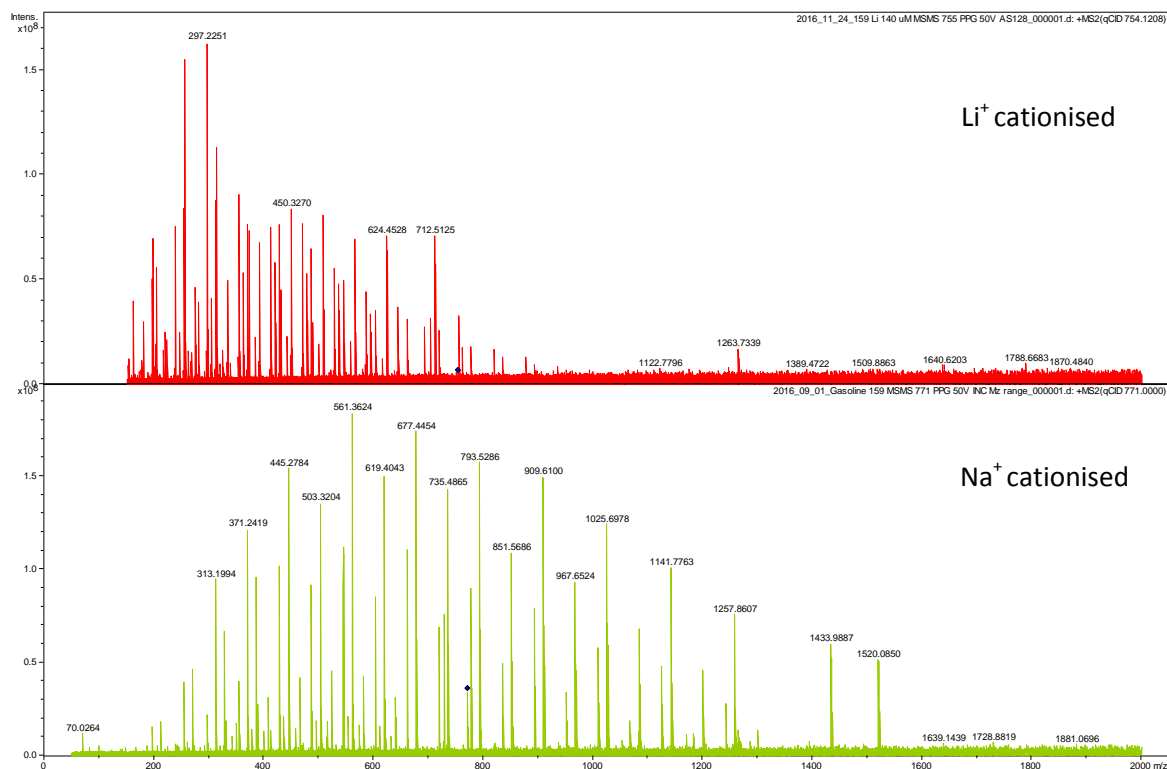an ionisation additive for ESI+ FT-ICR MS/MS was also investigated.

Figure 97 – ESI+ FT-ICR MS product ion scan of PPG (Top): gasoline 159 (MeOH + LiOAc) (Bottom): gasoline 159 (MeOH)

The ESI+ FT-ICR product ion mass spectrum (Figure 97, bottom) of the doubly sodiated PPG displays a series of doubly charged and singly charged fragment ions, including the [M + Na]$^+$ ion. The ESI+ FT-ICR product ion mass spectrum (Figure 97, top) of the doubly charged lithiated PPG results in a series of doubly charged fragment ions and very few singly charged species, especially at a greater *m/z* value than the precursor ion, when compared to the sodium adduct.

The relative intensity of the four fragmentation series, A, B, C and Z previously described is different upon the addition of lithium acetate when compared to the fragmentation of the sodiated molecule. This is displayed in the comparison of the ESI+ FT-ICR product ion mass spectra for the lithiated molecule (Figure 98, top), and the sodiated molecule (Figure 98, bottom). It must be noted that the peaks have shifted by - 16 *m/z* units, for the lithiated fragment ions when compared to the sodiated fragment ions, due to the difference in mass between the sodium and lithium cations. An increase in ion intensity of lithiated series A is observed.
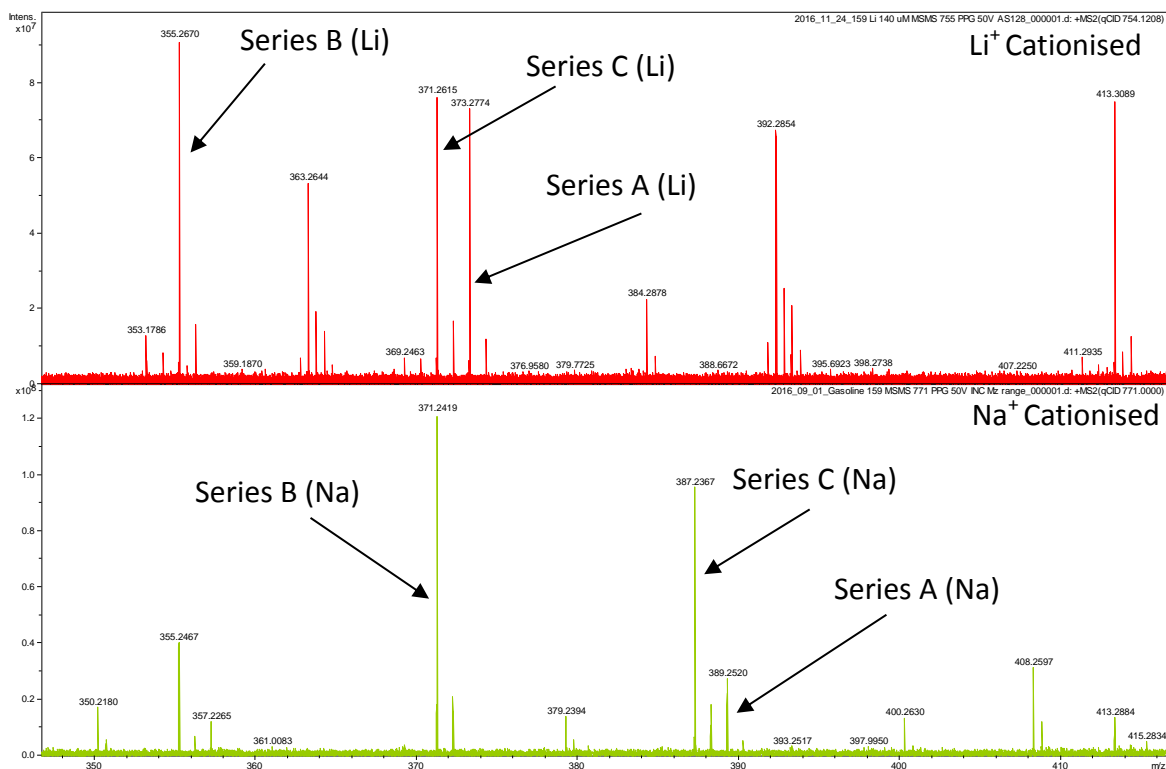
Figure 98 – ESI+ FT-ICR product ion spectrum for PPG (Top): gasoline 159 (MeOH + LiOAc)

(Bottom): gasoline 159 (MeOH)

5.3.3.1.2   Polypropylene glycol end group determination

The structure of the PPG can be calculated using the accurate mass measurement of the cationised molecule and the fragment ions. In addition, the lithiated molecule displays further fragmentation when compared to the sodiated molecule, which adds further evidence in structural determination.

Figure 99 - ESI+ FT-ICR product ion spectrum of m/z 771 at 50 V for 5 % gasoline 159 in methanol

The loss of 86.0963 m/z units from the sodiated molecule (m/z 1520.0850) to produce a fragment ion of m/z 1433.9887, corresponds to an elemental formula of $C_5H_{10}O$, which can be attributed to the loss of an ethyl group and an addition PPG unit. Thus, it is suggested that the PPG is terminated with an ethyl group, giving the ethylether structure displayed in Figure 100.
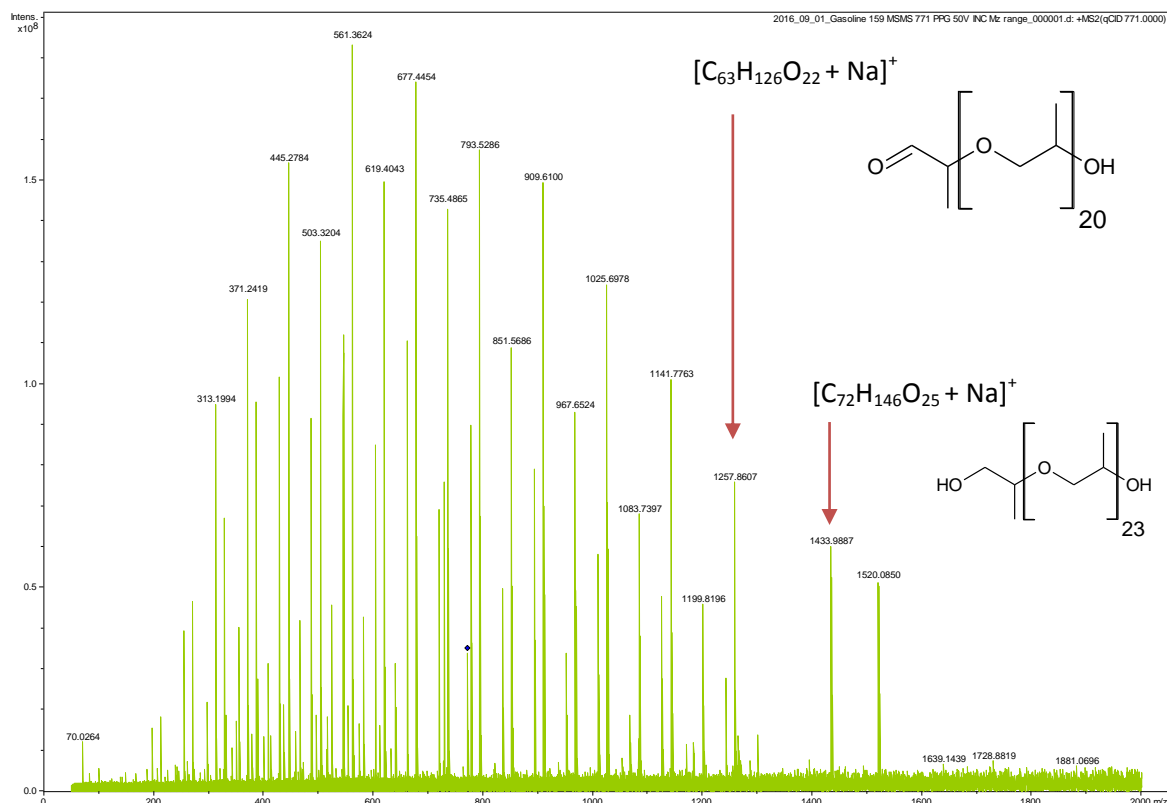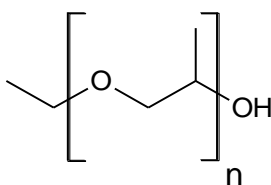

Figure 100 – Proposed structure of PPG

The ion with an m/z of 1257.8607 (Figure 99) can be attributed to an elemental formula of $[C_{63}H_{126}O_{22} + Na]^+$, a member of the C fragmentation series (Figure 96). The absence of fragmentation ions, and conformation of the continuation of the fragmentation series between m/z 1257.8607 and m/z 1433.9887 is overcome with the addition of lithium acetate as previously described.

To further investigate the structure of the PPG, MS/MS experiments were undertaken using PPG and deuterated sample solvents. As described previously, the addition of formic acid to the

gasoline forces the protonation of the PIB with the sample and suppresses the ionisation of the PPG. Thus for the deuteration experiments, only deuterated methanol was used.

It has previously been observed that the PPG increases by 1 *m/z* unit when deuterated, therefore *m/z* 772.5 was isolated (+1 *m/z* unit from non-deuterated), and fragmented *via* the same method as previously described. The resulting ESI+ FT-ICR product ion mass spectra are presented (Figure 101).
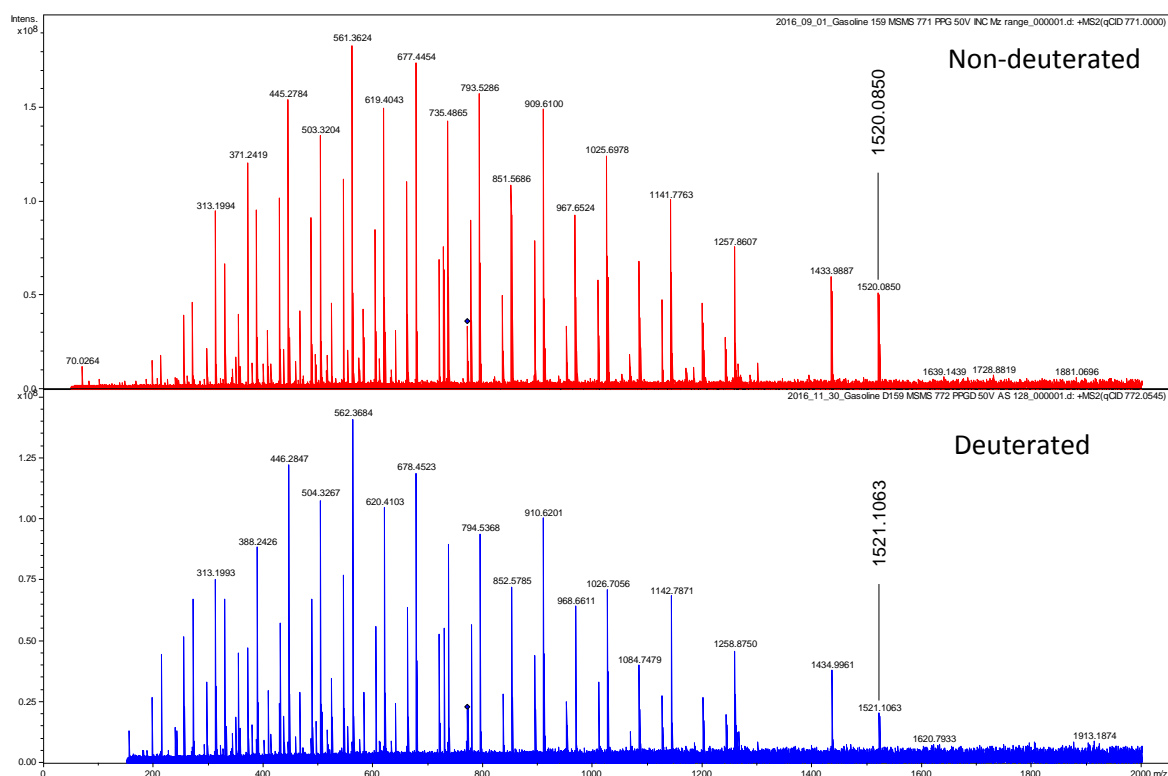
Figure 101 - ESI+ FT-ICR product ion spectra of *m/z* 772 at CID 50 V for 5 % gasoline 159 in deuterated methanol

All of the fragment ions (Figure 101) exhibit +1 *m/z* unit difference in the deuterated sample, when compared to the non-deuterated. This is due to the –OH group present as the end group on the molecule. The remainder of the molecule cannot contain any exchangeable hydrogen atoms. This is in good agreement with the suggested structure (Figure 100). Thus the deuterated structure is presented (Figure 102).

Figure 102 – Proposed structure for the deuterated PPG

5.4   Polymeric detergent additive determination summary

The structure of two derivatised polyisobutylene detergent additives and one derivatised polypropylene glycol fluidiser additive have been determined. This was achieved for additives at concentrations used within finished gasoline samples, without the use of pure/standard additive samples. Gasoline required little sample preparation *i.e.* a 5 % gasoline in methanol, and the addition of an ionisation additive.

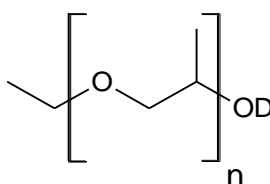Selectivity for specific polymeric fuel additives can be achieved with the use of ionisation additives (*i.e.* formic acid for the detection and identification of PIB-Mannich additives). Ionisation additives allow for determination of molecular mass, from the characteristic differences between the mass of the cations. Jackson *et al.*[86] described the increased intensity and intricacy of PPG fragmentation when using lithium acetate as an ionisation additive in ESI+ MS/MS experiments. Lithium acetate has been utilised in the similar manner for the QIT MS/MS fragmentation of PPG fuel additives within the gasoline matrix.

Atmospheric pressure ionisation techniques facilitate the detection of polymeric additives, which are not detected v*ia* traditional methods (*i.e.* GC-MS) due to their high molecular weight and thus low volatility.

For compounds to ionise by positive ion electrospray ionisation, they must contain a site for protonation and cationisation. Thus, electrospray renders the non-polar hydrocarbon matrix invisible, simplifying the mass spectrum while highlighting additives and polar compounds present.

The detection of compounds by ESI- indicates the presence of a site for deprotonation, *e.g*. derivatised PIB phenolic group. While ionisation of compounds by APPI+ provides insight into the π-electron systems present, and allows for further selectivity.

Ultra-high resolution mass spectrometry allows for determination of nominally isobaric compounds, and the deduction of elemental composition of ions through accurate mass measurement.

Tandem MS, provides insight into the structure of the ions v*ia* their characteristic fragmentation, which is enhanced when combined with ultra-high resolution mass spectrometry, as accurate mass measurement of the fragment ions can be obtained, and thus elemental composition used to aid structural elucidation.

Tandem MS in time (*i.e.* QIT) provides further information with regard to the structure of the ions, as all fragment ions are obtained from the predetermined precursor ion, rather than the possibility of fragment ions of fragment ions.

The number of exchangeable hydrogen atoms can be determined v*ia* deuterium exchange experiments, which aids in the identification of functional groups within the ions. The use of deuterium exchange with tandem MS, provides further structural information about the fragment ions observed (*i.e.* the location of the functional groups).

Whilst the majority of structural information can be obtained from mass spectrometric experimentation, chromatography affords the ability to negate ion suppression issues experienced by direct infusion experimentation. The use of chromatography was advantageous for highlighting the different chemistry between PIB A and PIB B, which only differed by CH_2 unit by MS.

Although multiple experiments are described for the determination of polymeric additives with gasoline, multiple instruments are not always necessarily required. The use of API-Orbitrap MS affords the ability to undertake high resolution tandem MS experimentation in time within one instrument, while integrating atmospheric pressure ionisation (*e.g.* ESI or APPI).

The presence of polymeric additives within the gasoline samples are presented in Table 9.

Table 9 – Presence of polymeric additives with gasoline samples

Series	Gasoline Sample #									
	155	156	158	160	162	167	159	161	164	166
PIB A	X	X	X	✓	✓	✓	✓	✓	✓	✓
PIB B	✓	X	X	X	X	X	X	X	X	X
PPG	X	X	X	✓	✓	✓	✓	X	✓	✓

Chapter 6:   Deposit forming reference fuel

6.1   Deposit forming reference fuel patent

US 8764854 B1 patent[24] describes the composition of a gasoline which produces a high amount of fuel injector and intake valve deposits, within a test engine. By using a gasoline that produces deposits, the effectiveness of detergent additives and engine hardware can be evaluated for their ability to keep internal combustion engines free from deposits.

It is believed by Innospec, that one of the gasoline samples provided has the composition described by patent US 8764854 B1. If this fuel could be identified, the constituent compounds could be investigated, with the intention of forming a correlation between the compounds identified within the fuel samples and the presence of deposits within the associated injectors.

The patent fuel is described as "a deposit-forming reference fuel composition comprises a high sulfur base fuel composition in an amount greater than 50 weight % based on total weight % of the deposit-forming reference fuel composition, wherein the high sulfur base fuel composition comprises greater than or equal to 200 ppm sulfur based on total sulfur content of the base fuel composition. The deposit-forming reference fuel composition also comprises a reactive diolefin dopant and a reaction initiating peroxide. The reaction initiating peroxide has an active oxygen content greater than or equal to 2 weight % based on total oxygen content of the reaction initiating peroxide and a half-life temperature of 80° C. to 200° C. The deposit-forming reference fuel composition is free from a detergent additive and has a concentration ratio of greater than 1:1 for the reactive diolefin dopant to the reaction initiating peroxide."[24]
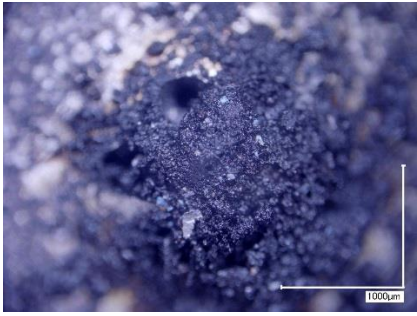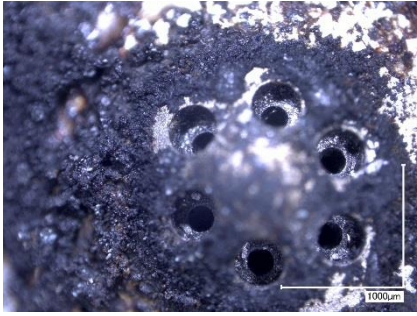
Candidates for the deposit reference fuel from the 10 gasoline samples can be reduced by eliminating the fuels which contain polyisobutylene detergent additives as the "fuel composition is free from a detergent additive". The detection of which has been described in the previous chapter. Gasolines 158 and 156 are the only samples in which PIB A or PIB B were not detected.
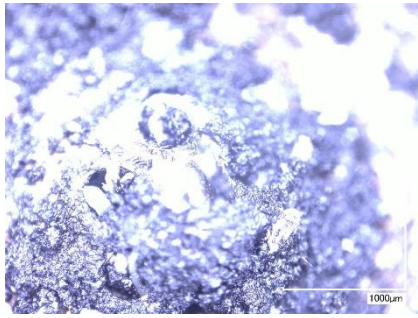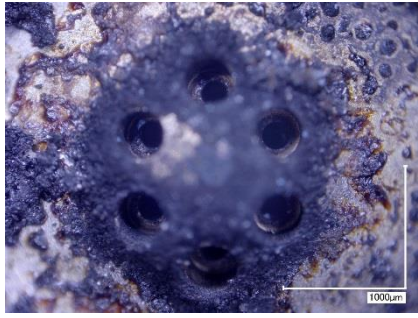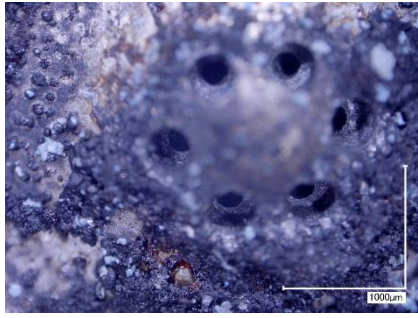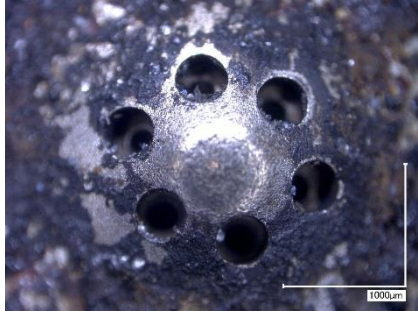
Another criteria of the patent was the "testing of the compositions disclosed herein has demonstrated the desired repeatable effect of injector plugging and desired amounts of high intake valve deposits", *i.e.* the deposit reference fuel must produce deposits within a test engine. Thus, the injectors associated with the gasoline samples were inspected for deposits; the presence of deposits within the injector nozzle would fulfil the criteria of the patent, and therefore remain a candidate for the deposit reference fuel.
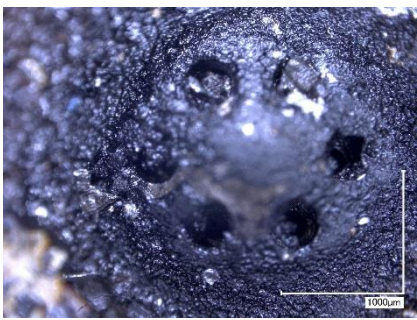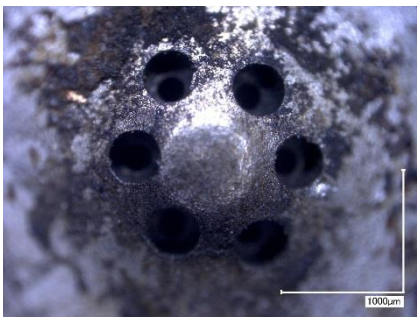
6.1.1 Injector deposit analysis by optical microscopy

The 10 gasoline samples were used in to power 10 test engines. One DISI injector from each test engine (*i.e.* an injector for each fuel sample) was analysed for injector nozzle deposits by optical microscopy. The injectors were deemed to contain deposits if one or more of the nozzle holes were obstructed by deposit, the severity of the deposition was not graded. Deposits on the outer surface of the injector were not considered to be detrimental to fuel delivery and thus were not of interest. Photographs of the injectors are presented in Table 10.

Table 10 – Photographs of the 10 injector tips, obtained v*ia* optical microscopy

Injector / Fuel Number	Injector Photograph	Injector Deposits
155		No Deposit Present
156		Deposit Present
158		No Deposit Present

159		Deposit Present
160		No Deposit Present
161		No Deposit Present
162		No Deposit Present
164		Deposit Present

166		Deposit Present
167		No Deposit Present

Injectors 156, 159, 164 and 166 were determined to contain injector deposits which would impact fuel flow and spray pattern. Thus gasolines 156, 159, 164 and 166 are suitable candidates for the deposit reference fuel. Although, as discussed previously, the fuel must be free from detergent additive (PIB A or B), only gasoline 156 satisfies both criteria. It is also noted that the deposits observed on injector 156 are the most severe when compared to the other deposited injectors (Table 10).

As previously discussed, gasoline 156 appears to be significantly different ($\approx$ 50 % similarity) to the remaining nine gasoline samples when the GC-MS data is compared via AnalyzerPro[TM]. Although, as discussed, GC-MS primarily provides information about the base hydrocarbon content of the fuel, the patent describes a "high sulfur base fuel composition in an amount greater than 50 weight % based on total weight % of the deposit-forming reference fuel composition, wherein the high sulfur base fuel composition comprises greater than or equal to 200 ppm sulfur based on total sulfur content of the base fuel composition". Thus the base fuel is likely to be considerably different from gasoline samples designed for normal engine operation, with sulphur levels approximately 10 times higher than most U.S. regular unleaded gasolines[24]. Investigations into the sulfur components of the gasoline samples would provide further evidence towards identifying the deposit reference fuel.
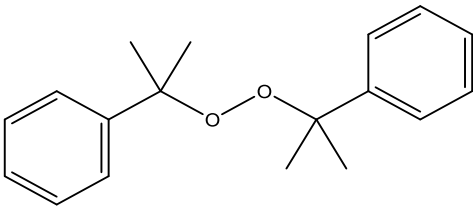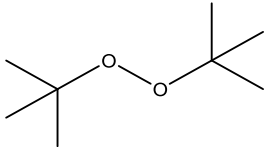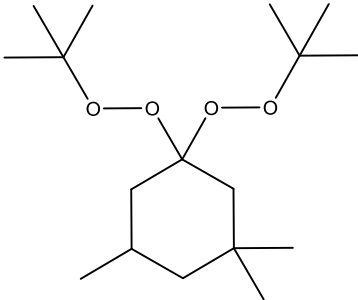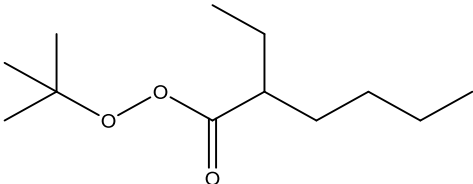
6.1.2 Reaction initiating peroxide and diolefin dopant

The deposit forming reference fuel patent[24] describes the addition of a peroxide and diolefin. The detection of these compounds within the gasoline 156 would further suggest that gasoline 156 is the fuel described by the patent.

Literature[80] suggest these compounds play role in the formation of deposits and gums within the fuel injectors, so development of methodology for the detection of these compounds with gasoline samples would allow screening for these potentially problematic compounds.

The peroxide and diolefin compounds described by the patent, are displayed in Table 11 & Table 12. Two of the peroxide compounds could not be obtained commercially.

Table 11 – Peroxide compounds described by the deposit reference fuel patent

Name	Structure	Acquired for Experimentation?
dicumyl peroxide		✔
di-t-butyl peroxide		✔
1,1-di(t-butylperoxy)-3,3,5-trimethylcyclohexane		✔
t-butyl peroxy-2-ethylhexanoate		X
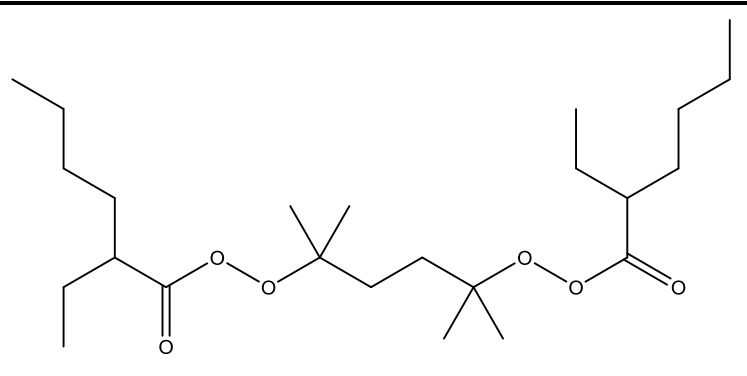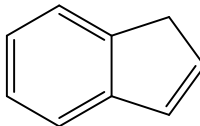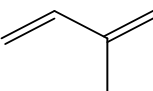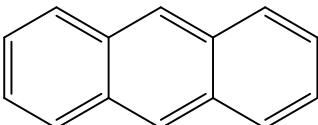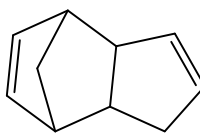
2,5-di(2-ethylhexanoylperoxy)-2,5-dimethylhexane		*X*

Table 12 - Diolefin compounds described by the deposit reference fuel patent

Name	Structure	Acquired for Experimentation?
indene		✔
isoprene		✔
anthracene		✔
dicyclopentadiene		✔

6.1.2.1   GC-MS of peroxide and diolefins

Initially the acquired compounds (Table 11 & Table 12) were subject to GC-MS analysis. The diolefins are suitable for GC-MS analysis, although the peroxide compounds are not. Characterised by a particularly weak O-O bond, the vaporisation and ionisation processes in GC-MS could result in thermal decomposition[87].

The compounds were analysed within a single chromatographic run at a concentration of 10,000 ppm each. The GC-MS TICC is presented (Figure 103).
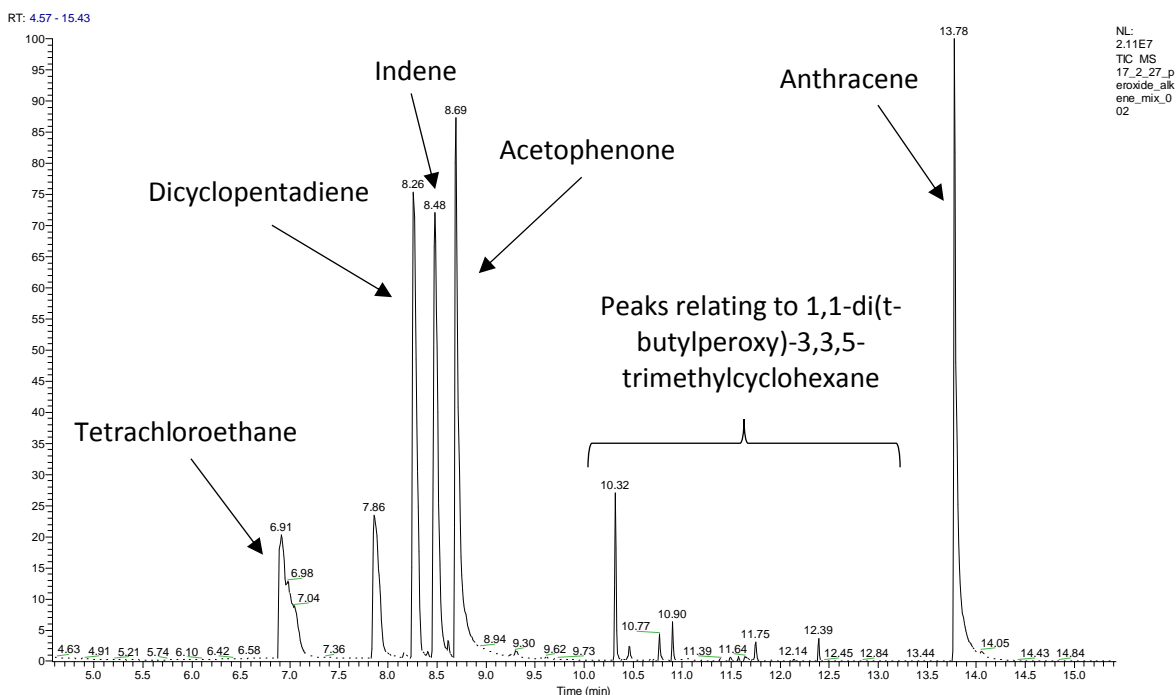
Figure 103 – GC-MS TICC of the diolefin/peroxide mix

The majority of the compounds are detected (identified from their mass spectra) with adequate separation. Isoprene and di-*tert*-butyl peroxide cannot be identified within the chromatogram (Figure 103), likely due to their volatility, and co-elution with the dichloromethane solvent peak. By reducing the solvent delay to 0 minutes, di-*tert*-butyl peroxide can be identified at a retention time of 4.0 minutes, characterised by its molecular ion *m/z* 146, and fragment ions of *m/z* 73 and 57. Isoprene is not observed.

1,1-di(t-butylperoxy)-3,3,5-trimethylcyclohexane cannot be identified within the chromatogram (Figure 103). The series of peaks from T_R: 10.30 to 12.40 min. can be attributed to this compound as they are present in the TICC for the single standard, possibly degradation products.

A peak for tetrachloroethane is present which appears to originate from the peroxide solutions (present in the TICC for each peroxide standard, when analysed separately).

The peak at T_R: 8.69 min. is identified as originating from the dicumyl peroxide standard from the TICC of the single standard. The mass spectrum for the peak (Figure 104) resembles that of acetophenone (identified library searching mass spectrum), and not of that of dicumyl peroxide.
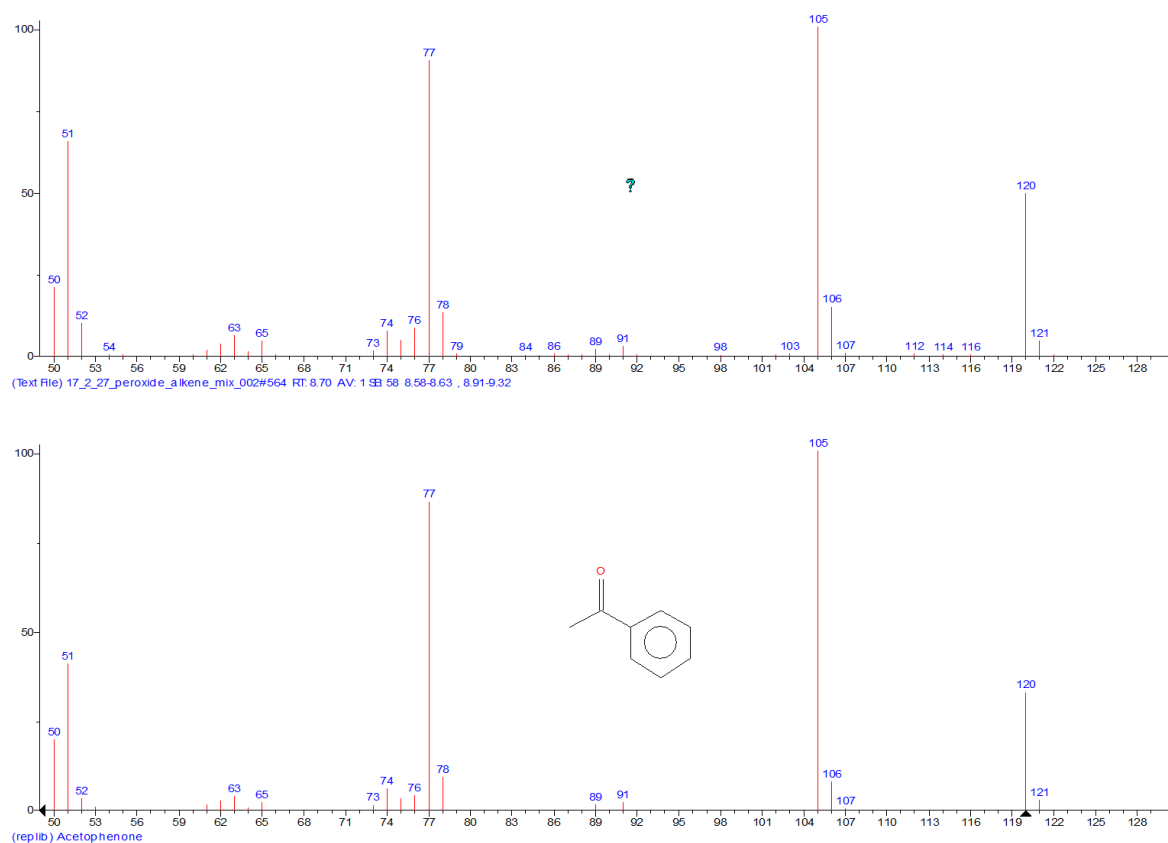
Figure 104 – Top: mass spectrum for the peak at T_R: 8.69 min. (Figure 103) Bottom: NIST library mass spectrum for acetophenone

Acetophenone is a decomposition product of dicumyl peroxide[88], and is likely to be combination of the relatively weak peroxide bond and the elevated temperatures experienced in the GC-MS injector, column, transfer line and/or ionisation source. Spetz *et al.*[89] described a method for the determination of dicumyl peroxide in workplace air, which overcame the issues of decomposition by lowering the injector temperature to 100 °C (currently 240 °C), the maximum column oven temperature to 120 °C (currently 320 °C) and transfer line temperature to 120 °C (currently 250 °C). By utilising these lower temperatures, Spetz *et al.*[89] kept thermal decomposition below 2 %.

In an attempt to replicate the results of Spetz *et al.*[89], the temperatures within the GC-MS were lowered and the effect on the mixture of peroxides was investigated. Initially, the temperature of the injection chamber of the GC was investigated, as it was possible that the dicumyl peroxide decomposed to acetophenone upon injection. Injector temperatures of 240 °C, 100 °C and 60 °C were investigated. The TICCs are shown in Figure 105.
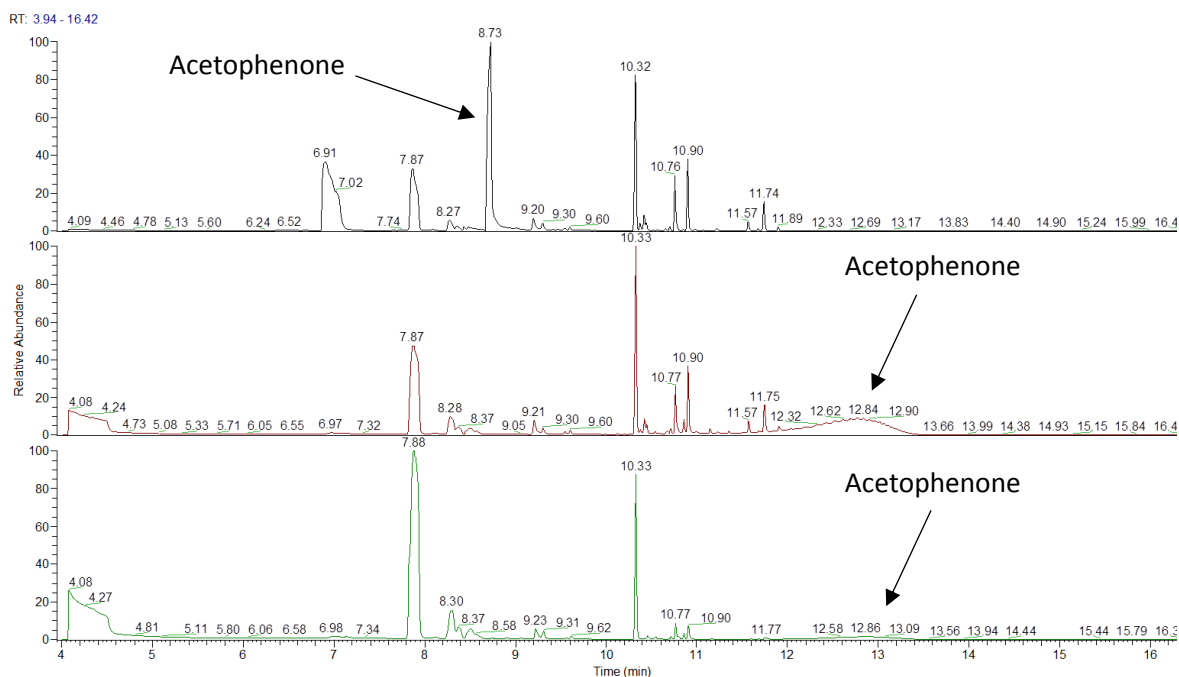
Figure 105 – TICCs for peroxide mixture with various injector temperatures (Top): 240 °C (Middle): 100 °C (Bottom): 60 °C

From the chromatograms (Figure 105), it is observed that dicumyl peroxide decomposes to acetophenone at lower injector temperatures. Although upon lowering the injector temperature to 100 °C, the peak for acetophenone has shifted retention time, and changed from a relative sharp peak to peak eluting over several minutes. The sharp peak produced with an injector temperature of 240 °C, suggests that the decomposition takes place in the injector. Whereas with an injector temperature of 100 °C, the temperature is likely to be insufficient to volatilise the dicumyl peroxide and thus be carried onto the column by the carrier gas. Decomposition would then take place on the column, producing the broad peaks at a longer retention time. Regardless of the change of retention time and peak shape, dicumyl peroxide remains undetectable.

A reduction in all of the GC temperatures was undertaken in an attempt to prevent decomposition of the dicumyl peroxide *i.e.* column oven temperature, injector temperature and transfer line temperature. A injector temperature of 120 °C, transfer line temperature of 100 °C and an over temperature program of 90 °C to 120 °C at 30 °C/min and then held for 25 min. followed by 120 °C to 320 °C at 30 °C/min and then held for 5 min. was used. The resulting chromatograms for the peroxide mixture is present (Figure 106).
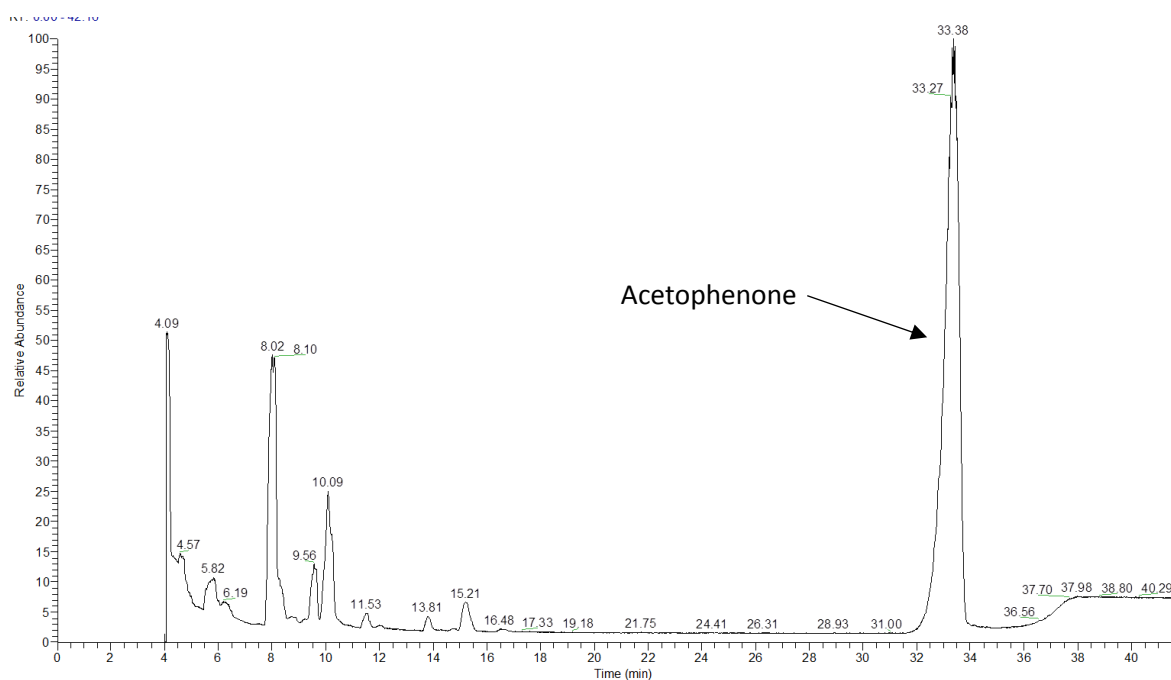
Figure 106 – TICC of peroxide mix (lowered temperatures)

Upon lowering the remaining temperatures within the GC, dicumyl peroxide is still undetectable and a peak is observed for the presence of acetophenone. Not only is dicumyl peroxide undetectable at these lower temperatures, these parameters are detrimental to the detection of other compounds within the gasoline matrix and the cleanliness of the GC-MS.

GC-MS is not a good technique for detection of the peroxides described by the patent. 1,1-di(t-butylperoxy)-3,3,5-trimethylcyclohexane is undetectable, although a series of peaks are present which are related to this compound, possibly degradation products. Dicumyl peroxide decomposes within the GC-MS to acetophenone and thus is undetectable, although, the presence of acetophenone within a gasoline sample could possible used as an indicator to the presence of dicumyl peroxide in the initial sample.

The diolefins described by the patent are readily detectable would good intensity *via* this GC-MS method. Although, the coelution of isoprene with the dichloromethane due to the volatility of isoprene is an issue.

6.1.2.2   Atmospheric pressure ionisation of peroxides and diolefins

Positive ion electrospray can be used to analyse the thermally labile peroxides due to the low thermal energy input into the molecules and subsequent ions during the ionisation process. The thermal energy is dissipated by the evaporation of the eluent.

Positive ion atmospheric pressure photo-ionisation can be used for the detection of diolefins. The same properties that make diolefins (conjugated double bonds) problematic with respect to

deposition within fuel injectors, are the same properties that make compounds suitable for ionisation by APPI+ (*i.e.* presence of π-electron systems). Thus, APPI+ can be used to selectively ionise these compounds within fuel samples, highlighting their presence with little interference from the hydrocarbon matrix observed v*ia* GC-MS techniques.

For both the analysis of the peroxides and the diolefins, the API techniques can be interfaced with UHPSFC. UHPSFC is a chromatographic technique which is suitable for the thermally labile peroxides due the low operating temperature, unlike that of GC, and the good compatibility of the supercritical CO_2 with gasoline, unlike the aqueous phases of reversed-phase HPLC. An ASTM method[90] existed for the detection dicumyl peroxide in resins utilising HPLC, although this was withdrawn in 2017.

6.1.2.2.1   UHPSFC-API MS of peroxide compounds

The peroxides described by the deposit forming reference fuel patent were analysed by UHPSFC-ESI+, to initially to identify whether they will ionise. Cationised molecules would be expected due to the high electron density around the peroxide bond.

6.1.2.2.1.1   UHPSFC-ESI+ MS of dicumyl peroxide

A 1000 ppm solution of dicumyl peroxide in methanol was analysed by UHPSFC-ESI+ MS equipped with a HSS C18 column (1.8 μm x 3.0 mm x 100 mm), utilising a 10 % - 40 % gradient of MeOH + 25 mM NH_4OAc modifier over 3 minutes.

The ammoniated molecule of dicumyl peroxide (Figure 108) is observed in the UHPSFC-ESI+ mass spectrum (Figure 107) at a retention time of 0.52 min. No evidence of decomposition is apparent, although acetophenone would not ionise by ESI+, thus would not appear in the BPICC (Figure 107, top). Acetophenone would respond to UV, therefore the UV chromatogram is also displayed (Figure 107, bottom), and no peaks are observed, this suggests acetophenone is not present.
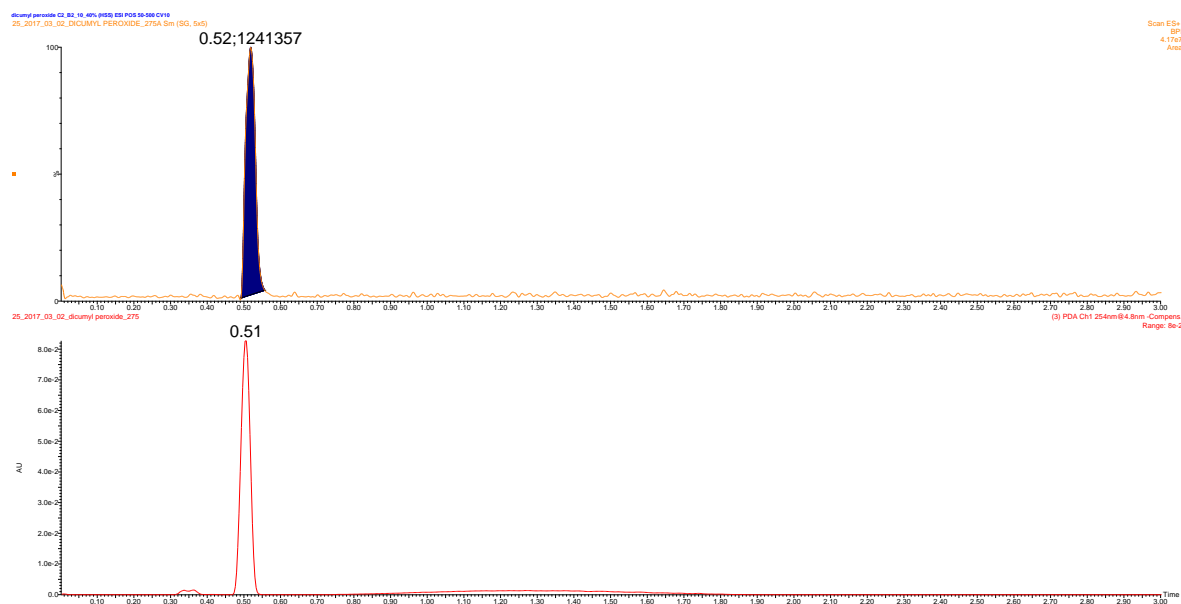
Figure 107 – (Top): UHPSFC-ESI+ MS BPICC of 1000 ppm dicumyl peroxide. (bottom): UHPSFC-UV
chromatogram of 1000 ppm dicumyl peroxide
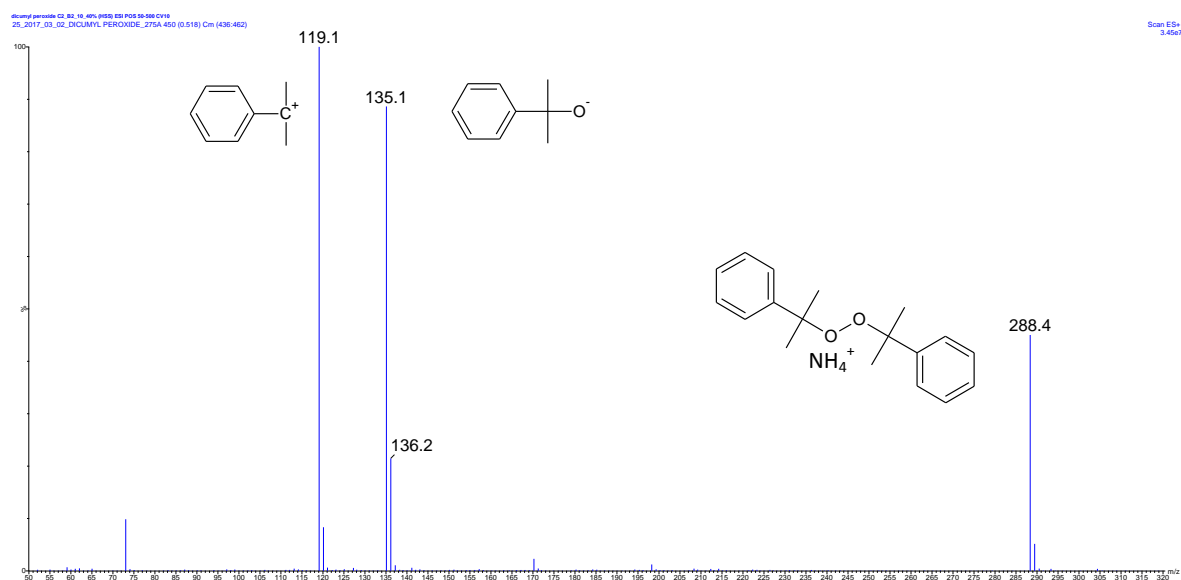
Figure 108 – UHPSFC-ESI+ mass spectrum for dicumyl peroxide, cone voltage of 10 V (T_R: 0.52
(Figure 107))

Fragmentation of the ammoniated molecule (*m/z* 288) is characteristic of a peroxide, with a
cleavage of the peroxide bond resulting in a fragment ion at *m/z* 135. An addition fragment ion
corresponding to the loss of a further oxygen is observed at *m/z* 119 (Figure 108).

The intensity of the chromatographic peak for dicumyl peroxide increases with increase cone
voltage. The UHPSFC-ESI+ mass spectra of dicumyl peroxide at each cone voltage are shown in
Figure 109.
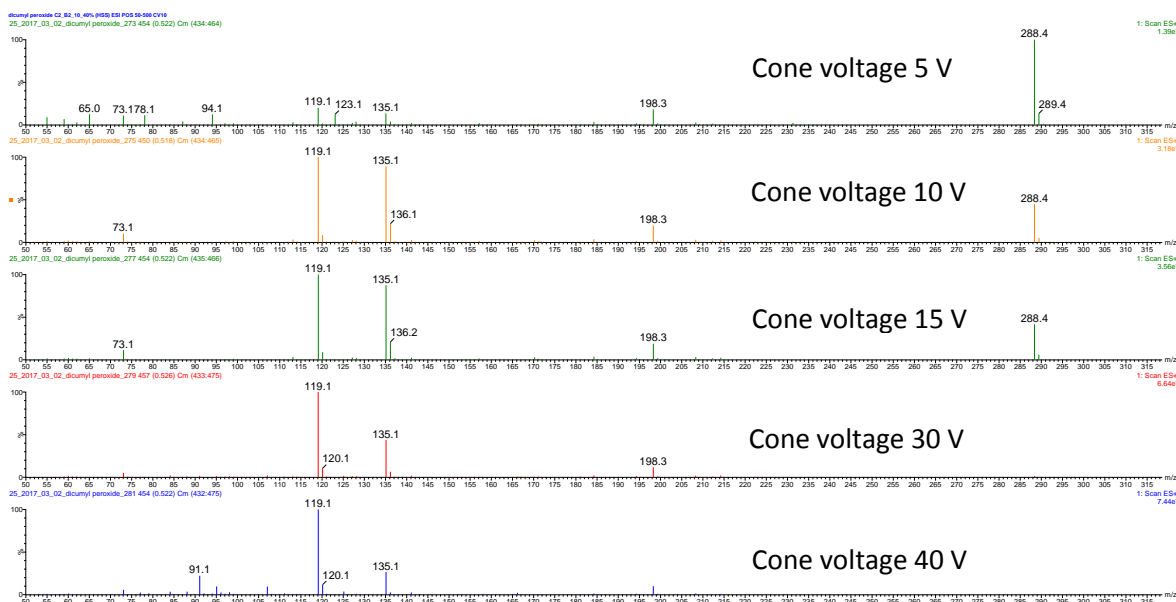
Figure 109 – UHPSFC-ESI+ MS mass spectra for dicumyl peroxide at cone voltages of 5, 10, 15, 30 & 40 V

At low collision energies of 5, 10 & 15 V, the ammoniated molecule is identified at *m/z* 288 (Figure 109). Fragment ions of *m/z* 135 and *m/z* 119 are detected with increasing intensity upon increasing the cone voltage. A gain of an order of magnitude in sensitivity is achieved by employing an in source CID voltage of 40 V when compared to 5 V, although the cationised molecule is not observed at the cone voltage. To further increase the sensitivity of the detection of dicumyl peroxide, SIR experimentation can be undertaken, utilising the base peak ion, *m/z* 119.

6.1.2.2.1.1.1 Detection of dicumyl peroxide in gasoline by UHPSFC-ESI+ MS

10 µL of a 10,000 ppm dicumyl peroxide methanolic solution was added to 990 µL of gasoline 159, to produce a sample of gasoline 159 spiked with 10 ppm dicumyl peroxide. This sample was initially analysed using the UHPSFC-ESI+ MS method for dicumyl peroxide method previously described (section 6.1.2.2.1.1), although the dicumyl peroxide co-eluted with other compounds within the gasoline matrix. To negate this co-elution, the methanol modifier/CO_2 gradient was changed to 0 % modifier between 0 min. and 1.50 min., which then increases to 40% at 2.30 min. and held until 5 min. The run time was increase from 3 min. to 5 min. to accommodate for the longer 100 % CO_2 hold time. The quadrupole was initially operated in scan mode, and then a SIR method for *m/z* 119 (the base peak for dicumyl peroxide), a cone voltage of 40 V was used, as this displayed the greatest sensitivity for the detection of dicumyl peroxide. BPICCs are presented for gasoline 159 using full scan (Figure 110, top), gasoline 159 spiked with 10 ppm dicumyl peroxide using full scan (Figure 110, middle) and gasoline 159 spiked with 10 ppm dicumyl peroxide using SIR for *m/z* 119 (Figure 110, bottom).
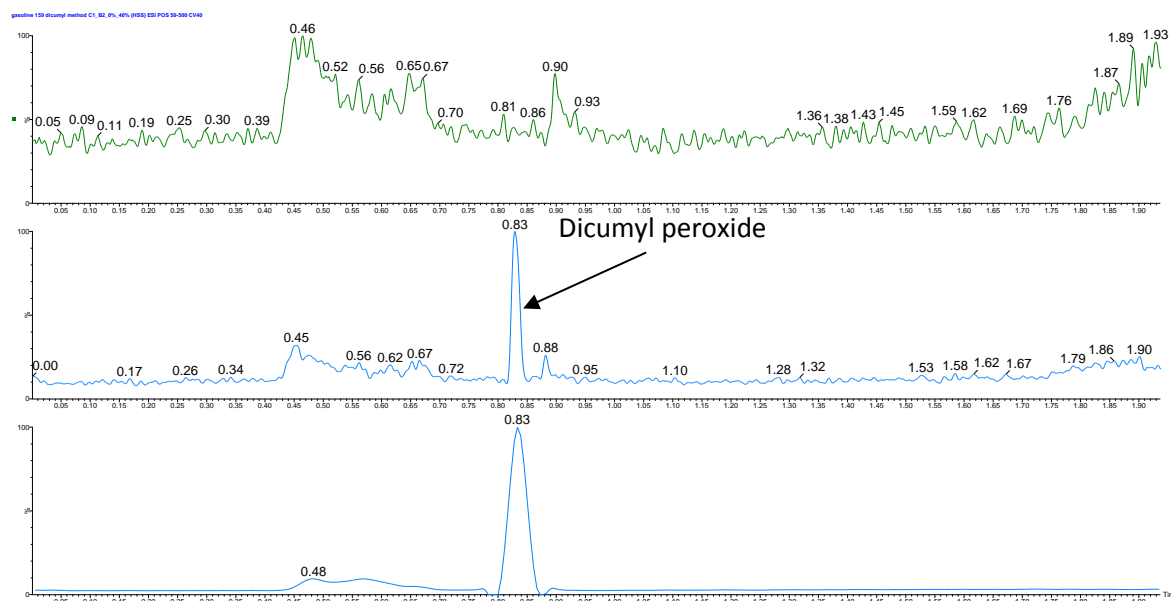
Figure 110 – (Top): UHPSFC-ESI+ MS BPICC of gasoline 159 (middle): UHPSFC-ESI+ MS BPICC of gasoline 159 spiked with 10 ppm dicumyl peroxide (bottom): UHPSFC-ESI+ MS SIR for *m/z* 119 BPICC of gasoline 159 spiked with 10 ppm dicumyl peroxide

Dicumyl peroxide (10 ppm) is identified at a T_R: of 0.83 minutes within the BPICC of the spiked gasoline sample. No co-elution with any compound within the gasoline matrix is observed. The use of SIR for *m/z* 119 increases the sensitivity by an order of magnitude.

Detection of dicumyl peroxide within gasoline samples has been achieved by UHPSFC-ESI+ MS. No decomposition of dicumyl peroxide is observed during the chromatographic and ionisation processes. The chromatographic peak corresponding to dicumyl peroxide is resolved from the other peaks within the gasoline matrix. Utilising an SIR method for *m/z* 119, a chromatographic peak for 10 ppm dicumyl peroxide in gasoline is observed with a signal to noise ratio of 47. To determine a value for LOD, further experimentation is required.

6.1.2.2.1.2   APPI+ MS of dicumyl peroxide

The structure of dicumyl peroxide contains two aromatic rings, making it a candidate for positive ion atmospheric pressure photo-ionisation, due to the π-electron systems. A toluene solution of 1000 ppm dicumyl peroxide was directly infused at 10.00 μL/min into the APPI source of a single quadrupole mass spectrometer at various vaporisation temperatures (150 °C to 650 °C and every 50 °C interval between). The mass spectra for vaporisation temperatures of 300 °C and 650 °C are presented (Figure 111).
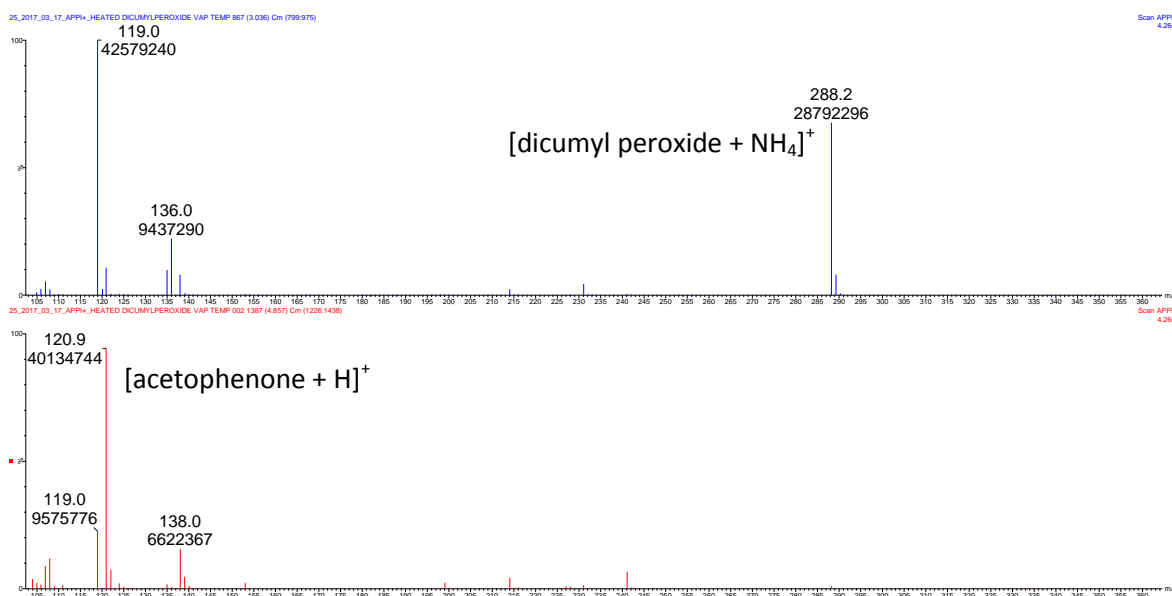
Figure 111 – APPI+ MS of dicumyl peroxide (top): vap. temp. 300 °C (bottom): vap. temp. 650 °C

At low temperatures, the ammoniated molecule for dicumyl peroxide is observed (Figure 111, top), although this is uncharacteristic for APPI+, where no adduct ion should form. Fragmentation for dicumyl peroxide is also observed with ions of m/z 119 and m/z 135 present. Upon increasing the temperature, the intensity of the ammoniated molecule decreases and the intensity of the fragment ions increase. The purpose of the vaporisation temperature is to vaporise and desolvate the molecules prior to ionisation in the gas phase, although it is possible that the elevated temperatures are causing the molecules to fragment.

An increase in the ion intensity of the m/z 121 (protonated acetophenone molecule) is observed with increases in vaporisation temperature. This would suggest the increase in temperature could be causing the dicumyl peroxide to decompose. The ion intensities of m/z 288 (ammoniated dicumyl peroxide), m/z 119 (dicumyl peroxide fragment) and m/z 121 (protonated acetophenone) can be plotted against APPI+ probe temperature, and the trends described are shown in Figure 112.
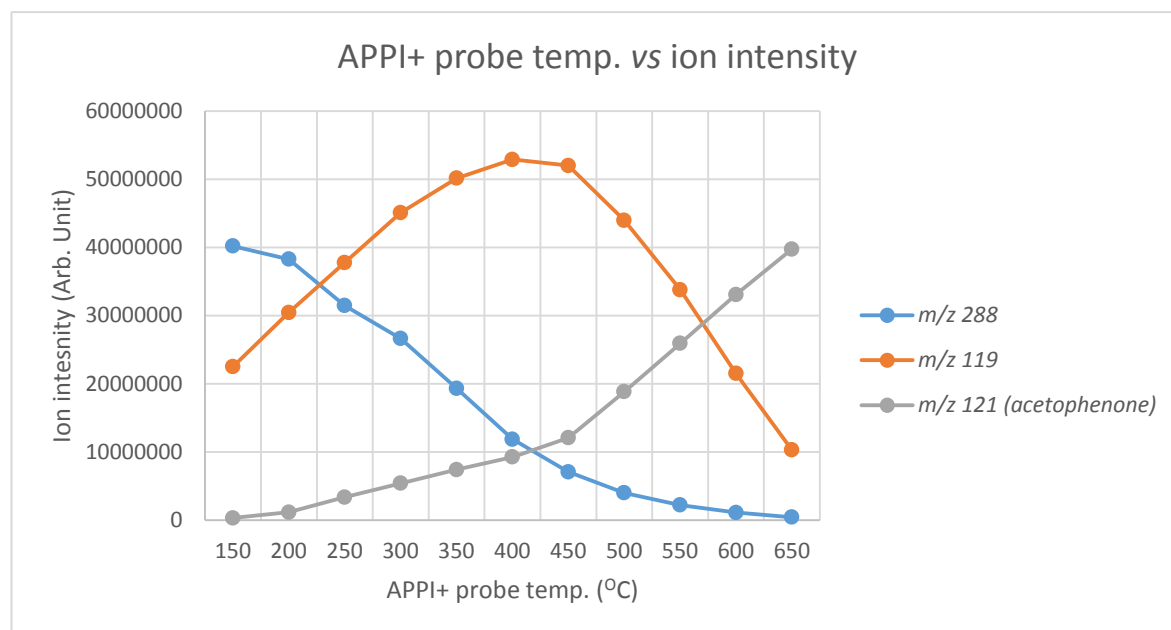
Figure 112 - Graph plotting APPI+ probe temperature *vs* ion intensity of ammoniated dicumyl peroxide (*m/z* 288), dicumyl peroxide fragment (*m/z* 119) and acetophenone (*m/z* 121)

APPI+ is not ideal for the analysis of dicumyl peroxide as the increased temperatures appear to induce decomposition, and the sensitivity at lower temperatures is significantly lower than that of ESI+ method described (6.1.2.2.1.1). In addition, the presence of the ammoniated dicumyl peroxide ion is not characteristic of APPI+ and is possibly formed v*ia* a droplet evaporation event within the APPI source.

6.1.2.2.1.3   UHPSFC-ESI+ MS of di-*tert*-butyl peroxide

A 10,000 ppm solution of di-*tert*-butyl peroxide in methanol was analysed by UHPSFC-ESI+ MS equipped with a HSS C18 column (1.8 µm x 3.0 mm x 100 mm), utilising a 10 % - 40 % gradient of MeOH + 25 mM NH_4OAc modifier over 3 minutes.

The ammoniated molecule of di-*tert*-butyl peroxide (*m/z* 164) (Figure 114) is identified within the UHPSFC-ESI+ MS BPICC (Figure 113) at a retention time of 0.40 min.
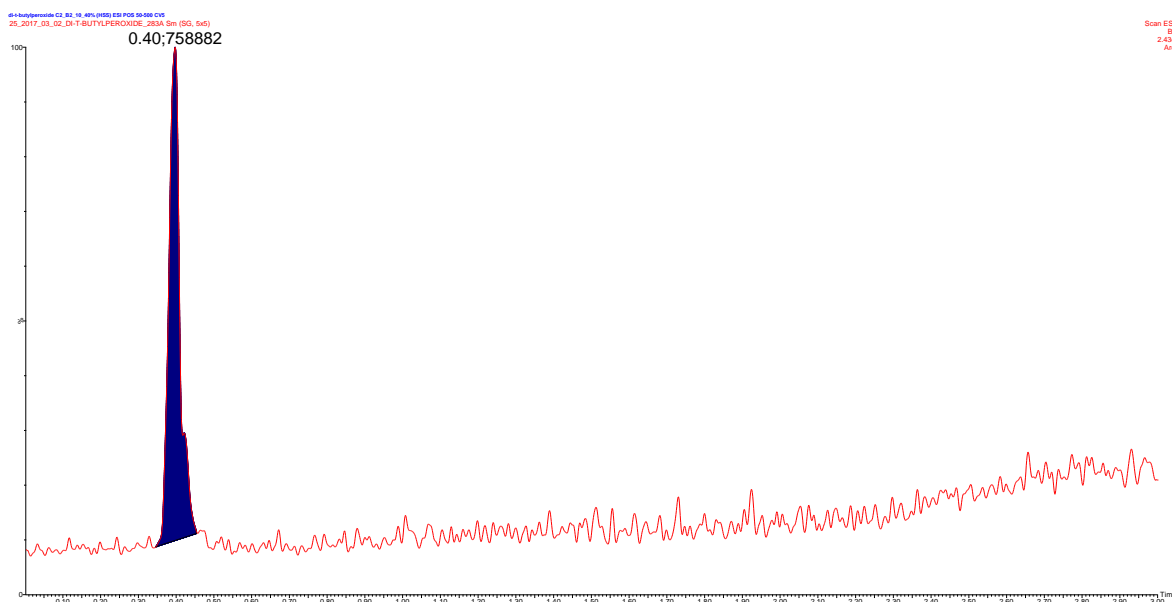
Figure 113 – UHPSFC-ESI+ MS BPICC of 10,000 ppm di-*tert*-butyl peroxide
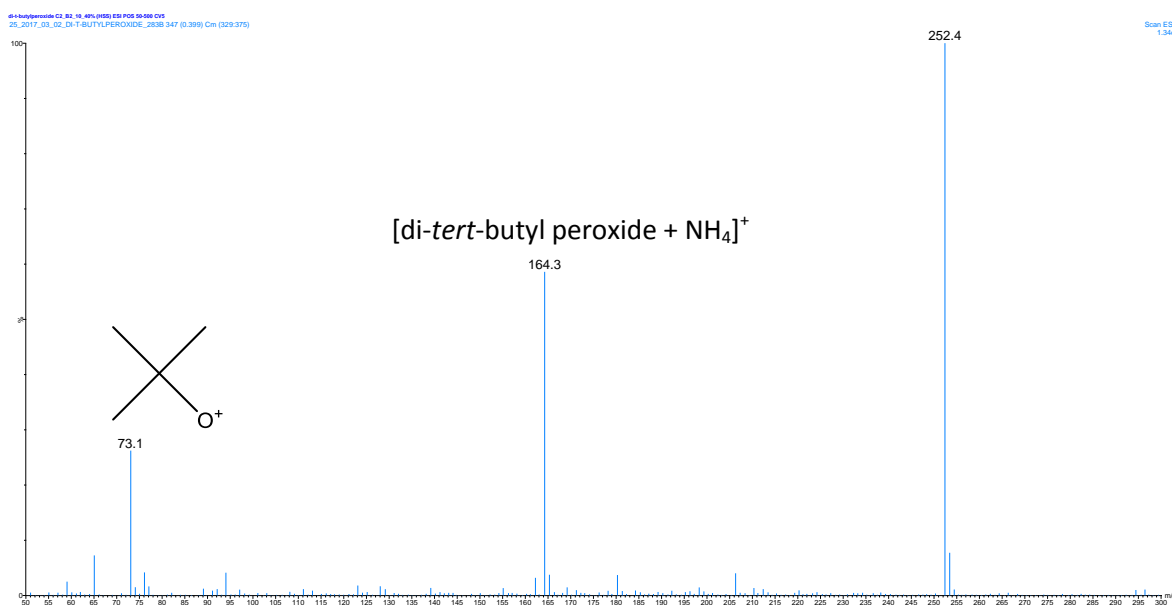
Figure 114 – UHPSFC-ESI+ mass spectrum of the peak at T_R: 0.40 min. in Figure 113.

The ESI+ mass spectrum (Figure 114) for the peak at T_R: 0.40 min. (Figure 113), at a in-source CID voltage of 5 V, can be identified as di-*tert*-butyl peroxide from the ammoniated molecule (*m/z* 164) and the fragment ion of *m/z* 73, originating from a from fragmentation of the peroxide bond, similar to that of dicumyl peroxide. An unidentified ion (*m/z* 252) is also observed in the ESI+ mass spectrum.

The effect of cone voltage on the fragmentation of di-*tert*-butyl peroxide was investigated.
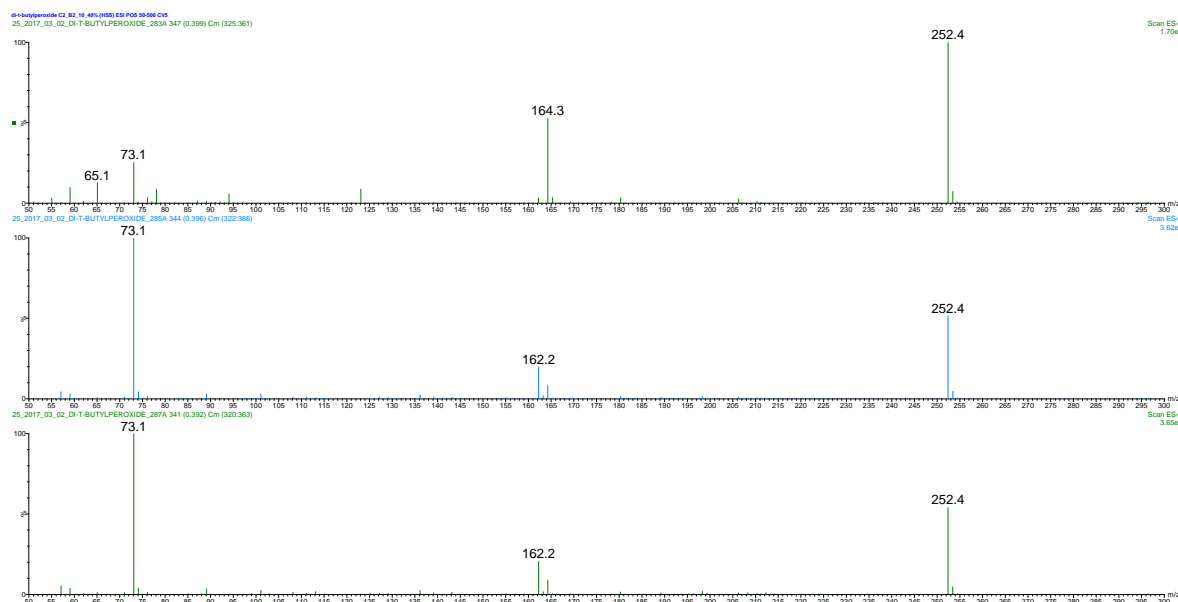
Figure 115 – UHPSFC-ESI+ mass spectra for di-*tert*-butyl peroxide at various cone voltages (top): 5 V (middle): 10 V (bottom): 15 V

From the ESI+ mass spectra (Figure 115) of di-*tert*-butyl peroxide at various cone voltages, it is observed that the ammoniated molecule readily fragments under low voltages (*i.e.* 5 V), and upon increasing the cone voltage from 5 V to 10 V and 15 V, the intensity of the ammoniated molecule is decreased, and the intensity of the fragment at *m/z* 73 increases. The intensity of the unidentified ion (*m/z* 252) remains constant throughout the in-source CID experiments.

The ion at *m/z* 252 shares a retention time with the ammoniated molecule of di-*tert*-butyl peroxide (*m/z* 164) as does the ion at *m/z* 162. MS/MS precursor and product ion scans show that *m/z* 252 and *m/z* 162 are related to each other as *m/z* 162 is present within the product ion mass spectrum of *m/z* 252, and *m/z* 252 is present within the precursor ion mass spectrum of *m/z* 162, while either is not related to *m/z* 164. Separation of the chromatographic peaks for *m/z* 252 and *m/z* 164 has not been achieved with changes in chromatographic conditions.

The current limit of detection for di-*tert*-butyl peroxide by UHPSFC-ESI+ is approximately 1000 ppm. Addition experimentation must be undertaken to identify the origin of ion responsible for *m/z* 252. The high LOD of di-*tert*-butyl peroxide by UHPSFC-ESI+ MS could be a result of *m/z* 252. *m/z* 252 could be formed through a reaction of di-*tert*-butyl peroxide, thus reducing the concentration of di-*tert*-butyl peroxide, or the presence of *m/z* 252 within the mass spectrum could be causing suppression of the ammoniated di-*tert*-butyl peroxide, due to the shared retention time.

6.1.2.2.2   Atmospheric pressure photo-ionisation (APPI) of diolefin compounds

As discussed in section 6.1.2.2, the properties of diolefins are ideal for analysis by APPI+ MS, *i.e.* the presence of π-electron systems. The selectivity of the diolefins and aromatic compounds by APPI+ MS negates the saturated hydrocarbon matrix of gasoline, simplifying the mass spectrum and highlighting the presence of these potentially problematic compounds with respect to deposit formation.

Initially, a 100 ppm solution of isoprene, anthracene, dicyclopentadiene and indene was prepared in toluene. This solution was directly infused, at a flow rate of 5 µL/min, into single quadrupole mass spectrometer equipped with an APPI source. Molecular ions were observed in the APPI+ mass spectrum (Figure 116) for indene, dicyclopentadiene and the anthracene at *m/z* 116, 132 and 178 respectively. Isoprene is not observed in the APPI+ mass spectrum (Figure 116).
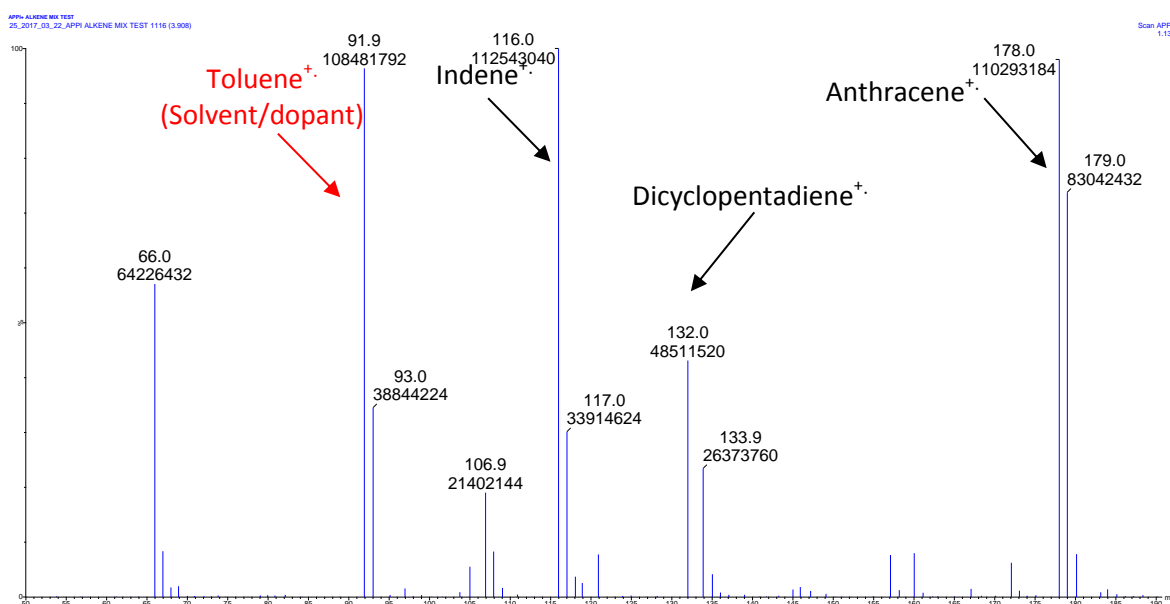
Figure 116 – APPI+ mass spectrum for 100 ppm per component of isoprene, indene, dicyclopentadiene and anthracene in toluene

The desolvation temperature was optimised for sensitivity at 600 °C for the detected compounds (anthracene, indene and dicyclopentadiene). In-source collision induced dissociation was also optimised, with a cone voltage of 30 V corresponding to a maximum intensity of the molecular ions.

6.1.2.3   UHPSFC-APPI+ MS

This section focuses on the application of UHPSFC-APPI+ for the detection of anthracene, dicyclopentadiene and indene within the gasoline matrix, utilising the optimised ionisation source

conditions described in the previous section. The benefit of chromatography over infusion is two-fold, reduction of ion suppression effects and the probable separation of isobaric compounds.

A 100 ppm per component toluene solution of anthracene, indene and dicyclopentadiene was analysed by UHPSFC-APPI+ MS equipped with a HSS C18 column (1.8 µm x 3.0 mm x 100 mm), utilising a 10 % - 40 % gradient of MeOH + 25 mM NH$_4$OAc modifier over 3 minutes. Toluene was used as dopant, a vaporisation temperature of 600 °C and a cone voltage of 30 V was used.

RICCs for the molecular ion of each compound are displayed in Figure 117.
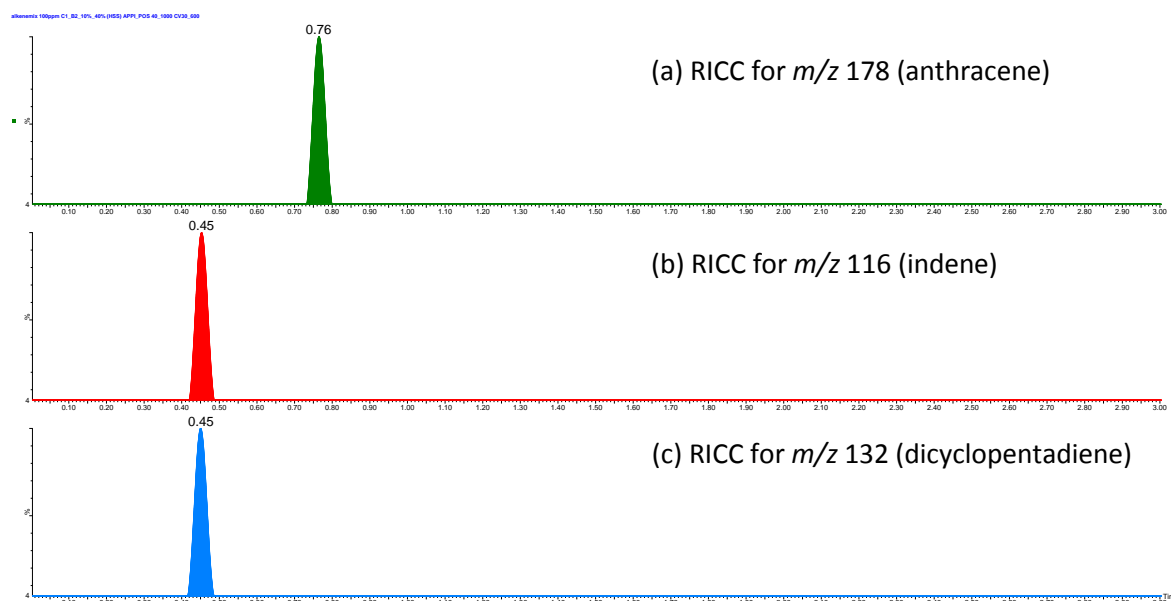
Figure 117 – UHPSFC-APPI+ MS RICC for (a): anthracene, *m/z* 178 (b): indene, *m/z* 116 (c): dicyclopentadiene, *m/z* 132

Anthracene is observed within the chromatogram (Figure 117) with a T$_R$: 0.76 min., whereas indene and dicyclopentadiene co-elute at T$_R$: 0.45 minutes.

To eliminate the possibility that the *m/z* 116 peak was a fragment of the dicyclopentadiene, the compounds were analysed individually. The RICC for *m/z* 116 of the indene samples displayed a peak at T$_R$: 0.45 min., thus the peak within the combined sample can be attributed to indene.

The co-elution can be expected since the structures of indene and dicyclopentadiene are similar (differing only by a methylene group).

In an attempt to develop a method for diolefins that would produce two distinct peaks for indene and dicyclopentadiene, a range of different SFC columns were used but separation of these two species was not achieved.

An SIR method was created for the molecular ions of anthracene, dicyclopentadiene and indene (m/z 178, 132 and 116 respectively), a limit of detection of approximately 100 ppb in toluene was achieved for the three compounds.

6.1.2.3.1 UHPSFC-APPI+ MS of gasoline samples

The 10 GDI test engine gasoline samples were analysed by UHPSFC-APPI+ MS using the method described in section 6.1.2.3 for the detection of anthracene, dicyclopentadiene and indene. Identification of these compounds within gasoline 156 would provide further evidence that gasoline 156 is the gasoline described by the deposit forming reference fuel patent[24].

RICCs were created for the molecular ions of anthracene (m/z 178), indene (m/z 116) and dicyclopentadiene (m/z 132) for each gasoline sample. Compounds were determined to be present, if a peak was detected in the RICC with the same retention time as observed within the toluene standards, see section 6.1.2.3. RICCs for gasoline 158 are presented as an example (Figure 118).
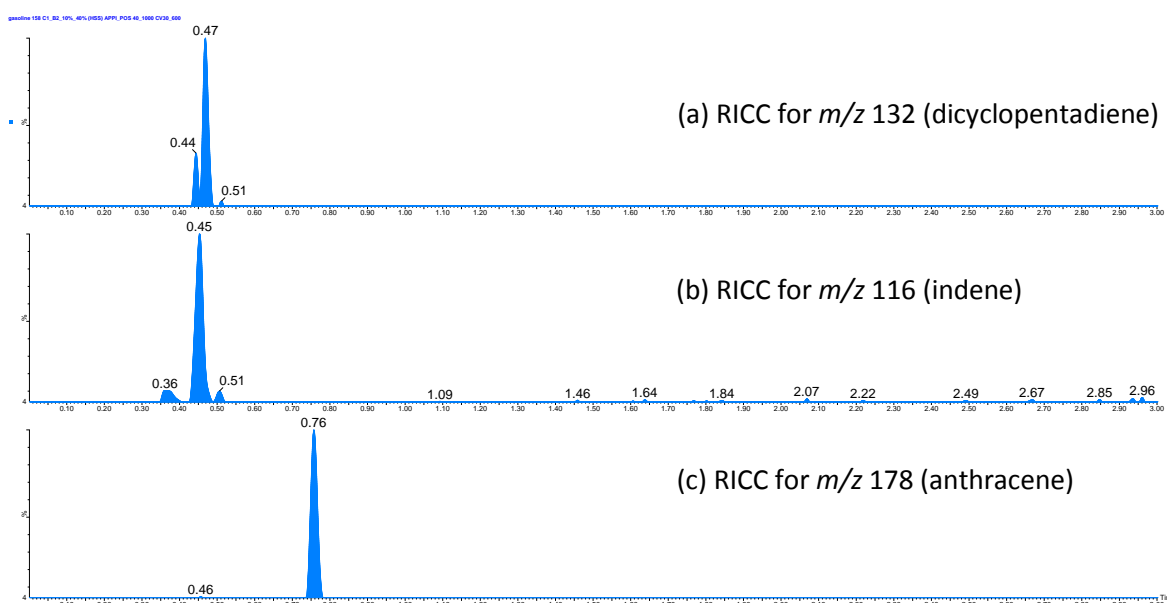
Figure 118 – UHPSFC-APPI+ MS RICCs of gasoline 158 for (a): dicyclopentadiene, m/z 132 (b): indene, m/z 116 (c): anthracene, m/z 178

The RICCs for anthracene, indene and dicyclopentadiene suggest these compounds are present in gasoline 158 (Figure 118). For further confirmation of the presence of these compounds, multiple reaction monitoring experimentation could be undertaken using a triple quadrupole MS. Here, the precursor ion is selected in the first quadrupole (*e.g.* the molecular ion), fragmentation of the precursor takes place in the second quadrupole, and the third quadrupole is set to only permit a stable trajectory for a known fragment ion of the precursor. This method would negate any issues

associated with the detection of isobaric ions with a similar retention time and significantly increase sensitivity for the targeted compounds.

The presence of anthracene, indene and dicyclopentadiene within the gasoline samples is shown within Table 13.

Table 13 – Presence of anthracene, indene and dicyclopentadiene within the gasoline samples by UHPSFC-APPI+ MS

Gasoline	Anthracene (*m/z* 178, T_R: 0.78 min.)	Indene (*m/z* 116, T_R: 0.45 min.)	Dicyclopentadiene (*m/z* 116, T_R: 0.45 min.)
155	✓	X	X
156	✓	X	X
158	✓	✓	✓
159	✓	X	X
160	✓	X	X
161	✓	X	X
162	✓	X	X
164	✓	✓	X
166	✓	X	X
167	✓	X	X

Anthracene is detected in all gasoline samples, indene is detected in gasoline 158 and 164, and dicyclopentadiene is only detected in gasoline 158. The presence of these compounds shows no correlation to the presence of deposits within the injector nozzles.

The chromatographic peak for anthracene within gasoline 156 is of a similar intensity to the anthracene peaks in the other gasolines, suggesting that the anthracene concentration is not greater than in other gasoline samples. Indene and dicyclopentadiene were not detected within gasoline 156. This evidence is not consistent with the deposit forming reference fuel patent, unless additional isoprene is present, which is currently undetectable by UHPSFC-APPI+ MS.

The deposit forming reference fuel describes the addition of either anthracene, isoprene, indene or dicyclopentadiene to promote deposit formation. Although, potentially problematic, diolefins

are not limited to these four compounds, but rather the class of compound in general. These compounds are detectable by GC-MS although, APPI+ provides selective ionisation for diolefins and aromatic compounds, while rendering the remainder of the gasoline matrix essential invisible.

Chapter 7: Conclusions

This project has focused on the development of chromatographic and mass spectrometric methods for the determination of polymeric detergent and fluidiser gasoline additives within a gasoline matrix. The project also focused on the comparison of the composition of gasoline samples which display the formation of injector deposits within DISI injectors to that of gasoline samples which do not display deposits. The aim of which was to identify deposit precursors within the gasoline samples.

The structure of two derivatised polyisobutylene detergent additives and one derivatised polypropylene glycol fluidiser additive have been determined. The additives were identified in finished gasoline samples at typically doping concentrations, without the use of pure standards for each polymeric additive. The gasoline samples required little sample preparation (*i.e.* a 5 % gasoline in methanol, and the addition of an ionisation additive).

GC-MS, typically used for gasoline analysis, is unsuitable for the detection of polymeric gasoline additives, due to their high molecular weight and low volatility.

Electrospray ionisation negates the issues experienced with GC-MS, as it is not necessary to volatilise the sample, high molecular weight and thermally labile compounds can be analysed directly. The two derivatised PIB molecules and the derivatised PPG molecule were detected using ESI+. The use of ESI also provided selectivity, whereby only the polar compounds within the gasoline matrix were detected, rendering the hydrocarbon matrix invisible, thus simplifying the mass spectra.

Further selectivity for the polymeric additives was achieved with the use of ionisation additives. The preparation of 5 % methanol + 25 mM formic acid promoted the ionisation of the derivatised polyisobutylene compounds, while suppressing the derivatised polypropylene glycol. The addition of 25 mM ammonium acetate permitted the detection of both the derivatised PIBs and the derivatised PPG molecules. While providing selectivity for the polymeric additives, the addition of ionisation additives permitted the identification of the molecular weight of each compound, by comparing the *m/z* of the same molecule when cationised with different cations.

Accurate mass measurement of the polymeric additives was undertaken using ESI+ FT-ICR MS. The accurate mass measurement of the difference between members of each oligomeric polymer series, identified the polymers as PIB and PPG. Using accurate mass of the ions and information obtained about the associated cations from ionisation additive experiments, potential end group

masses, and therefore elemental composition, could be calculated from linear regression of the oligomeric series.

Initially the incorrect end group was assigned to PIB A. This was due to a conference presentation displaying the identification of an isobaric and therefore identical elemental composition, PIB additive in gasoline. Although, the compound presented contained a primary amine, therefore two exchangeable hydrogen atoms were present. As the molecule has been shown to be protonated, three exchangeable hydrogen atoms are present under ESI+ conditions. Upon undertaking deuterium exchange experiments, an increase in 2 *m/z* units was observed, and thus two exchangeable hydrogen atoms must be present for the protonated molecule, one of which is from the cationising proton, and the other originating from a phenolic OH group. PIB B also contained two exchangeable hydrogen atoms for the protonated molecule.

The *m/z* of PIB B displayed the presences of an additional CH_2 group when compared to PIB A. The gasoline samples containing PIB A and PIB B were analysed by UHPSFC-ESI+ MS. Each member of the polymeric series of PIB A was baseline separated, whereas the members of the polymeric series of PIB B were unresolved from each other. This different chromatographic behaviour was unlikely to be a result of an increased chain length within the end group.

Tandem MS experimentation were utilised to investigate the structure of the polymeric additive end groups. PIB A and PIB B were determined to be PIB-Mannich compounds, characterised the loss of their di-butyl amine and di-methyl amine pendant arms respectively, under MS/MS conditions. The identification of the structure of the fragment ions was aided with the use of accurate mass measure and MS/MS experiments of the deuterated molecules. Further evidence for PIB-Mannich compounds was provided *via* the detection of PIB A and PIB B by APPI+ (highlights the presence of a π-electron system, the derivatised benzene ring), and ESI- (deprotonation of the phenolic OH group).

The addition of lithium acetate to gasoline as an ionisation additive aided structural determination of PPG additives within the fuel. The ESI+ MS/MS experiments of the lithiated PPG compounds displayed addition and more intense fragment peaks than that of the sodiated and ammoniated molecules. The PPG molecules proceeded to fragment by four fragmentation series under MS/MS conditions. Using these series, the PPG molecule was determined to contain an ethyl end group. This is consistent with an increase in 1 *m/z* unit when deuterated (terminating OH group) and the absence of the PPG from the APPI+ and ESI- mass spectra.

Although multiple experiments are described for the determination of polymeric additives in gasoline, multiple instruments are not always necessarily required. The use of API-Orbitrap MS

would afford the ability to undertake high resolution tandem MS experimentation in time within one instrument.

Another objective of the project was to correlated gasoline composition with DISI injector deposits. This has been guided by the suggestion that one of the gasoline samples is a deposit forming reference fuel described by patent US 8764854 B1.

The gasoline sample described by the patent must produce deposits, therefore the presence of injector deposits within the nozzle of the DISI injectors were investigated by optical microscopy. DISI injectors corresponding to gasoline samples 156, 159, 164 and 166 were found to contain injector deposits. The patent also describes that the fuel must be free from detergent additive. Utilising the polymeric additive detection and identification methods previously described, gasoline 156 was identified as the only gasoline to produce deposits and be free from detergent additives.

The patent also describes a different base fuel composition to that of commercially available gasoline samples. This was investigated by computational comparison of the similarity of the electron ionisable portion of each gasoline sample.

EI GC-MS affords high chromatographic resolution and detailed structural information from energetic fragmentation for the hydrocarbon base fuel and volatile additives in gasoline. Although it is limited to thermally stable and low molecular weight compounds. Gasoline samples can often appear near identical, with just varying concentrations of the compounds present. Subtle differences between the samples are difficult to identify manually. Automated processing of gasoline TICCs allows for rapid and comprehensive identification of compounds, and comparison between different samples. The use of SpectralWorks AnalyzerPro™ provides a gauge on the similarity of gasoline samples, by comparing the component fingerprint of a gasoline to another. Gasoline 156 has been identified as being very different compared to the other 9 gasoline samples (typically < 50 % similarity).

Gasoline 156 has been shown to produce injector deposits under test engine conditions, to be free from detergent additives and be most dissimilar to the other gasoline samples. From the gasoline samples present, 156 is the most likely candidate for the gasoline described by patent US 8764854 B1.

To provide further evidence for this identification and potentially correlate deposits within injectors to compounds within the gasoline samples. The presence of diolefins and peroxides, which are have been highlighted as potential deposit precursors, in the gasoline samples was investigated.

The detection of dicumyl peroxide, di-t-butyl peroxide and 1,1-di(t-butylperoxy)-3,3,5-trimethylcyclohexane by GC-MS was initially investigated. The particularly weak O-O bond present in the peroxides resulted in thermal decomposition when exposed to the temperatures present within the GC-MS. Detection of dicumyl peroxide and di-t-butyl peroxide were achieved by UHPSFC-ESI+ MS with no thermal decomposition.

The detection of anthracene, isoprene, indene or dicyclopentadiene has been achieved by GC-MS, although, UHPSFC-APPI+ MS provided selective ionisation for diolefins and aromatic compounds, while rendering the remainder of the gasoline matrix essential invisible.

No correlation has been made with the presence of these compounds in gasoline samples and the presence of DISI injector deposits.

Engine technology and gasoline composition are closely related, with advancements in engine hardware requiring adjustments to gasoline composition, thus it is essential to comprehensively understand the chemical make-up of gasoline samples. This work has displayed the versatility of mass spectrometry and chromatography towards achieving this goal.

List of References

1.   Akarapanjavit, N.; Boonchanta, P., Valve Seat Recession and Protection Due to Lead Phase Out in Thailand. *SAE Technical Paper 962029* **1996**.

2.   Kent, W. L.; Finnigan, F. T., The Effect of Some Fuel and Operating Parameters on Exhaust Valve Seat Wear. *SAE Technical Paper 710673* **1971**.

3.   Stępień, Z.; Oleksiak, S., Deposit Forming Tendency in Sparkignition Engines and Evaluation of Gasoline Detergent Additives Effectiveness. *Journal of KONES* **2009,** 16, 421-431.

4.   Wallington, T. J.; Kaiser, E. W.; Farrell, J. T., Automotive Fuels and Internal Combustion Engines: A Chemical Perspective. *Chem Soc Rev* **2006,** 35, (4), 335-347.

5.   Nunney, M. J., *Light and Heavy Vehicle Technology*. 4th ed. ed.; Butterworth-Heinemann: Amsterdam ; London, 2007.

6.   Richards, P.; Owen, K., *Automotive Fuels Reference Book*. Third ed.; SAE International: Warrendale, Pennsylvania, USA, 2014.

7.   Schaschke, C., *A Dictionary of Chemical Engineering*. First ed.

8.   Zhao, F.; Lai, M. C.; Harrington, D. L., Automotive Spark-Ignited Direct-Injection Gasoline Engines. *Prog Energ Combust* **1999,** 25, (5), 437-562.

9.   He, X.; Ratcliff, M. A.; Zig, B. T., Effects of Gasoline Direct Injection Engine Operating Parameters on Particle Number Emissions. *Energ. Fuel* **2012,** 26, (4), 2014-2027.

10.   Sandquist, H.; Denbratt, I.; Owrang, F.; Olsson, J., Influence of Fuel Parameters on Deposit Formation and Emissions in a Direct Injection Stratified Charge SI Engine. *SAE Technical Paper 2001-01-2028* **2001**.

11.   *ASTM D2699-16e1, Standard Test Method for Research Octane Number of Spark-Ignition Engine Fuel*; West Conshohocken, 2016.

12.   *ASTM D2700-16a, Standard Test Method for Motor Octane Number of Spark-Ignition Engine Fuel*; West Conshohocken, 2016.

13.   Foong, T. M.; Morganti, K. J.; Brear, M. J.; Da Silva, G.; Yang, Y.; Dryer, F. L., The Octane Numbers of Ethanol Blended with Gasoline and its Surrogates. *Fuel* **2014,** 115, 727-739.

14.   Farrell, A. E., Ethanol Can Contribute to Energy and Environmental Goals *Science* **2006,** 312, (5781), 1748-1748.

15.   Anderson, J.; Hardigan, P.; Ginder, J.; Wallington, T.; Baker, R., Implications of the Energy Independence and Security Act of 2007 for the US Light-Duty Vehicle Fleet. *SAE Technical Paper 2009-01-2770* **2009**.

16.   Barusch, M.; Mingle, J.; Payne, J.; Sigworth, H., The "World's First Detergent-Action Gasoline" (With 36 Years of Perspective),". *SAE Technical Paper 900149* **1990**.

17.   *Fuel Additives: Uses and Benefits*; Additive Technical Committee: 2013.

18.   Stępień, Z., Intake Valve and Combustion Chamber Deposits Formation - The Engine and Fuel Related Factors that Impact thier Growth. *Nafta-Gaz* **2014,** 4, 236-242.

Bibliography

19.   Aradi, A. A.; Colucci, W. J.; Scull, H. M.; Openshaw, M. J., A Study of Fuel Additives for Direct Injection Gasoline (DIG) Injector Deposit Control. *SAE Technical Paper 2000-01-2020* **2000**.

20.   Phillips, T. A. Corrosion Inhibitor for Liquid Fuels. US4737159, 1988.

21.   Tupa, R. C.; Dorer, C. J., Gasoline and Diesel Fuel Additives for Performance/Distribution/Quality. *SAE Technical Paper 841211* **1984**.

22.   Altin, O.; Eser, S., Carbon Deposition from Thermal Stressing of Petroleum Fuels. *Abstr Pap Am Chem S* **2004,** 228, U673-U673.

23.   Hilden, D. L., The Relationship of Gasoline Diolefin Content to Deposits in Multiport Fuel Injectors. *SAE Technical Paper 881642* **1988**.

24.   Studzinski, W. M.; Cummings, J. M. Reference Fuel Composition. US8764854 B1, 2014.

25.   Hallet, D. *Formation and Characterization of Carbon Deposits from Thermal Stressing of Gasoline and Diesel Fuels*; The Pennsylivania State University: 2003.

26.   Zerda, T. W.; Yuan, X.; Moore, S. M.; Leon, C. A. L. Y., Surface area, Pore Size Distribution and Microstructure of Combustion Engine Deposits. *Carbon* **1999,** 37, (12), 1999-2009.

27.   Mayers, P. S.; Uyehara, O. A.; Young, R. D. *Fuel Compostion and Vapourisation Effects on Combustion Chamber Deposits*; U.S. Dept. of Energy: 1981.

28.   Carlisle, H.; Frew, R.; Mills, J.; Aradi, A., The Effect of Fuel Composition and Additive Contenet on Injector Deposits and Performance of Air Assisted Direct Injection Spark Ignition (DISI) Research Engine. *SAE Technical Paper 2001-01-2030* **2001**.

29.   Ansomboon, J.; Wuttimongkolchai, A.; Pannoi, S.; Fuckuda, K., Characterisation of Deposits and Effect of Detergent Additives, Olefin Content and Engine Oil on Intake Valve Deposit Formation. *SAE Technical Paper 2000-01-2856* **2000**.

30.   Arters, D.; Bardasz, E.; Schiferl, E.; Fisher, D., A Comparison of Gasoline Direct Injection Part I - Fuel System Deposits and Vehicle Performance. *SAE Technical Paper 1999-01-1498* **1999**.

31.   Kinoshita, M.; Saito, A.; Matsushita, S.; Shibata, H.; Niwa, Y., Study of Deposit Formation Mechanism on Gasoline Injection Nozzle. *JSAE Rev* **1998,** 19, (4), 335-357.

32.   Arters, D.; Macduff, M., The Effect on Vehicle Performance of Injector Deposits in a Direct Injection Gasoline Engine. *SAE Technical Paper 2000-01-2021* **2000**.

33.   Dearn, K.; Xu, J.; Ding, H.; Xu, H., An Investigation into the Characteristics of DISI Injector Deposits using Advanced Analytical Methods. *SAE Int J Fuels Lubr* **2014,** 7, (3).

34.   Tswett, M., Physikalisch-chemische Studien über das Chlorophyll. Die Adsorption. *Ber dtsch botan* **1906,** 24, 316–323.

35.   Purnell, H., *Gas Chromatrography*. John Wiley and Sons Inc: New York, 1962.

36.   Van Deemter, J. J.; Zuiderweg, F. J.; Klinkenberg, A. V., Longitudinal Diffusion and Resistance to Mass Transfer as Causes of Nonideality in Chromatography. *Chem Eng Sci* **1956,** 5, (6), 271-289.

37.   Golay, M. J. E., Gas Chromatography. In First ed.; Butterworths: London, 1958.

38.   Golay, M. J. E., *Gas Chromatography*. Butterworths: London, 1958.

39.   Gohlke, R. S., Time-of-Flight Mass Spectrometry and Gas-Liquid Partition Chromatography. *Anal Chem* **1959,** 31, (4), 535-541.

40.   Teng, S. T.; Williams, A. D.; Urdal, K., Detailed Hydrocarbon Analysis of Gasoline by GC-MS (SI-PIONA). *Hrc-J High Res Chrom* **1994,** 17, (6), 469-475.

41.   Achten, C.; Puttmann, W., Method for Determination of Methyl Tert-Butyl Ether in Gasoline by Gas Chromatography. *J Chromatogr A* **2001,** 910, (2), 377-383.

42.   Kanai, H.; Inouye, V.; Goo, R.; Chow, R.; Yazawa, L.; Maka, J., GC/MS Analysis of MTBE, ETBE, and TAME in Gasolines. *Anal Chem* **1994,** 66, (6), 924-927.

43.   Frysinger, G. S.; Gaines, R. B., Comprehensive Two-Dimensional Gas Chromatography with Mass Spectrometric Detection (GC x GC/MS) Applied to the Analysis of Petroleum. *Hrc-J High Res Chrom* **1999,** 22, (5), 251-255.

44.   Phillips, J. B.; Beens, J., Comprehensive Two-Dimensional Gas Chromatography: A Hyphenated Method With Strong Coupling Between the Two Dimensions. *J Chromatogr A* **1999,** 856, (1-2), 331-347.

45.   Martin, A. J. P., Synge, R. L. M., A new form of chromatogram employing two liquid phases *Biochem J* **1941,** 35, (12), 1358-1368.

46.   Hsu, C.; Shi, Q., Prospects for Petroleum Mass Spectrometry and Chromatography. *Sci China Chem* **2013,** 56, (7), 833-839.

47.   Barman, B. N.; Cebolla, V. L.; Membrado, L., Chromatographic Techniques for Petroleum and Related Products. *Crit Rev Anal Chem* **2000,** 30, (2-3), 75-120.

48.   Berger, T. A., *Packed column SFC*. The Royal Society of Chemistry: Cambridge, 1995.

49.   Hoffmann, E. D.; Stroobant, V., *Mass Spectrometry : Principles and Applications*. Third ed.; J. Wiley: Chichester, West Sussex, England, 2007.

50.   Kienitz, H.; Aulinger, F., *Massenspektrometrie*. Verlag Chemie: Weinheim/Bergstrasse,, 1968.

51.   Gross, J. H., *Mass Spectrometry : A Textbook*. 2st ed.; Springer: New York, 2011.

52.   Konermann, L.; Ahadi, E.; Rodriguez, A. D.; Vahidi, S., Unraveling the Mechanism of Electrospray Ionization. *Anal Chem* **2013,** 85, (1), 2-9.

53.   Dole, M. M., L.L.; Hines, R.L., Mobley, R.C.; Ferguson, L.D.; Alice, M.B., Molecular Beams of Macroions. *J Chem Phys* **1968,** 49, (5), 2240-2249.

54.   Kebarle, P.; Verkerk, U. H., Electrospray: From Ions in Solution to Ions in the Gas Phase, What We Know Now. *Mass Spectrom Rev* **2009,** 28, (6), 898-917.

55.   Taylor, G.; McEwan, A., The Stability of a Horizontal Fluid Interface in a Vertical Electric Field. *J Fluid Mech* **1965,** 22, (01), 1-15.

56.   Van Berkel, G. J.; Kertesz, V., Using the Electrochemistry of the Electrospray Ion Source. *Anal Chem* **2007,** 79, (15), 5510-5520.

57.   Nguyen, S.; Fenn, J. B., Gas-Phase Ions of Solute Species from Charged Droplets of Solutions. *P Natl Acad Sci USA* **2007,** 104, (4), 1111-1117.

58.   Iribarne, J. V.; Thomson, B. A., Evaporation of Small Ions from Charged Droplets. *J Chem Phys* **1976,** 64, (6), 2287-2294.

59.   Dole, M.; Mack, L. L.; Hines, R. L.; Mobley, R. C.; Ferguson, L. D.; Alice, M. B., Molecular Beams of Macroions. *J Chem Phys* **1968,** 49, (5), 2240-2249.

Bibliography

60.   Wilm, M., Principles of Electrospray Ionization. *Mol Cell Proteomics* **2011,** 10, (7).

61.   Diehl, G.; Wasinski, F. A. H.; Roberz, B.; Luftmann, H.; Schmidt, T. C.; Andersson, J. T.; Karst, U., Liquid Chromatography/Electrochemistry/Mass Spectrometry as Screening Technique for Alcohols and Phenols in Fuels. *Microchim Acta* **2004,** 146, (2), 137-147.

62.   Crawford, K. E.; Campbell, J. L.; Fiddler, M. N.; Duan, P.; Qian, K.; Gorbaty, M. L.; Kenttamaa, H. I., Laser-Induced Acoustic Desorption/Fourier Transform Ion Cyclotron Resonance Mass Spectrometry for Petroleum Distillate Analysis. *Anal Chem* **2005,** 77, (24), 7916-7923.

63.   Zhan, D. L.; Fenn, J. B., Electrospray Mass Spectrometry of Fossil Fuels. *Int J Mass Spectrom* **2000,** 194, (2-3), 197-208.

64.   Rostad, C. E., Screening of Polar Components of Petroleum Products by Electrospray Ionization Mass Spectrometry. *Energ Fuel* **2005,** 19, (3), 992-997.

65.   Haddad, R.; Regiani, T.; Klitzke, C. F.; Sanvido, G. B.; Corilo, Y. E.; Augusti, D. V.; Pasa, V. M. D.; Pereira, R. C. C.; Romao, W.; Vaz, B. G.; Augusti, R.; Eberlin, M. N., Gasoline, Kerosene, and Diesel Fingerprinting via Polar Markers. *Energ Fuel* **2012,** 26, (6), 3542-3547.

66.   Carraze, B.; Delafoy, J.; Bertin, J.; Beziau, J. F.; Lange, C. M., Mass Spectral Fingerprints of Detergents in Gasolines using Electrospray Ionization. *Rapid Commun Mass Sp* **2004,** 18, (4), 451-457.

67.   Robb, D. B.; Covey, T. R.; Bruins, A. P., Atmospheric Pressure Photoionisation: An Ionization Method for Liquid Chromatography-Mass Spectrometry. *Anal Chem* **2000,** 72, (15), 3653-3659.

68.   Bos, S. J.; Van Leeuwen, S. M.; Karst, U., From Fundamentals to Applications: Recent Developments in Atmospheric Pressure Photoionization Mass Spectrometry. *Anal Bioanal Chem* **2006,** 384, (1), 85-99.

69.   Raffaelli, A.; Saba, A., Atmospheric Pressure Photoionization Mass Spectrometry. *Mass Spectrom Rev* **2003,** 22, (5), 318-331.

70.   Miller, P. E.; Denton, M. B., The Quadrupole Mass Filter - Basic Operating Concepts. *J Chem Educ* **1986,** 63, (7), 617-622.

71.   Amster, I. J., Fourier Transform Mass Spectrometry. *J Mass Spectrom* **1996,** 31, (12), 1325-1337.

72.   Marshall, A. G.; Hendrickson, C. L., Fourier Transform Ion Cyclotron Resonance Detection: Principles and Experimental Configurations. *Int J Mass Spectrom* **2002,** 215, (1-3), 59-75.

73.   Hipple, J. A.; Sommer, H.; Thomas, H. A., A Precise Method of Determining the Faraday by Magnetic Resonance. *Phys Rev* **1949,** 76, (12), 1877.

74.   Comisarow, M. B.; Marshall, A. G., Fourier Transform Ion Cyclotron Resonance Spectroscopy. *Chem Phys Lett* **1974,** 25, (2), 282-283.

75.   Marshall, A. G.; Hendrickson, C. L., Charge Reduction Lowers Mass Resolving Power for Isotopically Resolved Electrospray Ionization Fourier Transform Ion Cyclotron Resonance Mass Spectra. *Rapid Commun Mass Sp* **2001,** 15, (3), 232-235.

76.   March, R. E., An Introduction to Quadrupole Ion Trap Mass Spectrometry. *J Mass Spectrom* **1997,** 32, (4), 351-369.

77.   Willoughby, R. C.; Sheehan, E.; Mitrovich, S., *A Global View of LC/MS : How to Solve Your Most Challenging Analytical Problems*. First ed.; Pittsburgh, Pa., 1998.

78.   ASTM D2789-95, Standard test method for hydrocarbon types in low olefinic gasoline by mass spectrometry. In ASTM International: West Conshohocken, PA, 2011.

79.   ASTM D5769-15, Standard test method for determination of benzene, toluene, and total aromatics in finished gasolines by gas chromatography/mass spectrometry. In ASTM International: West Conshohocken, PA, 2015.

80.   Pradelle, F.; Braga, S. L.; Martins, A. R. F. A.; Turkovics, F.; Pradelle, R. N. C., Gum Formation in Gasoline and Its Blends: A Review. *Energ Fuel* **2015,** 29, (12), 7753-7770.

81.   Altgelt, K. H.; Boduszynski, M. M., *Composition and Analysis of Heavy Petroleum Fractions*. M. Dekker: New York, 1994.

82.   Marshall, A. G.; Rodgers, R. P., Petroleomics: Chemistry of the Underworld. *P Natl Acad Sci USA* **2008,** 105, (47), 18090-18095.

83.   Savory, J. J.; Kaiser, N. K.; McKenna, A. M.; Xian, F.; Blakney, G. T.; Rodgers, R. P.; Hendrickson, C. L.; Marshall, A. G., Parts-Per-Billion Fourier Transform Ion Cyclotron Resonance Mass Measurement Accuracy with a "Walking" Calibration Equation. *Anal Chem* **2011,** 83, (5), 1732-1736.

84.   Koster, S.; Duursma, M. C.; Boon, J. J.; Heeren, R. M. A., Endgroup Determination of Synthetic Polymers by Electrospray Ionization Fourier Transform Ion Cyclotron Resonance Mass Spectrometry. *J Am Soc Mass Spectr* **2000,** 11, (6), 536-543.

85.   Lynch, T.; Whitmarsh, S.; Wicking, C. In *Selective Ionisation With High Resolution Mass Spectrometry - The Future for Hyphenation in the Petrochemical Industry?*, HTC-14, Ghent, Belgium, 2016; Ghent, Belgium, 2016.

86.   Jackson, A. T.; Slade, S. E.; Thalassinos, K.; Scrivens, J. H., End-Group Characterisation of Poly(propylene Glycol)s by Means of Electrospray Ionisation-Tandem Mass Spectrometry (ESI-MS/MS). *Anal Bioanal Chem* **2008,** 392, (4), 643-650.

87.   Rondeau, D.; Vogel, R.; Tabet, J. C., Unusual Atmospheric Pressure Chemical Ionization Conditions for Detection of Organic Peroxides. *J Mass Spectrom* **2003,** 38, (9), 931-940.

88.   Di Somma, I.; Marotta, R.; Andreozzi, R.; Caprio, V., Dicumyl Peroxide Thermal Decomposition in Cumene: Development of a Kinetic Model. *Ind Eng Chem Res* **2012,** 51, (22), 7493-7499.

89.   Spetz, A.; Svanstrom, M.; Ramnas, O., Determination of Dicumyl Peroxide in Workplace Air. *Ann Occup Hyg* **2002,** 46, (7), 637-641.

90.   ASTM E1090-08, Standard Test Method for Dicumyl Peroxide and Dicumyl Peroxide Decomposition Products in Resins (Withdrawn 2017). In ASTM International: West Conshohocken, PA,, 2008.